12-2017

Synthesis and Characterization of Glycidyl Methacrylate-Based Graft Copolymer Functional Interfaces

Nikolay Brordinov

SYNTHESIS AND CHARACTERIZATION OF GLYCIDYL METHACRYLATE-BASED GRAFT COPOLYMER FUNCTIONAL INTERFACES

A Dissertation
Presented to
the Graduate School of
Clemson University

In Partial Fulfillment
of the Requirements for the Degree
Doctor of Philosophy
Material Science & Engineering

---

by
Nikolay Borodinov
December 2017

Accepted by:
Dr. Igor Luzinov, Committee Chair
Dr. Marek Urban
Dr. Olin Thompson Mefford
Dr. Mark Roberts

ABSTRACT

Modification of materials properties such as surface energy, wettability, ability to absorb, contain or release specific type of chemicals enables practical application of these materials in various scientific and engineering set-ups. However, designing protocol that could be easily adapted for different situations and simultaneously unlock multiple variations of the resulting properties is a non-trivial task. This dissertation is devoted to application of glycidyl methacrylate-based graft copolymers for the purposes of surface modification, establishing fundamental trends and dependencies of this process and exploring the possible range of applications. These materials have extremely valuable property to undergo controllable post-synthetic modifications including surface attachment and cross-linking. Deep understanding of the relationship between structure, properties and composition of these polymeric materials was made possible with the current study and can play pivotal role in introducing GMA-based functional interfaces into industrial practice.

First part of this dissertation is focused on GMA-copolymer films prepared by "grafting to" method. As I have demonstrated, such nanoscale layers are promising elements of photonic sensors leading to creation of new generation of highly selective devices. Photonic technologies represent state-of-the-art answer to chemical weapon proliferation and ensure safety and security of global population, which necessitates research in highly responsive but stable and reliable polymer films for chemical detection. Here, I show that GMA-copolymer films are not only able to fulfill this task, but also can

be actuated in a special way that allows them to operate as post-exposure sensing elements recording information of the chemical exposure. This groundbreaking finding has clear and evident applicability, but also great fundamental value as the investigation that I have performed gives new insights on the metastable polymer networks.

Second part of the dissertation is devoted to GMA-copolymers prepared by "grafting through" method which results in water-soluble polymers that enable use of GMA-based reactions in aqueous environment. This not only reduces the use of organic solvents in polymer processing, but also opens new venues of modification of objects such as enzymes that would not be able to be processed otherwise. Through the rigorous study of the synthesis and relevant properties, I have identified the possible range of resulting properties and highlighted composition-dependent trends which serve as a practical guide for preparation of copolymers with desired properties. I demonstrated the applicability of GMA-copolymers for preparation of thermally-stable polymer-enzyme conjugates, mechanically resistant drug-loaded coatings, chemical sensors and preparation of transparent conductive coatings using graphene oxide as a precursor.

Overall, this dissertation provides novel insights on surface modification of various materials and actualizes the role that GMA-based copolymers can play. Unique combination of fine control over surface properties and preparation practicality makes these materials a novel technological solution for advanced functional interface design.

DEDICATION

I dedicate this dissertation to my family who provided me with guidance, advice and moral support throughout my studies: my parents, Sergei Borodinov and Elena Prokhortseva, my grandfather Vyacheslav Prokhortsev and my grandmother Valentina Prokhortseva. I would like to give special dedication to my late grandfather Nikolay Borodinov and recently deceased grandmother Natalya Borodinova who passed away in 2014. I will always remember her kindness, wisdom and diligence that will always be my beacon in life.

ACKNOWLEDGEMENTS

First of all, I would like to thank my current advisor, Dr. Igor Luzinov, for the wonderful opportunity to work in his lab, learn from him and grow as a scientist under his guidance. I was truly blessed to have such wonderful scientific advisor whose support and kindness made my PhD studies an unforgettable journey.

Next, I would like to thank members of Dr. Luiznov's group: Misha Savchak, Charles Nikon, Dr. Anna Paola Soliani, Dr. Yuri Galabura, Dr. James Giammarco, Dr. Jake Townsend, Dr. Tugba Demir, Dr. Ruslan Burtovyy and Dr. Fehime Vatansever for their friendship and help during my work.

I would like to give special thanks to Artem Trofimov, Katie Burdette, Dr. Dmitry Gil, Pavel Aprelev, Mikhail Bredikhin, Anastasia Frank-Kamenetskii, Oleksandr Klep, Dr. Victor Maximov, Dr. Raisa Kiseleva, Dmitry Davydovich, Dr. Tigran Abramyan, Alexander Polman, Petr Kuznetzov, Ekaterina Kuznetzova and Tatyana Bashlakova-Nikolaeva for being my supportive friends who were always full of encouragement and compassion. I would like to acknowledge Dr. Vladimir Reukov and Dr. Peter Maksymovych for their guidance, help and valuable word of advice.

I would like to express my gratitude to the members of my committee, Dr. Marek Urban, Dr. Olin Thompson Mefford and Dr. Mark Roberts for providing me assistance and guidance with regard to my work.

I would like to thank Dr. Alexey Vertegel, Dr. Sergei Kalinin, Dr. Michel van Tooren, Dr. Anuradha Agarwal, Dr. Kathleen Richardson, Dr. Pingshan Wang, Dr. Vladimir Tsukruk and Dr. Sergiy Minko for the wonderful and enriching collaborative projects. Also, I want to acknowledge Kimberly Ivey for assisting in almost all my projects.

TABLE OF CONTENTS

TABLE OF CONTENTS (CONTINUED)

TABLE OF CONTENTS (CONTINUED)

TABLE OF CONTENTS (CONTINUED)

TABLE OF CONTENTS (CONTINUED)

LIST OF FIGURES

LIST OF FIGURES (CONTINUED)

LIST OF FIGURES (CONTINUED)

LIST OF FIGURES (CONTINUED)

LIST OF FIGURES (CONTINUED)

LIST OF FIGURES (CONTINUED)

LIST OF FIGURES (CONTINUED)

LIST OF TABLES

CHAPTER 1. INTRODUCTION

1.1. Introduction

This dissertation is devoted to the synthesis and characterization of graft copolymers containing epoxy monomeric units and their utilization for surface modification. The major goal of this work is to establish a structure-composition-property relationship and explore the applicability of graft copolymers as a versatile tool for controlling the surface and interfacial properties of various materials as well as establish new applications for grafting technology.

The reactive epoxy rings presented in the structure of the copolymers allow for the reactions with nucleophiles such as carboxyl, amino and hydroxyl groups. This enables the copolymers to react with the organic and inorganic surfaces and undergo cross-linking forming stable covalently attached networks. However, as the novel materials and technologies emerge, the issue of their realization in actual environments and conditions requires more variability and tunability of the coatings used for the surface modification. An additional complication that represents a significant challenge for materials scientists and engineers is that some practically important systems require water solubility and/or compatibility. Biomedical systems are one of the prominent examples of such behavior as they are able to successfully operate in a very narrow window of temperatures, pressures and solution compositions. Thus, in order to create a next generation of polymer surface modification agents, one has to consider three requirements of the proposed coating:

- the ability to control over its properties is a way that can delivers wide variation of the achieved properties through the identical procedures.
- the ability to use the reactivity of the coating within the actual systems of interest.
- the ability to use the similar modification protocols for a variety of substrates in a streamlined cost-effective procedure

Polyglycydyl methacrylate (PGMA) naturally satisfies these requirements as it is able to permanently bond to ceramic, metal and polymer surfaces due to intrinsically presented nucleophilic groups on their surface using “grafting to” method that implies creation of chemical bonds between reactive polymer of the substrate. In the case of the chemically inert materials, an air plasma exposure or chemical activation (piranha solution or base) can be used as a pre-treatment measures. This core property of PGMA is important for this work and serves as a primal motivation to focus on this particular polymer system in my dissertation. While grafting the polyglycydyl methacrylate macromolecular chains from the surface in the context of surface-initialed polymerization is indeed a well-explored path in research papers, its practicality is hindered by the certain limitations. First, “grafting from” set-up requires the substrate to be within the reactive media that may cause conflict with its functionality and represent somewhat of a technical challenge, while “grafting to” technique can be combined with any physical deposition method (spin-coating, drop-casting, dip-coating, spray coating).

Surface-initiated polymerization in the form of atom-transfer radical polymerization (ATRP) offers certain level of control over the polydispersity and structure of the coating. However, this control is limited to short chains only as otherwise the

reaction takes longer times, in addition, ATRP causes some concerns when applied to biological systems due to the usage of copper catalyst. Most importantly, "grafting from" requires the presence of the anchored initiator on the substrate surface while PGMA can interact with a surface directly in a one-step procedure and then undergo surface "grafting to" modifications. These considerations prompted me to explore the usage of pre-emptively synthesized PGMA and GMA-containing copolymers for the purposes of surface modification as opposed to the *in-situ* polymerization.

The previous studies on PGMA-based materials were mainly focused on thin polymer brushes and the physical and chemical peculiarities of their behavior. For instance, as the new chemical sensor set-ups are rising to their prominence, the call for the new methods of tailoring their response and maximizing the useful signal has to be answered. Enrichment polymer layers that effectively concentrate the analyte of interest in the vicinity of the sensor element by swelling in its vapors are a viable solution to this challenge. However, this application requires usage of thicker films (100 – 1000 nm) with adjustable chemical affinity that can be tailored to be more sensitive to specific chemicals. Biomedical systems are yet another example of the application that is very demanding in terms of the property variability. For instance, the hydrophobicity of the coatings plays crucial role in its interaction with human body and protein adhesion. In this regard, the special focus of this dissertation will be made on exploring the ways to diversify thickness and the chemical composition of the grafted coatings beyond levels of 10-100 nm typically used.

Finally, this dissertation considers the ability to use reactivity of PGMA in certain systems imposing a number of requirements on the polymer coating. Specifically, water-

soluble poly(oligo(ethylene glycol) methyl ether methacrylate) (OEGMA) copolymer with glycidyl methacrylate maintains the reactivity towards nucleophilic chemical groups which opens up opportunities for ecologically friendly surface modification performed in aqueous media rather than in organic solvents. It is demonstrated that this copolymer is able to covalently bind to colloid substrates dispersed in water under ambient conditions.

The present dissertation is structured as follows. **Chapter 2** will introduce the basic fundamentals of the polymer grafting technology as well as provide with an in-depth analysis of the recent trends and most important areas of application with a special emphasis put on GMA and OEGMA as building blocks for surface modification. Next three chapters consider synthesis, structure and properties of GMA copolymers obtained by "grafting to" approach. **Chapter 3** is dedicated to the synthesis of such materials and one of their main functional characteristic – swelling in the vapors of volatile organic compounds. **Chapter 4** will explore the usage of these materials for the purposes of chemical sensing and the pathways to increase the stability of copolymer-based devices to gamma irradiation. **Chapter 5** is going to be centered on a fundamentally new material called nanofoam which is a metastable GMA copolymer film. This chapter will also display its high potential to serve as a post-exposure chemical sensor.

Water-soluble GMA copolymers synthesized by "grafting through" method will be discussed in three following chapters. **Chapter 6** will consider the synthetic aspects of the copolymerization as well as outline the relationship between the composition and properties of the product. **Chapter 7** will introduce the applications of these materials for the surface modification of the solid surfaces for the purposes of chemical sensing and

orthopedic implant coating. Finally, **Chapter 8** will highlight the modification of colloid objects such as graphene oxide and proteins for the purposes of hydrophilic/hydrophobic compatibilization and thermal stabilization, respectively.

CHAPTER 2. LITERATURE REVIEW

2.1. The overview of polymer grafting for surface modification

Organic polymers are a versatile class of materials that find their applications in adhesives, binders, industrial coatings, varnishes, fibers, resins, composite materials, filtration membranes, active components of solar cells and sensors to name a few.[1-4] The possibility to alter their basic properties by an appropriate selection of synthesis, processing and modification protocols is a fundamental basis for a widespread usage of polymers that is further expanding as new approaches and findings emerge. One of the most powerful pathways to broaden the spectrum of polymer properties is preparation of graft-copolymers. In this scenario, the initial polymer molecule that may or may not be a part of a cross-linked network is augmented with another polymer chain. This way the properties of two individual components are combined within the same material. The result is a unique combination of behaviors designed according to fit the application.

A special case of grafting is the modification of the material surface. In this case, the bulk properties such as mechanical moduli, electronic structure and porosity can be effectively utilized in a system that imposes certain prerequisites for the event happening at the interface. Most common surface properties include, but are not limited to wettability, swellability, morphology, cytotoxicity and mechanical robustness. Polymer grafting in principle allows for the fine control over these qualities thus attracting keen interest from very distant disciplines within materials science community. The overall number of research papers dedicated to the polymer grafting is enormous and keeps on growing.

However, the citation clustering analysis is capable of providing a clearer overview on the issue. **Figure 2.1** displays the citation map generated using Web of Science search engine using search words “polymer grafting surface modification”, “anchoring polymer layer”, “adhesion improvement polymer grafting”, “polymer brush modification surface grafting” spanning from 2000 to 2017 and processed using in VOSviewer.

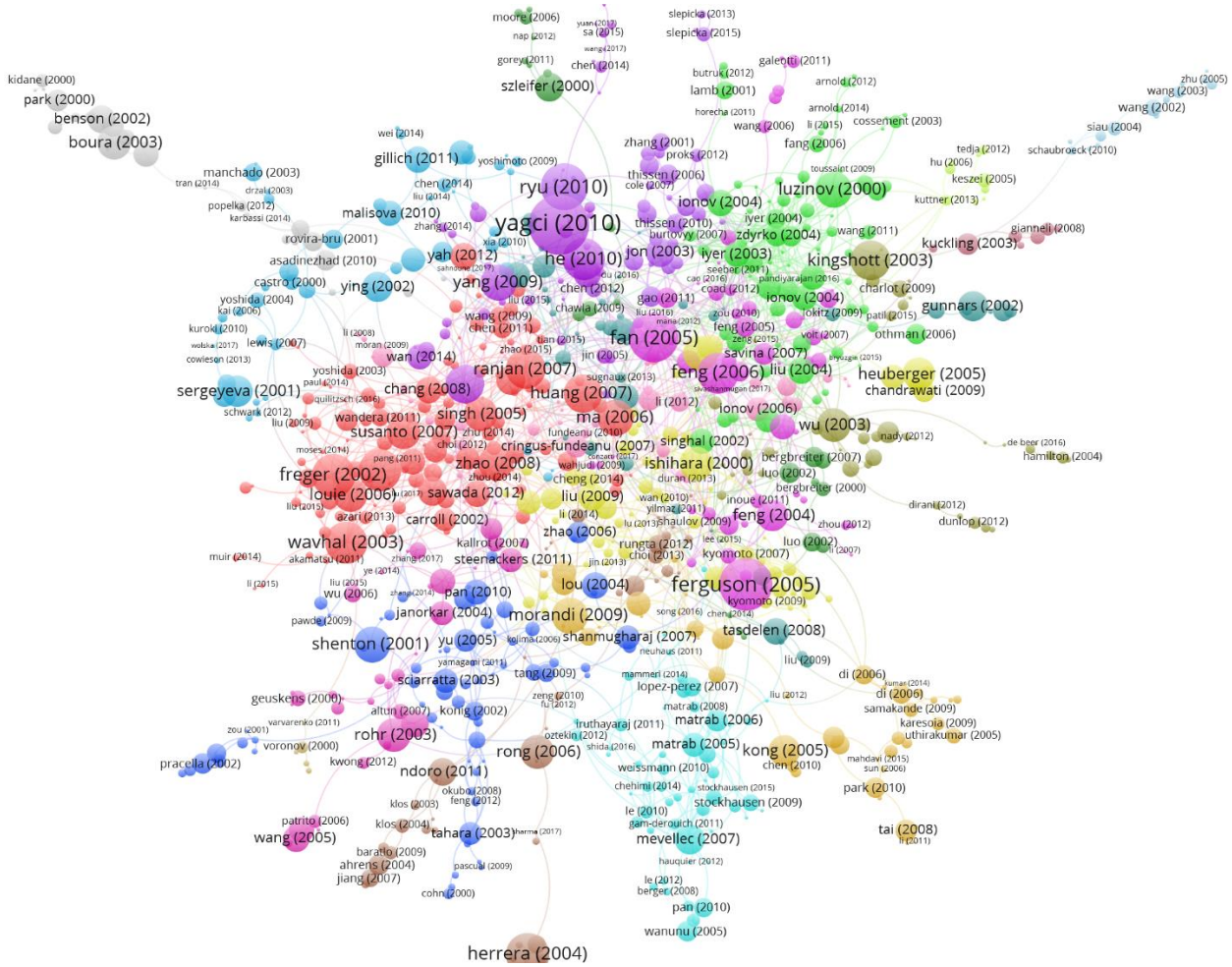

Figure 2.1. The citation map generated using search words “polymer grafting surface modification”, “anchoring polymer layer”, “adhesion improvement polymer grafting”, “polymer brush modification surface grafting” spanning from 2000 to 2017.

It is quite clear that this topic is naturally separated into a number of distinct clusters where the items (individual publications) heavily cite each other while mentioning of the items in other clusters is less pronounced. Clusters may correspond to a certain group of scientists creating a research topic, collaborating or competing within a field. In this dissertation I use this citation map to provide a detailed review of the most important research papers in the field and characterize the scope of the studies relevant at this moment.

Alternative method of investigating and visualizing the citation space is the keyword analysis (**Figure 2.2**). Using the same selection of papers as before, it is possible to map the keywords most commonly occurring together as well as color the nods of the graph (this time corresponding to the certain keyword) according to the year of publication. Now it is possible to see the main trends of the research in this area. The central nod of this graph is occupied by the atom-transfer radical polymerization which is a powerful technique that provides the ability to synthesize surface-attached polymers of controlled configuration, composition and polydispersity. The related topic of brushes which are polymer chains densely bonded to the interface is also in the center of attention of these studies. Note that the terms like adhesion, adsorption, coatings, interface and self-assembled monolayers are expected in the paper selection with the search words given. Interestingly enough, another heavily used keyword is nanoparticles. While it is too general to discern between various applications of such structures, it indicates the strong tendency of the grafting studies to facilitate the operations with nanoscale objects as opposed to being applied to the solid surfaces exclusively.

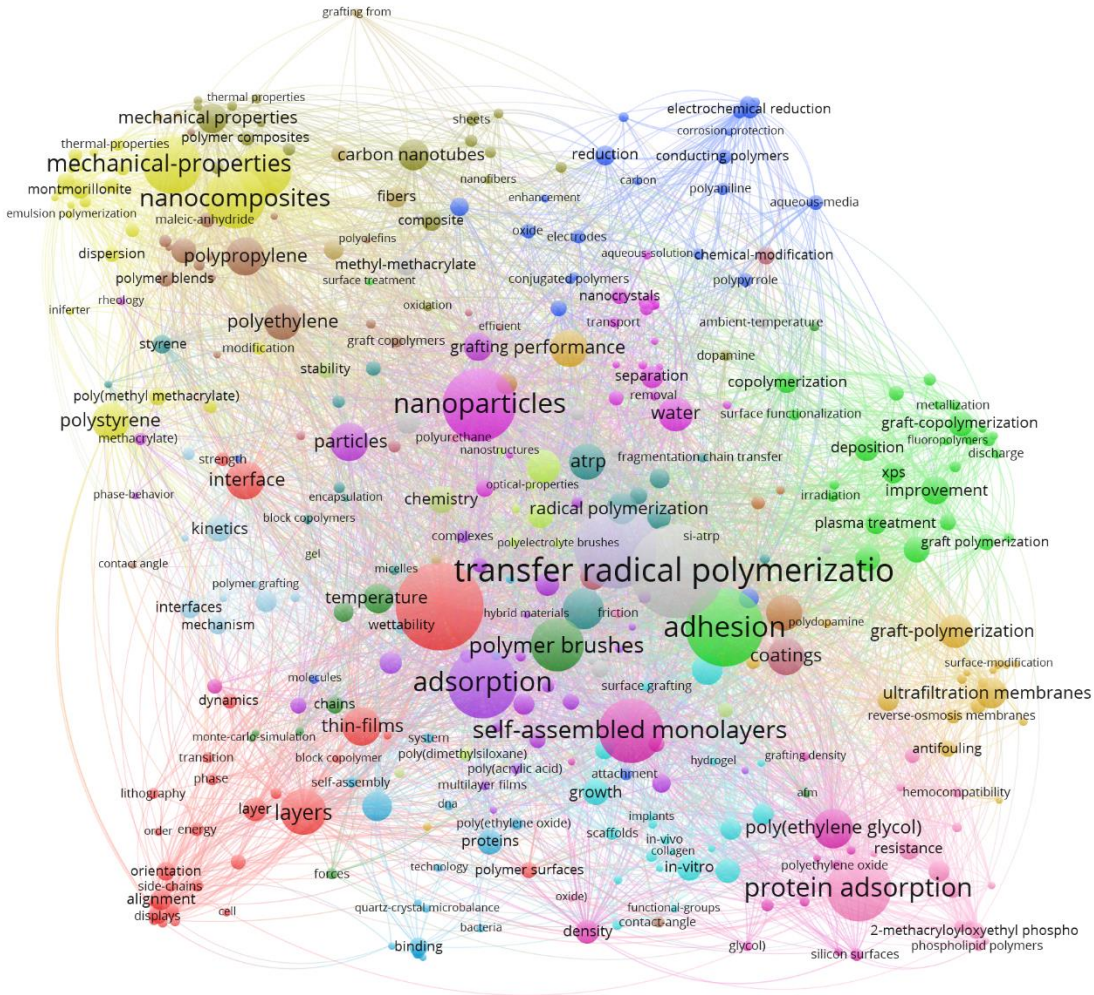

Figure 2.2. The keyword map generated using search words "polymer grafting surface modification", "anchoring polymer layer", "adhesion improvement polymer grafting", "polymer brush modification surface grafting" spanning from 2000 to 2017 and colored according to the cluster assignment.

The specific topics that are being investigated in details over the last 17 years include a very diverse group of fields outlining the interests of industry as well as basic research community. Keywords belonging to the same topic tend to appear in the papers together providing an overall understanding of the goals, methods and objects of the

respective studies. Another useful method of representation of this data is to color the nods according to the dates of publication (**Figure 2.3**).

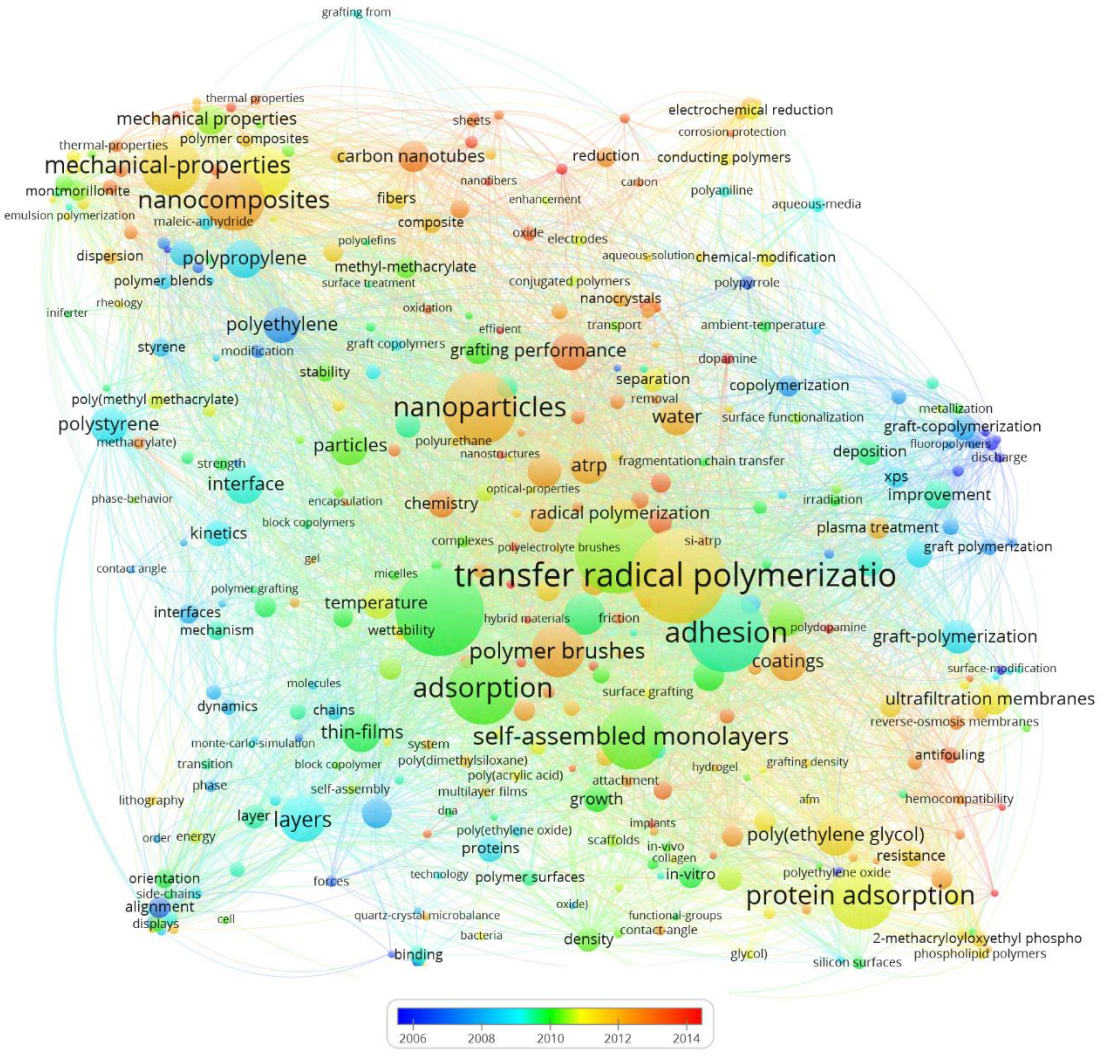

Figure 2.3. The keyword map generated using search words “polymer grafting surface modification”, “anchoring polymer layer”, “adhesion improvement polymer grafting”, “polymer brush modification surface grafting” spanning from 2000 to 2017 and colored according to the year of publication.

Novel classes of composites including nanocomposites (yellow) are a large area of interest due to opportunities that these materials may open for applications demanding the

combination of light weight and good mechanical performance. New generation of carbon systems such as nanotubes and graphene sheets are closely connected to this topic (dark yellow). It is worth noticing that investigation of the carbon nanostructure modifications by polymer grafting methods is a very recent trend (**Figure 2.3**). The flexible electronics and electrode design prompt the search for the methods of synthesis and optimization of the materials performance. Thus, the electrochemical reduction and conducting polymers is another important area of application for grafting (blue).

The improvement of adhesion between surfaces done by plasma treatment, irradiation-related techniques and graft copolymerization is large field of interest with clear applications in materials compatibilization (green). As the demand for purification and filtration systems is constantly increasing in the modern world, the improvement of current ultrafiltration membranes (orange) is starting to gain momentum. One the most recent trends is tackling the fouling issue when the membrane pores are getting blocked hence decreasing its performance. By controlling the adhesion between the surface of the material and the particles participating in the filtration, it is possible to regulate this process. The modification of the membrane interface by the means of polymer grafting is a very advantageous solution.

A close topic which, however, spans way further than membrane science only, is protein adhesion and repellency (pink). The poly(ethylene glycol) is a non-cytotoxic water-soluble polymer that is a key component of many systems where the need for protein repellency is strongly pronounced. Biomedical applications (purple, blue and light blue) of polymer grafting are neighboring fields that are of particular practical interest as the

advances in this fiend my significantly improve the current state of biotechnology and patient quality of life. Finally, there is a large cluster of keywords (red) that corresponds to the general properties of the grafted polymer layers and their physical properties.

In summary, a brief analysis of the literature of the topic of polymer grafting reveals that there are numerous fields that request advances in surface properties delivered by the means of polymer grafting. One of the strongest advantages of this approach is that once the basic procedure is established, it can be successfully transferred between different systems with some minor case-specific adjustments. However, besides development of general modifications protocols, one needs to recognize the current trends and demonstrate the applicability of these protocols for the demands of the day. In turn, it will ensure that particular method of surface modification by graft-copolymers is going to be able to serve the challenges that are going to arise in the future. This consideration has shaped the contents of the current dissertation to contain as the investigation of fundamental properties of PGMA graft-copolymers and pathways to their synthesis and property control, as the examples of their usage in the practice.

The following sections of the literature review will be dedicated to the description of the basic principles of polymer grafting as well as detailed analysis of the relevant studies on the topic of graft copolymer surface modification.

2.2. Basic concepts of polymer grafting

As it has been indicated before, the general idea of graft-copolymer is the combination of the main chain and the pending chain of different natures to obtain the

desired materials property. However, this configuration may be achieved in different ways that provides certain level of flexibility when designing the graft-copolymer for a specific case. There are three methods to achieve this architecture of the copolymer commonly referred to as "grafting from", "grafting to" and "grafting through".[5] Each of them has certain advantages as well as drawbacks which are going to be specified below.

"Grafting from" is a strategy of graft-copolymer synthesis that implies the polymerization of the grafted chain initialed by the active moieties presented on the main chain (**Figure 2.4**).[6-8]

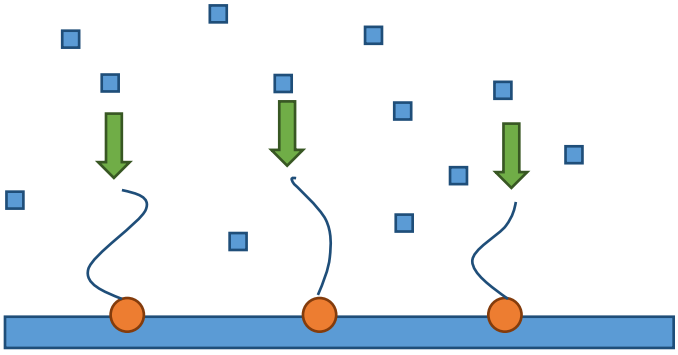

Figure 2.4. The schematics of the "grafting from" concept.

This concept has certain advantages that make it extremely prominent solution for many tasks that rise in the research. First, it is applicable to a wide variety of monomers, essentially, the macroinitiator (the main polymer chain) is a subtype of initiators. While the kinetics of this process may differ from the most common cases of polymerization reaction due to the hindered diffusion of the monomers,[9] the process may proceed yielding the growth of the pending polymer chain. Second, using some modern techniques of controlled radical polymerization such as atom-transfer radical polymerization and

reversible addition-fragmentation chain transfer, it is possible to generate the pending chains with very low size distribution.[10] Third, these techniques allow for the preparation of the pending chains composed of blocks of different monomers.[11] However, this technique has several limitations that stand in the way of its usage for certain systems. "Grafting from" involves the reactive media that *in-situ* polymerization is occurring in, which may constitute an issue for substrates that are sensitive to the environmental conditions. Most prominent examples of these systems are biological systems that may or may not preserve their activity upon being subjected to the conditions required for the polymerization. Another crucial challenge is the necessity to have the polymerization initiator on the main chain or on the surface being modified. Usage of reactive silicon compounds is a very common solution for the modification of solid surfaces.[12] Finally, as the process of pending chain growth takes place during the modification, which may take long time and hence be impractical as the scale of operation increases.

"Grafting to" is another technique involving grafting of the pre-emptively synthesized oligomers or polymers possessing the reactive end group to the reactive main chain (**Figure 2.5**).[13-14]

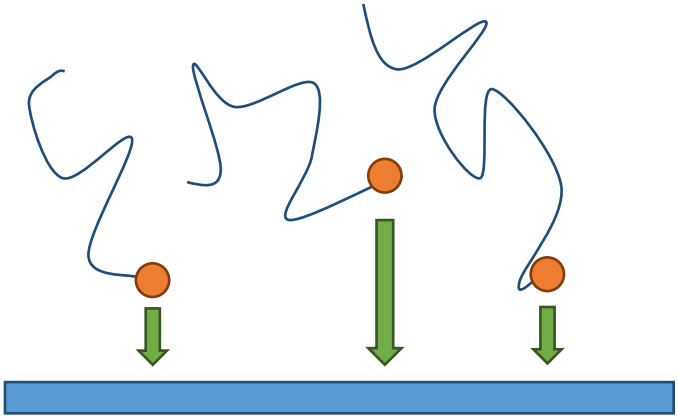

Figure 2.5. The schematics of the “grafting to” concept

This method is associated with certain processing conveniences. Most importantly, the processes of pending chain synthesis and the attachment to the main chain are separated in space and time. This eliminates the issue of compatibilization between the reaction conditions of these two processes and as long as the oligomer with reactive end group is available. In this case, controlled polymerization techniques may be used during the first step, in fact, the pending chain of any nature can be considered making the diversity of the modifications available truly uncontested by any other grafting method. Typically, click-chemistry or usage of epoxy rings in the main chain structure are employed in such post-polymerization modification of the main chain. However, the “grafting to” technique is also subject to a number of constraints. The availability of the reactive oligomer and its price definitely have to be thoroughly reviewed before the implementation of the protocol can be favored. Most importantly, as this process requires a reaction, the issues of reactive oligomer diffusion becomes a serious problem that may manifest itself as the passivation of the surface by very reactive end group or general dewetting issue both of which stand in the way of oligomer diffusion into the bulk of the polymer being modified.

"Grafting through" is one more approach for the synthesis of graft-copolymers[15]. In this case, the copolymerization of the macromolecular monomers is considered[16] (**Figure 2.6**).

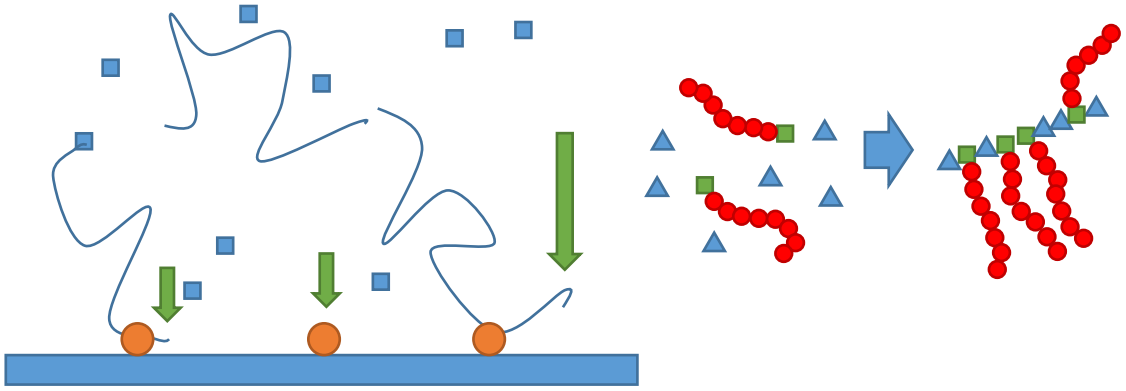

Figure 2.6. The schematics of the "grafting through" concept, left – surface-bound carbon-carbon double bonds, right – macromonomer polymerization

Just like in the case of "grafting through", the variety of the pending chains is limited only by the availability of the macromonomers. Aside from that, the appropriate selection of polymerization conditions can construct virtually any distribution of the pending chains. However, if the "grafting through" techniques proceeds through the macromonomer of very high molecular weight or through the surface-attached macromonomer, the growing chain may experience significant steric hindrance while entering the polymer coil. This not only slows down the reaction but potentially can completely halt it.

It is necessary to mention that usage of these approaches is not mutually exclusive, for example, a copolymer prepared using "grafting through" approach can be successfully attached to the surface in "grafting to" protocol or macromonomer polymerization can be

initiated from the substrate. Although this factor potentially may introduce certain level of ambiguity to the methodology of the synthesis associated with the respective technique, it is substantial that all these approaches have the same general purpose which is a combination of various polymers in a single material with main chain-pending chain molecular architecture. In the particular instant of PGMA-based systems, the pivotal ability of epoxy groups to participate in post-polymerization modifications including cross-linking is retained and inherited by corresponding graft-copolymers.

2.3. Representative examples of polymer grafting applications

2.3.1. Composite and nanocomposite preparation

As various nanostructured materials enter the realm of practical applications, the engineering aspects of their functionalization become crucially important for further advances in this field of materials science.[17] Scaling down the elements of electronic devices,[18] creating new generations of composites[19] and electronic materials[20-22], exploring the opportunities presented by the exfoliated layered systems[23-24] are the key topics of the day. Specifically, nanostructured allotropic modifications of carbon are in the focus of special attention. However, their dispersibility in various media is limiting its processing and overall applicability. There are two general approaches that are employed to perform surface modification of nanoscale objects[25]: physical sorption and chemical bonding. For example, dopamine is able to undergo polymerization on a variety of organic and inorganic substrates including carbon fibers[26] and then subsequently serve as an anchor layer for the further reactions. This strategy using non-covalent interactions can be utilized even in the

absence of active groups. However, in many practical cases the presence of the chemical bonding can provide better stability of the coating and more robust interface as it can be finely tuned for a specific case of the surrounding matrix.[27] This is where the versatility of surface modification performed by polymer grafting comes into play where the small alterations to the general protocol can yield surfaces with different properties. An additional activation of the substrate may be needed to provide chemical groups for polymerization initiation ("grafting from"), propagation ("grafting through") or post-synthetic reaction ("grafting to"). **Figure 2.7** displays a typical example of such activation. As the surface of native titanium dioxide cannot directly interact with polyethylene glycol (PEG), it was first coated with plasma-polymerized n-allylamine polymer. The amino groups that were formed during this process reacted with PEG dialdehyde resulting in covalent attachment of the polyethylene glycol chain. Another method employed to perform surface activation is a non-specific oxidation of inert surfaces[28]. However, some materials, such as graphene oxide, silica nanoparticles or nanofibrillated cellulose readily possess the chemical groups that are capable of taking part in the reactions. The reactive silanes[29], azides[30], diamines[31], epoxy rings[32] and norbornenes[33] are frequently used to introduce the chosen chemistry of interest. Surface-initiated ATRP[34-35] or "grafting to"[36] modification can be performed on the next step finally delivering the desired functionality.

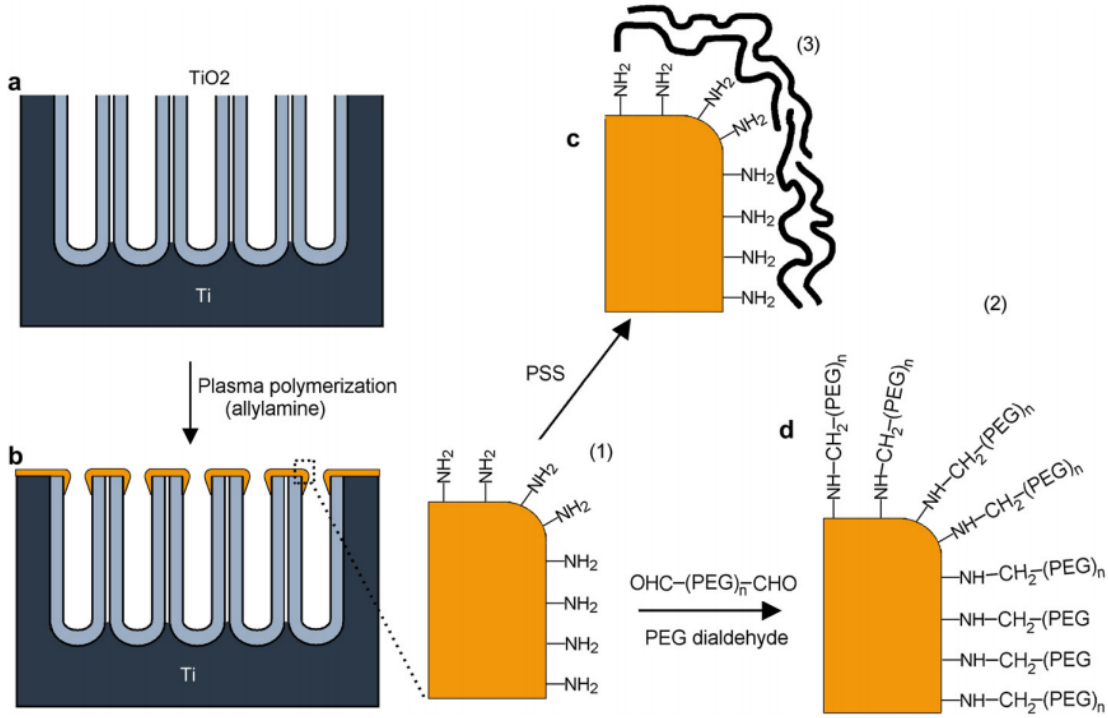

Figure 2.7. Scheme for the tailoring of the surface functionalities on TiO2 nanotube films: a) bare TiO2 nanotube arrays, b) plasma polymerization of n-allylamine polymer (AAPP), c) electrostatic adsorption of poly(sodium styrenesulfonate (PSS) on AAPP and d) covalent attachment of polyethylene glycol (PEG) on APPP . The picture is adopted with permission from [25].

2.3.2. Polymer grafting for filtration membranes

Membrane technologies is one of the most practically important fields of chemical engineering, as the growing population of a rapidly urbanizing world demands large amounts of clean water, which intensifies search for new highly-efficient methods of water purification and desalination.[37] Another vitally crucial applications of membranes are protein solution concentration and biomedical separation. The optimization of their operation includes the increase in selectivity and flux that can lead to more efficient and cost-effective filtration. The key mechanisms of filtration membrane performance losses

include fouling[38] (physical blocking of the flux by the particles presented in the solution) and chain and polar group reorientation in the surface region[39] which makes one-time plasma treatment insufficient for the long-term durability of the polymer membranes. For example, long-time performance of modified membranes can be drastically improved with polymer coating as exemplified in **Figure 2.8**. The flux through the membrane is one of the most fundamental characteristics of a membrane and is vitally important to applicability of a given prototypes in practice. Consequently, polymer surface modification can heavily contribute to making filtration more attractive from technological and economical points of view.

In order to combat these effects, the surface of the membrane is coated with the hydrophilic polymers which makes attachment of hydrophobic particles thermodynamically unfavorable[40]. Polar macromolecules such as PEG[41], zwitter-ionic polymers[42-43] and polyelectrolytes[44] are used in order to provide the prevent clogging of the pores and increase the lifetime of the filtration elements. One of the interesting aspects of the membrane polymer grafting is that radiation of UV light are often considered to be the initiators of the polymerization[45]. Photoinitiator entrapment may be performed as a surface pre-treatment[43] which ensures that the protocol of the membrane modification is scalable. However, ATRP is still a viable technique that is used when the exploring new options of surface property tailoring, for example, it can be used to synthesize ion-exchange membranes using the commercially available microporous membranes as a precursor[46].

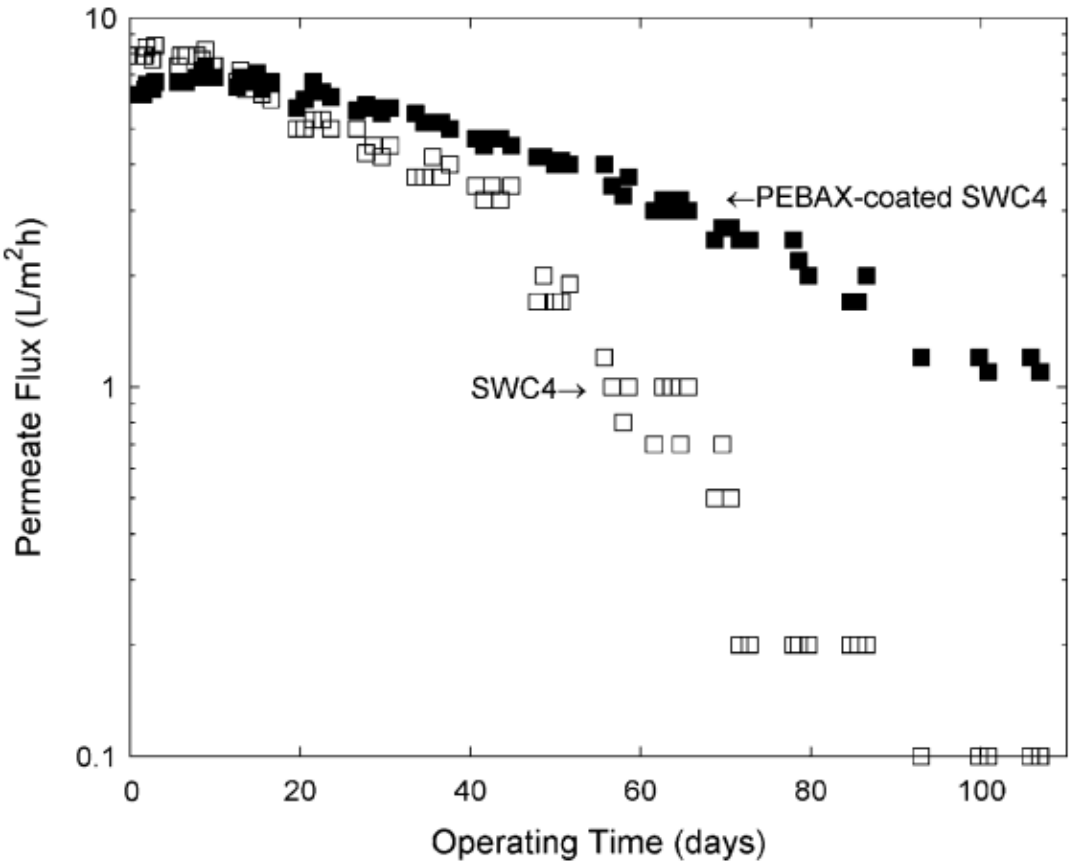

Figure 2.8. Flux through uncoated (open squares) and 1 wt.% PEBAX 1657-coated (black squares) SWC4 membranes during treatment of an oil/surfactant/water emulsion. Data are plotted on a semi-logarithmic scale. The coated membrane maintains a slower rate of flux decline than the uncoated sample, resulting in consistently higher flux values after 15 days. The picture is adopted with permission from [38].

2.3.3. Biomedical applications of graft-copolymers

Active usage of polymer grafting for the filtration membranes for hemodialysis ("artificial kidney" systems) suggests that the same concept can be applied to the modification of biological implants and targeted drug-delivery.[47-49] Encapsulation of the active compounds[50] can significantly improve its efficiency as the transport and stability issues are resolved by polymer modification and can help to provide visual information

about distribution of certain types of cell in a living organism. These systems,[51-52] however, are subject to rigorous studies investigating their biocompatibility and addressing the possible concern of toxicity towards the human organism. This significantly limits the range of chemistries that can potentially be a part of biomedical device. The use of oligo(ethylene glycol) methyl ether methacrylate-based polymer systems has become prominent in the recent years as polyethylene glycol is one of a few polymers that pose no danger and are routinely used in food industry.[53-55] PEG-coated nanoparticles can go through the body and if the loading of these structures is fluorescent, it is possible to provide the actual information about their distribution as they pass through living organism (**Figure 2.9**). Such insights are extremely valuable for visualizing medically-relevant information and designing safer and more efficient treatment for various diseases.

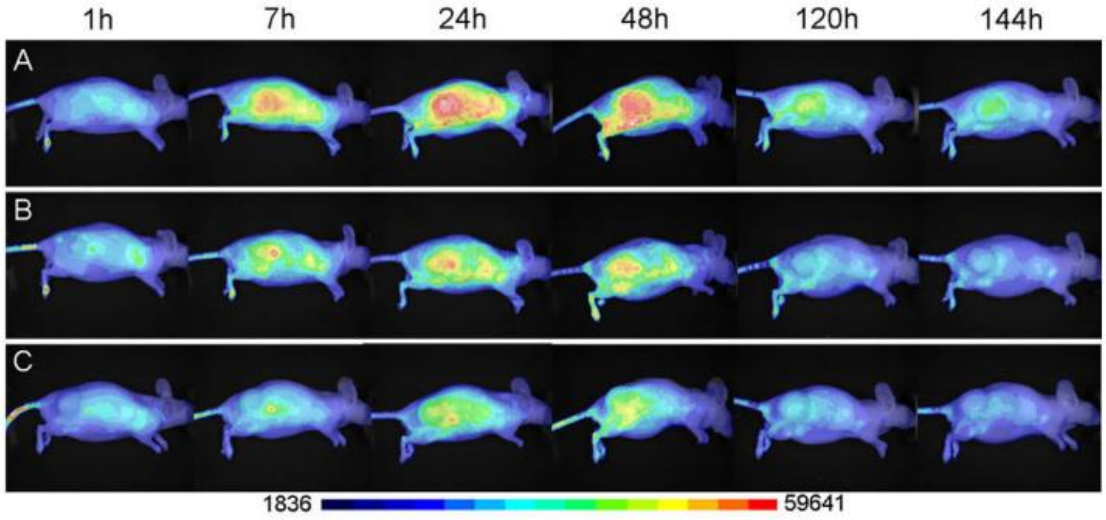

Figure 2.9. Fluorescence images (200 ms integration time, color scale with contrast fixed between 1836 and 59,641) are recorded at different times after injection and superimposed to visible light images (in white and black) for three types of fluorescent lipid nanoparticles coated with PEG. The picture is adopted with permission from [50] and highlight the tumor in a mouse.

2.3.4. Polymer grafting for sensing applications

Determination of specific analytes presence and concentration remains among the most demanded tasks in the area of analytical chemistry, which is important for research laboratories, industrial processing control, homeland security, defense and environmental monitoring. Modern science accommodates extremely sensitive and reliable means of analysis like mass-spectrometry, enzyme-linked immunosorbent assay (ELISA) and X-ray photoelectron spectroscopy (XPS), which can be used for precise qualitative and quantitative analysis of wide range of compounds.[56-58] However, those techniques may require elaborative sample preparation and vast amount of energy to operate. Also the instruments employed are expensive and ponderous, which is utterly undesirable for such applications as volatile compounds field monitoring, disposable biological tests, and lab-on-a-chip designs. This provides the demand for small devices with low power consumption and low production and operation cost which can effectively determine certain chemical or group of chemicals.[59-61]

There are several numerical parameters that characterize the performance of a sensor. The first key parameter is selectivity that displays the sensor ability to differentiate between various analytes.[62] According to specific requirements of the analytical task high selectivity (e.g. to a single analyte in the presence of similar ones) or threshold selectivity limited to certain class of objects is needed. Another important characteristic of the sensing device is sensitivity,[63-64] which is the ratio of the produced signal to the value of initial input. Other important characteristics are limit of detection (LOD)[65] and limit of quantification (LOQ)[66] which stand for the minimal input signal that can distinguish the

presence of the analyte from its absence and the minimal input signal above which qualitative comparison of the two input signals by the value of output signal is available, respectively.[67-68] Noise intensity which reflects the level of random fluctuation of the signal intrinsic to the analytical device. Those parameters of sensor system are determined by both sensor design and fundamental characteristics of an active material which provides the response.

The general concept of polymer surface modification applied for the sensor development has one significant advantage: the ability to transfer the successful solution found for one sensor system into another.[69] Here, enrichment polymer layers increase the local concentration of the analyte and/or provide the desired range of selectivity. The fundamentals of the improvements of the response observed in this case is based on the changing physical properties of the EPL associated with the swelling, which can be picked up by an appropriate set-up.

This naturally leads to a large number of sensing approaches that utilize changing mechanical, electrical and optical properties of the polymer. Quartz microbalance[70-72] and microcantilever[73] arrays are powerful techniques that allow for monitoring of the mechanical properties which changes as a result of polymer incorporating the solvent molecules and undergoing the plasticization. The changes of optical properties such as UV-Vis absorbance and photoluminesence[74-75] or infrared absorbance[76] can be used for the sensor design as the swelling may manifest itself in the alteration in the spectra in the corresponding region of electromagnetic radiation (an example of EPL for FTIR-based sensing set-up is shown in **Figure 2.10**). The evanescent wave propagating from the crystal

detects changes in FTIR absorption, and if the polymer layer is swollen with chemical vapors, the signal is going to be much stronger than if the crystal would directly interact with the atmosphere with no coating. In essence, polymer layers act as enthalpic trap attracting chemical in concentrations higher than in surrounding medium.

Monitoring the electrical properties such as capacity[77-78] or resistivity[79] or creating the electrode ion-selective coatings using the graft polymers[80-82] is another viable strategy as it allows to readily use the electric signal in the circuit without the necessity of converting it.

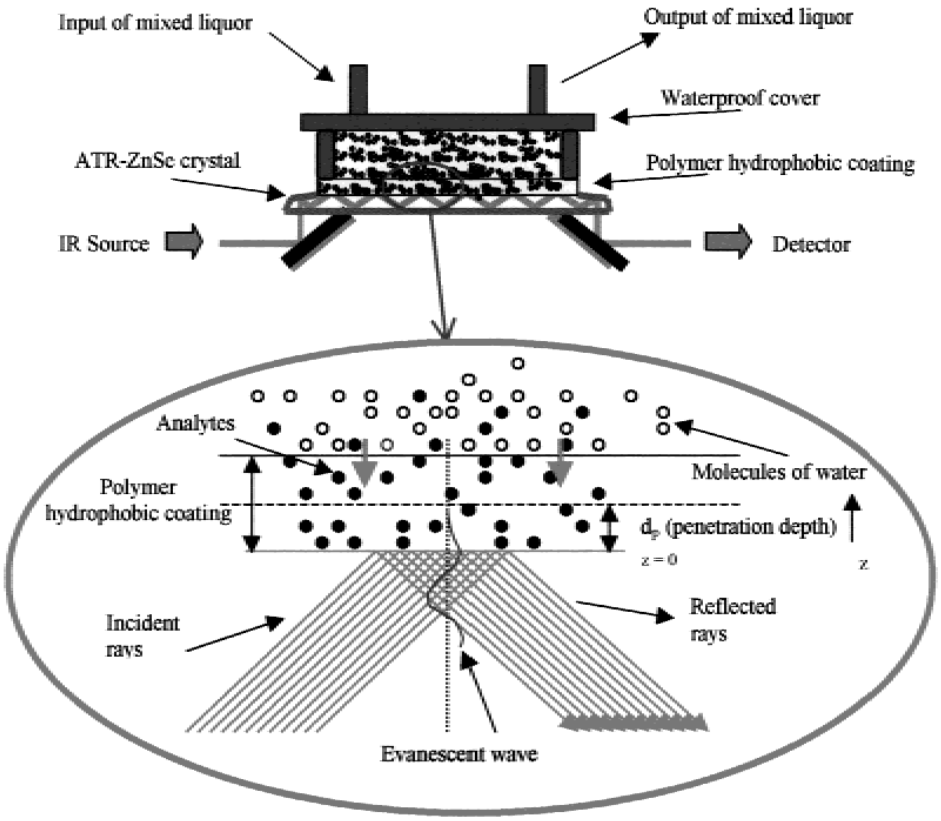

Figure 2.10. The ATR-FTIR sensor. Enrichment of chlorinated analytes in the polymer-coating medium. The evanescent wave concept. The picture is adopted with permission from [83].

2.4. Poly(glycidyl methacrylate) for surface modification

Poly(glycidyl methacrylate) is an excellent starting point for surface modification and creation of enrichment polymer layers.[84-88] It is available through radical polymerization and it can be copolymerized with other monomers. The epoxy groups of the synthesized product can react with nucleophilic groups leading to opening of the epoxy ring enabling covalent binding to the surface and post-synthesis modification. Once the PGMA layer has been prepared, its composition can be modified thus tuning the ability to respond to different VOC of interest. "Grafting to" offers significant flexibility of the modification agent and the volume fraction of this agent in the resulting film. However, it is crucial to be able to control this process in order to achieve the better control over the properties of the sensor.

Previous work done in Dr. Luzinov's group has thoroughly characterized the grafting of polymer chains to thin PGMA layers, however, in order to fulfill the sensitivity requirement, the enrichment polymer layer needs to have higher thickness that also depend on the application. Most importantly, PGMA epoxy groups can react with nucleophilic groups (such as hydroxyl, carboxyl and amino) which opens wide opportunities for post-synthesis modification.[89-91] As the opening of an epoxy group by a nucleophile generates hydroxyl group, PGMA can be thermally cross-linked forming stable permanent network layer.[92-93]

2.5. Oligo(ethylene glycol) methyl ether methacrylate for "grafting through"

Poly(oligo(ethylene glycol) methyl ether methacrylate) (POEGMA) has drawn significant attention over the recent years due to its thermosensitivity,[94] protein repellency,[95] and ability to compatibilize materials with water.[45] OEGMA monomers bear reactive methacrylate fragment that is capable of undergoing polymerization while oligo(ethylene glycol) provide water compatibility to the synthesized molecule. Thus, POEGMA can be considered as a comb-shape graft copolymer where oligo(ethylene glycol) is grafted to the methacrylate backbone. The balance between hydrophilic and hydrophobic parts of the molecule results in thermal switching properties that strongly depend on the side chain length.[96] It is well established that poly(ethylene glycol) demonstrates low toxicity and does not trigger immune system response,[97] which facilitates the use of POEGMA for biological applications,[98-101] Amphiphilic POEGMA-based systems show high potential to be an efficient platform for drug delivery[102-104] and immobilization of biomolecules.[105]

2.6. Summary.

The natural versatility of polymers expanded by grafting finds numerous applications in such relevant fields as composite materials, filtration technologies, biomedical applications as well as sensor design. Among other platforms, PGMA and

POEGMA-based systems are especially promising as they provide access to easily controllable post-synthesis modifications and water-solubility.

2.7. References.

1. Hergenrother, P. M., The use, design, synthesis, and properties of high performance/high temperature polymers: an overview. *High Performance Polymers* **2003,** *15* (1), 3-45.
2. Kocherginsky, N. M.; Tan, C. L.; Lu, W. F., Demulsification of water-in-oil emulsions via filtration through a hydrophilic polymer membrane. *Journal of Membrane Science* **2003,** *220* (1-2), 117-128.
3. Coleman, J. N.; Khan, U.; Blau, W. J.; Gun'ko, Y. K., Small but strong: A review of the mechanical properties of carbon nanotube-polymer composites. *Carbon* **2006,** *44* (9), 1624-1652.
4. Thompson, B. C.; Frechet, J. M. J., Organic photovoltaics - Polymer-fullerene composite solar cells. *Angewandte Chemie-International Edition* **2008,** *47* (1), 58-77.
5. Zhang, L.; Li, W.; Zhang, A., Synthesis and applications of polymer molecular brushes. *Prog. Chem.* **2006,** *18* (7-8), 939-949.
6. Olivier, A.; Meyer, F.; Raquez, J. M.; Damman, P.; Dubois, P., Surface-initiated controlled polymerization as a convenient method for designing functional polymer brushes: From self-assembled monolayers to patterned surfaces. *Progress in Polymer Science (Oxford)* **2012,** *37* (1), 157-181.
7. Littunen, K.; Hippi, U.; Johansson, L. S.; Österberg, M.; Tammelin, T.; Laine, J.; Seppälä, J., Free radical graft copolymerization of nanofibrillated cellulose with acrylic monomers. *Carbohydrate Polymers* **2011,** *84* (3), 1039-1047.
8. Xu, Y.; Becker, H.; Yuan, J.; Burkhardt, M.; Zhang, Y.; Walther, A.; Bolisetty, S.; Ballauff, M.; Müller, A. H. E., Double-grafted cylindrical brushes: Synthesis and characterization of poly(lauryl methacrylate) brushes. *Macromolecular Chemistry and Physics* **2007,** *208* (15), 1666-1675.
9. Shinoda, H.; Matyjaszewski, K., Structural control of poly(methyl methacrylate)-g-poly(lactic acid) graft copolymers by atom transfer radical polymerization (ATRP). *Macromolecules* **2001,** *34* (18), 6243-6248.
10. Lele, B. S.; Murata, H.; Matyjaszewski, K.; Russell, A. J., Synthesis of uniform protein-polymer conjugates. *Biomacromolecules* **2005,** *6* (6), 3380-3387.
11. Barner, L.; Pereira, S.; Sandanayake, S.; Davis, T. P., Reversible addition-fragmentation chain transfer graft copolymerization of styrene and m-isopropenyl-alpha,alpha '-dimethylbenzyl isocyanate from polypropylene lanterns: Solid phases for scavenging applications. *Journal of Polymer Science Part a-Polymer Chemistry* **2006,** *44* (2), 857-864.

12. Castellano, M.; Gandini, A.; Fabbri, P.; Belgacem, M. N., Modification of cellulose fibres with organosilanes: Under what conditions does coupling occur? *Journal of Colloid and Interface Science* **2004,** *273* (2), 505-511.
13. Ionov, L.; Zdyrko, B.; Sidorenko, A.; Minko, S.; Klep, V.; Luzinov, I.; Stamm, M., Gradient polymer layers by "grafting to" approach. *Macromolecular Rapid Communications* **2004,** *25* (1), 360-365.
14. Minko, S.; Patil, S.; Datsyuk, V.; Simon, F.; Eichhorn, K. J.; Motornov, M.; Usov, D.; Tokarev, I.; Stamm, M., Synthesis of adaptive polymer brushes via "grafting to" approach from melt. *Langmuir* **2002,** *18* (1), 289-296.
15. Henze, M.; Mädge, D.; Prucker, O.; Rühe, J., "Grafting through": Mechanistic aspects of radical polymerization reactions with surface-attached monomers. *Macromolecules* **2014,** *47* (9), 2929-2937.
16. Cho, H. Y.; Krys, P.; Szczes??niak, K.; Schroeder, H.; Park, S.; Jurga, S.; Buback, M.; Matyjaszewski, K., Synthesis of Poly(OEOMA) Using Macromonomers via "grafting-Through" ATRP. *Macromolecules* **2015,** *48* (18), 6385-6395.
17. Keszei, S.; Matkó, S.; Bertalan, G.; Anna, P.; Marosi, G.; Tóth, A., Progress in interface modifications: from compatibilization to adaptive and smart interphases. *European Polymer Journal* **2005,** *41* (4), 697-705.
18. Lupan, O.; Ursaki, V. V.; Chai, G.; Chow, L.; Emelchenko, G. A.; Tiginyanu, I. M.; Gruzintsev, A. N.; Redkin, A. N., Selective hydrogen gas nanosensor using individual ZnO nanowire with fast response at room temperature. *Sensors and Actuators B-Chemical* **2010,** *144* (1), 56-66.
19. Rong, M. Z.; Zhang, M. Q.; Ruan, W. H., Surface modification of nanoscale fillers for improving properties of polymer nanocomposites: a review. *Materials Science and Technology* **2006,** *22* (7), 787-796.
20. Zhang, J. T.; Zhao, X. S., Conducting Polymers Directly Coated on Reduced Graphene Oxide Sheets as High-Performance Supercapacitor Electrodes. *Journal of Physical Chemistry C* **2012,** *116* (9), 5420-5426.
21. Zhang, H. B.; Yan, Q.; Zheng, W. G.; He, Z. X.; Yu, Z. Z., Tough Graphene-Polymer Microcellular Foams for Electromagnetic Interference Shielding. *Acs Applied Materials & Interfaces* **2011,** *3* (3), 918-924.
22. Gomez, H.; Ram, M. K.; Alvi, F.; Villalba, P.; Stefanakos, E.; Kumar, A., Graphene-conducting polymer nanocomposite as novel electrode for supercapacitors. *Journal of Power Sources* **2011,** *196* (8), 4102-4108.
23. Nicolosi, V.; Chhowalla, M.; Kanatzidis, M. G.; Strano, M. S.; Coleman, J. N., Liquid Exfoliation of Layered Materials. *Science* **2013,** *340* (6139), 1420-+.
24. Coleman, J. N.; Lotya, M.; O'Neill, A.; Bergin, S. D.; King, P. J.; Khan, U.; Young, K.; Gaucher, A.; De, S.; Smith, R. J.; Shvets, I. V.; Arora, S. K.; Stanton, G.; Kim, H. Y.; Lee, K.; Kim, G. T.; Duesberg, G. S.; Hallam, T.; Boland, J. J.; Wang, J. J.; Donegan, J. F.; Grunlan, J. C.; Moriarty, G.; Shmeliov, A.; Nicholls, R. J.; Perkins, J. M.; Grieveson, E. M.; Theuwissen, K.; McComb, D. W.; Nellist, P. D.; Nicolosi, V., Two-Dimensional Nanosheets Produced by Liquid Exfoliation of Layered Materials. *Science* **2011,** *331* (6017), 568-571.

25. Vasilev, K.; Poh, Z.; Kant, K.; Chan, J.; Michelmore, A.; Losic, D., Tailoring the surface functionalities of titania nanotube arrays. *Biomaterials* **2010,** *31* (3), 532-540.
26. Chen, S.; Cao, Y.; Feng, J., Polydopamine As an Efficient and Robust Platform to Functionalize Carbon Fiber for High-Performance Polymer Composites. *ACS Applied Materials & Interfaces* **2014,** *6* (1), 349-356.
27. Ma, P. C.; Mo, S. Y.; Tang, B. Z.; Kim, J. K., Dispersion, interfacial interaction and re-agglomeration of functionalized carbon nanotubes in epoxy composites. *Carbon* **2010,** *48* (6), 1824-1834.
28. Nunes, A.; Amsharov, N.; Guo, C.; Van den Bossche, J.; Santhosh, P.; Karachalios, T. K.; Nitodas, S. F.; Burghard, M.; Kostarelos, K.; Al-Jamal, K. T., Hybrid Polymer-Grafted Multiwalled Carbon Nanotubes for In vitro Gene Delivery. *Small* **2010,** *6* (20), 2281-2291.
29. Roghani-Mamaqani, H.; Haddadi-Asl, V.; Khezri, K.; Zeinali, E.; Salami-Kalajahi, M., In situ atom transfer radical polymerization of styrene to in-plane functionalize graphene nanolayers: grafting through hydroxyl groups. *Journal of Polymer Research* **2014,** *21* (1).
30. He, H.; Gao, C., General Approach to Individually Dispersed, Highly Soluble, and Conductive Graphene Nanosheets Functionalized by Nitrene Chemistry. *Chemistry of Materials* **2010,** *22* (17), 5054-5064.
31. Choi, W.; Endo, S.; Oyaizu, K.; Nishide, H.; Geckeler, K. E., Robust and efficient charge storage by uniform grafting of TEMPO radical polymer around multi-walled carbon nanotubes. *Journal of Materials Chemistry A* **2013,** *1* (9), 2999.
32. Zou, H. L.; Lin, S. D.; Tu, Y. Y.; Liu, G. J.; Hu, J. W.; Li, F.; Miao, L.; Zhang, G. W.; Luo, H. S.; Liu, F.; Hou, C. M.; Hu, M. L., Simple approach towards fabrication of highly durable and robust superhydrophobic cotton fabric from functional diblock copolymer. *Journal of Materials Chemistry A* **2013,** *1* (37), 11246-11260.
33. Johnson, J. A.; Lu, Y. Y.; Burts, A. O.; Xia, Y.; Durrell, A. C.; Tirrell, D. A.; Grubbs, R. H., Drug-Loaded, Bivalent-Bottle-Brush Polymers by Graft-through ROMP. *Macromolecules* **2010,** *43* (24), 10326-10335.
34. Lee, S. H.; Dreyer, D. R.; An, J.; Velamakanni, A.; Piner, R. D.; Park, S.; Zhu, Y.; Kim, S. O.; Bielawski, C. W.; Ruoff, R. S., Polymer Brushes via Controlled, Surface-Initiated Atom Transfer Radical Polymerization (ATRP) from Graphene Oxide. *Macromolecular Rapid Communications* **2010,** *31* (3), 281-288.
35. Matrab, T.; Chancolon, J.; L'hermite, M. M.; Rouzaud, J.-N.; Deniau, G.; Boudou, J.-P.; Chehimi, M. M.; Delamar, M., Atom transfer radical polymerization (ATRP) initiated by aryl diazonium salts: a new route for surface modification of multiwalled carbon nanotubes by tethered polymer chains. *Colloids and Surfaces A: Physicochemical and Engineering Aspects* **2006,** *287* (1-3), 217-221.
36. Zhu, Y. H.; Sundaram, H. S.; Liu, S. J.; Zhang, L.; Xu, X. W.; Yu, Q. M.; Xu, J. Q.; Jiang, S. Y., A Robust Graft-to Strategy To Form Multifunctional and Stealth Zwitterionic Polymer-Coated Mesoporous Silica Nanoparticles. *Biomacromolecules* **2014,** *15* (5), 1845-1851.

37. Parkinson, J.; Zhang, S. J., Polymer-carbon nanotube nanocomposites for water purification and desalination. *Abstracts of Papers of the American Chemical Society* **2014,** *248*.
38. Louie, J. S.; Pinnau, I.; Ciobanu, I.; Ishida, K. P.; Ng, A.; Reinhard, M., Effects of polyether–polyamide block copolymer coating on performance and fouling of reverse osmosis membranes. *Journal of Membrane Science* **2006,** *280* (1-2), 762-770.
39. Yasuda, H.; Sharma, A. K.; Yasuda, T., Effect of orientation and mobility of polymer molecules at surfaces on contact angle and its hysteresis. *Journal of Polymer Science: Polymer Physics Edition* **1981,** *19* (9), 1285-1291.
40. Susanto, H.; Ulbricht, M., Photografted thin polymer hydrogel layers on PES ultrafiltration membranes: characterization, stability, and influence on separation performance. *Langmuir* **2007,** *23* (14), 7818-7830.
41. Chen, X. R.; Tang, B. X.; Luo, J. Q.; Wan, Y. H., Towards high-performance polysulfone membrane: The role of PSF-b-PEG copolymer additive. *Microporous and Mesoporous Materials* **2017,** *241*, 355-365.
42. Zhao, J.; Shi, Q.; Luan, S.; Song, L.; Yang, H.; Shi, H.; Jin, J.; Li, X.; Yin, J.; Stagnaro, P., Improved biocompatibility and antifouling property of polypropylene non-woven fabric membrane by surface grafting zwitterionic polymer. *Journal of Membrane Science* **2011,** *369* (1-2), 5-12.
43. Yang, Y.-F.; Li, Y.; Li, Q.-L.; Wan, L.-S.; Xu, Z.-K., Surface hydrophilization of microporous polypropylene membrane by grafting zwitterionic polymer for anti-biofouling. *Journal of Membrane Science* **2010,** *362* (1-2), 255-264.
44. Carroll, T.; Booker, N. A.; Meier-Haack, J., Polyelectrolyte-grafted microfiltration membranes to control fouling by natural organic matter in drinking water. *Journal of membrane science* **2002,** *203* (1), 3-13.
45. Meng, J.; Li, J.; Zhang, Y.; Ma, S., A novel controlled grafting chemistry fully regulated by light for membrane surface hydrophilization and functionalization. *Journal of Membrane Science* **2014,** *455*, 405-414.
46. Singh, N.; Husson, S. M.; Zdyrko, B.; Luzinov, I., Surface modification of microporous PVDF membranes by ATRP. *Journal of Membrane Science* **2005,** *262* (1-2), 81-90.
47. Xue, M. Q., *Modification and Tribological Study on Implant Polymers of Hip Prosthesis*. 2009; p 865-866.
48. Mora-Huertas, C. E.; Fessi, H.; Elaissari, A., Polymer-based nanocapsules for drug delivery. *International Journal of Pharmaceutics* **2010,** *385* (1-2), 113-142.
49. Patri, A. K.; Majoros, I. J.; Baker, J. R., Dendritic polymer macromolecular carriers for drug delivery. *Current Opinion in Chemical Biology* **2002,** *6* (4), 466-471.
50. Goutayer, M.; Dufort, S.; Josserand, V.; Royere, A.; Heinrich, E.; Vinet, F.; Bibette, J.; Coll, J. L.; Texier, I., Tumor targeting of functionalized lipid nanoparticles: Assessment by in vivo fluorescence imaging. *Eur. J. Pharm. Biopharm.* **2010,** *75* (2), 137-147.
51. Chiriac, A. P.; Nita, L. E.; Diaconu, A.; Bercea, M.; Tudorachi, N.; Parnfil, D.; Mititelu-Tartau, L., Hybrid gels by conjugation of hyaluronic acid with poly(itaconic anhydride-co-3,9-diviny1-2,4,8,1 0-tetraoxaspiro (5.5)undecane) copolymers. *International Journal of Biological Macromolecules* **2017,** *98*, 407-418.

52. Zhou, L.; Cheng, R.; Tao, H.; Ma, S.; Guo, W.; Meng, F.; Liu, H.; Liu, Z.; Zhong, Z., Endosomal pH-Activatable Poly(ethylene oxide)-graft-Doxorubicin Prodrugs: Synthesis, Drug Release, and Biodistribution in Tumor-Bearing Mice. *Biomacromolecules* **2011,** *12* (5), 1460-1467.
53. Geng, F.; Huang, Q.; Wu, X. F.; Ren, G. D.; Shan, Y. Y.; Jin, G. F.; Ma, M. H., Co-purification of chicken egg white proteins using polyethylene glycol precipitation and anion-exchange chromatography. *Sep. Purif. Technol.* **2012,** *96*, 75-80.
54. Martin, A.; Mattea, F.; Gutierrez, L.; Miguel, F.; Cocero, M. J., Co-precipitation of carotenoids and bio-polymers with the supercritical anti-solvent process. *J. Supercrit. Fluids* **2007,** *41* (1), 138-147.
55. Dong, B. Y.; Manolache, S.; Somers, E. B.; Wong, A. C. L.; Denes, F. S., Generation of antifouling layers on stainless steel surfaces by plasma-enhanced crosslinking of polyethylene glycol. *Journal of Applied Polymer Science* **2005,** *97* (2), 485-497.
56. Deng, A. P.; Himmelsbach, M.; Zhu, Q. Z.; Frey, S.; Sengl, M.; Buchberger, W.; Niessner, R.; Knopp, D., Residue analysis of the pharmaceutical diclofenac in different water types using ELISA and GC-MS. *Environmental Science & Technology* **2003,** *37* (15), 3422-3429.
57. Huang, C. H.; Sedlak, D. L., Analysis of estrogenic hormones in municipal wastewater effluent and surface water using enzyme-linked immunosorbent assay and gas chromatography/tandem mass spectrometry. *Environmental Toxicology and Chemistry* **2001,** *20* (1), 133-139.
58. Banerjee, D.; Shchukarev, A., XPS in environmental studies: Improvement of arsenic analysis in natural samples. *Journal of Electron Spectroscopy and Related Phenomena* **2007,** *156*, LVI-LVI.
59. Ghafar-Zadeh, E.; Sawan, M.; Therriault, D., A 0.18-mu m CMOS capacitive sensor lab-on-chip. *Sensors and Actuators a-Physical* **2008,** *141* (2), 454-462.
60. Ghafar-Zadeh, E.; Sawan, M., A Hybrid Microfluidic/CMOS Capacitive Sensor Dedicated to Lab-on-Chip Applications. *Ieee Transactions on Biomedical Circuits and Systems* **2007,** *1* (4), 270-277.
61. Fernandes, A. C.; Duarte, C. M.; Cardoso, F. A.; Bexiga, R.; Cardoso, S.; Freitas, P. P., Lab-on-Chip Cytometry Based on Magnetoresistive Sensors for Bacteria Detection in Milk. *Sensors* **2014,** *14* (8), 15496-15524.
62. Bakker, E.; Pretsch, E.; Buhlmann, P., Selectivity of potentiometric ion sensors. *Analytical Chemistry* **2000,** *72* (6), 1127-1133.
63. Sakai, G.; Matsunaga, N.; Shimanoe, K.; Yamazoe, N., Theory of gas-diffusion controlled sensitivity for thin film semiconductor gas sensor. *Sensors and Actuators B-Chemical* **2001,** *80* (2), 125-131.
64. Zhang, S. P.; Bao, K.; Halas, N. J.; Xu, H. X.; Nordlander, P., Substrate-Induced Fano Resonances of a Plasmonic: Nanocube: A Route to Increased-Sensitivity Localized Surface Plasmon Resonance Sensors Revealed. *Nano Letters* **2011,** *11* (4), 1657-1663.
65. Ceresa, A.; Radu, A.; Peper, S.; Bakker, E.; Pretsch, E., Rational design of potentiometric trace level ion sensors. A Ag+-selective electrode with a 100 ppt detection limit. *Analytical Chemistry* **2002,** *74* (16), 4027-4036.

66. Mocak, J.; Bond, A. M.; Mitchell, S.; Scollary, G., A statistical overview of standard (IUPAC and ACS) and new procedures for determining the limits of detection and quantification: Application to voltammetric and stripping techniques (technical report). *Pure and Applied Chemistry* **1997,** *69* (2), 297-328.
67. Loock, H.-P.; Wentzell, P. D., Detection limits of chemical sensors: Applications and misapplications. *Sensors and Actuators B-Chemical* **2012,** *173*, 157-163.
68. Uhrovcik, J., Strategy for determination of LOD and LOQ values - Some basic aspects. *Talanta* **2014,** *119*, 178-180.
69. Janata, J.; Josowicz, M., Conducting polymers in electronic chemical sensors. *Nature materials* **2003,** *2* (1), 19-24.
70. Feng, F.; Zheng, J. W.; Qin, P.; Han, T.; Zhao, D. Y., A novel quartz crystal microbalance sensor array based on molecular imprinted polymers for simultaneous detection of clenbuterol and its metabolites. *Talanta* **2017,** *167*, 94-102.
71. Erbahar, D. D.; Harbeck, M.; Gumus, G.; Gurol, I.; Ahsen, V., Self-assembly of phthalocyanines on quartz crystal microbalances for QCM liquid sensing applications. *Sensors and Actuators B-Chemical* **2014,** *190*, 651-656.
72. Chen, Q.; Tang, W.; Wang, D.; Wu, X.; Li, N.; Liu, F., Amplified QCM-D biosensor for protein based on aptamer-functionalized gold nanoparticles. *Biosensors & Bioelectronics* **2010,** *26* (2), 575-579.
73. Abu-Lail, N. I.; Kaholek, M.; LaMattina, B.; Clark, R. L.; Zauscher, S., Micro-cantilevers with end-grafted stimulus-responsive polymer brushes for actuation and sensing. *Sensors and Actuators B-Chemical* **2006,** *114* (1), 371-378.
74. Gerrans, K.; Luhrs, A.; Feider, C.; Margerum, L. D., Silica nanoparticles functionalized with polyamidoamine (PAMAM) dendrimers as platforms for photoluminescence (PL) sensing of copper and cyanide ions. *Journal of Colloid and Interface Science* **2016,** *470*, 276-283.
75. Li, F.; Wang, X. D.; Xia, Z. G.; Pan, C. F.; Liu, Q. L., Photoluminescence Tuning in Stretchable PDMS Film Grafted Doped Core/Multishell Quantum Dots for Anticounterfeiting. *Advanced Functional Materials* **2017,** *27* (17).
76. Luzinova, Y.; Zdyrko, B.; Luzinov, I.; Mizaikoff, B., In situ trace analysis of oil in water with mid-infrared fiberoptic chemical sensors. *Analytical chemistry* **2012,** *84* (3), 1274-80.
77. Panasyuk-Delaney, T.; Mirsky, V. M.; Wolfbeis, O. S., Capacitive Creatinine Sensor Based on a Photografted Molecularly Imprinted Polymer. *Electroanalysis* **2002,** *14* (3), 221-221.
78. Peng, H.; Soeller, C.; Vigar, N.; Kilmartin, P. A.; Cannell, M. B.; Bowmaker, G. A.; Cooney, R. P.; Travas-Sejdic, J., Label-free electrochemical DNA sensor based on functionalised conducting copolymer. *Biosensors & Bioelectronics* **2005,** *20* (9), 1821-1828.
79. Niu, L.; Luo, Y. L.; Li, Z. Q., A highly selective chemical gas sensor based on functionalization of multi-walled carbon nanotubes with poly(ethylene glycol). *Sensors and Actuators B-Chemical* **2007,** *126* (2), 361-367.

80. Qin, Y.; Peper, S.; Radu, A.; Ceresa, A.; Bakker, E., Plasticizer-free polymer containing a covalently immobilized Ca2+-selective lonophore for potentiometric and optical sensors. *Analytical Chemistry* **2003,** *75* (13), 3038-3045.
81. Qin, Y.; Bakker, E., A copolymerized dodecacarborane anion as covalently attached cation exchanger in ion-selective sensors. *Analytical Chemistry* **2003,** *75* (21), 6002-6010.
82. Khoshniyat, A.; Hashemi, A.; Sahari, S.; Sharif, A.; Shamsipur, M., Investigation of Interactions of Cationic and Anionic Polyacrylamaides with Modified Nanoclays by Potentiometric Sensors. *Sensor Letters* **2011,** *9* (5), 1814-1822.
83. Acha, V.; Meurens, M.; Naveau, H.; Agathos, S. N., ATR-FTIR sensor development for continuous on-line monitoring of chlorinated aliphatic hydrocarbons in a fixed-bed bioreactor. *Biotechnology and bioengineering* **2000,** *68* (5), 473-87.
84. Bliznyuk, V.; Galabura, Y.; Burtovyy, R.; Karagani, P.; Lavrik, N.; Luzinov, I., Electrical conductivity of insulating polymer nanoscale layers: environmental effects. *Physical Chemistry Chemical Physics* **2014,** *16* (5), 1977-1986.
85. Lin, P. T.; Giammarco, J.; Borodinov, N.; Savchak, M.; Singh, V.; Kimerling, L. C.; Tan, D. T. H.; Richardson, K. A.; Luzinov, I.; Agarwal, A., Label-free water sensors using hybrid polymer-dielectric mid-infrared optical waveguides. *ASC Applied Materials & Interfaces* **2015,** *7* (21), 11189-94.
86. Singh, V.; Lin, P. T.; Patel, N.; Lin, H.; Li, L.; Zou, Y.; Deng, F.; Ni, C.; Hu, J.; Giammarco, J.; Soliani, A. P.; Zdyrko, B.; Luzinov, I.; Novak, S.; Novak, J.; Wachtel, P.; Danto, S.; Musgraves, J. D.; Richardson, K.; Kimerling, L. C.; Agarwal, A. M., Mid-infrared materials and devices on a Si platform for optical sensing. *Science and Technology of Advanced Materials* **2014,** *15* (1), 014603.
87. Giammarco, J.; Zdyrko, B.; Petit, L.; Musgraves, J. D.; Hu, J.; Agarwal, A.; Kimerling, L.; Richardson, K.; Luzinov, I., Towards universal enrichment nanocoating for IR-ATR waveguides. *Chemical Communications* **2011,** *47* (32), 9104-9106.
88. Chyasnavichyus, M.; Tsyalkovsky, V.; Zdyrko, B.; Luzinov, I., Tuning fluorescent response of nanoscale film with polymer grafting. *Macromolecular rapid communications* **2012,** *33* (3), 237-41.
89. Soto-Cantu, E.; Lokitz, B. S.; Hinestrosa, J. P.; Deodhar, C.; Messman, J. M.; Ankner, J. F.; Kilbey, S. M., Versatility of alkyne-modified poly(glycidyl methacrylate) layers for click reactions. *Langmuir* **2011,** *27* (10), 5986-96.
90. Benaglia, M.; Alberti, A.; Giorgini, L.; Magnoni, F.; Tozzi, S., Poly(glycidyl methacrylate): a highly versatile polymeric building block for post-polymerization modifications. *Polymer Chemistry* **2013,** *4* (1), 124-124.
91. Safa, K. D.; Nasirtabrizi, M. H., One-pot, novel chemical modification of glycidyl methacrylate copolymers with very bulky organosilicon side chain substituents. *European Polymer Journal* **2005,** *41* (10), 2310-2319.
92. Borodinov, N.; Giammarco, J.; Patel, N.; Agarwal, A.; O'Donnell, K. R.; Kucera, C. J.; Jacobsohn, L. G.; Luzinov, I., Stability of Grafted Polymer Nanoscale Films toward Gamma Irradiation. *ACS Applied Materials & Interfaces* **2015,** *7* (34), 19455–19465.
93. Galabura, Y.; Soliani, A. P.; Giammarco, J.; Zdyrko, B.; Luzinov, I., Temperature controlled shape change of grafted nanofoams. *Soft Matter* **2014**, 2567-2573.

94. Du, Z.; Sun, X.; Tai, X.; Wang, G.; Liu, X., Optimizing conditions of preparation of thermoresponsive SiO2-POEGMA particles via AGET-ATRP. *Applied Surface Science* **2015,** *329*, 234-239.
95. Deng, X.; Smeets, N. M. B.; Wang, J.; Brennan, J. D.; Filipe, C. D. M.; Hoare, T., Poly(oligoethylene glycol methacrylate) Dip-Coating: Turning Cellulose Paper into a Protein-Repellent Platform for Biosensors. *Journal of American Chemical Society* **2014,** *136* (37), 12852–12855.
96. Lutz, J. F., Polymerization of oligo(ethylene glycol) (meth)acrylates: Toward new generations of smart biocompatible materials. *Journal of Polymer Science, Part A: Polymer Chemistry* **2008,** *46*, 3459-3470.
97. Brown, A. a.; Khan, N. S.; Steinbock, L.; Huck, W. T. S., Synthesis of oligo(ethylene glycol) methacrylate polymer brushes. *European Polymer Journal* **2005,** *41*, 1757-1765.
98. Hu, J.; Wang, G.; Zhao, W.; Liu, X.; Zhang, L.; Gao, W., Site-specific in situ growth of an interferon-polymer conjugate that outperforms PEGASYS in cancer therapy. *Biomaterials* **2016,** *96*, 84-92.
99. Smeets, N. M. B.; Patenaude, M.; Kinio, D.; Yavitt, F. M.; Bakaic, E.; Yang, F.-C.; Rheinstädter, M.; Hoare, T., Injectable hydrogels with in situ-forming hydrophobic domains: oligo(D,L-lactide) modified poly(oligoethylene glycol methacrylate) hydrogels. *Polymer Chemistry* **2014,** *5* (23), 6811-6823.
100. Shi, X.; Wang, Y.; Li, D.; Yuan, L.; Zhou, F.; Wang, Y.; Song, B.; Wu, Z.; Chen, H.; Brash, J. L., Cell Adhesion on a POEGMA-Modified Topographical Surface. *Langmuir* **2012,** *48* (49), 17011-17018.
101. Liu, M.; Leroux, J. C.; Gauthier, M. A., Conformation-function relationships for the comb-shaped polymer pOEGMA. *Progress in Polymer Science* **2014,** *48*, 111-121.
102. Skandalis, A.; Pispas, S., PLMA-b-POEGMA amphiphilic block copolymers: Synthesis and self-assembly in aqueous media. *Journal of Polymer Science Part A: Polymer Chemistry* **2017,** *55* (1), 155-163.
103. Wang, G.; Chen, M.; Guo, S.; Hu, A., Synthesis, self-assembly, and thermosensitivity of amphiphilic POEGMA-PDMS-POEGMA triblock copolymers. *Journal of Polymer Science, Part A: Polymer Chemistry* **2014,** *52* (18), 2684-2691.
104. Knop, K.; Pretzel, D.; Urbanek, A.; Rudolph, T.; Scharf, D. H.; Schallon, A.; Wagner, M.; Schubert, S.; Kiehntopf, M.; Brakhage, A. A.; Schacher, F. H.; Schubert, U. S., Star-shaped drug carriers for doxorubicin with POEGMA and POEtOxMA brush-like shells: A structural, physical, and biological comparison. *Biomacromolecules* **2013,** *14* (8), 2536-2548.
105. Sung, D.; Park, S.; Jon, S., Facile Immobilization of Biomolecules onto Various Surfaces Using Epoxide-Containing Antibiofouling Polymers. *Langmuir* **2012,** *28* (9), 4507-4514.

CHAPTER 3. SYNTHESIS OF PGMA GRAFT COPOLYMERS BY "GRAFTING TO" METHOD

3.1. Introduction

Polymers are one of the most versatile classes of materials that can be successfully used for novel sensor development. The chemical composition, crystallinity and mechanical properties of polymers can be altered in a well-controlled manner, they can be easily deposited by spin or dip coating solution or ink jet printing. Taking into account that polymers can also be chemically modified providing desired functional groups on the surface, they seem to be the perfect candidates for advanced device design.

The concept of enrichment polymer layer (EPL) that effectively increases the local concentration of the analyte at the surface of the sensing element has been recently introduced for the purposes of online monitoring.[1] Sensors for detection of chemicals in the environment have important and unique applications in law enforcement,[2-3] manufacturing,[4] and homeland security.[5-6] Sensing films or their arrays are typically needed to reach the required level of detection by selectively attracting analytes to the sensing element *via* physical/chemical interactions. In order to fulfill this role, polymer has to demonstrate significant swelling in the VOC of interest. Thus, the ability to adjust the EPL composition is crucial for their practical application. The thickness above the polymer coil monolayer can also improve the sensitivity of the device making more functional volume available to the interrogation. For example, photonic resonators that have

demonstrated to be a highly promising platform for volatile organic compound detection are capable of probing space located within the evanescence wave region.[7-8] The exact value of the depth of penetration depends on the refractive indices of the materials employed, specified in the case of silicon nitride and polymers, it has the values of 100-200 nanometers. This prompts the creation of thicker EPLs that could maximize the useful signal at the detector. In order to tackle this challenge, the thicker PGMA-based layers modified by "grafting to" approach as prospective EPLs have been put in the focus on this study.

This chapter focuses on the investigation of the details of the three-component gradient grafted film synthesis. The "grafting to" method (see **Figure 3.1**) has been used to modify the poly(glycidyl methacrylate) network with carboxy-terminated polystyrene and hydroxyl-terminated poly(2-vinyl pyridine) that were chosen because of their high ability to interact with aromatics and polar compounds, respectively. The key parameters responsible for the control over the melt grafting process have been calculated and the morphology-related peculiarities of three-component film swelling and collapse have been identified.

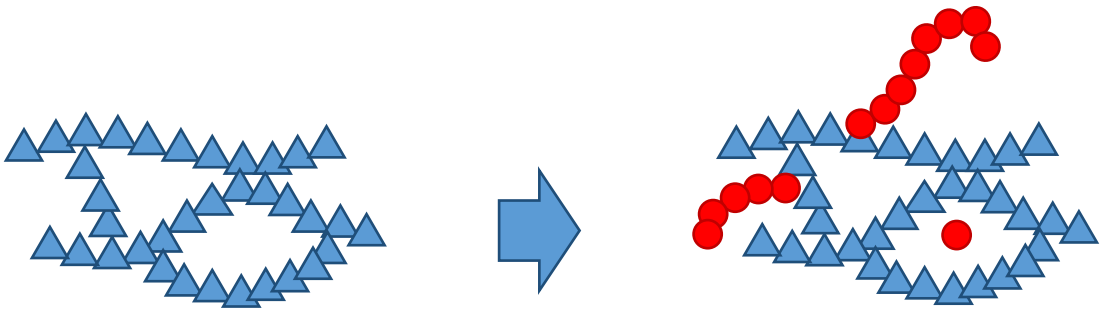

Figure 3.1. The scheme of "grafting to " method: a new polymer enters cross-linked network (blue).

3.2. Materials and methods

3.2.1. Materials

Glycidyl methacrylate (97%), azoisobutyronitrile (AIBN), poly(ethylene glycol) dimethyl ether (PEG) with number average molecular weight, Mn = 1,000 g/mol, sulfuric acid, and hydrogen peroxide (30%) were purchased from Sigma-Aldrich. Monocarboxyl-terminated PS with Mn = 2,000 g/mol and hydroxyl-terminated P2VP with Mn = 4,000 g/mol were purchased from Polymer Source Inc. Higher molecular weight non-reactive PS (Mn = 170,000 g/mol) was purchased from Sigma-Aldrich. One-sided polished silicon wafers with a thickness of 500 μm were purchased from University Wafer. All solvents used in this work were purchased from VWR International and used as received.

3.2.2. Synthesis of PGMA

PGMA has been prepared by free-radical polymerization. MEHQ inhibitor remover beads were added to GMA prior to synthesis. It has been filtered through the 0.2 μm syringe filters and placed alongside with MEK and AIBN initiator in a round bottom flask. The solution was kept under nitrogen purge for 45 min and then immersed into a water bath preheated to 50 °C. The overall monomer concentration was 0.5 mol L^{-1} and the AIBN concentration was 0.01 mol L^{-1}. The polymerization reaction was terminated after 1.5 h by opening flask to the ambient atmosphere and removal the reactor form the water bath. The resulting product was precipitated by diethyl ether, centrifuged and redissolved in MEK. This procedure was repeated three times in order to remove unreacted monomers and initiator. Gel permeation chromatography (Water Breeze) has been used to measure

PGMA molecular weight and polydispersity index which were found to be Mn=510,000 g/mol and PDI=2.2. Polystyrene monodisperse standards have been used for calibration.

3.2.3. Formation of three-component gradient films

Polished silicon wafers have been cleaned in an ultrasonic bath, immersed into hot piranha solution (sulfuric acid, hydrogen peroxide 3:1 mixture) for 30 min and then thoroughly washed with distilled water. Mayer Feintechnik dip coater, model D-3400 dip-coater has been used to deposit PGMA films from 1.5 wt% solution in chloroform. The polymer layers have been annealed at 130°C in vacuum oven and then washed with pure chloroform in order to remove ungrafted polymer. The typical sample size was 20x20 mm. PGMA-coated wafers have been further dip-coated into 1.2% monocarboxy-PS and 0.3% non-reactive high molecular weight PS. After evaporation of the solvent, the samples were placed on the temperature gradient stage[9] (**Figure 3.2**) with the temperature varying from 100 °C to 150 °C. After 6 h, the PS grafting samples were removed from the stage and thoroughly washed with chloroform (three to four times) to remove any ungrafted PS. P2VP coating has been applied by dip-coating of the PS-modified PGMA films 1.5% monohydroxy-P2VP and 1.5% PEG chloroform solution. Samples were further annealed on the gradient stage turned 90° from the direction used for the previous modification stage. The gradient stage temperature was set to range from 80 °C to 130 °C. Six parallel films have been prepared to collect larger sampling statistics.

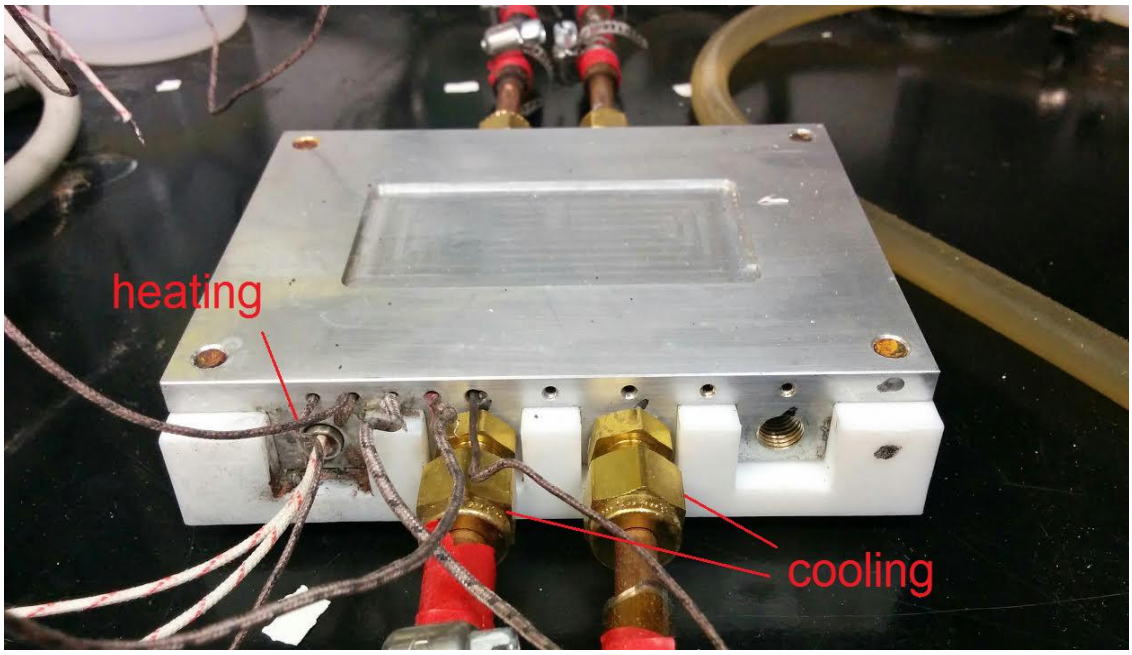

Figure 3.2. The scheme of the thermal stage used to prepare the gradient samples (designed by Anna Paola Soliani).

3.2.4. Atomic force microscopy

Dimension 3100 atomic force microscope (Digital Instruments) has been used to characterize the morphology of the PGMA layer before and after polystyrene grafting. Samples were analyzed in tapping mode at the scan rate 1 Hz.

3.2.5. Measurement of the film thicknesses

Spectroscopic reflectometry was performed with a home-built reflectometer (based on the EDMUND Industrial optic spectrometer, **Figure 3.3**) at an angle of incidence of 0°. Wavelengths ranging from 400 nm to 1000 nm were used. The thicknesses and refractive indices of the films were calculated by fitting experimental reflectance using Fresnel equations.[10] The reflectometer has a 2D scanning feature.

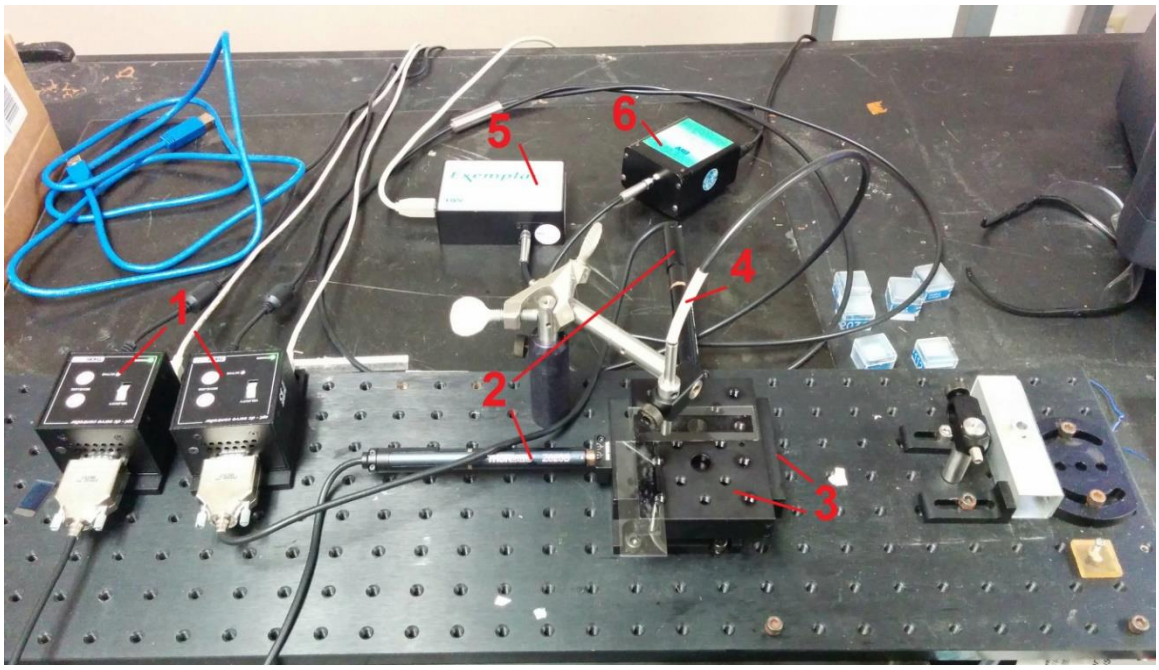

Figure 3.3. The scheme of home-built ellipsometer: 1) motor stage controllers, 2) motors, 3) translation stages, 4) waveguide, 5) spectrometer, 6) light source

Specifically, it consists of two T-Cube DC Servo motor controllers connected to a computer *via* USB and controlled by a LabView graphical user interface, two Thorlabs Z825B motors, two Thorlabs 25 mm motorized translation stages, a waveguide, a BWTEK BRC115P-V-ST1 Exemplar spectrometer, which is also connected to the computer *via* USB and controlled by the LabView graphical user interface, and a light source. A Si wafer was used for calibration of the optical system at the beginning of the measurement. Fitting of the reflectivity data used an empirical Sellmeier refractive index model[11] with two parameters. Thickness and light source overall intensity drift correction are two other variables, so the total fitting process estimates best fit based on four parameters. A total of 440 points on a 20×20 mm scan with 1 mm resolution were measured with 20 ms acquisition time per point. The polymer films were measured at 2 mm resolution on a

10×11 scan four times, and the resulting thicknesses were averaged using Dixon's Q-criteria (90% confidence) to exclude outliers.

3.3. Modification of thick PGMA films by "grafting to" method

3.3.1. The motivation for the study

Poly(glycidyl methacrylate) is well-known material for the creation of surface-attached anchoring layers.[12] Its unique ability to interact with nucleophilic groups through the opening of the epoxy rings provides the polymer with the ability to covalently bind to surfaces. In case of ultrathin films the coating is consisted of polymer molecules spread on the interface. It is essential that not all the epoxy groups are consumed during this process and the resulting anchoring layer can be further modified by grafting. The reactivity of this layer is determined by mobile "loops" which are parts of polymer chain are extended from the interface as opposed to "train" sections directly bound with the surface.[13] While this approach is a viable solution for the advanced and versatile surface functionalization,[14-15] the usage of these films for sensing applications require more variability of the layer itself as well as generally thicker layers.

Grafting is a flexible tool for performing polymer modification.[16] While PGMA provides the structural integrity of the surface-attached cross-linked layer, its affinity towards the analytes of interest can be tuned by the means of post-deposition modification. As it was previously demonstrated,[17] low molecular weight compounds can be easily grafted to the PGMA cross-linked network through vapor or melt procedure. However, when the polymer chain is used for modification of a thicker PGMA film via grafting, the

system is getting more complicated as miscibility of two chemically different polymers as well as transport phenomena can completely halt the grafting reaction. In this dissertation, I investigate how to overcome these difficulties and design protocol that would result in controllable high-efficiency modification of the initial PGMA surface-attached film using two polymers – polystyrene and poly(2-vinyl pyridine). While PGMA shows strong swelling in some solvents like acetone or chloroform, addition of PS and P2VP is expected to provide the EPL some affinity to aromatic compounds and polar compounds capable of forming the hydrogen bonds, respectively.

3.3.2. The preparation difficulties of the "grafting to" protocol in the case of thicker films

It is essential that the "grafting to" process consists of two steps - diffusion and consequent chemical reaction. As the vapors or molten low molecular weight chemicals swell the polymer layer, hydroxyl, carboxyl and amino groups start to interact with PGMA through nucleophilic epoxy opening. End-functionalized polymers are capable of interacting with oxirane rings in a similar fashion, however, the transport of the chains to the reaction site may be significantly hindered. In essence, grafting of polymer and oligomer molecules has another dimension of preparation difficulty. Moreover, these difficulties also differ depending on the system investigated, hence, it is hard to design a single universal protocol that would work for any initial layer thickness and polymer grafted. In this dissertation I tackled grafting of P2VP and PS due to their expected effect on the EPL affinity to a given set of chemicals. As it turns out, the grafting of these two polymers is not a trivial synthetic task. As PGMA layers have relatively large thickness

(more than polymer chain monolayer), the desired pattern of the grafting include uniform penetration of the new polymer chains inside the already formed network (**Figure 3.4**). Grafting of polymer studied here is challenging as the requirements of uniformity (PS) and penetration (P2VP) are somewhat difficult to achieve during the "grafting to" process.

Carboxy-terminated reactive polystyrene and PGMA have significant difference in surface energy which causes molten layer of PS to deteriorate into droplets. This leads to non-uniform modification of the initial layer and disrupts the modification process (**Figure 3.4**). However, this effect can be mitigated by the usage of high-molecular weight polystyrene that does not participate in reaction by itself but rather provides the molten polymer layer with dewetting delayed due to the high viscosity of high molecular weight PS. This stabilizes the layer of molten polystyrene and allows for efficient diffusion of PS-COOH into PGMA network.

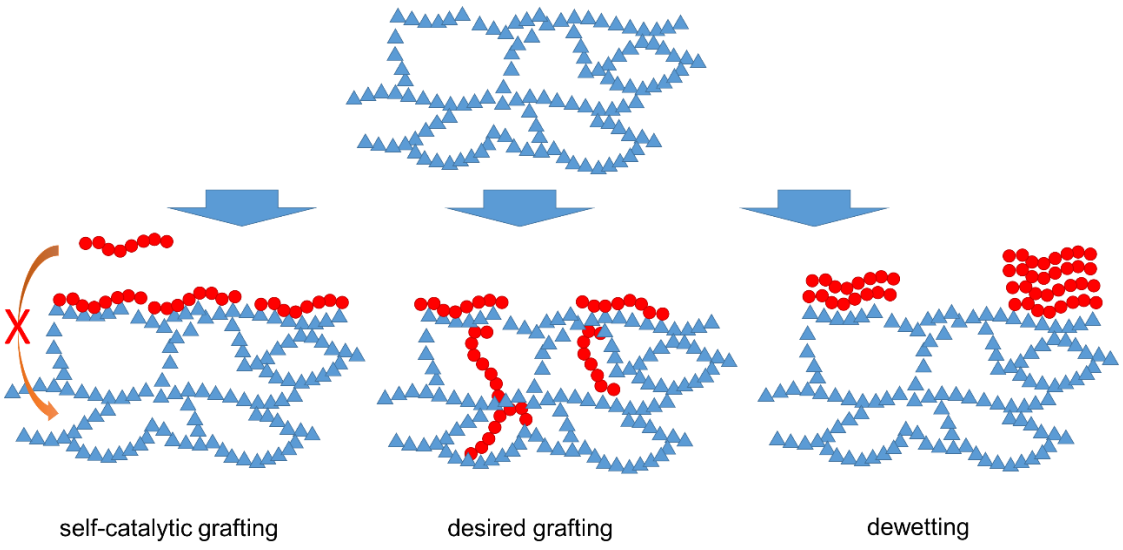

Figure 3.4. "Grafting to": PGMA network (blue triangles) is modified with a polymer chain (red circles). Self-catalytic grafting and dewetting prevent deep modification of the network.

On the other hand, grafting of P2VP is complicated by self-catalytic grafting. Specifically, the polymer itself promotes opening of the epoxy rings thus the grafting becomes controlled by the diffusion rather than by the reaction rate. Initial experiments showed that 10 nm increase in layer thickness due to P2VP grafting happens quickly and in a reproducible manner, however, as the penetration of the chains into the network is blocked (**Figure 3.4**), the higher grafting efficiencies cannot be achieved without additional measures. This effect is very characteristic for thicker PGMA films, so in order to promote the diffusion and slow down the reaction hydroxyl-terminated polymer is used instead of carboxy-terminated one. In addition, the synthesis is done in the media of molten polyethylene glycol dimethyl ether. At the grafting temperatures (70˚C and above) PEG melts and does not evaporate serving as a solvent that decreases the activity of hydroxyl groups. Using this approach, it is possible to perform uniform efficient grafting of the PGMA base layer.

These examples highlight that the fundamental understanding of the underlying physical processes is essential to design an efficient protocol for "grafting to" PGMA surface-attached networks.

3.3.3. Control over the grafting process: the "grafting to" activation energy

Once the general grafting procedure has been established, the methods to control this process were put in the scope of the research. Preparation of grafted films with specific grafting extent is necessary for advanced design of EPLs and manufacturing of sensors with desired properties. Such control can be achieved by control of the reaction temperature assuming that the kinetics of grafting is Arrhenius-like.

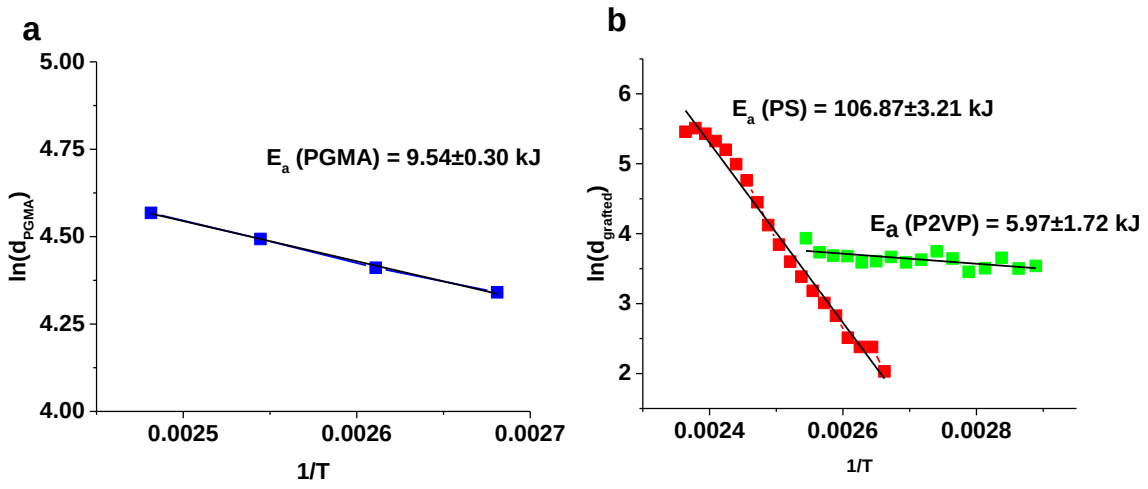

Figure 3.5. The Ahrennius plot of the thickness profile of PGMA (a) on the piranha-treated silicon wafer and the grafted thickness of PS and P2VP (b) on the uniform PGMA layer.

To obtain such information about the grafting process, the application of a temperature gradient to the film during the grafting process can be successfully used. As it is shown on **Figure 3.5**, this approach indeed yields gradient of the grafted thickness. This data is valuable for the establishing control over the grafting procedure: by selecting an appropriate temperature of the process one can regulate the grafting thickness. When it is plotted in Arrhenius coordinates (thickness logarithm versus inverse temperature), the effective activation energy of the grafting process can be extracted by performing the linear fit of the experimental data.

Grafting of PGMA to piranha-activated silicon wafer has activation energy of 9.5 J/mol. The grafting of PS-COOH and P2VP-OH into the 100 nm thick PGMA base layer has activation energies of 106.8 J/mol and 6.0 J/mol, respectively. These values are in well correspondence with the nature of both processes: as pyridine rings of P2VP promote the reaction with the epoxy, activation energy is significantly decreased as compared to non-

catalytic PS-COOH grafting. Thus, the key parameters that allow for precise control over the modification process and create a two-component gradient film have been verified.

3.3.4. Preparation of two orthogonal chemical gradients.

EPLs with chemical composition varying across the surface are extremely valuable tools for observation of the trends of composition-dependent behavior. In this case, using gradient of polymer grafting I am going to track swelling in different VOCs to characterize the response of designed sensor layer. The modification of PGMA film can be done sequentially. Here PS gradient is created according to the findings presented earlier and then P2VP gradient is applied at 90˚C angle so directions of the two gradients are orthogonal. This way the composition of the points varies across the sample which gives more data regarding the swelling phenomena. **Figure 3.6** displays the typical picture of thickness profile of the base PGMA layer (**Figure 3.6a**), PS grafted layer (**Figure 3.6b**) and P2VP grafted layer (**Figure 3.6c**) which was applied on the (PS)/PGMA polymer film. As it turns out, the resulting P2VP gradient is not orthogonal to the PS gradient: apparently, the increase in PS content promotes the P2VP grafting. Indeed, grafted P2VP thickness increases with grafted PS thickness until certain point, after which it gradually declines (**Figure 3.6d**). Such an unusual behavior can be explained by taking into an account the peculiarities of modified PGMA films swelling, which is going to be discussed in **Chapter 4**. The transport and distribution of the substances used for modification plays crucial role in the determining the outcome of grafting.

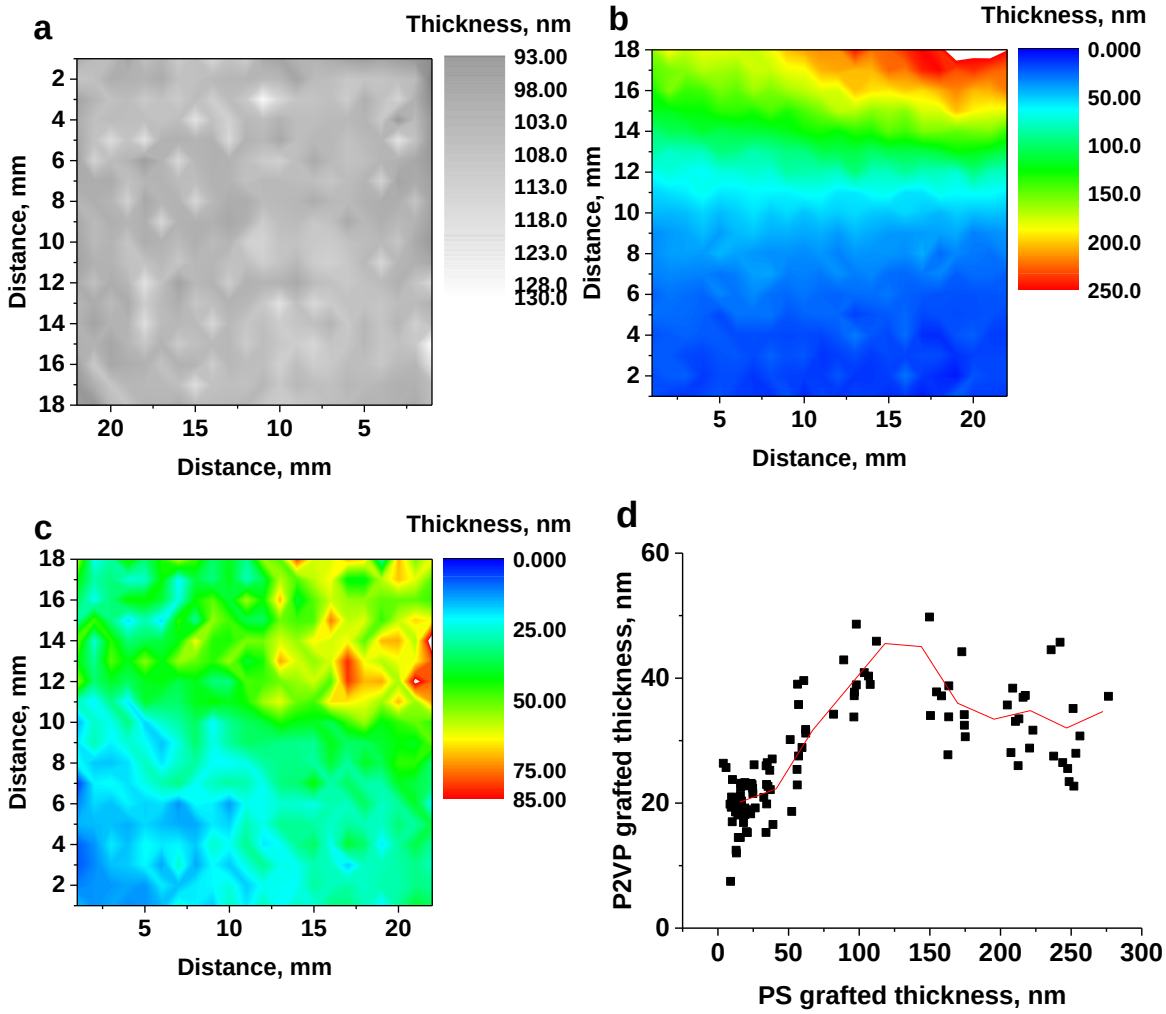

Figure 3.6. The typical thickness map of grafted PGMA layer (a) and the gradients of grafted thicknesses of PS (b) and P2VP (c). The modification of (PS)/PGMA with P2VP: P2VP grafted thickness vs PS grafted thickness.

3.4. Structure of the PGMA films modified by "grafting to method"

The preparation of the PGMA base layers in this study has been done by dip-coating of the piranha pre-treated silicon wafers in the chloroform solution of PGMA followed by

annealing at elevated temperature and removal of the ungrafted polymer. The morphology of this film is uniform as indicated on **Figure 3.7a**. It is essential that the resulting PGMA layer is an attached to the surface cross-linked network. The curing process is initialed from the surface where hydroxyl groups of activated silicon wafer open the adjacent epoxy rings of glycidyl methacrylate units. This yields a chemical bond with the surface and formation of another hydroxyl group that in its turn is capable of reacting with epoxy groups as well.

As the result, PGMA consists of densely cross-linked "stems" where polymer chains are tightly bound by a series of cross-links propagating from the silicon wafer into the surface of polymer layer. These "stems" are separated by "strands" of non-cross-linked PGMA that have low amount of cross-links and demonstrate high mobility. When the PS-COOH grafting is performed, these loose sections of polymer chains are the ones where polystyrene is being predominantly grafted to.

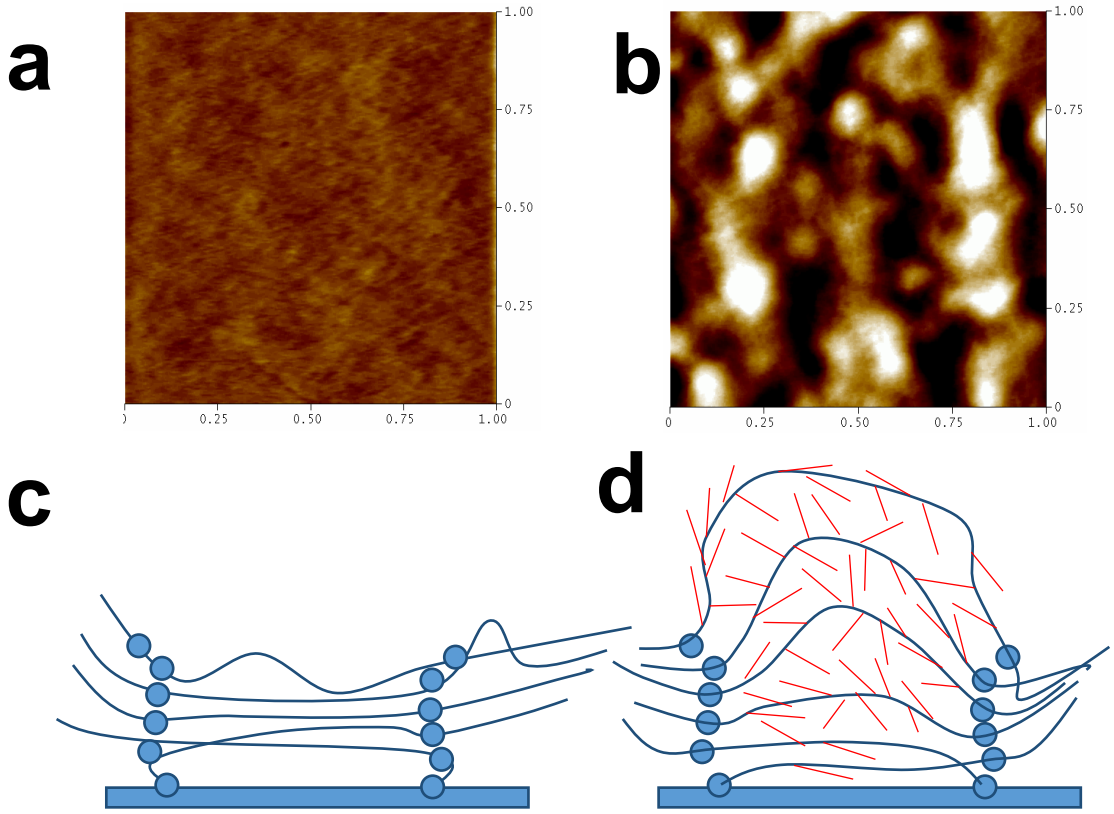

Figure 3.7. The morphology of PGMA (a) and polystyrene-modified PGMA (b) layers and their respective shematic representations (c, d).

The "stems" of heavily cross-linked material take extended conformation allowing "strands" to react with carboxyl groups of polystyrene. Subsequently, the resulting films show much higher roughness (**Figure 3.7b**) highlighting the "strand" areas where grafting is more efficient. The cartoon on **Figure 3.7c,d** demonstrates the basics of the PGMA cross-linked layer structure and the product of its modification by PS-COOH. Note, that both PS and P2VP used for modification have molecular weight lower that corresponding critical entanglement molecular weights.

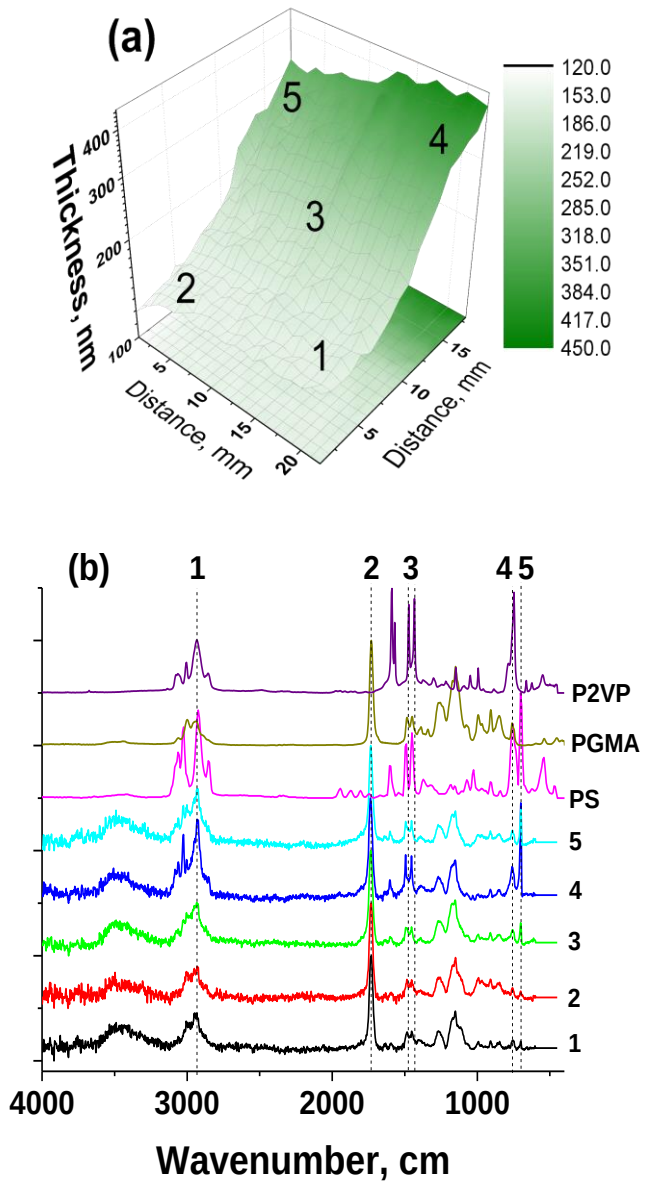

Figure 3.8. (a) Thickness of the representative three component gradient grafted layer *versus* surface coordinate. **(b)** FTIR spectra of one-component dip-coated films (made of PGMA, PS, and P2VP) and the gradient polymer layer at different locations. The approximate location on the gradient film is marked on **(a)**. The peaks marked are: (1) C-H stretching: 2930 cm^{-1}, (2) carbonyl: 1730 cm^{-1}), (3) C-H bending overlapping with aromatic C=C and C=N stretching: 1400-1500 cm^{-1}, (4-5) C-H bending: 750 and 700 cm^{-1})

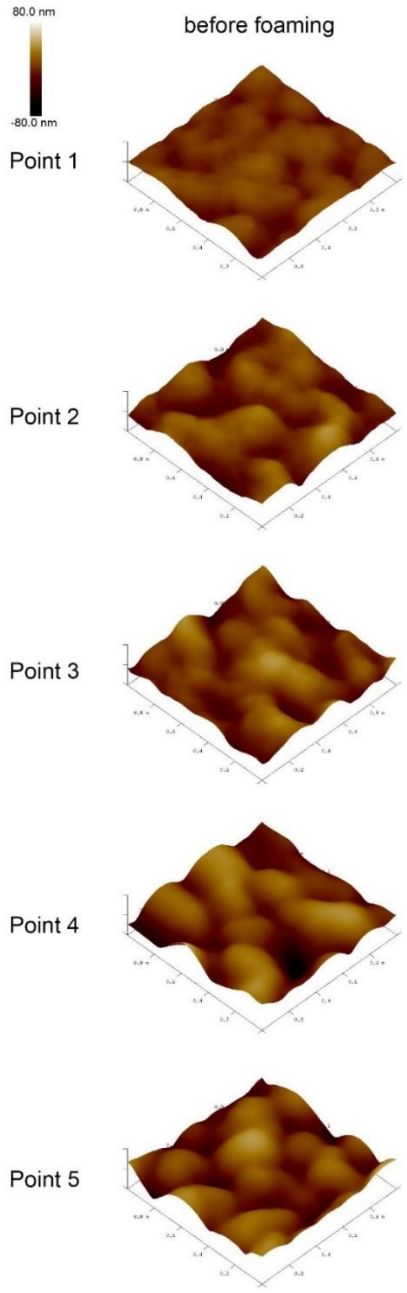

Figure 3.9. AFM (1x1 microns) topographical images for the gradient grafted layer at different locations. The approximate location on the gradient film is marked on **Figure 3.8(a)**.

A Fourier transform infrared spectroscopy (FTIR) analysis of the resulting gradient film confirmed **(Figure 3.8b**) that the chemical composition significantly varies across the film. In fact, the ratios between intensities of the major IR absorption peaks, such as C−H stretching (2930 cm^{-1}), carbonyl (1730 cm^{-1}), C−H bending overlapping with aromatic C=C and C=N stretching (1400−1500 cm^{-1}), and C−H bending (750 and 700 cm^{-1}), are unique for different locations of the three-component grafted film. There are at least five principal compositional areas that can be virtually identified on the sample (**Figure 3.8**) with PGMA/PS/P2VP ratios roughly on the level of: **(1)** 10/1/2, **(2)** 10/2/1, **(3)**10/5/3, **(4)** 10/20/6, and **(5)** 10/20/4. Atomic force microscopy (AFM) images of the three-component film (**Figure 3.9**) clearly show that these areas possess somewhat similar surface morphologies. In general, the AFM route-mean-square (RMS) roughness of the grafted films is on the level of 7−20 nm with a higher roughness in the areas with higher PS and P2VP contents indicating higher roughness is connected with the mutual immiscibility of the PS, P2VP, and PGMA macromolecules.

3.5. Conclusions

In this chapter the preparation of the PGMA-based graft copolymer film has been studied in details. The 2D scanning reflectometer set-up has been constructed for the acquisition of big data arrays of polymer layer thickness. The formation of surface-attached cross-linked layer and its subsequent modification has been characterized on each step of the process. As it turns out, the process of the three-component gradient film preparation can be controlled by the annealing temperature variation across the sample and can be roughly expressed in terms of Arrhenius activation energy. The "grafting to" procedure was found to generate non-uniformities across the modified surface. The PGMA-based network consist of densely cross-linked "stems" and loose heavily modified "strands", which is a key finding that dictates the properties of EPLs and hence influences the performance of the sensor assembly.

3.6. References

1. Xiong, Y.; Ye, Z. B.; Xu, J.; Liu, Y. C.; Zhang, H. Y., A microvolume molecularly imprinted polymer modified fiber-optic evanescent wave sensor for bisphenol A determination. *Analytical and Bioanalytical Chemistry* **2014,** *406* (9-10), 2411-2420.
2. Wren, S. P.; Nguyen, T. H.; Gascoine, P.; Lacey, R.; Sun, T.; Grattan, K. T. V., Preparation of novel optical fibre-based Cocaine sensors using a molecular imprinted polymer approach. *Sensors and Actuators B: Chemical* **2014,** *193*, 35-41.
3. Winther-Jensen, O.; Kerr, R.; Winther-Jensen, B., Alcohol vapour detection at the three phase interface using enzyme-conducting polymer composites. *Biosensors & bioelectronics* **2014,** *52*, 143-6.
4. Luzinova, Y.; Zdyrko, B.; Luzinov, I.; Mizaikoff, B., Detecting trace amounts of water in hydrocarbon matrices with infrared fiberoptic evanescent field sensors. *Analyst* **2012,** *137* (2), 333-341.

5. Mlsna, T. E.; Cemalovic, S.; Warburton, M.; Hobson, S. T.; Mlsna, D. a.; Patel, S. V., Chemicapacitive microsensors for chemical warfare agent and toxic industrial chemical detection. *Sensors and Actuators B: Chemical* **2006,** *116* (1-2), 192-201.
6. Mizaikoff, B., Mid-IR Fiber-Optic Sensors. *Analytical Chemistry* **2003,** *260A*.
7. Lin, P. T.; Giammarco, J.; Borodinov, N.; Savchak, M.; Singh, V.; Kimerling, L. C.; Tan, D. T. H.; Richardson, K. a.; Luzinov, I.; Agarwal, A., Label-Free Water Sensors Using Hybrid Polymer–Dielectric Mid-Infrared Optical Waveguides. *ACS Applied Materials & Interfaces* **2015,** *7*, 11189-11194.
8. Giammarco, J.; Zdyrko, B.; Petit, L.; Musgraves, J. D.; Hu, J.; Agarwal, A.; Kimerling, L.; Richardson, K.; Luzinov, I., Towards universal enrichment nanocoating for IR-ATR waveguides. *Chemical Communications* **2011,** *47* (32), 9104-9104.
9. Soliani, A. P. PhD thesis. Synthesis and characterization of chemically functionalized shape memory nanofoams for unattended sensing applications. Clemson University, 2014.
10. Siqueiros, J. M.; Regalado, L. E.; Machorro, R., DETERMINATION OF (N,K) FOR ABSORBING THIN-FILMS USING REFLECTANCE MEASUREMENTS. *Applied Optics* **1988,** *27* (20), 4260-4264.
11. Yovcheva, T.; Vlaeva, I.; Bodurov, I.; Dragostinova, V.; Sainov, S., Refractive index investigation of poly(vinyl alcohol) films with TiO2 nanoparticle inclusions. *Appl. Optics* **2012,** *51* (32), 7771-7775.
12. Zdyrko, B.; Swaminatha Iyer, K.; Luzinov, I., Macromolecular anchoring layers for polymer grafting: comparative study. *Polymer* **2006,** *47* (1), 272-279.
13. Iyer, K. S.; Zdyrko, B.; Malz, H.; Pionteck, J.; Luzinov, I., Polystyrene layers grafted to macromolecular anchoring layer. *Macromolecules* **2003,** *36*, 6519-6526.
14. Zou, J.; Zdyrko, B.; Luzinov, I.; Raston, C. L.; Iyer, K. S., Regiospecific linear assembly of Pd nanocubes for hydrogen gas sensing. *Chemical communications (Cambridge, England)* **2012,** *48* (7), 1033-5.
15. Zdyrko, B.; Klep, V.; Li, X.; Kang, Q.; Minko, S.; Wen, X.; Luzinov, I., Polymer brushes as active nanolayers for tunable bacteria adhesion. *Materials Science and Engineering: C* **2009,** *29* (3), 680-684.
16. Bhattacharya, a.; Misra, B. N., Grafting: A versatile means to modify polymers: Techniques, factors and applications. *Progress in Polymer Science (Oxford)* **2004,** *29*, 767-814.
17. Borodinov, N.; Giammarco, J.; Patel, N.; Agarwal, A.; O'Donnell, K. R.; Kucera, C. J.; Jacobsohn, L. G.; Luzinov, I., Stability of Grafted Polymer Nanoscale Films toward Gamma Irradiation. *ACS Applied Materials & Interfaces* **2015,** *7* (34), 19455–19465.

CHAPTER 4. SWELLING ABILITY AND GAMMA-RADIATION ROBUSTNESS OF GRAFT COPOLYMERS FOR VOC SENSOR COATING

4.1. Introduction

Organic polymers possess unique functionalities and physical properties that can be utilized for a number of electronic and optical applications, ranging from memory devices to optical sensors.[1-9] As electronic/optical systems are scaled down to micron/submicron sizes, it has become critical to employ uniform, stable, and precisely located nanoscale polymer films in these devices.[3-4, 8, 10-14] To this end, chemically grafted polymer layers have recently been explored in the fabrication of components for a number of electronic and optical systems.[8, 10, 13-17] Covalent bonding to the substrate prevents the delocalization of the nanoscale polymer films, as a result of temperature/environmental variations and fluctuations. To this end, this chapter focuses on practical aspects of polymer-based sensor design. As the primary function of enrichment polymer layers is to be able to swell in the vapors of the volatile organic compounds, the detailed investigation of three-component EPL ability to respond to vapors of acetone, toluene, methanol and chloroform has been done.

Moreover, for a number of applications, functional polymer films must be designed to operate in challenging environments, such as high-energy gamma-ray radiation. Ionizing radiation is well recognized for influencing mechanical properties, chemical composition, molecular weight, and the cross-linking extent of irradiated polymers.[18-19] The effects of

irradiation on a number of polymers are known and understood. For instance, polymers such as polystyrene, aromatic polyamides, and polysulfones possess significant resistance to radiation damage, but others like polypropylene and poly(meth)acrylates will readily degrade upon exposure to ionizing radiation.[20-24] However, the radiation stability of ultrathin grafted polymer films has not been thoroughly investigated, nor have effective mitigation strategies been outlined for these films. This is in spite of the fact that nanoscale polymer films have been considered to be employed in gamma-ray irradiation dosimetry.[25-27] Therefore, in order to identify the application range for the systems containing grafted films, it is important to determine their radiation stability. In particular, this range is crucial for the devices being employed in orbiting satellites, defense related applications, and the devices located in the vicinity of nuclear facilities or radioactive objects.[28-29] To this end, this chapter also considers the influence of gamma-ray irradiation on submicron polymer grafted films, and explores avenues for improving their stability towards radiation.

In terms of applications, the polymer thin films employed in sensor devices for the detection of chemical and biological substances are in the focus of this chapter.[30-32] In fact, it is well established that EPLs deposited on the surface of (optical) sensors can significantly improve their analytical performance, by attracting compounds of interest and increasing their local concentration in the vicinity of the sensing elements.[12, 33-35] The effective and reliable functioning of an EPL is dependent on two main factors: the permanency of the chemical structure and the ability to absorb a significant amount of the chemical of interest through swelling. Both of these parameters can be significantly affected by an EPL's exposure to gamma radiation, which is known to cause polymer cross-

linking (decreasing its ability to swell), as well as significant changes in the polymer chemical structure and molecular weight.

PGMA belongs to the methacrylate polymer family, which is notoriously unstable when exposed to ionizing itradiation.[24] The effects of gamma-ray irradiation on the PGMA material and PGMA ultrathin films in terms of their chemical composition and swellability (cross-linking) are being thoroughly investigated. Then, the grafting of low molecular substances and polymers, as well as the incorporation of nanoparticles, is shown to significantly increase the stability of the nanoscale PGMA layer towards ionizing radiation.

Once the principal trend the preparation of the three-component PGMA-based graft-polymer layers and their stability towards gamma-radiation has been investigated, I studied the response of EPL on sensor elements, optical resonators. Here, the evanescent wave racetrack photonic resonators are used to create the sensing device. These structures have shown high potential for the creation of novel generation of chemical sensors.[36] In this chapter, the coating of the resonators with PGMA-based EPL is being performed as well as characterization of its signal drift due to the gamma radiation.

This way, this chapter will provide a comprehensive knowledge about the fundamentals of PGMA-based graft copolymer film response, its viability for the operation in a challenging environment and the functioning of the EPL on the actual sensor element. These devices are able to show strong response after large doses of gamma-radiation and provide the capability of chemical vapor online monitoring.

4.2. Materials and methods

4.2.1. Materials

The PGMA was synthesized according to the procedure described in **Chapter 3**. Gel permeation chromatography (Water Breeze) has been used to measure PGMA molecular weight and polydispersity index which were found to be Mn=510,000 g/mol and PDI=2.2. Polystyrene monodisperse standards have been used for calibration. Glycidyl methacrylate (97%), azoisobutyronitrile (AIBN), poly(ethylene glycol) dimethyl ether (PEG) with number average molecular weight, Mn = 1,000 g/mol, sulfuric acid, and hydrogen peroxide (30%) were purchased from Sigma-Aldrich. Monocarboxy-terminated PS with Mn = 2,000 g/mol and hydroxyl-terminated P2VP with Mn = 4,000 g/mol were purchased from Polymer Source Inc. Higher molecular weight non-reactive PS (Mn = 170,000 g/mol) was purchased from Sigma-Aldrich. The dimethylphenylsilanol (DMPS) and 4-amino-2,2,6,6-tetramethylpiperidine-1-oxyl (4-amino-TEMPO) were purchased from Sigma Aldrich. The Au nanoparticles were purchased from Nanoprobes. They are stabilized with 1-mercapto-(triethyleneglycol)methyl ether and have diameters of 5±1 nm. The sulfuric acid and hydrogen peroxide were purchased from Sigma Aldrich and LabChem Inc., respectively, and mixed at a 3:1 ratio to prepare the "piranha" solution. The synthesis of the BaF_2 nanoparticles was conducted by Katie R. O'Donnell working under Dr. Luiz Jacobsohn at Department of Materials Science and Engineering in Clemson University, according to the procedures described elsewhere.[37-38] In brief, the synthesis was carried out via the solution precipitation method, using ammonium di-noctadecyldithiophosphate (ADDP) as a ligand. A solution of the host and rare earth,

RE dopant metal nitrates dissolved in water was added to a solution of NH_4F dissolved in 1:1 ethanol:water, together with ADDP, to form nanoparticles in suspension. The barium fluoride nanoparticles have an average size of 30 nm. One-sided polished silicon wafers with a thickness of 500 μm were purchased from University Wafer. All solvents used in this work were purchased from VWR International and used as received.

4.2.2. Formation of three-component gradient films and the thickness measurement

The preparation of three-component graft-copolymer films and the thickness measurement have been described in detail in **Chapter 3**.

4.2.3. Solvent exposure of the gradient nanofoam films

The swelling of the three-component polymer layers has been performed according to the following procedure: the sample was put inside the glass reflectometer cell and scanned, then the selected solvent (toluene, methanol, acetone or chloroform) in a bucket has been placed in the cell. After 20 min exposure, the sample was scanned again. The ratio of the thicknesses after and before the solvent exposure yielded the swelling ratio.

4.2.4. Fabrication of films for the radiation exposure studies

A dip-coating process from solution was employed to deposit a precursor polymer film on the silicon wafers using a dip-coater D-3400 (Mayer Feintechnik). Prior to the dip-coating, the silicon wafers were first cleaned in D.I. (deionized) water for one hour using an ultrasonic bath, then placed in a piranha solution (3:1 concentrated sulfuric acid/30% hydrogen peroxide) at ~ 80 ºC and sonicated for one hour, and finally rinsed several times with D.I. water. The polymer solutions for the coating were prepared with

concentrations of 0.5%, 1%, 1.5%, and 2 % w/v PGMA and 2% w/v PS. Chloroform was used as the solvent for all polymers. The polymer layers were deposited on the silicon surface by dip-coating at 320 mm/min.

In general, the PGMA layers were fabricated according to the previously published procedure.[39-40] Layers were annealed for 3 h at 130°C in a vacuum oven, to anchor them to the silicon wafer. After annealing, the samples were rinsed 4 times with chloroform to remove any ungrafted polymer. For the PS grafting, the procedure described in detail elsewhere was followed.[40] In brief, the carboxy terminated PS (70%) was mixed in chloroform with high molecular weight PS (30%), to avoid dewetting during the polymer attachment. The mixture was dip-coated above the already grafted PGMA layer. Next, the PS was incorporated into the PGMA layer via melt grafting at 130°C for 3 h. After annealing, the samples were rinsed 4 times with chloroform to remove any ungrafted polymer. To obtain the 4-amino-TEMPO/PGMA and DMPS/PGMA grafted layers, the procedure described in detail elsewhere was followed.[41] Briefly, 4-amino-TEMPO and DMPS were vapor-grafted into an already grated 70 nm PGMA layer at 130°C for 1 h in a Schlenk tube. Next, the films were thoroughly washed with chloroform in order to remove any ungrafted substances. To obtain the nanoparticles/PGMA films, barium fluoride and gold particles were dispersed in a PGMA chloroform solution, and dip-coated on the silicon wafer surface. The dry w/w contents of the barium fluoride and gold in the polymer films were 40% and 16%, respectively.

4.2.5. Characterization of the films during the radiation robustness study.

Changes in the polymer layer thickness were registered with ellipsometry in order to estimate the extent of the grafting. The cross-linking extent of the nanoscale layers was estimated by solvent vapor swelling, and monitored by in-situ ellipsometric measurements. For the swelling analysis, the following procedure was utilized.[11-12] It was conducted by placing the wafer covered with the films in a closed cell with a bucket of analyte. Ellipsometry was performed with a COMPEL automatic ellipsometer (InOmTech, Inc.), at an angle of incidence of 70°. The refractive index for the layers was assumed to be 1.5. Atomic force microscopy (AFM) studies were performed on a Dimension 3100 (Digital Instruments, Inc.) microscope. The tapping mode was used to image the surface morphology of the PGMA and PS/PGMA films, using silicon tips with spring constants of 50 N/m at scan rates in the range of 0.51 Hz.

Differential scanning calorimetry (DSC) (Model 2920; TA Instruments) was carried out at a heating rate of 20°C/min. The FTIR spectra of the polymer nanoscale layers on 0.5 mm thick Si wafers were acquired using Thermo Nicolet 6700 FTIR spectrometry, equipped with the transmission accessory. A clean Si wafer from the same batch was used as a baseline for the transmission measurements, and 256 scans were averaged. For acquiring the ATR FTIR spectra of the bulk PGMA, the Thermo Nicolet Magna 550 FTIR spectrometer with the Thermo-Spectra Tech Endurance Foundation Series Diamond ATR accessory was used, and 16 scans were averaged. An ATR correction and baseline correction were performed using Thermo Scientific

OMNIC software, versions 8.0 and 6.1. Deconvolution of the peaks and peak integration were completed using Origin MicroCal 6.1.

4.2.6. Irradiation

A Gammacell 220 gamma research irradiator, which produces energies gamma rays with energies equal to 1.17 and 1.33 MeV during ^{60}Co decay, was used to irradiate the polymer samples studied here. The dose rate was 7 krad/min calibrated with respect to the water. Absorption lengths for gamma-ray irradiation in this range are much larger than the thicknesses of the samples tested. Therefore, that the damage can be considered to be produced homogeneously throughout the material. The irradiation of the samples has been performed by Qingyang Du and Vivek Singh at Massachusetts Institute of Technology under the guidance of Dr. Agarwal.

4.2.7. Coating of photonic racetrack resonators.

Fabrication of SiN_x resonators followed the standard Si microfabrication processes and also has been performed by Qingyang Du and Vivek Singh. Thin film nitride was grown onto silicon wafers with 3 μm thermal oxide using LPCVD. Photolithography was performed on an i-line stepper to define the resonator patterns in SiN_x, Subsequently, the patterns were transferred to the film by a reactive ion etch using a mixture of CF_4 and CHF_3 gases. The as-fabricated silicon nitride waveguide has dimensions of 800 nm (width) and 400 nm (height), the radius of the resonator is 50 μm. 3 sensors consisting of 4 arrays with coupling gap varying from 600 nm up to 900 nm have been made. PGMA base layer was applied to all three resonators. Polystyrene and poly(2-vinyl pyridine) were grafted to the PGMA base layers on the respective sensors.

4.3. Results on the swelling of the PGMA films modified by "grafting to method"

As swelling of the enrichment polymer layers in analyte vapors is directly related to their primary function to attract chemicals, its composition dependence has to be studied in detail. Three-component gradient films that have been described in **Chapter 3** were used for the investigations. Here, I discuss the behavior predicted by the theory describing swelling of surface-attached network and explain the observed deviations.

4.3.1. Swelling of surface attached polymer networks.

The introduction of chemicals into the EPL leads to the change of its dielectric permittivity, density, Young's modulus and refractive index that can be detected with an appropriate sensor device. Essentially, EPL is an enthalpic trap where the energetically favorable interactions between solvent molecule and polymer result in solvent concentrating within the functional film. Thus, the phenomenon of swelling is defined by the balance between the elastic energy of deformed polymer network that opposes the swelling and the free energy of mixing which favors the swelling.[42] Thus, the investigation of the swelling of three component EPL film is necessary to establish its practical applicability for sensing application. In order to study this, the thickness at the point across the three-component films in dry state and in methanol, toluene, acetone and chloroform vapors was measured. This solvent selection provides good insight on the affinity of the EPL towards hydrogen bond-forming analytes (methanol), aromatic compounds (toluene)

and polar chemicals (acetone). Chloroform interacts well with a very wide range of polymers, so swelling it its vapor reflects the general ability to expand.

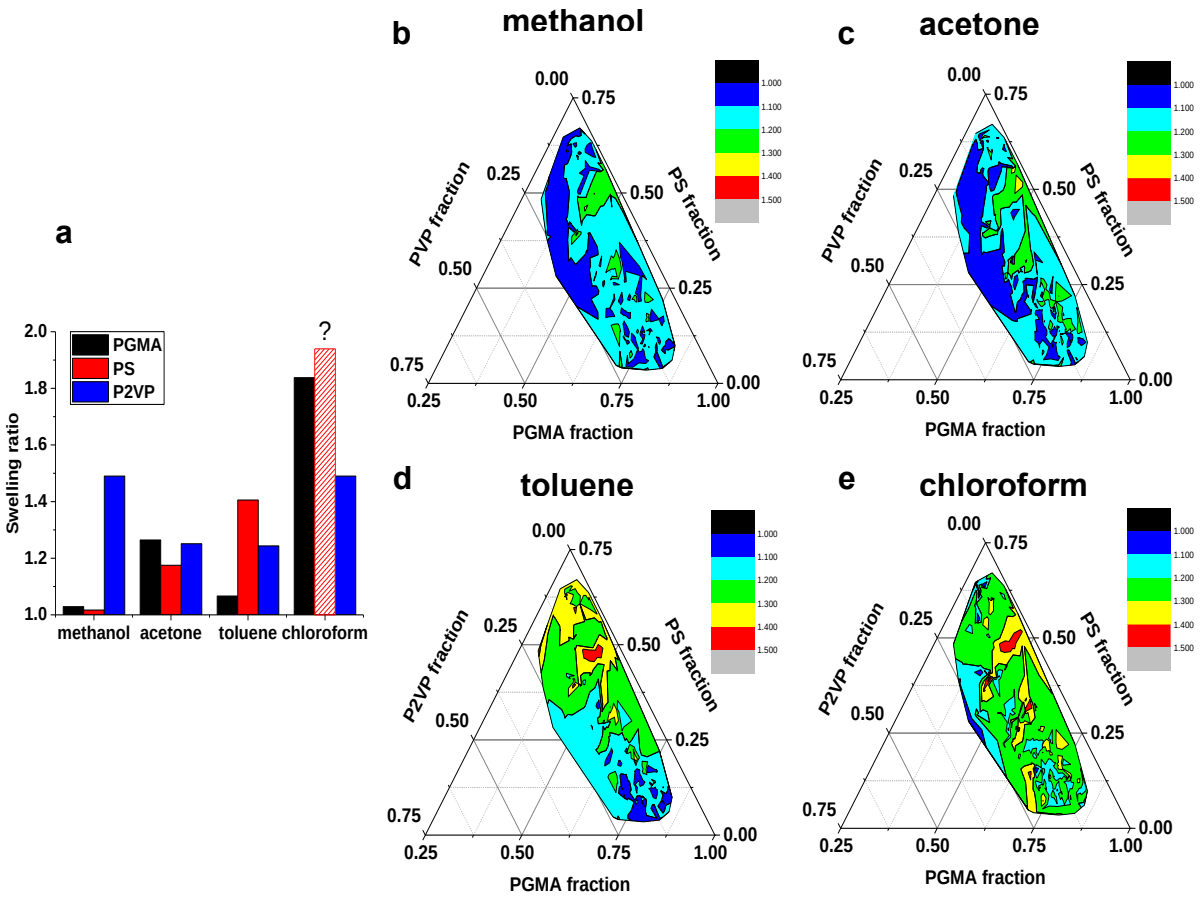

Figure 4.1. Swelling of the ungrafted polymers in methanol, acetone, toluene and chloroform vapors (a). The polystyrene of the selected molecular weight dewets in chloroform vapor as a result of swelling, so while the exact swelling extent of swelling cannot be measured, it is estimated to be very high. The composition-dependent pattern of the swelling of three-component graft-copolymer films in vapors of methanol (b), acetone (c), toluene (d) and chloroform (e).

According to the theory of swelling of thin surface-attached polymer networks[42-43] swelling extent α which is a ratio of thicknesses before and after solvent exposure, it must be strongly affected by the Flory-Huggins parameter χ which varies across the film with

the composition (N_c is the number of segments between crosslinks, d is the number of dimensions that the network can expand to).

$$\alpha \sim \left[\frac{1}{(1/2 - \chi) N_c} \right]^{-1/(d+2)} \tag{9}$$

All three polymers used here have close glass transition temperature (80˚C for P2VP, 56˚C for PGMA and 79 ˚C for PS of selected molecular weights) which is well above room temperature. As the solvent is introduced into the polymer film, the plasticization of the EPL occurs. The swelling of the ungrafted polymers was characterized in order to probe their ability to interact with vapors of solvents of varying thermodynamic affinity (**Figure 4.1a**).

It is clearly seen that methanol show significant swelling extent only for P2VP, toluene – for P2VP and PS while acetone and chloroform show similar response (polystyrene swells so well in chloroform vapors that even thick films dewet from the silicon wafer surface). So basing on the theory, points on the film with high P2VP and PS content should show maximum swelling for methanol and toluene, respectively.

4.3.2. Swelling of PGMA-based networks

Figure 4.1b-e shows the "sweet spot" at 0.5 PS – 0.1 PVP – 0.4 PGMA which shows maximum swelling for all solvents. While this observation is indeed contradicting to the theory, one must consider the assumptions that have been done in order to derive the theoretical equations. Specifically, the equation considers expansion of the network with uniform cross-linking density. However, in our case an essentially phase separated system

is observed where tightly cross-linked “stems” and loose “strands” predominantly affected by grafting coexist. Swelling of these “strands” generates little mechanical stress as no entanglements of the PGMA chains or grafted PS/P2VP chains hinder chain mobility. Initially, the increase of the grafted polymers volume ratio promotes swelling as more PS and P2VP chains are available for the interaction with the solvents diffusing into the polymer layer which would not normally cause swelling of pure PGMA layer. **Figure 4.2** displays the relationship between grafted thickness of polymers and the swelling extent in toluene, acetone, methanol and chloroform. As evident from the graph, at certain grafting level the density of PS and P2VP chains becomes so high that they start to compete for the space with the solvent molecules. This result in the initial increase of the swelling with the grafted thickness followed by slow decline which is well observed for methanol and acetone that peak at 100-150 nm grafted thickness. The same trend was observed for P2VP grafting into PS-modified PGMA network, as the first stage of the “grafting to” process is the transport of the chemicals into the polymer layer, it is directly related to the swelling and it governed by the same principles.

When the “overall expansion extent” is plotted as the ratio of sum of the grafted thickness and the thickness gained by the exposure to the vapors (**Figure 4.2**, red lines), for all of the solvents this “overall expansion” reaches maximum value of 0.8-1 and then levels off highlighting the competition between grafted chains and the solvent.

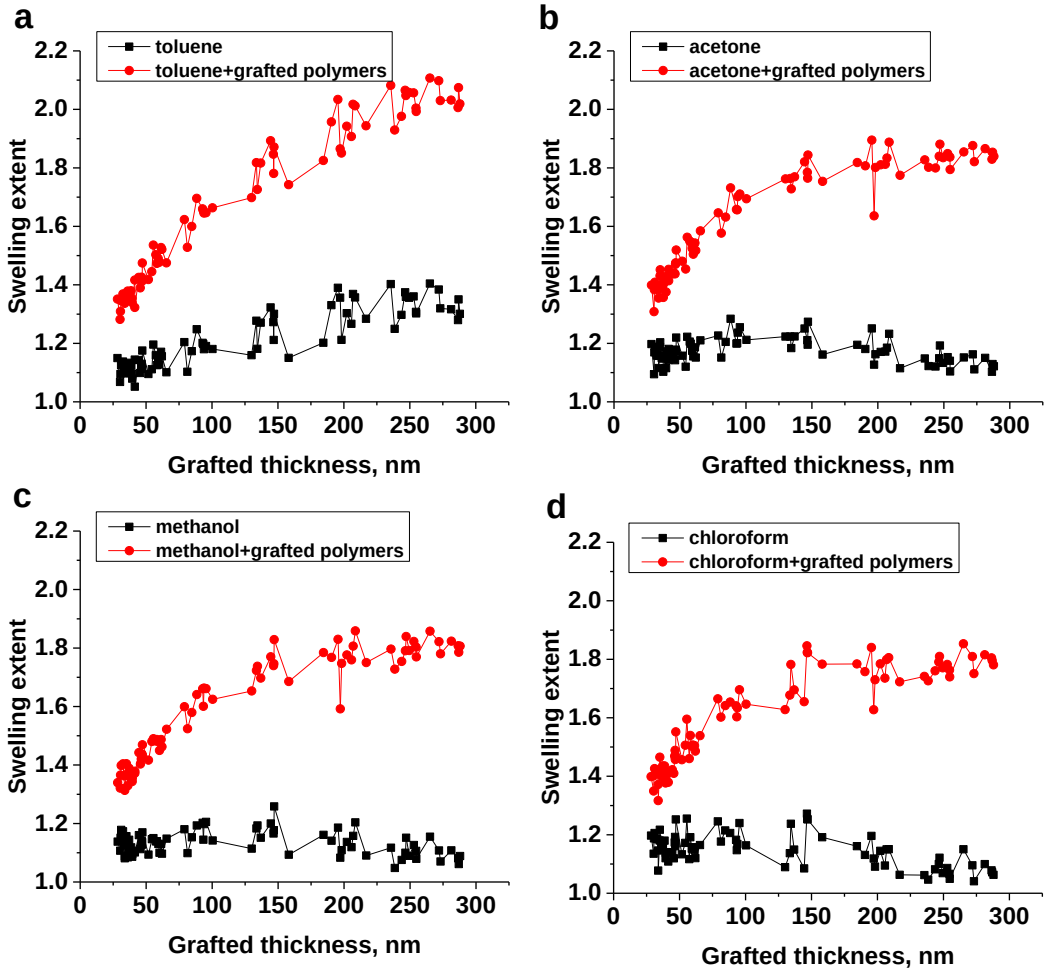

Figure 4.2. Swelling of the three-component films in toluene (a), acetone (b), methanol (c) and chloroform (d) as a function of grafted thickness (PS+P2VP) (black lines). The swelling calculated considering the grafted polymer (red lines).

Thus, the general tendencies of the three-component EPL swelling in vapors of volatile organic compounds have been identified. As it turns out, the structure of PGMA-based network consisting of tightly cross-linked "stems" and mobile "strands" plays a decisive role in its expansion. Increase of the volume fraction of the grafted chains facilitates swelling until they start to compete with the solvent molecules for the space.

This leads to the formation of a "sweet spot" that shows maximum swelling for all studied solvents regardless of their nature.

4.4. PGMA stability to gamma radiation

To obtain the EPL thin layer, the PGMA is initially deposited on the sensor elements by dip-coating, spin-coating, or drop-casting from solution, and annealed at elevated temperatures.[10-12] The polymer films are anchored via the "grafting to" approach.[44] During annealing, in addition to a surface functional groups-epoxy reaction, a cross-linking reaction between the epoxy groups occurred. In essence, the PGMA layer is fabricated as a thin internally cross-linked film, covalently bound to the surface using its epoxy group functionalities.[44-46] The epoxy groups of the PGMA not involved in the reaction with the surface and cross-linking can be used for the grafting of other polymer chains, to modify the chemical composition of the nanoscale film.

Typically for polymers exposed to gamma-ray irradiation: (a) bond cleavage resulting in molecular weight decrease, (b) cross-linking of the polymer molecules leading to network formation and an increase in molecular weight, (c) carbon dioxide release because of carbonyl groups elimination, and (d) double bond formation that occurs as the result of radical recombination can be expected.[19] In this respect, the closest analogue to PGMA, the gamma-ray radiation stability of which has been rigorously studied, is poly(methyl methacrylate) (PMMA).[21, 47-50] PMMA has been extensively used as an engineering plastic, organic glass, and a positive photoresist for electron beam

lithography.[24] It is well documented that the radiation stability of PMMA is low in comparison with many other polymers.

4.4.1. Radiation stability of bulk PGMA

It is necessary to point out that the data on the gamma-ray irradiation stability of PGMA has not been reported in the scientific literature. Therefore, to understand the behavior of the PGMA nanoscale films upon their exposure to ionizing radiation, the influence of gamma-ray irradiation on the PGMA bulk material was first studied. **Figure 4.3a** displays the ATR FTIR spectra of the bulk PGMA samples subjected to different doses of irradiation. First of all, the development of the conjugated ester was observed (peak at 1280 cm^{-1}) during the PGMA material irradiation. In addition, the dose increase causes the intensive formation of carbon-carbon double bonds, which is indicated by the presence of an IR peak located at 1640 cm^{-1}. This process is well documented for PMMA degradation under irradiation.[24, 51-53] The formation of conjugated esters occurs when a hydrogen atom is abstracted from the cut polymer main chain, and the resulting radical undergoes β-scission, resulting in the formation of a neighboring double bond and ester group.

With respect to the molecular weight, two main effects of ionizing irradiation on polymers have been identified: (a) chain scission decreasing molecular weight, and (b) cross-linking increasing molecular weight.[54] Extensive cross-linking also leads to the formation of a non-soluble fraction (gel-fraction) of polymer material. When the well-studied PMMA is exposed to gamma-ray irradiation, it experiences an extensive main-chain scission/decrease in molecular weight. The polymer is not capable of cross-linking.[54-

[56] It is necessary to highlight a significant difference between the PGMA and PMMA macromolecules, which is the presence of reactive epoxy groups in the PGMA structure. Under irradiation a certain amount of epoxy groups is consumed, as indicated by the decreasing of the 900 cm^{-1} band (**Figures 4.3a,b**).

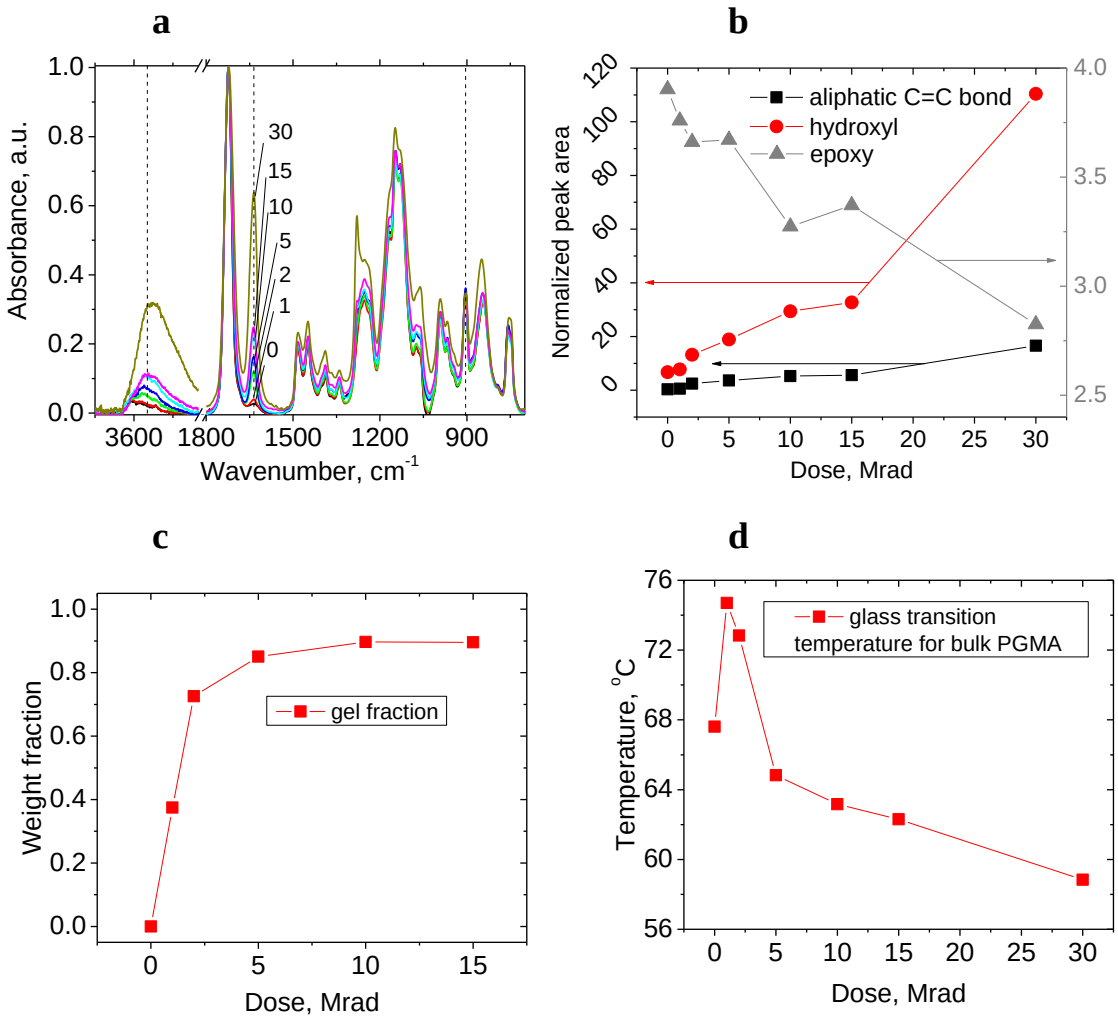

Figure 4.3. Gamma-radiation effects on bulk PGMA. (a) FTIR spectra of bulk PGMA samples before and after irradiation normalized by carbonyl peak, (b) areas of C=C peak, hydroxyl and epoxy peaks as a function of irradiation dose for bulk PGMA samples normalized by carbonyl peak, (c) gel-fraction of bulk PGMA samples versus dose of gamma radiation. d) Glass transition temperature of bulk PGMA samples as a function of irradiation dose. Lines are guide for eyes only.

It is improbable that the epoxy groups are reacting with the radical species formed during the irradiation, since the PGMA is routinely obtained (including this work) by radical polymerization, which implies no interaction between the oxirane group and polymer chain carrying radical. Therefore, the nucleophile-type initiation of the epoxy polymerization with alcohol and/or carboxyl groups[57] is responsible for the decrease in the epoxy group concentration. In fact, in the PGMA FTIR spectra, the presence of a small amount of hydroxyl groups was observed in the 3500 cm^{-1} spectral region (**Figure 4.3a**).

The presence of the hydroxyl signal in the spectra indicated that prior to the irradiation, a small fraction of (a) epoxy groups in the macromolecules was opened, yielding hydroxyls, and/or (b) glycidyl methacrylate groups were hydrolyzed yielding carboxylic groups. During irradiation, the increased mobility of the (newly formed by chain scission) short chains facilitates the reaction between the hydroxyl and epoxy groups, since the shorter chains are less restricted from reptation movements than the original "frozen" below glass transition temperature (Tg) long chain.[58] The process is also driven by the increase in the concentration of the hydroxyl groups in the course of irradiation (**Figure 4.3a**). In the irradiated PMMA samples, a similar increase in the hydroxyl functionalities was observed, and suggested to originate from the oxidative degradation of the polymer.[24]

In principle, these FTIR results indicate that under irradiation, PGMA simultaneously undergoes bond cleavage/chain scission and cross-linking via the epoxy groups. Both processes change the chemical nature of the polymer, but influence its physical behavior in opposite directions: (a) cross-linking leads to an increase in the effective molecular weight, formation of the network, and decrease in the mobility of the

macromolecule constituting material, while (b) bond cleavage/chain scission leads to a decrease in the effective molecular weight and an increase in the mobility of the macromolecule constituting material. It is necessary to point out that the level of cross-linking can be critical for the polymer layer employed as the EPL, since the extensive cross-linking decreases the ability of the enrichment layers to swell and attract the compounds of interest to the sensor elements.

In order to evaluate the level of the PGMA cross-linking, the amount of the gel-fraction in the irradiated material was determined as a function of the gamma-ray irradiation dose. It was found that a dose increase up to 5 Mrad leads to an increase in the gel-fraction (**Figure 4.3c**). A further dose increase does not produce a significant change in the gel-fraction. Therefore, it appears that the cross-linking dominates the bond cleavage until reaching a dose of 5 Mrad. The thermal behavior of the irradiated polymer to reveal additional details of the degradation processes was studied. **Figure 4.3d** shows the results of the DSC measurements of the PGMA glass transition temperature, which mostly reflects changes in the level of cross-linking and the molecular weight of the polymer chains. The Tg rises from 68^{o}C to 75^{o}C at the initial (1 Mrad) stage of the radiation treatment. Further irradiation leads to a gradual Tg decrease, which reaches 59^{o}C after a dose of 30 Mrad. This result indicates that, initially, the formation of the polymer network hinders the mobility of polymer chains, and increases the thermal energy required to achieve long-range chain motions. However, when the dose reaches 5 Mrad, the chains in the network are cleaved to a certain extent, removing the excessive restrictions imposed on the chain movements by the cross-linking. The resulting effect is the growing number of shorter

chains within the network with a lower Tg. These data shows the critical importance of monitoring the chemical composition of the nanoscale polymer layer, as well as its ability to swell when the radiation dose increases.

4.4.2. Radiation stability of PGMA nanoscale films

50 nm PGMA layer grafted to a silicon wafer was used to study the influence of radiation on chemically grafted nanoscale films. First, within the range studied (dose up to 15 Mrad) the thickness of the film is unchanging. This result indicates that a measurable amount of the gaseous products is not formed during irradiation. In order to monitor the chemical changes of the irradiated PGMA nanoscale films, FTIR analysis before and after each step of the irradiation treatment was performed for the grafted layers (**Figure 4.4a-c**). The number of carbonyl groups in the films slightly increases under gamma-ray irradiation (**Figure 4.4a,c**). It was documented that both the loss of carbonyls (primarily caused by –COOH group elimination) and formation of new ketone carbonyls can occur under irradiation.[47, 51]

As for the bulk PGMA, the formation of a conjugated ester (peak at 1280 cm^{-1}) and double bond (peak at 1640 cm^{-1}) upon irradiation (**Figure 4.4a,b**) was observed. According to the infrared data, gamma-ray irradiation also induces the formation of hydroxyl groups in PGMA, while the intensity of the oxirane (epoxy) ring vibration (ca. 900 cm^{-1}) gradually decreases (**Figure 4.4c**). This observation corresponds to the epoxy ring opening, accompanied by a hydroxyl peak appearing at ca. 3500 cm^{-1}. The area of the epoxy peak located at 900 cm^{-1} decreases 6 times for pure PGMA nanofilm after 15 Mrad, while the OH peak gradually increases with the increasing dose. The increase in the intensity of the

OH peak is in agreement with results previously reported for ion irradiated amorphous carbon thin films.[59] This supports the mechanism of the epoxy rings opening being directly related to the hydroxyl-mediated reaction. In general, the FTIR results show that the radiation induced degradation of the PGMA grafted layer follows the same pathway as the degradation of the bulk polymer.

Additionally, it was investigated how the extent of the PGMA film swelling in acetone vapor (the ratio between the thickness of the swollen film to its initial thickness) changes as a function of the radiation dose. The measurements allow the estimation of the level of the film cross-linking. **Figure 4.4** shows that the swellability of the film in acetone gradually decreases with the dose. The results clearly indicate that gamma-ray irradiation causes significant cross-linking of the 50 nm PGMA films. It was reported that gamma-ray irradiation can increase the surface roughness of the polymer materials.[60] Therefore, in order to investigate the surface morphology change in the irradiated PGMA nanofilms, the samples were imaged by AFM in the tapping mode (**Figure 4.4e**). The surface morphology of the irradiated polymer layers was found to be uniform and even, while the PGMA films remained smooth throughout the irradiation process, showing no discernible changes up to at least 15 Mrad.

In general, irradiation has a significant effect on the chemical composition and swelling extent of the nanoscale PGMA films. The changes definitely decrease the sensing ability of the PGMA based EPLs; therefore, strategies to increase the radiation stability of the PGMA based nanoscale films need to be identified.

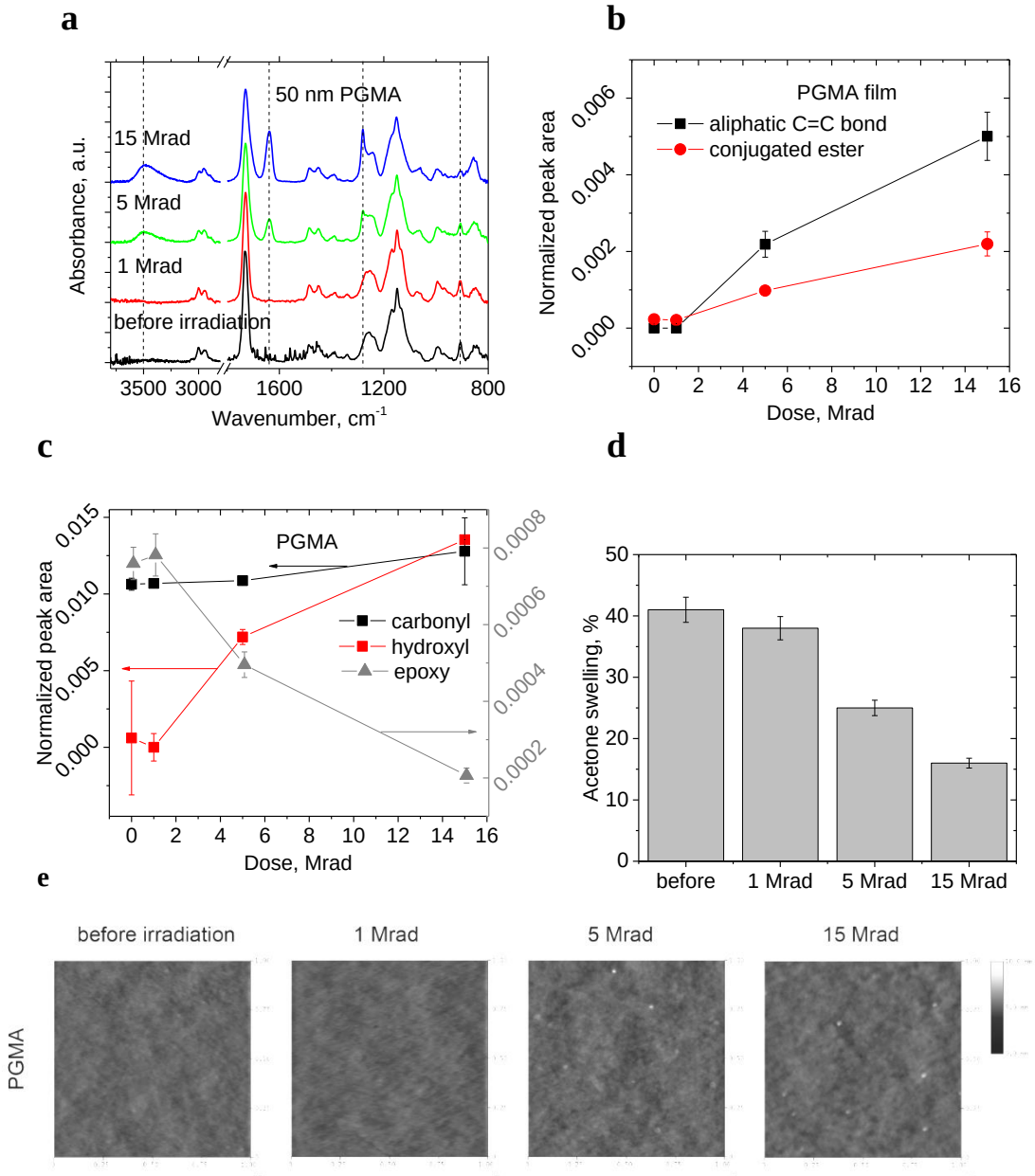

Figure 4.4. Gamma-radiation effects on PGMA grafted film. (a) FTIR spectra of PGMA film before irradiation, after 1, 5 and 15 Mrad gamma irradiation (15 Mrad), (b) the areas of aliphatic carbon-carbon double bond and conjugated ester as a function of irradiation dose normalized by PGMA content; (c) the areas of carbonyl, hydroxyl (left axis) and epoxy (right axis) peaks normalized by PGMA content as a function of irradiation dose; (d) Swelling extent in acetone vapour for PGMA films versus gamma radiation dose, (e) AFM images (height bar is 10 nm, scan size 1 μm by 1μm) of PGMA films. Lines are guide for eyes only.

4.5. Mitigation strategies for nanoscale PGMA films

The general approach for the mitigation of the radiation effect on the PGMA nanoscale films is depicted in **Figure 4.5**. It is well known that gamma-ray irradiation initially causes the formation of radicals that are further involved in multiple reactions, including interactions with the oxygen present in the air, chain transfer reactions by hydrogen abstraction, and termination by recombination or disproportionation[24].

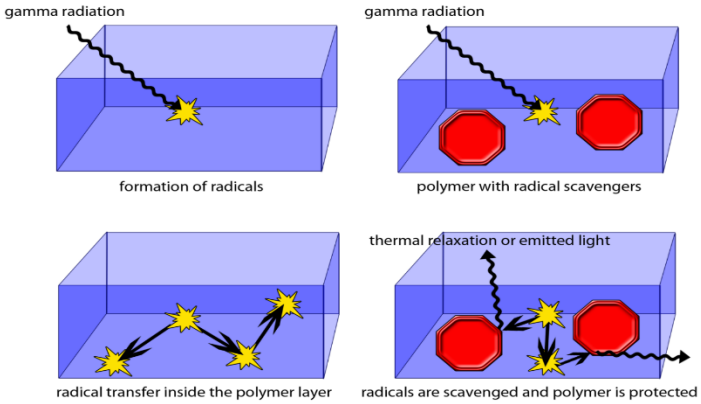

Figure 4.5. The strategy of gamma-radiation damage mitigation for the grafted polymer layers: radical scavengers are protecting polymer by terminating radical propagation within the film.

These processes cause critical morphological, topological, and chemical changes, thus, extensively alternating the properties of the polymer materials. In order to mitigate the outcome of the irradiation on the polymer films, free-radical scavengers can be introduced into the film. In this scenario, when a radical reaches the scavenger, more stable species with negligible propagation constants are formed, which further react, resulting in the formation of stable compounds. In other words, the presence of stabilizers alternates the pathway of the polymer film interaction with gamma radiation, providing significant

resistance towards radical-induced degradation. In this work, several strategies for radical scavenging were explored.

4.5.1. Grafting of PS to PGMA film

In order to increase the stability of the PGMA film towards ionizing radiation, it can be modified with further grafting of the macromolecules that are robust against the radiation. Polystyrene (PS), where the presence of the aromatic rings provides effective scavenging of the radicals, has high resistance towards the radiation,[54-55, 61] which makes it a perfect candidate to be a stabilizer. For instance, for the poly(methyl acrylate)-PS copolymer, in-situ radical monitoring demonstrated that the concentration of radiation-induced radicals drops 6 times when the copolymer composition is changed from pure poly(methyl acrylate) to PS.[62] Chain scission and radiation-induced cross-linking (which are mutually opposite processes) are the general mechanisms of PMMA and PS degradation, respectively. It was confirmed, by evaluating the radiation yield (per 100eV absorbed), that the PS tends to be cross-linked, while the chain scission is observed to be almost 4 times less for the polymer.[54] It is apparent that the PS macromolecules can be used to improve the PGMA stability towards radiation.

In order to modify the PGMA film, monocarboxy-terminated PS was deposited by dip-coating, and then melt-grafted (~ 25 nm) via a reaction between the carboxylic and epoxy groups into a pre-annealed PGMA (~25 nm) layer. In order to avoid dewetting, high molecular weight polystyrene was introduced into the grafting mixture. In addition to the ellipsometry measurements, the presence of aromatic double bonds (peaks at 1490 cm^{-1} and 1450 cm^{-1}) in the FTIR spectra of the grafted film confirmed the anchoring of the PS

chains (**Figure 4.6a**). The resulting grafted films were subjected to 1, 5, and 15 Mrad of gamma-radiation, and were characterized with FTIR, AFM, and ellipsometry. It appeared that the incorporation of polystyrene into the PGMA layer achieves the goal of increasing the radiation stability of the film in terms of swelling (cross-linking). For the PS/PGMA layers, the extent of swelling does not decrease, even after a 15 Mrad dose (**Figure 4.6b**). It appears that the effective scavenging of the radicals by aromatic rings in the PS-modified films prevents the macromolecules constituting the layer from intensive cross-linking.

The FTIR data also indicates the efficiency of the grafted polystyrene chains as stabilizers for the PGMA nanofilms. According to the infrared data, gamma-ray irradiation leads to the decrease of hydroxyl groups, aliphatic carbon-carbon double bonds, and the disappearance of the epoxy groups (**Figures 4.6a, c, and d**). It is necessary to point out that the hydroxyl peak areas normalized to the PGMA content are almost 2 times lower for the PS/PGMA, which indicates that free radicals can be effectively captured by aromatic rings. This conjecture is confirmed by the fact that the PS/PGMA nanofilm demonstrates only twofold oxirane ring intensity loss after 15 Mrad. As consistent with the changes in the 1640 cm^{-1} carbon-carbon double bond peak area, polystyrene suppresses the double bond formation by a factor of 4 (**Figure 4.5c** and **Figure 4.6c**). As for the PGMA films, no change in the carbonyl ester peak and a gradual increase in the carbonyl ketone peak (1710 cm^{-1}) were observed for the PS/PGMA film. The area of the aromatic double bonds (peaks at 1490 cm^{-1} and 1450 cm^{-1}) stays constant within the statistical errors. Therefore, the polystyrene benzene rings are not affected by gamma-ray irradiation to the extent detectable by FTIR.

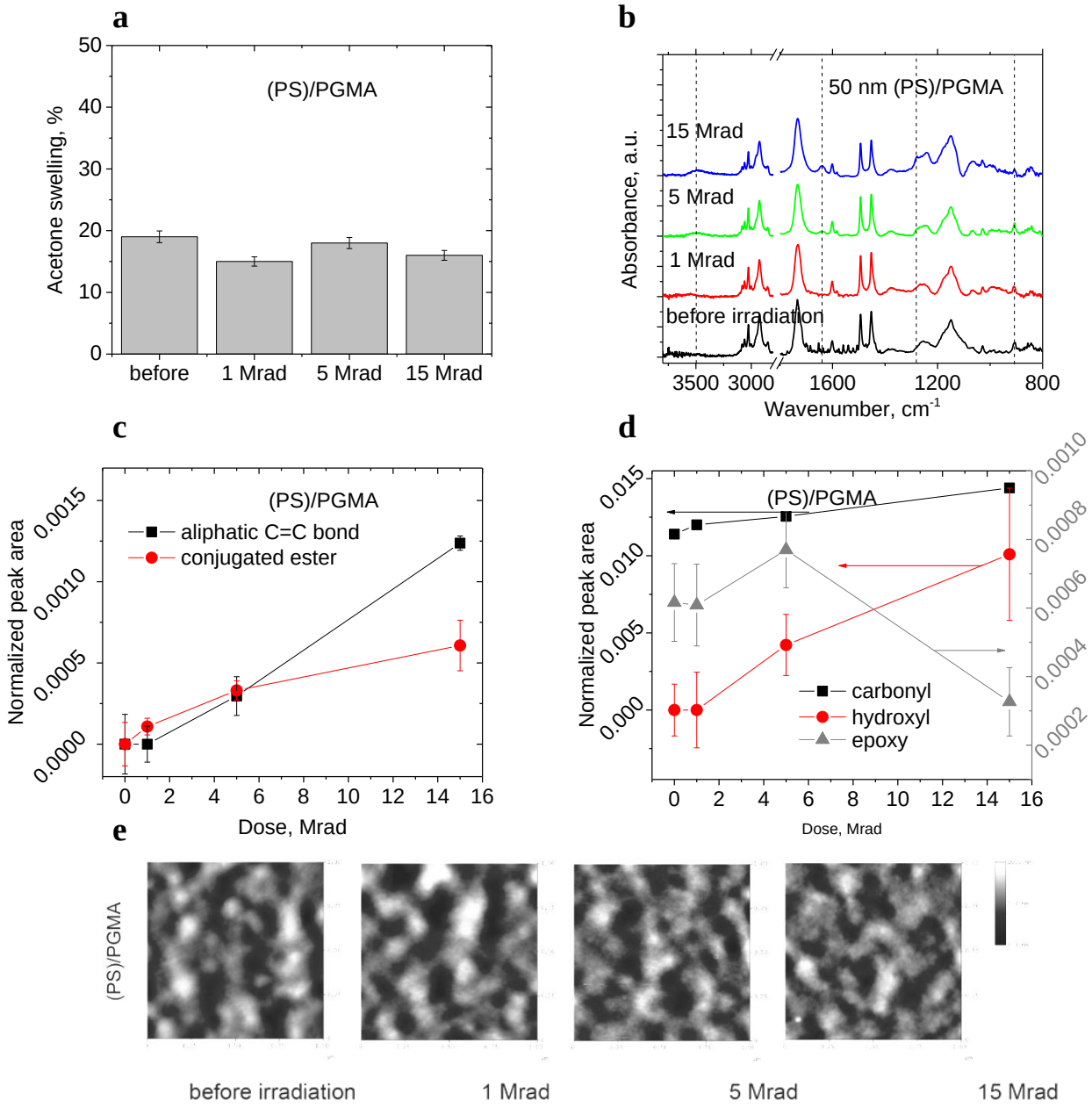

Figure 4.6. Gamma-radiation effects on PGMA enrichment polymer layer modified by PS grafting. (a) Swelling extent in acetone vapour upon gamma radiation; (b) FTIR spectra of (PS)/PGMA film before irradiation, after 1 and 15 Mrad gamma irradiation; (c) the areas of aliphatic carbon-carbon double bond and conjugated ester normalized by PGMA content as a function of irradiation dose; (d) the areas of carbonyl, hydroxyl (left axis) and epoxy (right axis) peaks normalized by PGMA content as a function of irradiation dose; (e) AFM images (height bar is 10 nm, scan size 1 μm by 1μm). Lines are guide for eyes only.

The surface morphology of the PS/PGMA films was followed in the course of gamma-ray irradiation. It was observed that the PS/PGMA polymer layer shows significantly higher surface roughness in comparison with the base PGMA layer; however, the film is uniform at the micron level and no dewetting was observed. As it turns out, the surface morphology of the (PS)/PGMA films was not affected by gamma-ray irradiation, even at a 15 Mrad dose (**Figure 4.6e**).

Dose	PGMA		PS/PGMA		DMPS/PGMA		4-Amino-TEMPO/PGMA		Au NPs/PGMA		BaF_2 NPs/PGMA	
Carbonyl x10^3												
0	**10.64**	*0.39*	**11.40**	*0.06*	**11.75**	*0.75*	**21.01**	*1.38*	**9.92**	*1.79*	**8.59**	*0.48*
1	**10.69**	*0.08*	**12.00**	*0.03*	**11.81**	*0.60*	**19.34**	*0.87*	**10.04**	*1.77*	**8.69**	*0.29*
15	**12.78**	*2.18*	**14.40**	*0.26*	**13.35**	*0.83*	**20.96**	*0.81*	**10.68**	*2.09*	**9.64**	*0.08*
Epoxy x10^5												
0	**7.60**	*0.42*	**6.16**	*1.13*	**3.10**	*0.29*	**0.60**	*0.09*	**5.19**	*0.51*	**4.23**	*0.68*
1	**7.82**	*0.55*	**6.09**	*1.19*	**2.29**	*0.37*	**0.50**	*0.11*	**5.20**	*0.42*	**3.93**	*0.76*
15	**2.06**	*0.19*	**3.26**	*1.00*	**n/a**	-	**n/a**	-	**n/a**	-	**n/a**	-
Hydroxyl x10^3												
0	**0.61**	*3.71*	**n/a**	-	**10.47**	*2.60*	**10.67**	*3.14*	**n/a**	-	**n/a**	-
1	**n/a**	-	**n/a**	-	**16.96**	*3.52*	**12.50**	*4.15*	**1.08**	*0.53*	**0.78**	*0.00*
15	**13.54**	*0.07*	**8.21**	*4.29*	**18.78**	*0.90*	**7.49**	*4.46*	**3.40**	*0.23*	**17.66**	*2.52*
Aliphatic carbon-carbon double bond x10^3												
0	**n/a**	-	**n/a**	-	**0.02**	*0.01*	**n/a**	-	**n/a**	-	**n/a**	-
1	**n/a**	-	**n/a**	-	**0.08**	*0.06*	**n/a**	-	**0.23**	*0.15*	**n/a**	-
15	**5.00**	*0.63*	**1.24**	*0.04*	**0.95**	*0.29*	**n/a**	-	**3.57**	*0.48*	**1.98**	*0.25*
Conjugated ester x10^3												
0	**0.23**	*0.12*	**n/a**	-	**0.10**	*0.04*	**n/a**	-	**0.33**	*0.09*	**0.36**	*0.07*
1	**0.21**	*0.12*	**0.11**	*0.05*	**0.29**	*0.09*	**n/a**	-	**0.45**	*0.11*	**0.43**	*0.06*
15	**2.20**	*0.31*	**0.61**	*0.16*	**0.58**	*0.04*	**0.04**	*0.09*	**1.51**	*0.23*	**0.96**	*0.13*

Table 4.1. The areas of peaks of interest for PGMA, Au NPs/PGMA, BaF2 NPs/PGMA, (PS)/PGMA, (DMPS)/PGMA and (4-Amino-TEMPO)/PGMA enrichment polymer layers before irradiation and after 1 and 15 Mrad. Averaged values of the peak areas are given in bold on the left and corresponding standard deviations are given in italic on the right.

4.5.2. Grafting of P2VP to PGMA film

As the structure of P2VP is similar to polystyrene, it is reasonable to expect somewhat close protective action when P2VP is grafted to PGMA nanoscale layer. In order to investigate this, (P2VP)/PGMA films have been subjected to gamma irradiation to study the changes in chemical composition and swelling. Similar to the irradiation of unmodified PGMA, the development of the conjugated ester (peak at 1280 cm^{-1}) during irradiation is observed. The formation of carbon-carbon double bonds (indicated by the presence of an IR peak located at 1640 cm^{-1}) points out the hydrogen atom abstraction from the polymer main chain, followed by β-scission resulting in the formation of a neighboring double bond and ester group. The epoxy groups are also consumed, as indicated by the decreasing of the 900 cm^{-1} band he amount of hydroxyl groups increasing with the dose was observed in the 3500 cm^{-1} spectral region. The protective effect of PVP is well-pronounced – the intensity of carbon-carbon aliphatic double bond for (PVP)/PGMA films normalized by PGMA content is 2.7 times lower than in case of unmodified PGMA films. However, polystyrene is still more efficient additive - intensity of carbon-carbon aliphatic double bond is 5.6 times lower than in case of unmodified PGMA films and the epoxy groups are still present even after 15 Mrad while (PVP)/PGMA completely loses them at this dose.

As evident from the **Figure 4.7**, the swelling in acetone decreases as the radiation dose increases which is a result of radiation-induced cross-linking. Unmodified PGMA film loses 61% of its swelling ratio after 15 Mrad of gamma radiation (as it was show during the second year) while (PVP)/PGMA loses only 48%. This is a demonstration of

the protective action of PVP which is, however, lower than PS where no swellability loss was observed.

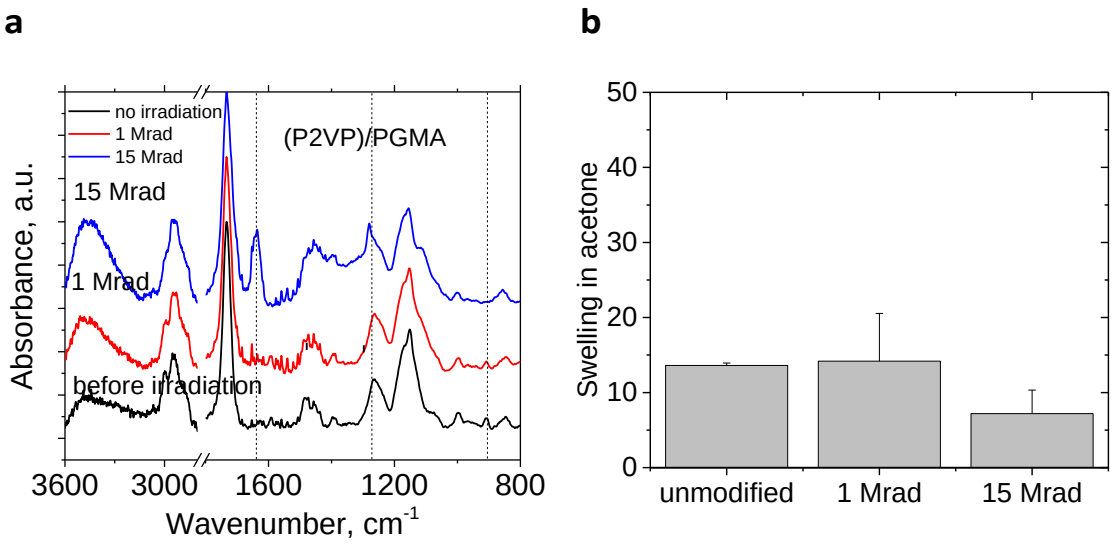

Figure 4.7. Gamma-radiation effects on PGMA enrichment polymer layer modified with P2VP: FTIR spectra before irradiation after 1 and 15 Mrad gamma irradiation (a). Swelling extent in acetone vapour upon gamma radiation (b).

4.5.3. Grafting of hindered amines to PGMA film

The addition of hindered amines, which arrest the radical driven degradation of polymers, is widely used for the UV/light stabilization of polymers.[63-65] Therefore similar strategy was employed to increase the ionizing radiation stability of the grafted PGMA films. The mechanism of hindered amine action is complex, and involves multiple steps of radical coupling and regeneration. Since gamma radiation directly creates free-radicals, hindered amine light stabilizers (HALS) may be extremely effective in preventing the damage to the polymer film. For example, polypropylene stability towards gamma-ray radiation can be significantly increased by the addition of bis(2,2,6,6-tetramethyl-4-piperidinyl) decanedioate or bis(1,2,2,6,6- pentamethyl-4-piperidinyl) decanedioate at the 0.125%

level.[66] HALS are scavenging radicals via the formation of nitroxide radicals, which then react with radicals formed as a result of irradiation.[65] In this respect, 4-amino-TEMPO, a stable nitroxide radical possessing an amino group was selected to employ for the PGMA grafted layer stabilization. This group is necessary for the covalent anchoring of the molecule to the PGMA chain via the group reaction with the epoxy groups of PGMA.

The 4-amino-TEMPO was grafted into the PGMA layer by vapor grafting. It is necessary to point out that the grafting density was rather high. Specifically, the initial thickness of the PGMA layer, measured using the ellipsometer, increased from 70 nm to 160 nm. The modification of the PGMA layer has significantly decreased the extent of the acetone swelling (**Figure 4.8a**). This effect is observed because of the 4-amino-TEMPO primary amine group, which is capable of reacting twice with the epoxy rings, increasing the level of the film cross-linking.

According to the FTIR spectroscopy data, 4-amino-TEMPO is highly efficient in terms of protecting the film from changing its chemical composition: the formation of carbon-carbon double bonds was not observed, and the formation of conjugated esters is negligible (**Figure 4.8b**, **Table 4.1**). This type of behavior was assigned to the effective radical recombination of the free radicals formed as result of irradiation, and the stable free radicals grafted to the PGMA. The efficiency of radical scavenging is extremely high, so the chain scissions are arrested; however, the cross-linking density grows, which is reflected by the drastic decrease in swelling ability, even after 1 Mrad. This important fact shows the low efficiency of the HALS and their derivatives as enrichment polymer layer

stabilizers, since the excessive cross-linking leads to a decrease in the EPL's ability to interact with volatile organic compounds.

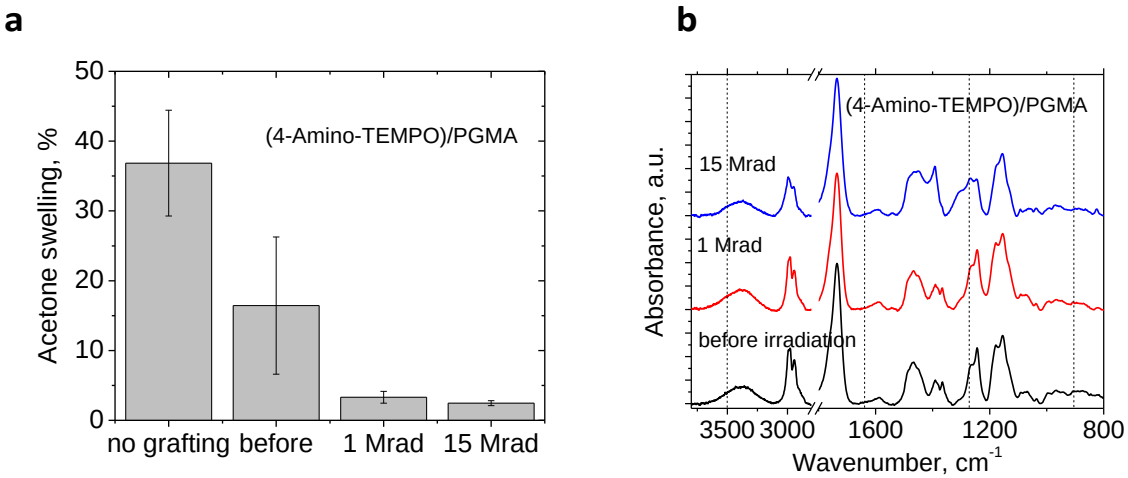

Figure 4.8. Gamma-radiation effects on PGMA enrichment polymer layer modified with 4-Amino-TEMPO: (a) Swelling extent in acetone vapor upon gamma radiation, (b) FTIR spectra before irradiation, after 1 and 15 Mrad gamma irradiation.

4.5.4. Radiation stability of DMPS-stabilized PGMA films

The usage of low molecular weight compounds containing aromatic structures[67] grafted to the main chain of the polymer being stabilized is a fruitful approach that can lead to decreased cross-linking levels. Moreover, multiple studies show the efficiency of phenylsiloxane-based compounds as active layers or modifiers for use in sensor applications.[68-70] The high affinity of these polar polymers to the nitro compounds, coupled with relative hydrophobicity, represents significant interest in the creation of new generations of explosive detection systems. As such, phenylsiloxane/phenylsilane (e.g. DMPS) may be an effective ionizing radiation resistance additive for the polymer layer, which simultaneously increases the affinity of the polymer layer to the polar compounds.

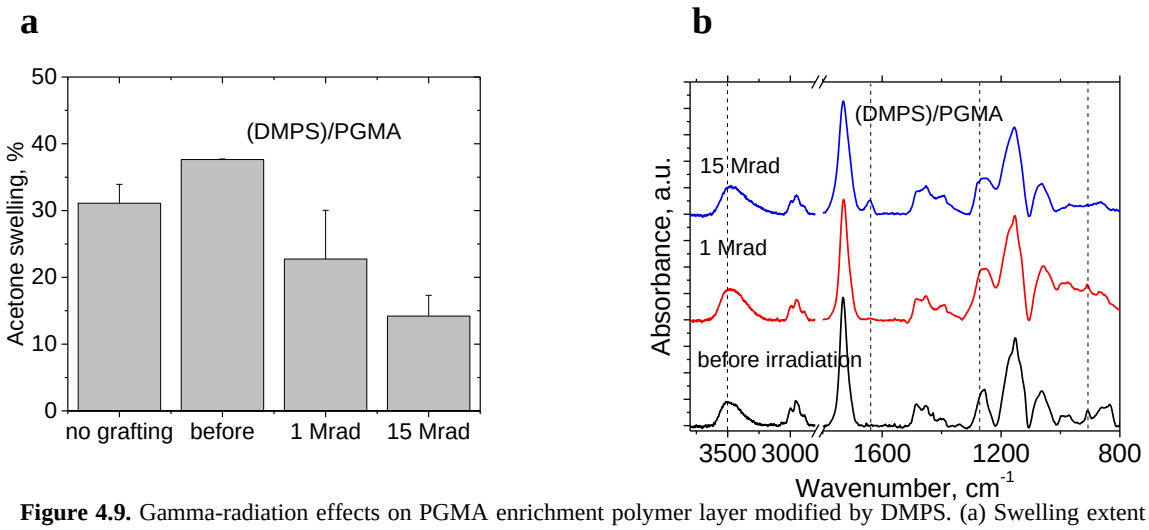

Figure 4.9. Gamma-radiation effects on PGMA enrichment polymer layer modified by DMPS. (a) Swelling extent in acetone vapour upon gamma radiation; (b) FTIR spectra before irradiation, after 1 and 15 Mrad gamma irradiation

To this end, DMPS was grafted into the PGMA nanoscale layer using the same procedure as the one used for the 4-amino-TEMPO. The initial thickness of the PGMA layer, measured by the ellipsometer, increased from 70 nm to 85 nm (or by 20%) during vapor grafting, via the reaction of the silanol group of DMPS with the epoxy group of PGMA. It was found that the DMPS modification increases the extent of acetone swelling for the PGMA nanolayers (**Figure 4.9a**). First, the results indicate that there is no significant additional cross-linking of the film associated with the DMPS anchoring. The swelling increase was associated with the increased polarity in the films after grafting, due to the formation of a significant amount of hydroxyl groups, which is evident from the FTIR spectra (band located at 3500 cm^{-1}).

The grafted DMPS turned out to be an efficient ionizing radiation protection additive. In general, the additive significantly suppresses the formation of double bonds (**Figure 4.9b**), thus preventing the chemical radiation-induced changes of the chemical composition of the EPL. However, slight increase in the bands located at 1280 cm^{-1} and

1640 cm^{-1} was still observed as the irradiation dose increased. It was also found that the area of the carbonyl peak increases following the same trend as the non-modified PGMA layer (**Table 4.1**). The area of the hydroxyl group increases, while the epoxy peak ceases to exist after a 15 Mrad dose. The opening of the oxirane ring leads to the formation of new hydroxyl groups, in addition to the ones that have already been presented in the films after DMPS grafting.

The evaluation of the swelling in acetone was conducted in order to estimate the cross-linking suppression activity of the DMPS. It was found (**Figure 4.9a**) that irradiation significantly decreases the swelling and, therefore, increases the level of the cross-linking. In fact, the acetone swelling of the DMPS/PGMA film after 15 Mrad is almost the same as that for the non-modified PGMA film. Therefore, the DMPS does not provide significant protection from cross-linking, while arresting the C=C bond formation.

4.5.5. Incorporation of gold and BaF_2 nanoparticles into the PGMA film

Inorganic nanoparticles are another promising class of candidates for the protection of the polymer nanoscale layers from free-radical attacks. For instance, it is known that the addition of nanoparticles to the polymers increases their thermal stability. Zinc oxide, polyhedral oligomeric silsesquioxane (POSS), carbon nanotubes/nanoparticles, and clay particles have been intensively studied for this purpose.[71] The thermal stability increase of PMMA, modified with AlOOH, Al_2O_3, TiO_2, and Fe_2O_3 nanoparticles, is related to the following factors: the restriction of chain movements, trapping of the radicals by the surface of the nanoparticle, and chemical bonding to the metal oxide surfaces via

methoxycarbonyl groups.[72] The presence of the free-radical scavenging ability encourages the use of inorganic nanoparticles for polymer film stabilization.

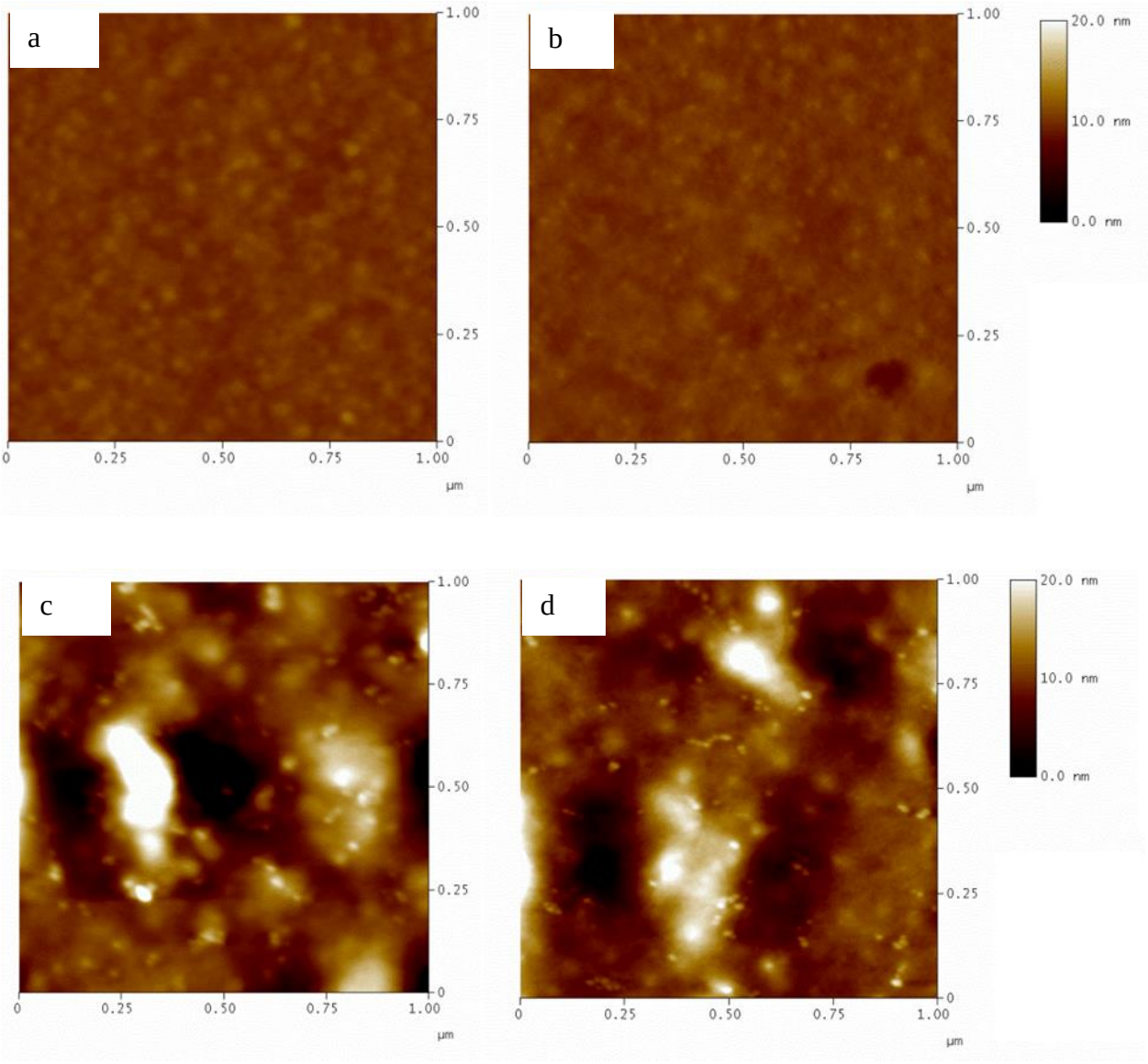

Figure 4.10. AFM of hydrid enrichment polymer layers. (a) Au NPs/PGMA before irradiation; (b) Au NPs/PGMA after 1 Mrad irradiation; (c) BaF2 NPs/PGMA before irradiation; (d) BaF2 NPs/PGMA after 1Mrad irradiation.

It is known that gold nanoparticles are capable of generating short-lived radicals by abstracting halogen or protons, with consequent scavenging of the formed radical species.[73]

This effect hinders the Au nanoparticle-related organic catalysis, while providing the evidence of a strong radical affinity towards the gold surface. In order to investigate the stabilizing activity of the gold nanoparticles, hybrid organic/inorganic Au NPs/PGMA films were prepared. The concentration of the nanoparticles in the film was 16% w/w (1.3% v/v). According to the AFM imaging, the films have a smooth morphology (**Figure 4.10**), and the nanoparticles are evenly distributed across the film. In general, the particles demonstrated limited potential for polymer film protection against ionizing radiation. Specifically, the swelling of the hybrid films does not change significantly at a small radiation dose (1 Mrad), but drops significantly after 15 Mrad of gamma-ray irradiation (**Figure 4.11a**). At the high dose, the carbon-carbon double bonds are intensively formed, as well as the hydroxyl groups (**Figure 4.19b**).

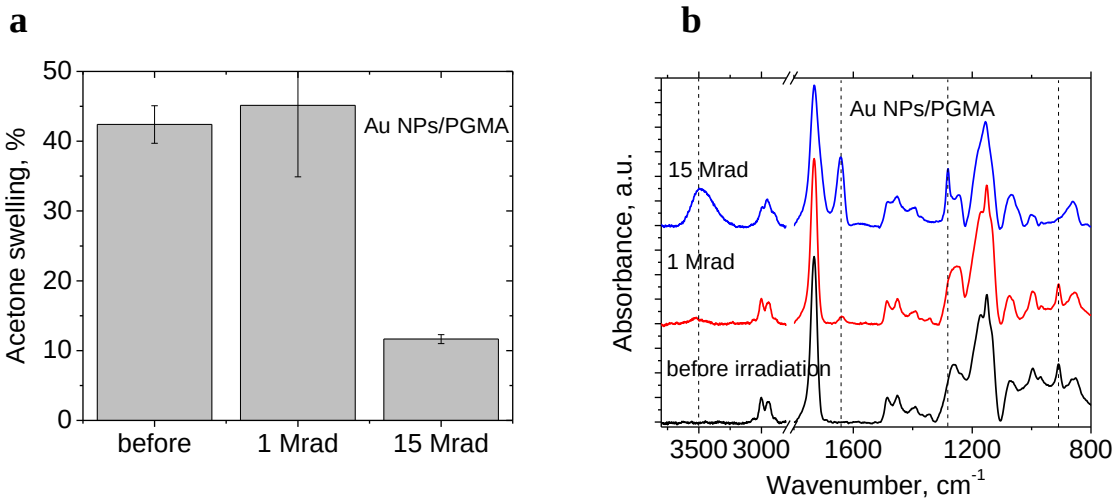

Figure 4.11. Gamma-radiation effects on hybrid 5 nm Au nanoparticles/PGMA polymer layer. (a) Swelling extent in acetone vapor for Au NPs/PGMA nanofilms upon gamma radiation; (b) FTIR spectra of Au NPs/PGMA film before irradiation, after 1 and 15 Mrad.

Additionally, scintillator nanoparticles (BaF_2) were tested, which convert high energy ionizing radiation into light, as radiation stabilizers for the grafted nanoscale

polymer layer (characteristics of the nanoparticles are provided in SI). The PGMA/BaF_2 film contains approximately 40% w/w (12% v/v) nanoparticles, which are distributed within the films in small agglomerates. At the lower (1 Mrad) dose, these hybrid nanoscale films demonstrated a certain stability towards gamma-ray irradiation. For the higher irradiation dose (15 Mrad), the extensive formation of the double bonds (**Figure 4.12a**), as well as film cross-linking (**Figure 4.12b**), was clearly observed. An increase in the carbonyl peak area also occurs while the irradiation dose increases (**Table 4.1**). Thus, the BaF_2 nanoparticles are actually protecting the film from gamma-ray irradiation; however, this effect is weaker than that for the (macro)molecular stabilizers.

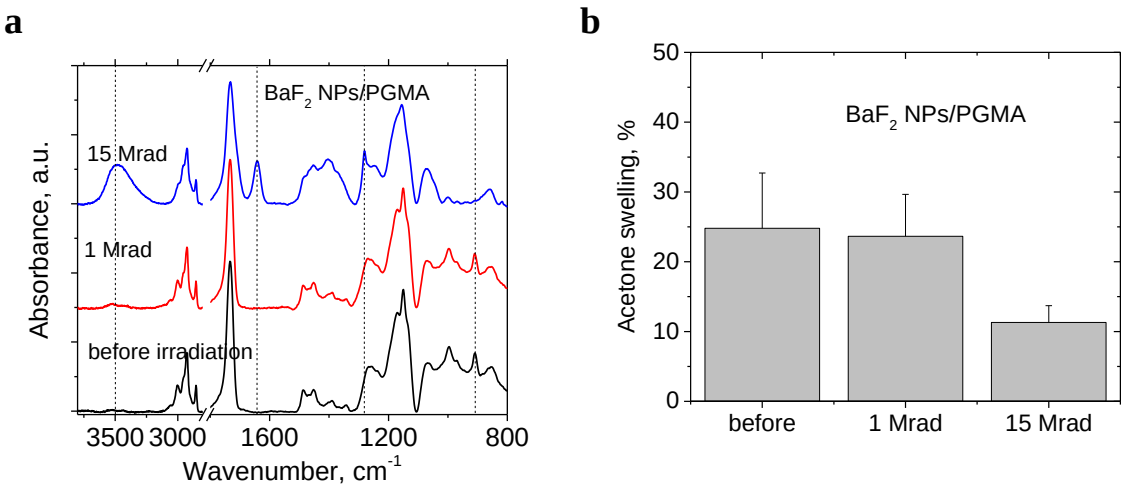

Figure 4.12. Gamma-radiation effects on hybrid 30 nm BaF2 nanoparticles/PGMA polymer layer. (a) FTIR spectra before irradiation, after 1 and 15 Mrad gamma irradiation; (b) Swelling extent in acetone vapour upon gamma radiation.

4.5.6. Comparison of the radiation stabilizer efficiencies

According to the comparative normalized FTIR spectra (**Figures 4.13a** and **4.13b**), the stability of the nanoscale film stabilizers is estimated as the area of the carbon-carbon double bond formation changes in the following order: 4-amino-

TEMPO>DMPS>PS>BaF_2 NPs>P2VP>Au NPs>pure PGMA. Whereas the cross-linking suppression activity changes in a different order (**c**): PS>>DMPS≈BaF_2NPs≈AuNPs≈pure PGMA≈P2VP>>4-amino-TEMPO. Despite the fact that the DMPS and 4-amino-TEMPO provided more significant protection against the radiation-related chemical changes, PS is a more promising candidate for the sensing application, because it is not undergoing extensive cross-linking, even after the high dose (15 Mrad), and continues to show the same swelling extent as the non-irradiated film.

However, since the EPLs are intended for use in chemical detection systems, the changes in the chemical affinity of the PS/PGMA layers should be estimated, to evaluate the probability of false-positives and false-negatives in the EPL-based sensors. In order to do this, the irradiated and non-irradiated (PS)/PGMA films were exposed to a group of solvents with different polarities. In the experiment, the estimated affinity of the film towards acetone, chloroform, and toluene does not change significantly upon irradiation (**Figure 4.13d**). However, the PS/PGMA layer shows a significant increase in the polar ethanol and decrease in the non-polar hexane swelling extent upon irradiation. These results indicate that chemical changes influence the nanoscale polymer layer response, after gamma-ray irradiation. Specifically, the formation of the hydroxyl groups increases the polarity of the nanoscale film, which is responsible for the observed changes in the extents of the ethanol and hexane swelling.

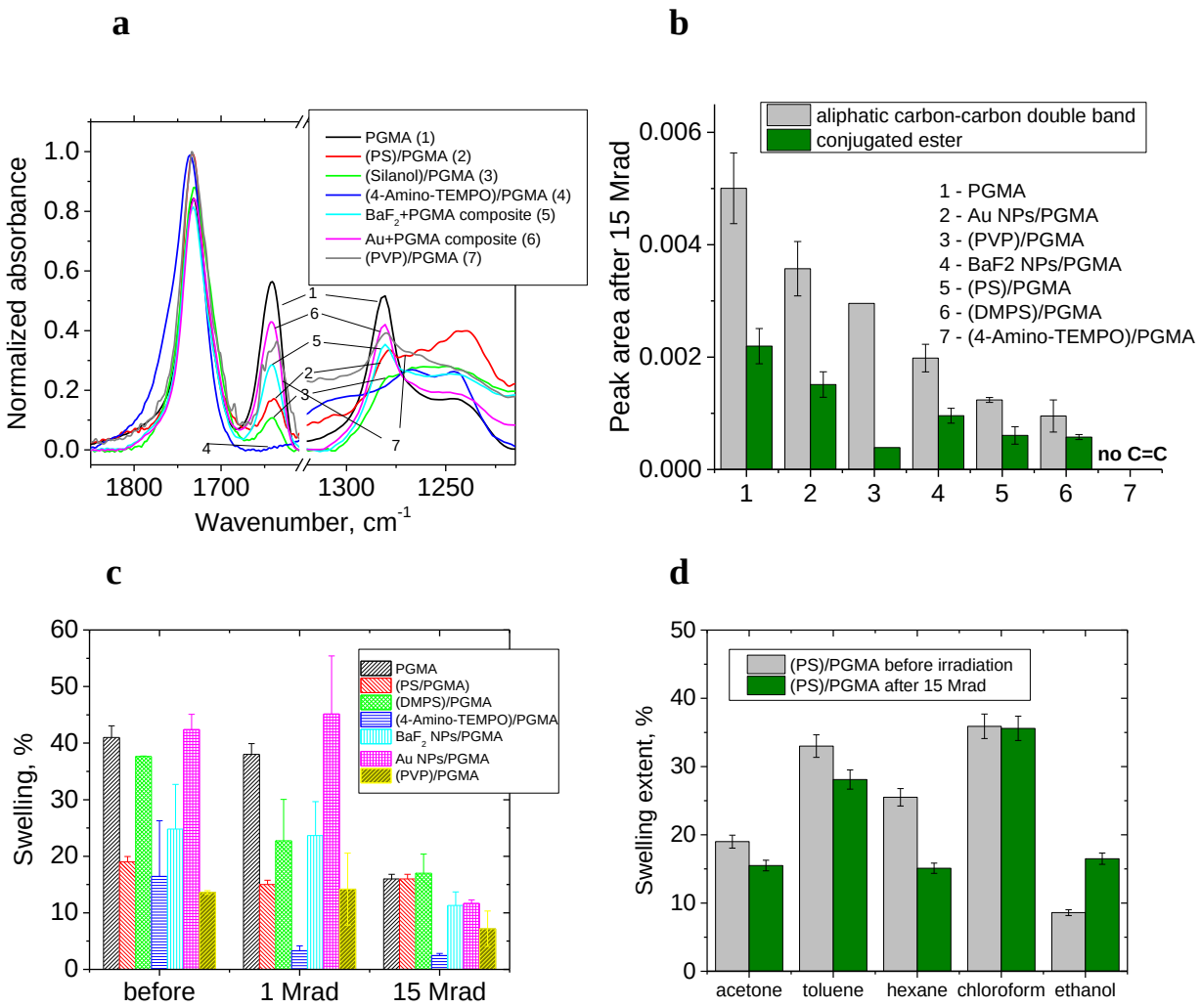

Figure 4.13. (a) FTIR of enrichment polymer layers with magnified carbonyl/C=C and conjugated ester regions; (b) the intensity of double bond and conjugated ester peaks normalized by layer thickness for PGMA, Au NPs/PGMA, BaF2 NPs/PGMA, PS/PGMA, (P2VP)/PGMA, DMPS/PGMA and 4-Amino-TEMPO/PGMA polymer layers; (c) swelling of enrichment polymer layers in acetone; (d) swelling of PS/PGMA films in acetone, toluene, hexane, chloroform and ethanol before and after 15 Mrad irradiation.

4.6. Coating of the racetrack resonators with EPLs.

Once the principal stability of EPL has been thoroughly investigated, it is possible to study the performance of the actual sensors and their stability to gamma irradiation. This is the final goal of the Defense Threat Reduction Agency-sponsored grant and important

advancement for the field of photonic circuits. Here we used photonic racetrack resonators manufactured by Qingyang Du at Massachusetts Institute of Technology under the guidance of Dr. Agarwal. The thickness of the polymer layers was 100 nm (PGMA-coated sensor), 195 nm ((PS)/PGMA-coated sensor) and 125 nm ((PVP)/PGMA coated sensor). Then each sensor was subsequently cleaved into 4 individual arrays of waveguides The irradiation and optical measurements also have been conducted by Mr. Du.

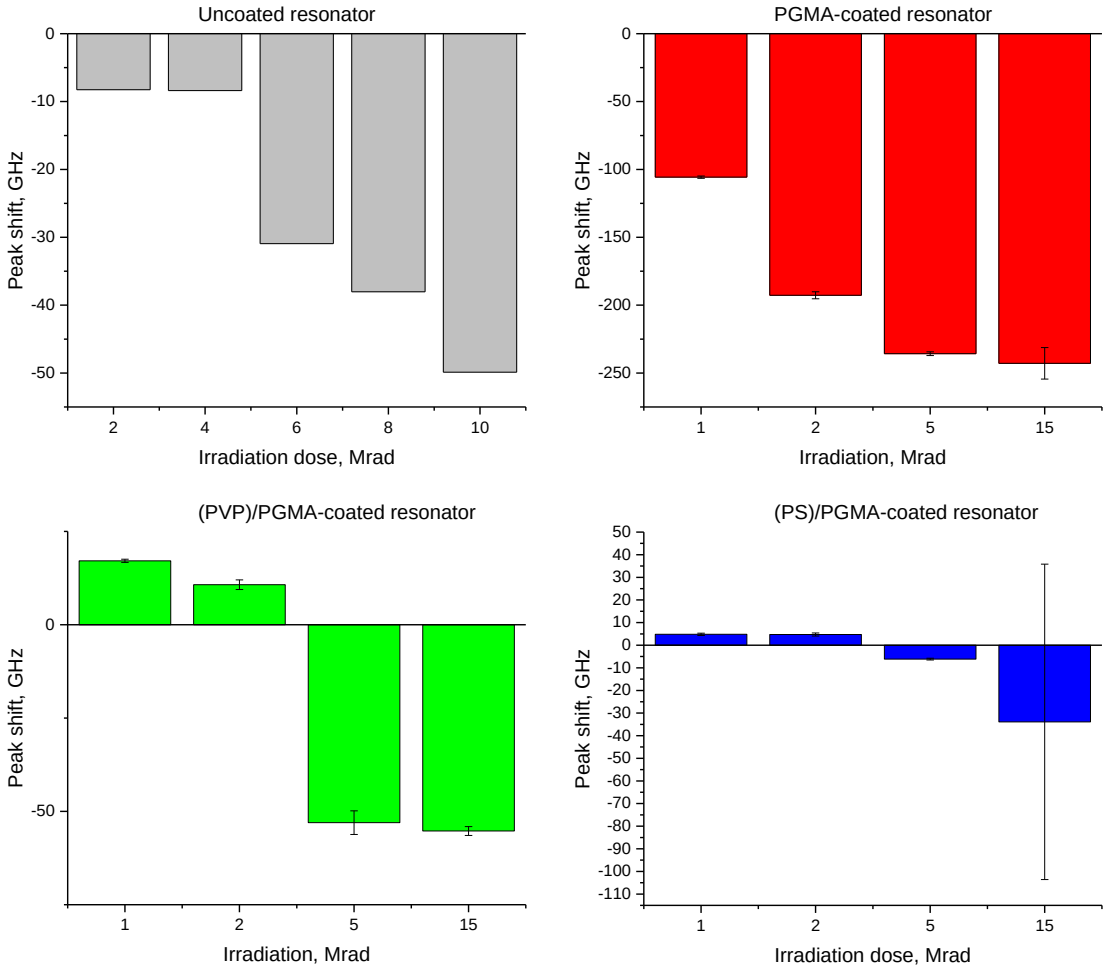

Figure 4.14. The shift of resonant frequency of the uncoated and PGMA, (PS)/PGMA, (PVP)/PGMA-coated resonators.

As it is shown on **Figure 4.14**, irradiation of the uncoated resonator causes strong resonant peak shift due to the changes to the silicon nitride that the waveguide is made of. This effect in intrinsic to the sensor system, however, damage dealt to the polymer layer can cause additional shifts as the refractive index of the EPL is changed as a result of irradiation. In fact, PGMA-coated resonators show very large drift of resonant frequency while (P2VP)/PGMA and (PS)/PGMA-coated devices have much higher robustness which is consistent with the previous findings. The presence of resonance shift raises as important issue that gamma-radiation affects the reading of the sensor which calls for additional measures in order to avoid false negatives and false positives during sensor operation in the field. Apart from the actual sensor that can be exposed to volatile organic compounds the complete analytical set-up requires a sealed backup. This backup sensor must have the same structure and be isolated from the environment, however, it must not be shielded from gamma radiation. During the measurement the readings of the backup sensor must be taken into an account during the processing of the actual environmental sensor data so the effects of the gamma radiation will be compensated at any dose.

4.7. Conclusions

In this chapter the general trend in composition-dependent graft copolymer film swelling and gamma-radiation stability have been outlined. The study of the swelling of the three-component films in vapors of solvents of different chemical nature demonstrated that increase of the grafting extent promotes swelling of “strands” resulting in formation of “sweet spot” on the composition diagram that has maximum swelling in any solvent

studied here. The influence of gamma-ray irradiation on nanoscale PGMA grafted films have been investigated, and the avenues for improving their stability towards ionizing radiation were identified. First of all, it was determined that for pure PGMA layers, a significant level of cross-linking was observed due to irradiation. The cross-linking is accompanied by the formation of conjugated ester, carbon double bonds, hydroxyl groups, ketone carbonyls, and the elimination of epoxy groups. PS, P2VP, DMPS, 4-amino-TEMPO, BaF2, and gold nanoparticles were incorporated into the films, and were found to mitigate different aspects of the radiation damage.

Also, this chapter reports graft-copolymer coatings of actual photonic resonators which is driven by the practical applications and necessity to characterize the device and its response as a whole. Nitride resonators coated with PGMA, (PS)/PGMA, (PVP)/PGMA have been irradiated and the resonator peak shift has been determined as the dose increased from 1 to 15 Mrad. This is crucial for the analysis of the data recorded on the resonators subjected to gamma irradiation.

4.8. References

1. Huang, X.; Han, S.; Huang, W.; Liu, X., Enhancing solar cell efficiency: the search for luminescent materials as spectral converters. *Chemical Society reviews* **2013,** *42*, 173-201.
2. Cho, B.; Kim, T.-W.; Song, S.; Ji, Y.; Jo, M.; Hwang, H.; Jung, G.-Y.; Lee, T., Rewritable Switching of One Diode-One Resistor Nonvolatile Organic Memory Devices. *Adv. Mater.* **2010,** *22* (11), 1228-1232.
3. Hu, Z. J.; Tian, M. W.; Nysten, B.; Jonas, A. M., Regular arrays of highly ordered ferroelectric polymer nanostructures for non-volatile low-voltage memories. *Nat. Mater.* **2009,** *8* (1), 62-67.

4. Ling, Q. D.; Liaw, D. J.; Zhu, C. X.; Chan, D. S. H.; Kang, E. T.; Neoh, K. G., Polymer electronic memories: Materials, devices and mechanisms. *Prog. Polym. Sci.* **2008,** *33* (10), 917-978.
5. Wang, G.; Kim, T. W.; Lee, T., Electrical transport characteristics through molecular layers. *J. Mater. Chem.* **2011,** *21* (45), 18117-18136.
6. Silvi, S.; Constable, E. C.; Housecroft, C. E.; Beves, J. E.; Dunphy, E. L.; Tomasulo, M.; Raymo, F. M.; Credi, A., All-Optical Integrated Logic Operations Based on Chemical Communication between Molecular Switches. *Chemistry-A European Journal* **2009,** *15* (1), 178-185.
7. Bundgaard, E.; Krebs, F., Low band gap polymers for organic photovoltaics. *Solar Energy Materials and Solar Cells* **2007,** *91* (11), 954-985.
8. Zhitenev, N. B.; Sidorenko, A.; Tennant, D. M.; Cirelli, R. A., Chemical modification of the electronic conducting states in polymer nanodevices. *Nat. Nanotechnol.* **2007,** *2* (4), 237-242.
9. Raymo, F. M., Digital processing and communication with molecular switches. *Adv. Mater.* **2002,** *14* (6), 401-414.
10. Bliznyuk, V.; Galabura, Y.; Burtovyy, R.; Karagani, P.; Lavrik, N.; Luzinov, I., Electrical conductivity of insulating polymer nanoscale layers: environmental effects. *Physical Chemistry Chemical Physics* **2014,** *16* (5), 1977-1986.
11. Chyasnavichyus, M.; Tsyalkovsky, V.; Zdyrko, B.; Luzinov, I., Tuning fluorescent response of nanoscale film with polymer grafting. *Macromolecular rapid communications* **2012,** *33* (3), 237-41.
12. Giammarco, J.; Zdyrko, B.; Petit, L.; Musgraves, J. D.; Hu, J.; Agarwal, A.; Kimerling, L.; Richardson, K.; Luzinov, I., Towards universal enrichment nanocoating for IR-ATR waveguides. *Chemical Communications* **2011,** *47* (32), 9104-9106.
13. Whiting, G. L.; Snaith, H. J.; Khodabakhsh, S.; Andreasen, J. W.; Breiby, D.; Nielsen, M. M.; Greenham, N. C.; Friend, P. H.; Huck, W. T. S., Enhancement of charge-transport characteristics in polymeric films using polymer brushes. *Nano Letters* **2006,** *6* (3), 573-578.
14. Pinto, J. C.; Whiting, G. L.; Khodabakhsh, S.; Torre, L.; Rodriguez, A. B.; Dalgliesh, R. M.; Higgins, A. M.; Andreasen, J. W.; Nielsen, M. M.; Geoghegan, M.; Huck, W. T. S.; Sirringhaus, H., Organic thin film transistors with polymer brush gate dielectrics synthesized by atom transfer radical polymerization. *Advanced Functional Materials* **2008,** *18* (1), 36-43.
15. Rutenberg, I. M.; Scherman, O. A.; Grubbs, R. H.; Jiang, W. R.; Garfunkel, E.; Bao, Z., Synthesis of polymer dielectric layers for organic thin film transistors via surface-initiated ring-opening metathesis polymerization. *Journal of the American Chemical Society* **2004,** *126* (13), 4062-4063.
16. Kim, J. H.; Bohra, M.; Singh, V.; Cassidy, C.; Sowwan, M., Smart Composite Nanosheets with Adaptive Optical Properties. *ACS Appl. Mater. Interfaces* **2014,** *6* (16), 13339-13343.
17. Chen, C. M.; Niu, X. Y.; Han, C.; Shi, Z. S.; Wang, X. B.; Sun, X. Q.; Wang, F.; Cui, Z. C.; Zhang, D. M., Reconfigurable optical interleaver modules with tunable

wavelength transfer matrix function using polymer photonics lightwave circuits. *Opt. Express* **2014,** *22* (17), 19895-19911.
18. Akiyama, Y.; Sodaye, H.; Shibahara, Y.; Honda, Y.; Tagawa, S.; Nishijima, S., Study on gamma-ray-induced degradation of polymer electrolyte by pH titration and solution analysis. *Polymer Degradation and Stability* **2010,** *95* (1), 1-5.
19. O'Donnell, J., Chemistry of radiation degradation of polymers. In *Radiation effects on polymers*, Clough, R. L. S., S.W., Ed. American Chemical Society: Washington, DC, 1991; pp 402-413.
20. Fried, J. R., *Polymer Science and Technology*. 3rd ed.; Prentice Hall: Upper Saddle River, NJ, 2014; p 663.
21. Kudoh, H.; Sasuga, T.; Seguchi, T., High energy ion irradiation effects on polymer materials—Let dependence of G value of scission of polymethylmethacrylate (PMMA). *Radiation Physics and Chemistry* **1997,** *50* (3), 299-302.
22. Bhattacharya, A., Radiation and industrial polymers. *Prog. Polym. Sci.* **2000,** *25* (3), 371-401.
23. Busfield, W.; O'Donnell, J., Effects of gamma radiation on copolymers of styrene and methyl methacrylate in the solid state. *Journal of Polymer Science:* **1975,** *237*, 227-237.
24. Moore, J. A. C., J.O., Degradation of poly(methyl methacrylate). In *Radiation effects on polymers*, Clough, R. L.; Shalaby, S. W., Eds. American Chemical Society: Washington, DC, 1991; pp 156-192.
25. Martins Bazani, D. L.; Hempel Lima, J. P.; de Andrade, A. M., MEH-PPV Thin Films for Radiation Sensor Applications. *IEEE Sensors Journal* **2009,** *9* (7), 748-751.
26. Lima Pacheco, A. P.; Araujo, E. S.; de Azevedo, W. M., Polyaniline/poly acid acrylic thin film composites: a new gamma radiation detector. *Materials Characterization* **2003,** *50* (2-3), 245-248.
27. Laranjeira, J. M. G.; Khoury, H. J.; de Azevedo, W. M.; de Vasconcelos, E. a.; da Silva, E. F., Polyaniline nanofilms as a monitoring label and dosimetric device for gamma radiation. *Materials Characterization* **2003,** *50* (2-3), 127-130.
28. Kaoumi, D.; Weber, W. J.; Hattar, K.; Ribis, J., Introduction: Characterization and modeling of radiation damage on materials: state of the art, challenges, and protocols. *Journal of Materials Research* **2015,** *30* (9), 1157-1157.
29. Lee, J.-R.; Park, S.-J.; Seo, M.-K.; Baik, Y.-K.; Lee, S.-K., A study on physicochemical properties of epoxy coating system for nuclear power plants. *Nuclear Engineering and Design* **2006,** *236* (9), 931-937.
30. McQuade, D. T.; Pullen, a. E.; Swager, T. M., Conjugated polymer-based chemical sensors. *Chemical Reviews* **2000,** *100*, 2537-74.
31. Harsányi, G., Polymeric sensing films: new horizons in sensorics? *Materials Chemistry and Physics* **1996,** *43* (1-3), 199-203.
32. Thomas, S. W.; Joly, G. D.; Swager, T. M., Chemical sensors based on amplifying fluorescent conjugated polymers. *Chemical Reviews* **2007,** *107*, 1339-86.
33. Fan, X.; Du, B. Y., Selective detection of trace p-xylene by polymer-coated QCM sensors. *Sensors and Actuators B: Chemical* **2012,** *166*, 753-760.

34. Meilikhov, M.; Furukawa, S.; Hirai, K.; Fischer, R. A.; Kitagawa, S., Binary Janus Porous Coordination Polymer Coating for Sensor Devices with Tunable Analyte Affinity. *Angew. Chem.-Int. Edit.* **2013,** *52* (1), 341-345.
35. David, N. A.; Wild, P. M.; Djilali, N., Parametric study of a polymer-coated fibre-optic humidity sensor. *Meas. Sci. Technol.* **2012,** *23* (3), 8.
36. Giammarco, J.; Zdyrko, B.; Petit, L.; Musgraves, J. D.; Hu, J.; Agarwal, A.; Kimerling, L.; Richardson, K.; Luzinov, I., Towards universal enrichment nanocoating for IR-ATR waveguides. *Chemical Communications* **2011,** *47* (32), 9104-9104.
37. Jacobsohn, L. G.; Sprinkle, K. B.; Roberts, S. a.; Kucera, C. J.; James, T. L.; Yukihara, E. G.; DeVol, T. a.; Ballato, J., Fluoride Nanoscintillators. *Journal of Nanomaterials* **2011,** *2011*, 1-6.
38. Jacobsohn, L. G.; Kucera, C. J.; James, T. L.; Sprinkle, K. B.; DiMaio, J. R.; Kokuoz, B.; Yazgan-Kukouz, B.; DeVol, T. a.; Ballato, J., Preparation and Characterization of Rare Earth Doped Fluoride Nanoparticles. *Materials* **2010,** *3* (3), 2053-2068.
39. Tsyalkovsky, V.; Burtovyy, R.; Klep, V.; Lupitskyy, R.; Motornov, M.; Minko, S.; Luzinov, I., Fluorescent Nanoparticles Stabilized by Poly(ethylene glycol) Containing Shell for pH-Triggered Tunable Aggregation in Aqueous Environment. *Langmuir* **2010,** *26* (13), 10684-10692.
40. Galabura, Y.; Soliani, A. P.; Giammarco, J.; Zdyrko, B.; Luzinov, I., Temperature controlled shape change of grafted nanofoams. *Soft Matter* **2014,** *10* (15), 2567-2573.
41. Liu, Y.; Klep, V.; Zdyrko, B.; Luzinov, I., Synthesis of high-density grafted polymer layers with thickness and grafting density gradients. *Langmuir* **2005,** *21* (25), 11806-11813.
42. Toomey, R.; Freidank, D.; Rühe, J., Swelling Behavior of Thin, Surface-Attached Polymer Networks. *Macromolecules* **2004,** *37* (3), 882-887.
43. Ruhe, J.; Toomey, R., Surface-attached polymer networks: Synthesis and swelling behavior. *ABSTRACTS OF PAPERS …* **2003**, 157-158.
44. Zdyrko, B.; Luzinov, I., Polymer Brushes by the "Grafting to" Method. *Macromolecular Rapid Communications* **2011,** *32* (12), 859-869.
45. Zdyrko, B.; Klep, V.; Luzinov, I., Synthesis and Surface Morphology of High-Density Poly(ethylene glycol) Grafted Layers. *Langmuir* **2003,** *19* (24), 10179-10187.
46. Iyer, K. S.; Luzinov, I., Effect of macromolecular anchoring layer thickness and molecular weight on polymer grafting. *Macromolecules* **2004,** *37* (25), 9538-9545.
47. Peng, J. S.; Ming, L.-J.; Lin, Y.-S.; Lee, S., EPR study of radical annihilation kinetics of γ-ray-irradiated acrylic (PMMA) at elevated temperatures. *Polymer* **2011,** *52*, 6090-6096.
48. Sousa, a. R.; Araújo, E. S.; Carvalho, a. L.; Rabello, M. S.; White, J. R., The stress cracking behaviour of poly(methyl methacrylate) after exposure to gamma radiation. *Polymer Degradation and Stability* **2007,** *92* (8), 1465-1475.
49. Muisener, P. A. O.; Clayton, L.; D'Angelo, J.; Harmon, J. P.; Sikder, A. K.; Kumar, A.; Cassell, A. M.; Meyyappan, M., Effects of gamma radiation on poly(methyl methacrylate)/single-wall nanotube composites. *Journal of Materials Research* **2002,** *17* (10), 2507-2513.

50. Araujo, P. L. B., Polyaniline nanofibers as a new gamma radiation stabilizer agent for PMMA. *eXPRESS Polymer Letters* **2007,** *1*, 385-390.
51. Williams, J. L., Stability of polypropylene to gamma radiation. In *Radiation effects on polymers*, Clough, R. L.; Shalaby, S. W., Eds. American Chemical Society: Washington, DC, 1991; pp 556-568.
52. Choi, J. O.; Moore, J. A.; Corelli, J. C.; Silverman, J. P.; Bakhru, H., Degradation of poly(methylmethacrylate) by deep ultraviolet, x-ray, electron-beam, and proton-beam irradiations. *J. Vac. Sci. Technol. B* **1988,** *6* (6), 2286-2289.
53. Miller, K. J.; Hellman, J. H.; Moore, J. A., Conformations of poly(methyl methacrylate) and its degraded forms upon radiation. *Macromolecules* **1993,** *26* (18), 4945-4952.
54. Busfield, W.; O'Donnell, J., Effects of gamma radiation on copolymers of styrene and methyl methacrylate in the solid state. *Journal of Polymer Science* **1975,** *49* (1), 227-237.
55. Busfield, W. K.; Odonnell, J. H.; Smith, C. A., Radiation degradation of poly(styrene-co-methylmethacrylate). 2. Protective effects of styrene on volatile products, chain scission and flexural strength. *Polymer* **1982,** *23* (3), 431-434.
56. Shultz, A. R.; Roth, P. I.; Rathmann, G. B., Light scattering and viscosity study of electron-irradiated polystyrene and polymethacrylates. *Journal of Polymer Science* **1956,** *22* (102), 495-507.
57. Gedan-Smolka, M.; Lehmann, D.; Cetin, S., Basic investigations for development of new curing mechanisms for powder coatings. *Prog. Org. Coat.* **1998,** *33* (3-4), 177-185.
58. Welp, K. a.; Wool, R. P.; Agrawal, G.; Satija, S. K.; Pispas, S.; Mays, J., Direct Observation of Polymer Dynamics: Mobility Comparison between Central and End Section Chain Segments. *Macromolecules* **1999,** *32*, 5127-5138.
59. Jacobsohn, L. G.; Freire Jr, F. L., Germanium implantation into amorphous carbon films. *Nuclear Instruments and Methods in Physics Research Section B: Beam Interactions with Materials and Atoms* **2001,** *175-177*, 442-447.
60. Güven, O.; Alacakir, A.; Tan, E., An atomic force microscopic study of the surfaces of polyethylene and polycarbonate films irradiated with gamma rays. *Radiation Physics and Chemistry* **1997,** *50* (2), 165-170.
61. Bowmer, T.; Cowen, L., Degradation of polystyrene by gamma irradiation: Effect of air on the radiation induced changes in mechanical and molecular properties. *Journal of Applied Polymer Science* **1979,** *24* (2), 425-439.
62. Kellman, R.; Hill, D. T. J.; D.S., H.; O'Donnell, J.; Pomery, P. J., Gamma radiolysis of styrene-co-methyl acrylate copolymers: an electron spin resonance study

In *Radiation effects on polymers*, Clough, R. L.; Shalaby, S. W., Eds. American Chemical Society: Washington, DC, 1991; pp 119-134.
63. Gou, X.; Liu, D.; Hua, C.; Zhao, J.; Zhang, W., Synthesis and properties of multifunctional hindered amine light stabilizers. *Heterocyclic Communications* **2014,** *20* (1), 15-20.

64. Paine, M. R. L.; Barker, P. J.; Blanksby, S. J., Characterising in situ activation and degradation of hindered amine light stabilisers using liquid extraction surface analysis-mass spectrometry. *Analytica Chimica Acta* **2014,** *808*, 190-8.
65. Malatesta, V.; Neri, C.; Ranghino, G., Molecular mechanics and dynamics studies of polysiloxane-based hindered amine light stabilizers (HALS). *Macromolecules* **1993,** *26*, 4287-4292.
66. Falicki, S.; Gosciniak, D. J.; Cooke, J. M.; Cooney, J. D.; Carlsson, D. J., Polypropylene stabilization during gamma irradiation and during post-gamma storage. *Polymer Degradation and Stability* **1994,** *43* (1), 117-124.
67. Garcia-Uriostegui, L.; Dionisio, N.; Burillo, G., Evaluation of 2-vinylnaphthalene and 4-vinylbiphenyl as antirads to increase the radiation resistance of poly(vinyl chloride). *Polymer Degradation and Stability* **2013,** *98* (7), 1407-1412.
68. Mlsna, T. E.; Cemalovic, S.; Warburton, M.; Hobson, S. T.; Mlsna, D. a.; Patel, S. V., Chemicapacitive microsensors for chemical warfare agent and toxic industrial chemical detection. *Sensors and Actuators B: Chemical* **2006,** *116* (1-2), 192-201.
69. Patel, S. V.; Mlsna, T. E.; Fruhberger, B.; Klaassen, E.; Cemalovic, S.; Baselt, D. R., Chemicapacitive microsensors for volatile organic compound detection. *Sensors and Actuators B: Chemical* **2003,** *96* (3), 541-553.
70. Burcu, D.; Viktorya, A.; Sema, Ö. A., Computational Insight into the Explosive Detection Mechanisms in Silafluorene- and Silole-Containing Photoluminescent Polymers. *Journal of Physical Chemistry C* **2014,** *118* (12), 6385−6397.
71. Chrissafis, K.; Bikiaris, D., Can nanoparticles really enhance thermal stability of polymers? Part I: An overview on thermal decomposition of addition polymers. *Thermochimica Acta* **2011,** *523*, 1-24.
72. Chrissafis, K.; Bikiaris, D., Can nanoparticles really enhance thermal stability of polymers? Part I: An overview on thermal decomposition of addition polymers. *Thermochimica Acta* **2011,** *523* (1-2), 1-24.
73. Ionita, P.; Spafiu, F.; Ghica, C., Dual behavior of gold nanoparticles, as generators and scavengers for free radicals. *Journal of Materials Science* **2008,** *43* (19), 6571-6574.

CHAPTER 5. SYNTHESIS AND SENSING PROPERTIES OF GRAFT COPOLYMER NANOFOAM LAYER

5.1. Introduction

The previous chapters of this dissertation were dedicated to synthesis and swellability of multicomponent PGMA-based graft copolymer network. The combinatorial approach used there can in principle be used to investigate other properties of such materials, including the collapse of the metastable state referred to as nanofoam in the present chapter. Besides applications in sensor technologies that are discussed here, it provides a new prospective on the fundamental properties of PGMA networks modified by "grafting to" method.

The vast majority of sensor devices, and, therefore, sensing films, are designed to allow the online monitoring to give a rapid response in the presence of an analyte. The ability of the polymer films to recover their initial pre-exposure properties is considered to be one of the key features of the devices while irreversibility is commonly viewed as a drawback.[1-2] However, there is also a significant demand for systems employed for off-line sensing, where the occurrence of a chemical event can be detected and analyzed post-factum. In this case, the information can be recorded through the occurrence of a chemical reaction[3-8] or long-lasting physical changes in the structure of the active sensor material.[9-10] For instance, off-line sensing systems are essential in situations where chemical

events/incidents might occur but no power and/or connectivity are available. These systems are also important when forensic evidence (*e.g.* environmental monitoring or international treaty verification) is needed. This requires the development of sensors/sensing polymer films that are capable of accumulating essentially an encrypted signal and be readable in a post-exposure regime. It is necessary to point out that the current polymer materials being developed for off-line sensing are tailored very specifically to identify certain chemical events. Therefore, in order to detect new substances or chemical events, alternative polymer films or film arrays have to be developed and tested. To this end, an original and effective approach to the fabrication of polymer films that are able to record the presence of a variety of volatile chemical compounds in an off-line regime is reported here. The film is made of gradient polymer nanofoam, a tunable sensing material with structurally built-in sensing and recording capabilities.

In general, the nanofoam film is a surface-grafted cross-linked polymer network in a metastable extended configuration that can relax back a certain degree upon exposure to external stimuli. Recently, a uniform (without a chemical composition gradient) fabrication of the nanofoam and its response to temperature variation has been reported.[11] Specifically, the grafted nanofoam was shown to possess the behavior of a shape-memory material[12] exhibiting gradual mechanical contraction at the nanometer scale as the temperature was increased. By modification of the nanofoam with polymer grafting, an absolute nanoscale mechanical response of the porous polymer film can be tuned.

Since the contraction of the nanofoam is caused by forces associated with conformational changes of stretched macromolecular chains, it became obvious that the

relaxation of the chains can be caused similarly by plasticization of the extended grafted polymer chains with the volatile chemical compounds absorbed by the nanofoam.[13] The degree of the chain relaxation is associated with the thermodynamic affinity between the polymer chains and the volatile compounds. Therefore, the key point in the design of the detecting/monitoring platform reported here is the grafted nanofoam that has prescribed chemical gradients and, therefore, also possesses a gradually changing local affinity to volatile substances along the surface. On exposure to specific analytes, the film locally and irreversibly changes its internal structure at the nanolevel. The structural transformation resulting from the exposure causes significant changes in the thickness and density profile of the polymeric film, which in turn affect local optical properties such as refractive index and optical absorption. The changes in local film morphology under exposure are irreversible and provide a permanent record or 'fingerprint' for the chemical event of interest. This permanent modification in the film nanostructure can be directly detected *via* changes in the film surface profile and/or the optical characteristics of the light propagating in the waveguide. It is important to highlight that the initial surface profile and structure of the nanofoam film is encrypted by the unique conditions that were used to fabricate the nanoporous film and practically impossible to be replicated without prior knowledge.

Specifically, in this chapter I have used the three-component gradient PGMA-based coatings described in previous chapters to prepare nanofoam. I have followed the patterns of collapse of the extended conformation as a result of exposure to chemical vapors and demonstrated that these patterns are, in fact, solvent-specific. In collaboration with Dr.

Kimerling's group from MIT, I have demonstrated the working example of nanofoam-based sensor where an array of photonic microdisk resonators acts as a sensing element.

5.2. Materials and methods

5.2.1. Foaming of the PGMA-based polymer thin films

The foaming was conducted inside a foaming stage, which consists of a vacuum chamber where swelling and solvent sublimation takes place, and a copper temperature-regulated table that was cooled with liquid nitrogen. The table was equipped with a thermocouple that was used to control the temperature of the sample. The gradient films were swollen in a solvent good for all polymers (chloroform) and placed on the temperature-regulated sample table to freeze in their swollen state. The foaming stage was kept at −90 °C using liquid nitrogen, with the subsequent solvent removal (sublimation) done under reduced pressure (50 mTorr).

5.2.2. Solvent exposure of the gradient nanofoam films

The samples were exposed to saturated vapors of one of three solvents, toluene, methanol, or acetone, for 40 min. The film thickness profiles were measured and then the samples were re-foamed. A total of three exposures were done for each solvent.

5.2.3. Preparation of silicon nitride microresonators

Fabrication of the SiN_x resonators followed the standard Si microfabrication processes.[13] Thin film nitride was grown onto silicon wafers with 3 μm thermal oxide using LPCVD. Photolithography was performed on i-line stepper to define the resonator patterns in the SiN_x. Subsequently, the patterns were transferred to the film by a reactive ion etch

using a mixture of CF_4 and CHF_3 gases. The fabricated silicon nitride waveguide has dimensions of 800 nm (width) by 400 nm (height), and the radius of the resonator is 50 μm. Fabrication of the SiN_x resonators has been performed by Qingyang Du and Vivek Singh working under supervision of Dr. Agarwal and Dr. Kimerling in MIT.

5.2.4. Polymer coating of the silicon nitride photonic resonators

The PGMA layer was deposited on the surface of all three resonator arrays used in this study by dip-coating. PS and P2VP were grafted to the PGMA layers on the surface of respective resonators following the procedure analogous to the one used for the gradient preparation. To reach a high level of grafting, the PS was grafted at 150 °C and the P2VP was grafted at 120 °C. Each layer was subsequently foamed and cleaved into four individual arrays of waveguides so that each array could be exposed to the corresponding solvent.

5.2.5. Optical transmission measurement

All transmission measurements were performed on a Newport waveguide measurement system with a tunable laser (1525–1610 nm) coupled to the input facet and a LUNA Optical Vector Analyzer (OVA) coupled to the output facet of the devices with low loss, lens-tip optical fibers. The optical transmission spectrum was characterized on a Newport Auto Align workstation and an optical vector analyzer (LUNA Technologies OVA-5000) with a built-in tunable laser. Near-infrared wavelength light was coupled in and out through the bus waveguide using a tapered lens-tip fiber. All measurements were performed at a constant temperature of 19.7 ± 0.2 °C. The resonator samples were placed on a static stage while the input and output fibers were on precise software-controlled,

motorized three-axis stages that allow movements as small as 10 nm. The input fiber was aligned by observing the waveguide mode exiting the output facet using an infrared (IR) camera. The output fiber was then aligned using an optical power meter to read the power being coupled out of the output facet. These measurements have been performed by Qingyang Du and Vivek Singh working under supervision of Dr. Agarwal and Dr. Kimerling in MIT. The resulting pre-exposure and post-exposure spectra for each waveguide were plotted together. Lorentz peak function was used for the fitting of the corresponding peaks using Origin 2016 software. The peak shift was calculated as the difference between the Lorentz fit centers of the nanofoam spectra before and after exposure. The peak shift values for waveguides of the same array were averaged.

5.3. Gradient nanofoam film: principles of formation and operation

The fabrication of the gradient nanofoam film is achieved in four major steps (**Figure 5.1**). Firstly, a film made of polymer possessing epoxy groups in monomeric units is deposited on a surface. Secondly, the film is cross-linked *via* a reaction of the epoxy groups to create a coating that is non-soluble yet is able to swell. Next, the film is grafted with different polymers capable of reacting with the remaining (unreacted) epoxy functionality. The extent of the film reaction with each polymer is dependent on the spatial location within the film. In essence, a gradient film whose chemical composition varies in two directions isd generated. In this way every point of the film possesses its own unique composition. Finally, the film is submerged in a solvent or solvent mixture so that it swells

and is freeze-dried under reduced pressure. Thus, following the removal of the solvent(s) by sublimation, a nanoporous polymer film is obtained.

The resulting film is below the glass transition temperature (T_g) at the temperatures of operation and possesses the behavior of a nanoscale shape-memory material, which exhibits mechanical action under external stimulus (**Figure 5.1**). More specifically, the coating (which is *not* in thermodynamic equilibrium in the porous state) is able to 'remember' its original non-porous shape determined by the network elasticity. Exposure of the film to a chemical vapor that interacts with the macromolecules in the film causes plasticization of the film. As soon as the macromolecules attract a sufficient amount of the target chemical, the T_g of the polymer chains decreases. Therefore, the chains become mobile and the film shrinks. Since the film possesses a graded chemical composition, different locations of the film interact in different ways with the target chemical. Specifically, certain regions of the film that have a higher thermodynamic affinity to a chemical shrink to a higher extent, creating a unique thickness pattern for that specific chemical (**Figure 5.1**). The resulting changes in local film morphology are irreversible and provide a permanent record or 'fingerprint' for the chemical event of interest.

The obtained record is encrypted by the knowledge of: (i) unique conditions that were used to fabricate the nanoporous film and (ii) level of the film response upon chemical vapor exposure. In fact, the nanofoam film is produced in two principal steps: synthesis of the gradient polymer film, followed by freeze-drying of the film swollen in a solvent (or solvent mixture). Therefore, the initial surface profile and level of response of the film to the presence of chemical vapors is encrypted by an operator *via*: (a) film composition at

nano/micro/macro-levels controlled during synthesis; (b) solvent composition, which controls the degree of film swelling prior to and during freeze drying; and (c) freeze-drying conditions, which include pressure and temperature. Indeed, during the preliminary studies it was experimentally determined that these are the parameters controlling the nanofoam morphology and behavior. All of these manipulations are practically impossible to replicate without prior knowledge of the procedures.

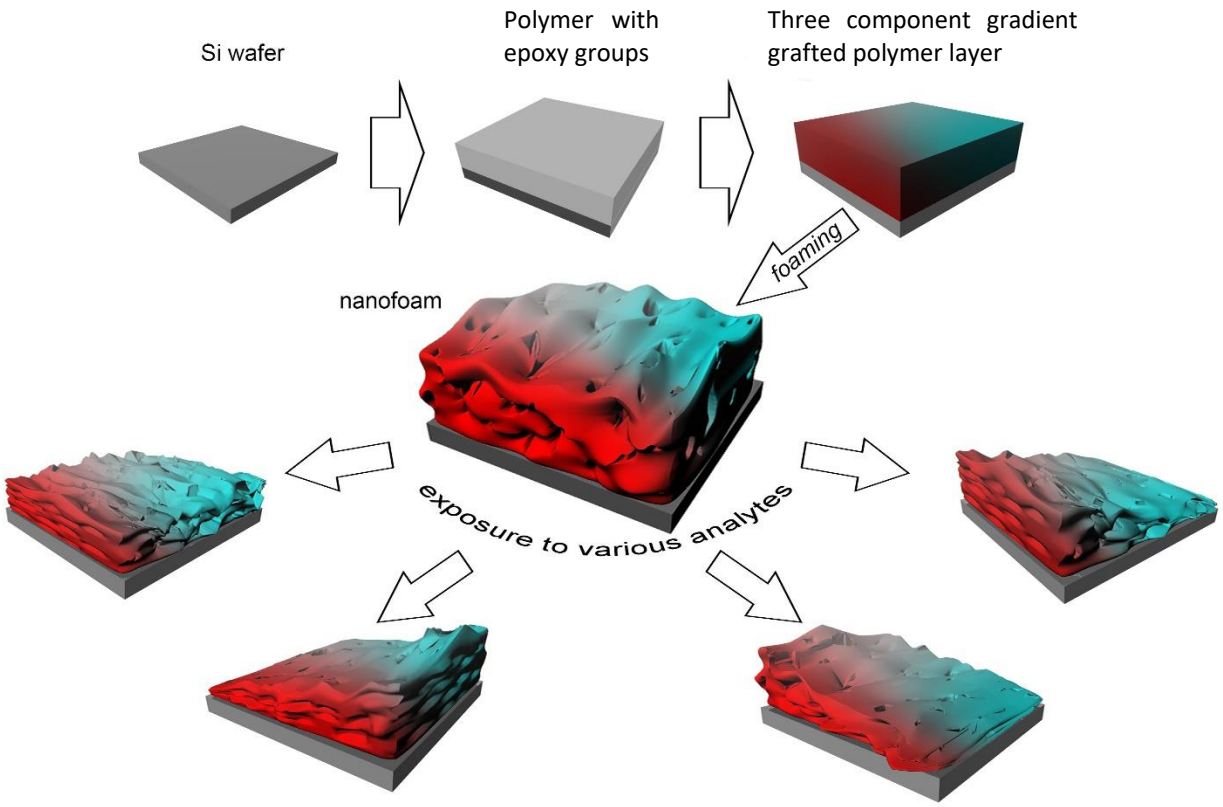

Figure 5.1. Schematic for the nanofoam film synthesis and operation. Once foamed, the gradient polymer layer can collapse in a solvent-specific way creating unique permanent pattern.

In general, the concept of encryption presumes the presence of the ‘message’, protected by the ‘key’, which should be known to decipher the ‘massage’. In this case, the

"message" is the history of the chemical vapor exposure that leaves the unique signature of nanofoam collapse. The 'key' is the knowledge of the pattern produced as nanofoam is exposed to particular chemical vapor. Once the film collapses upon exposure to a chemical vapor, the only way to erase the pattern is *via* heating the film to above T_g or exposing it to a number of solvents to collapse the surrounding region entirely. These manipulations would provide a clear and definite record of tampering with the device.

5.4. Formation of the nanofoam film

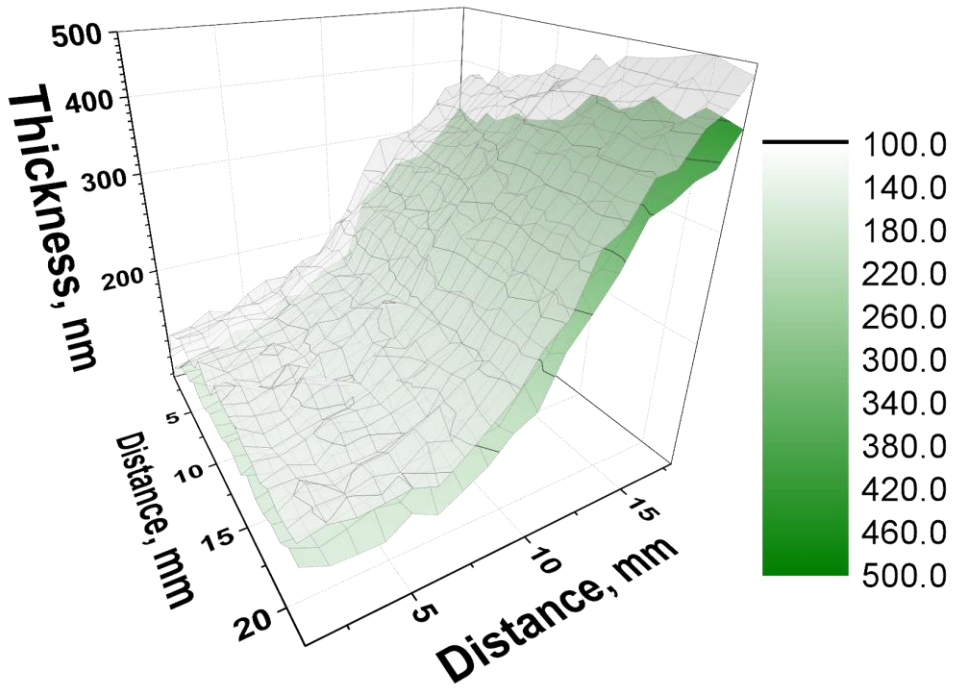

Figure 5.2. Thickness of the representative gradient grafted layer *versus* surface coordinate before (bottom) and after (top) the foaming.

The foaming consisted of swelling the grafted polymer layer in chloroform followed by freeze-thawing and sublimation of the solvent. Chloroform was selected as it is a good solvent for all three polymers constituting the film and can be frozen at −59 °C, an experimentally reachable temperature. To swell the polymer film, a small amount of the solvent was placed drop-wise on the film surface. Next, the sample was cooled to freeze the chloroform. Finally, the solvent was sublimated under reduced pressure. From visual inspection it was clear that the transparent grafted film became opaque after the solvent sublimation. The loss of transparency indicated a scattering of light because of pore formation. **Figure 5.2** shows the thickness map of the typical fabricated nanofoam gradient polymer films in comparison with a map of the film before the foaming procedure. The thickness of the gradient film (measured by reflectometry) increased in all compositional areas by 17 ± 4%. AFM imaging showed a significant change in morphology of the gradient film after the foaming (**Figure 5.3**).

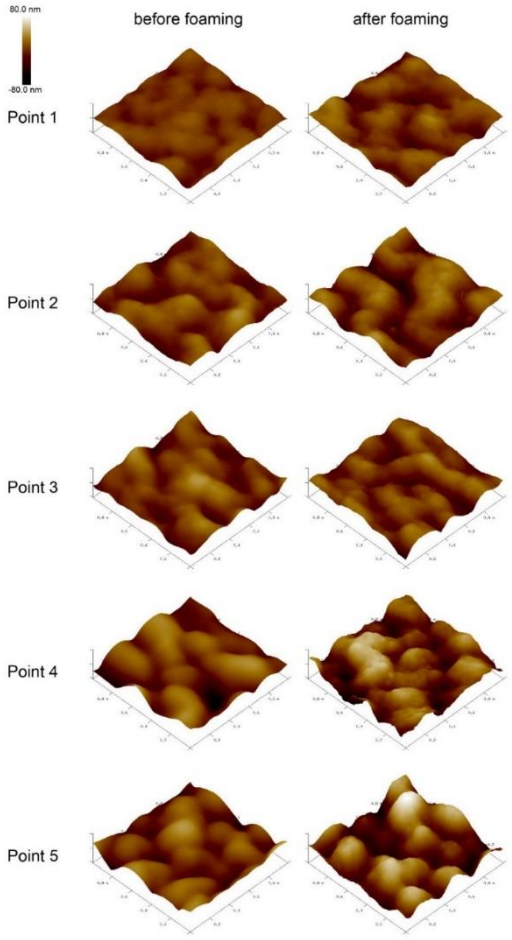

Figure 5.3. AFM (1x1 microns) topographical images for the gradient grafted layer at different locations before and after the foaming. The approximate location on the gradient film is marked on **Figure 3.6.**

Specifically, a formation of pores and a corresponding increase in film roughness were observed. RMS roughness of the film increased from 7−20 nm to 12−27 nm due to development of the open pores within the layer. To identify whether the grafted nanofoam had pores throughout the film, an experiment to visualize pore locations in the grafted nanofoam layer was conducted. Specifically, a 'nanotomography' approach was utilized to analyze the inner structure of the grafted film after solvent sublimation.[11, 14] This approach is based on a step-by-step air plasma etching of the film with a subsequent step-by-step AFM analysis of the etched surface, after which the morphology inside the film is revealed. Low-power air plasma (at 1 minute intervals) was used to etch the film. Reflectometry measurements were used to track the thickness of the etched polymer film after each step. Results of the experiment are presented on **Figures 5.4 and 5.5.** The AFM imaging revealed that, in fact, pores were situated not only on the surface but also throughout the foamed layer. The sizes of the interconnected and open pores inside the film were estimated to be between 10 nm and 200 nm.

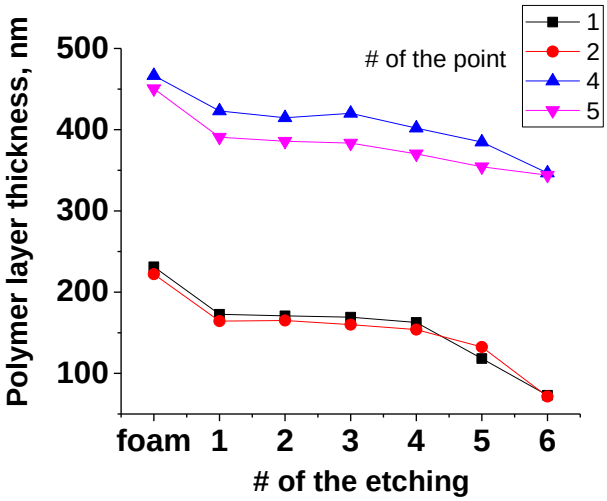

Figure 5.4. Thickness of the nanofoam polymer layer in course of the plasma etching at different points on the gradient sample indicated on **Figure 3.8**.

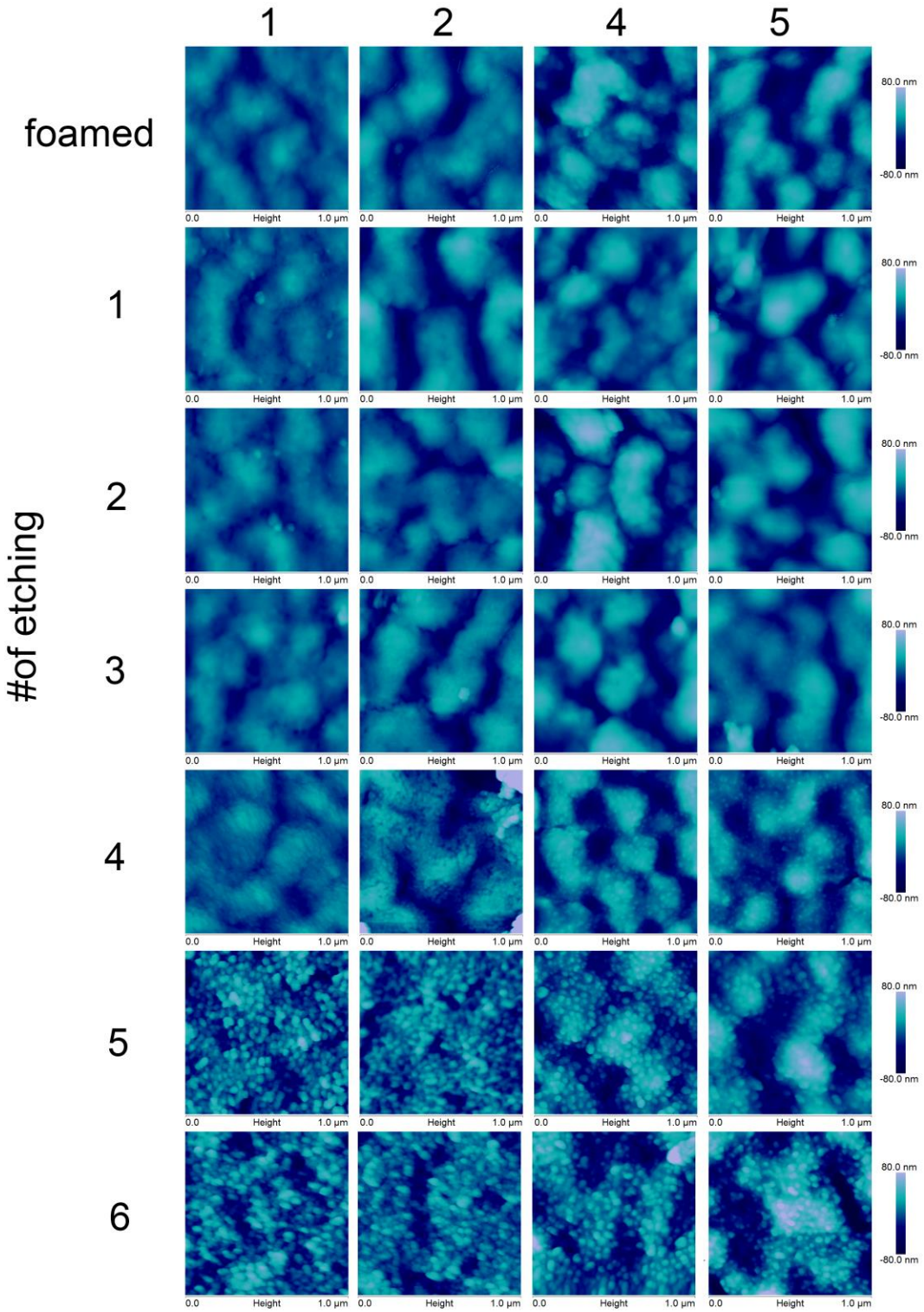

Figure 5.5. AFM images of the nanofoam gradient film before and in course of the plasma etching at different points on the gradient sample indicated on **Figure 3.6**.

5.5. Operation of the nanofoam film as a sensing/recording element

In order to characterize the response of the gradient nanofoam polymer layer to the vapors of volatile organic compounds, the nanofoam samples were exposed to methanol, toluene, or acetone. The solvents were selected based on their affinity to the macromolecules constituting the gradient nanofoam.[15-16] Acetone was selected as it is a good solvent for PGMA and a moderate solvent for PS and P2VP. Toluene was chosen as it is a good solvent for PS, moderate for PGMA, and bad for P2VP. Methanol was selected as it is a good solvent for P2VP, but bad for the other two components. This set of solvents covers predominantly van der Waals, polar, and hydrogen bonding between a solvent molecule and polymer layer. After the exposure, the samples were evacuated from the solvent vapor and allowed to dry overnight. Next, their thicknesses were mapped using the scanning reflectometer. The extent of collapse at any one point of the sample is defined by a dimensionless parameter alpha:

$$\alpha = 1 - (d_{exposed} - d_{initial})/(d_{foamed} - d_{initial}) \quad (1)$$

where $d_{initial}$, d_{foamed}, and $d_{exposed}$ are the initial thickness of the film at the given point, the thickness after foaming, and the thickness after exposure to the solvent vapors, respectively. A higher value of the parameter alpha indicates a higher degree of collapse of the nanofoam. Specifically, the parameter reflects the relative value of the film collapse normalized by the thickness gained during foaming, or it shows the fraction of the added

(*via* foaming) thickness that is gone as the result of the vapor exposure. This parameter was selected as it allows a straightforward comparison of degree of collapse for points on the nanofoam with different absolute thicknesses.

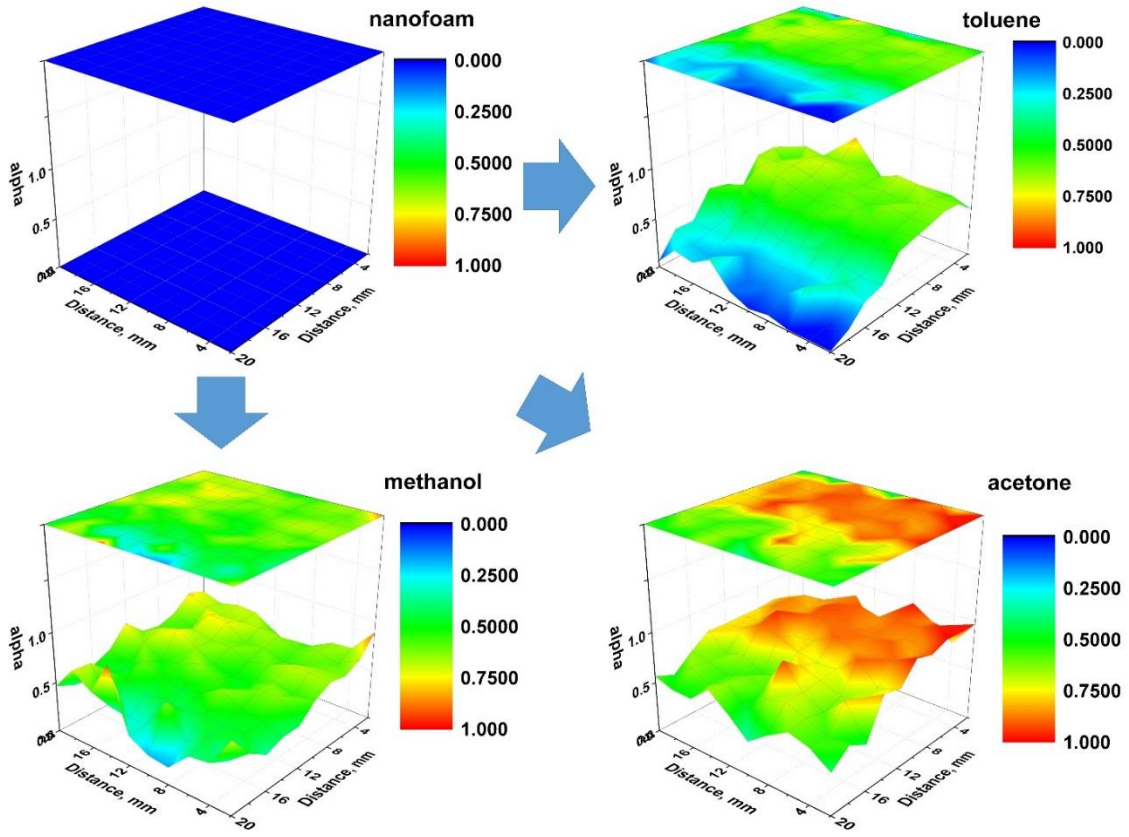

Figure 5.6. Collapse extent (α) of gradient nanofoam film caused by exposure to vapors of toluene, methanol and acetone. Three solvent generate drastically different patterns of collapse. The data was averaged for 3 parallel gradient samples.

Figure 5.6 shows the collapse extent (α), equal to 0 for the non-exposed gradient nanofoam (**Figure 5.6a**) and the nanofoam exposed to toluene, methanol and acetone **(Figures 5.6b, 5.6c, and 5.6d**) averaged from 3 parallel experiments. As it is evident from **Figure 5.6**, each solvent generates its own pattern of collapse, which is defined by the

interplay between the thermodynamic affinity of the solvent to the polymer layer and the grafting density of PS and P2VP. The observed film collapse is permanent and does not change with time at room temperature. The obtained result clearly demonstrates that the nanofoam gradient polymer film can be used for off-line sensing and encrypted recording of chemical events and differentiation between them.

In order to perform a more detailed investigation of the composition-dependent nanofoam response, the collapse data was plotted in a triangular diagram (**Figure 5.7**). One could expect that, for example, the PS-rich regions would interact with toluene more efficiently than the rest of the film and cause stronger collapse. As it turns out, the nanofoam collapse follows another pattern. The comparison with the swelling phase diagrams (**Figure 4.1**) indicates that high values of the swelling in a specific solvent observed at a given point on the film do not correspond to the higher values of the nanofoam response to the same solvent. One could hypothesize that swelling of the foamed structure is a necessary pre-requisite for the collapse of the nanofoam as it is essentially a plasticization phenomena, however, the increase of PGMA content leads to increase of parameter α for all the studied solvents while the increase of PS and P2VP content lead to decrease of the film responsiveness (**Figure 5.8**). The individual plots reflect the collapse of three-component nanofoam in a specified vapor as a function of the grafted thickness for PGMA, PS and P2VP. The overall behavior of the collapse is generally very similar for the chemicals studied: the high PGMA content promotes collapse, PS content acts in the opposite direction. This phenomena clearly demonstrates that the volumetric expansion of

the graft-copolymer network due to sorption of chemicals is not directly related to the post-exposure response of the nanofoam.

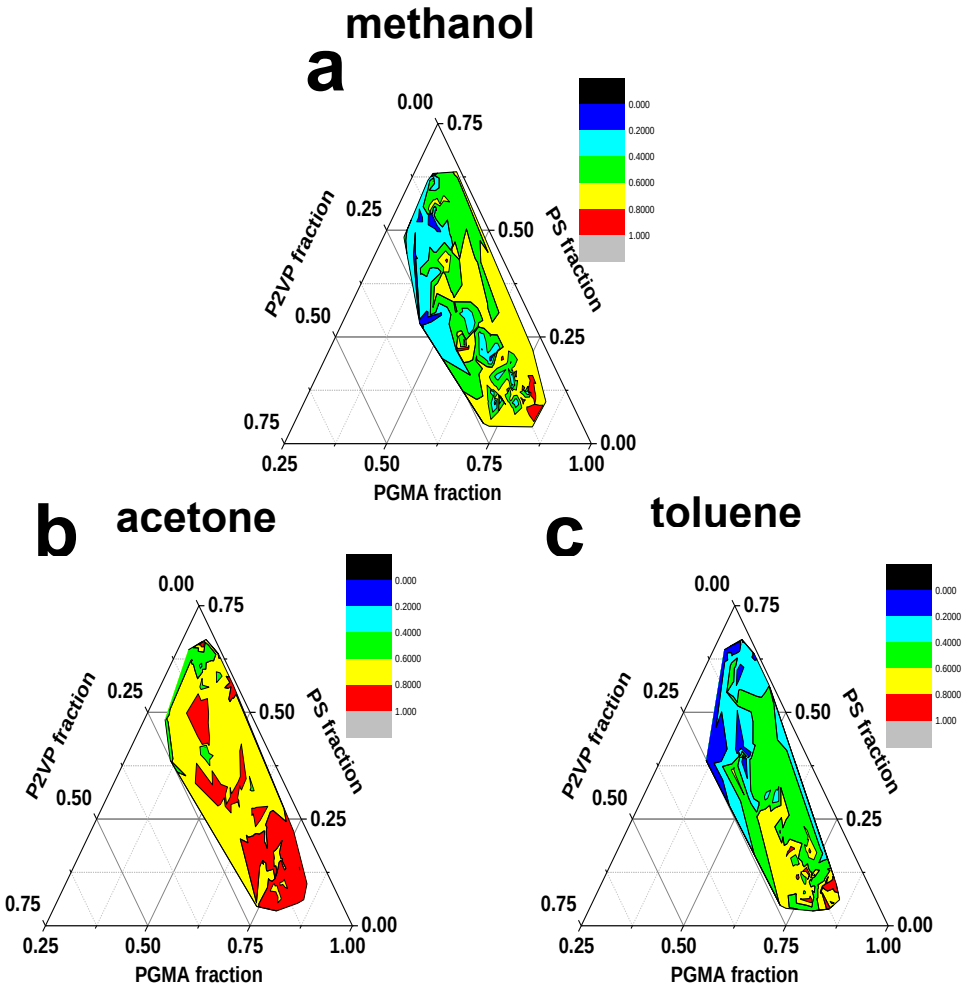

Figure 5.7. Composition-dependent collapse of the three-component nanofoam in methanol (a), acetone (b) and toluene (c) vapors.

The possible explanation of this effect is that PGMA-based graft-copolymer films are essentially nanostructured materials composed of "stems" and "strands" (**Figure 5.9**). The deformation of "strands" generates little mechanical stress, which promotes their swelling, however this portion of the network apparently is not associated with the

formation of any metastable states of the polymer conformation. On contrary, “stems” are intrinsically stiffer, and their limited mobility at temperatures below glass transition is a primal reason for the nanofoam being metastable at room temperatures. The solvent molecules interacting with the “stem” polymer chains plasticize it and cause the collapse of the polymer film. However, there is a heavy competition between “stem” and “strands” for the inclusion of the solvent molecules, and as the amount of grafted material is increased, the solvent molecules tend to be incorporated within “strands”.

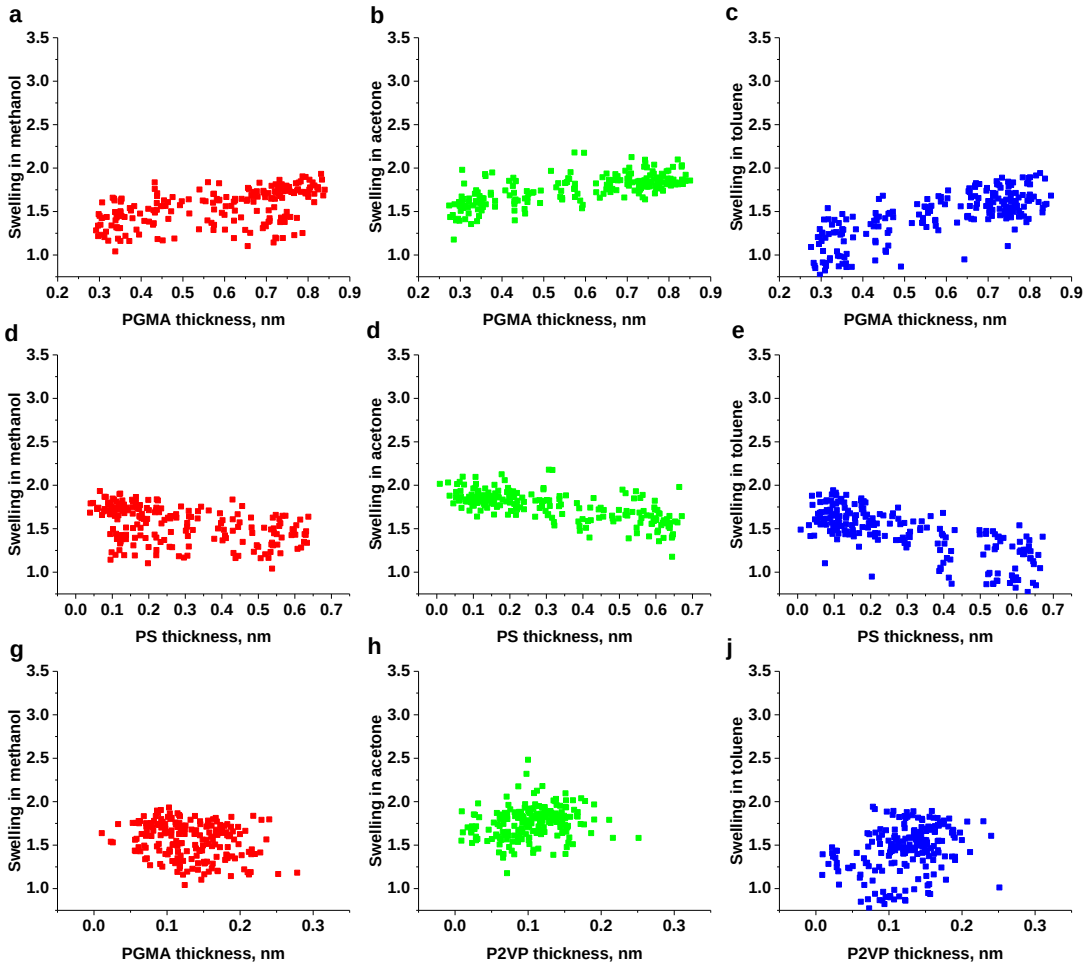

Figure 5.8. Composition-dependent collapse of the three-component nanofoam as a function of respective polymer thickness at a specific point of the film for methanol (a, d, g,), acetone (b, d, h) and toluene (c, e, j).

The grafted chains, P2VP and PS, offer great variability of the polymer affinity to the various solvents, and as the swelling of these regions leads to little elastic stress, more solvent molecules are presented in the “strands”. Consequently, “stems” do not effectively interact with the solvent and their structure is not altered during the exposure. This explains why the PGMA-rich regions of the nanofoam show more collapse then the strongly swelling “sweet spot” region: there is little enthalpic trap for the solvent to interrupt the plastification of the metastable network. This is a very important notion for the future practical application of the nanofoam for the novel sensor applications: the post-exposure response is a function of the most mechanically strained region capable of being is a metastable state.

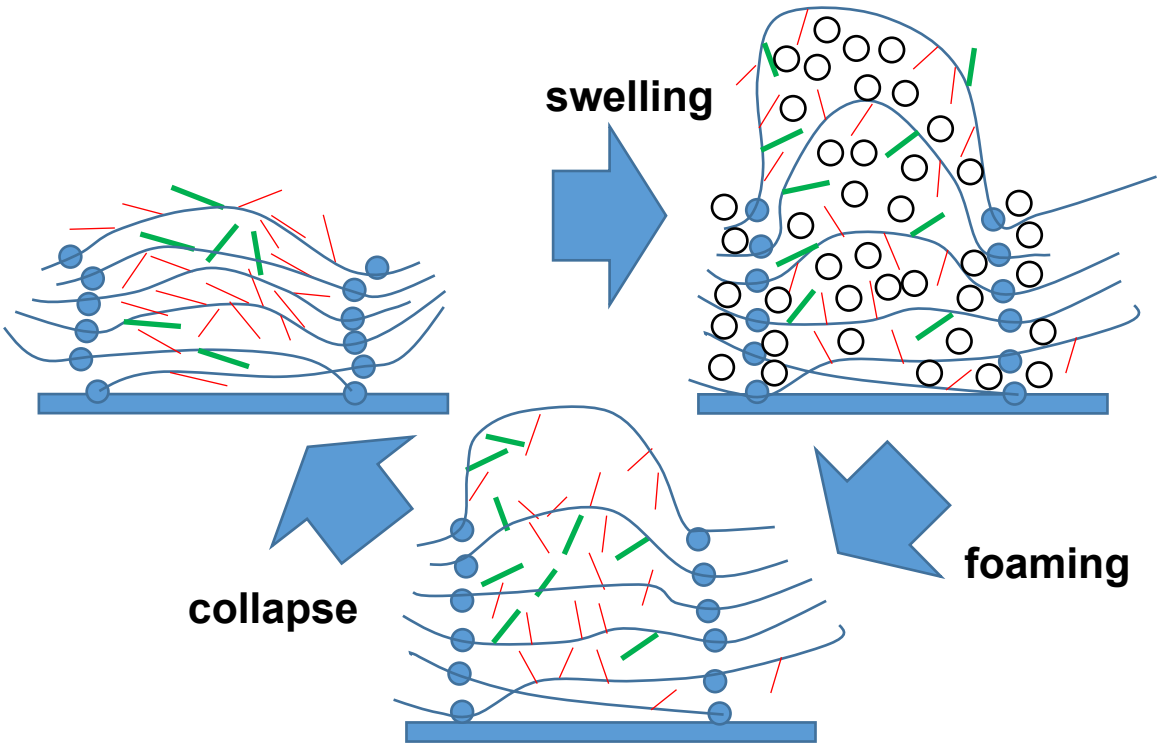

Figure 5.9. The schematic representation of the three-component polymer network undergoing swelling and foaming.

5.6. Monitoring of nanofoam collapse with microring resonators

Sensing/recording nanofoam films were prepared and interrogated on the surface of microring optical resonators (**Figure 5.10**). Microresonators are extremely sensitive to perturbations in the refractive index of their surroundings as well as any changes in optical absorption.[13, 17-18] They offer two different modes of detection that can be exploited for various monitoring applications. As shown in **Figure 5.10c**, a change in the refractive index of the surroundings is reflected as a shift in the resonant peak position while the introduction of optical absorption leads to a change in the peak height or extinction ratio. An effective surface modification of the arrays of optical resonators *via* grafting of nanoscale polymer films for sensing applications was recently demonstrated.[13, 19] In this work, nanofoam films (single composition, without a gradient) were prepared on the surfaces of optical resonators and the refractive indices of the films were measured before and after exposure to the solvent vapors. The custom arrays of microring resonators (made of infrared transparent silicon nitride) were fabricated on silicon wafers covered with 3 μm of thermally-grown SiO_2. **Figure 5.10a** shows a microphotograph of the resonators. The diameter of a microring resonator is 100 μm (0.1 mm). The size of the typical nanofoam film made in this work is on the order of 20×20 mm. Therefore, the array, in principle, can allow optical interrogation of the refractive index and optical absorption at different locations on the nanofoam film.

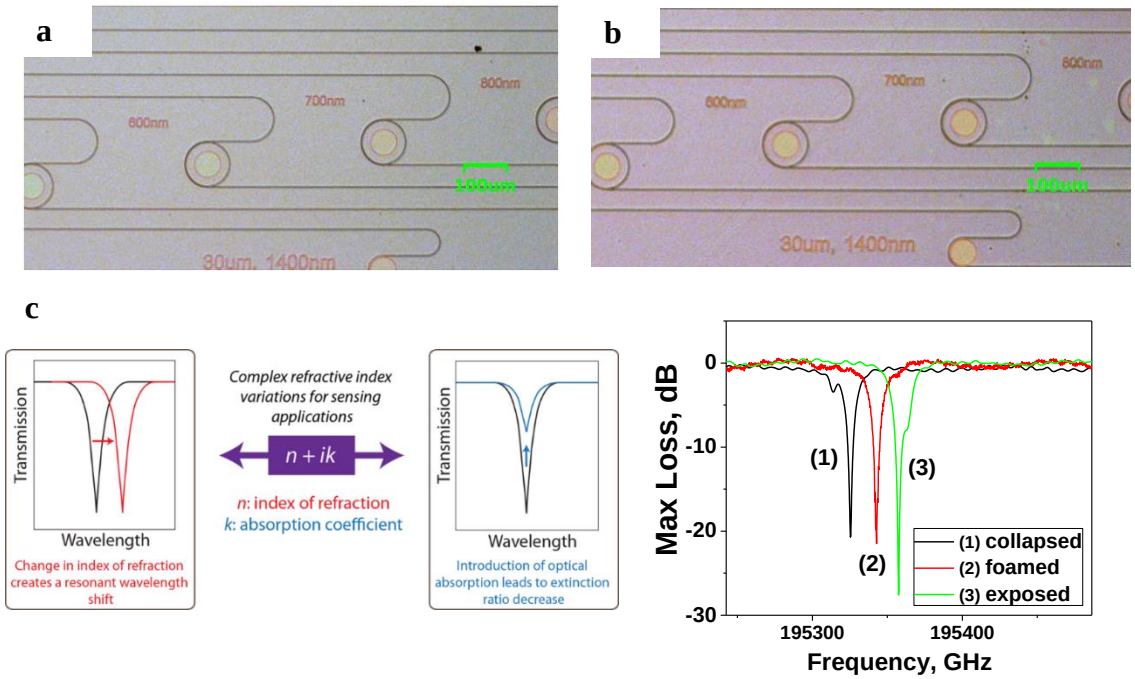

Figure 5.10. Optical micrographs of the microdisc resonators (a) as fabricated and (b) modified with PS/PGMA grafted layer. (c) The microresonator resonance peak alteration in case of changing refractive index (shift) and infrared absorption (peak damping). (d) Example of change in spectrum of the microring resonator covered with nanofoam.

Figure 5.10b shows that a typical grafted layer quite evenly covers the optical devices. Each larger array with a foamed polymer layer was cleaved into four identical waveguide arrays. The transmission spectrum of each waveguide on the array was acquired before exposure to any solvent to characterize the spectra of the foam coating. Optical testing demonstrated that the devices were not destroyed during the modification (polymer layer deposition and foaming) procedure.

Then, the four arrays of microring resonators were exposed to vapors of methanol, acetone, toluene, or chloroform. Vapor contact lasted for 1 h and then the samples were left in ambient air overnight to allow the solvent to fully evaporate. The resonance peaks were subsequently recorded again and compared with the recordings acquired before the

solvent exposure. Also, to obtain the optical characteristics of the collapsed (non-foamed) grafted layers, the refractive index was measured for the samples that were rinsed in chloroform and then dried. The data obtained was averaged for the waveguides of the same array as it was found that the coupling gap had no systematic effect on the peak shift. A typical result of these measurements is presented in **Figure 5.10d**. It is evident that the refractive index changes significantly when the grafted layer is foamed and exposed to a solvent.

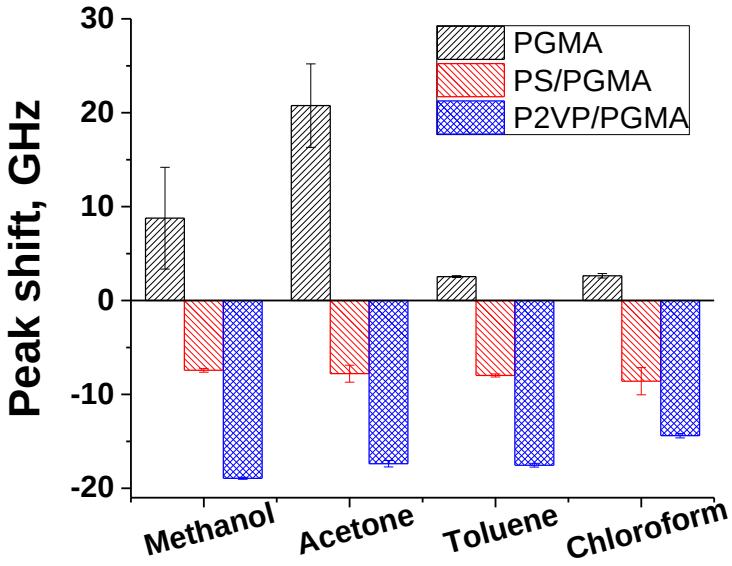

Figure 5.11. Results of optical transmission measurements for the microring resonators covered with 3 different nanofoams exposed to four different solvent vapors.

Figure 5.11 summarizes the results of the measurements for the different nanofoam/solvent vapor combinations. In fact, the volatile organic compounds generate a solvent-specific refractive index change that varies with the chemical composition of the nanofoam film. As evident from the comparison between the solvent responses, it is

possible to generate unique solvent signatures using three channels of information: PGMA, PS/PGMA, and P2VP/PGMA-coated resonator response. This is a direct demonstration of the ability of microring resonator arrays covered with nanofoams to record the presence of chemicals for further detection in a post-exposure regime. It was also found that the most sensitive to the exposure of the solvents (used in this work) are microring resonators covered with PGMA and P2VP/PGMA nanofoams. On the other hand, the resonators covered with PS/PGMA nanofoam shows lower level of optical response. Since the collapse of the nanofoam is dependent on the film composition and grafting density it is foreseen foresee that by adjusting those parameters optical response of the resonators can be tuned to obtain higher sensitivity to exposure to a particular chemical vapor of interest.

5.7. Conclusions

In conclusion, it was demonstrated that the gradient grafted nanofoam films are able to record the presence of volatile chemical compounds in an off-line regime. Namely, exposure of the nanofoam polymer layer to the solvent vapors causes a controllable collapse of the porous structure that is found to be dependent on the chemical nature of the nanofoam. The collapse is irreversible and solvent-specific, allowing for the use of the nanofoams in the recording of chemical events. The sensing/recording nanofoam films can be prepared and interrogated on the surface of microring optical resonators. It was determined that exposure of the microring resonators covered with the nanofoam films to solvent vapors generates a solvent-specific refractive index change that varies with the chemical composition of the nanofoam film. The collapse of the metastable nanofoam

network is associated with structural changes in the “stems”, so PGMA-rich regions demonstrate stronger response for all studied solvents. This provides new insights on the fundamentals of the nanofoam physics and the mechanism of its collapse.

5.8. References

1. Wang, D.-H.; Cui, Y.-Z.; Tao, F.-R.; Niu, Q.-F.; Li, T.-D.; Xu, H., A novel film of conjugated polymer grafted onto gelatin for detecting nitroaromatics vapor with excellent inhibiting photobleaching. *Sensors and Actuators B: Chemical* **2016,** *225*, 319-326.
2. Potyrailo, R. A.; Surman, C.; Nagraj, N.; Burns, A., Materials and Transducers Toward Selective Wireless Gas Sensing. *Chemical Reviews* **2011,** *111* (11), 7315-7354.
3. Chan, C.-Y.; Guo, J.; Sun, C.; Tsang, M.-K.; Tian, F.; Hao, J.; Chen, S.; Yang, M., A reduced graphene oxide-Au based electrochemical biosensor for ultrasensitive detection of enzymatic activity of botulinum neurotoxin A. *Sensors and Actuators B-Chemical* **2015,** *220*, 131-137.
4. Zhang, Y.; Zhao, H.; Wu, Z.; Xue, Y.; Zhang, X.; He, Y.; Li, X.; Yuan, Z., A novel graphene-DNA biosensor for selective detection of mercury ions. *Biosensors & bioelectronics* **2013,** *48*, 180-187.
5. Vaille, J. R.; Ravotti, F.; Garcia, P.; Glaser, M.; Matias, S.; Idri, K.; Boch, J.; Lorfevre, E.; McNulty, P. J.; Saigne, E.; Dusseau, L., Online dosimetry based on optically stimulated luminescence materials. *Ieee Transactions on Nuclear Science* **2005,** *52* (6), 2578-2582.
6. Angelini, E.; Grassini, S.; Neri, A.; Parvis, M.; Perrone, G.; Ieee, Plastic Optic Fiber Sensor for Cumulative Measurements. In *I2mtc: 2009 Ieee Instrumentation & Measurement Technology Conference, Vols 1-3*, 2009; pp 1619-1623.
7. Rakow, N. A.; Suslick, K. S., A colorimetric sensor array for odour visualization. *Nature* **2000,** *406* (6797), 710-713.
8. McQuade, D. T.; Pullen, A. E.; Swager, T. M., Conjugated polymer-based chemical sensors. *Chemical reviews* **2000,** *100* (7), 2537-2574.
9. Zhang, Y.; Qiu, J.; Hu, R.; Li, P.; Gao, L.; Heng, L.; Tang, B. Z.; Jiang, L., A visual and organic vapor sensitive photonic crystal sensor consisting of polymer-infiltrated SiO2 inverse opal. *Physical Chemistry Chemical Physics* **2015,** *17* (15), 9651-9658.
10. You, B.; Ho, C.-H.; Zheng, W.-J.; Lu, J.-Y., Terahertz volatile gas sensing by using polymer microporous membranes. *Optics Express* **2015,** *23* (3), 2048-2048.
11. Galabura, Y.; Soliani, A. P.; Giammarco, J.; Zdyrko, B.; Luzinov, I., Temperature controlled shape change of grafted nanofoams. *Soft Matter* **2014,** *10* (15), 2567-2573.

12. Xie, T.; Page, K. A.; Eastman, S. A., Strain-Based Temperature Memory Effect for Nafion and Its Molecular Origins. *Advanced Functional Materials* **2011,** *21* (11), 2057-2066.
13. Singh, V.; Lin, P. T.; Patel, N.; Lin, H.; Li, L.; Zou, Y.; Deng, F.; Ni, C.; Hu, J.; Giammarco, J.; Soliani, A. P.; Zdyrko, B.; Luzinov, I.; Novak, S.; Novak, J.; Wachtel, P.; Danto, S.; Musgraves, J. D.; Richardson, K.; Kimerling, L. C.; Agarwal, A. M., Mid-infrared materials and devices on a Si platform for optical sensing. *Science and Technology of Advanced Materials* **2014,** *15* (1), 014603.
14. Usov, D.; Gruzdev, V.; Nitschke, M.; Stamm, M.; Hoy, O.; Luzinov, I.; Tokarev, I.; Minko, S., Three-Dimensional Analysis of Switching Mechanism of Mixed Polymer Brushes. *Macromolecules* **2007,** *40* (24), 8774-8783.
15. Bliznyuk, V.; Galabura, Y.; Burtovyy, R.; Karagani, P.; Lavrik, N.; Luzinov, I., Electrical conductivity of insulating polymer nanoscale layers: environmental effects. *Physical Chemistry Chemical Physics* **2014,** *16* (5), 1977-1986.
16. Ionov, L.; Sidorenko, A.; Stamm, M.; Minko, S.; Zdyrko, B.; Klep, V.; Luzinov, I., Gradient mixed brushes: "Grafting to" approach. *Macromolecules* **2004,** *37* (19), 7421-7423.
17. Hu, J. J.; Sun, X. C.; Agarwal, A.; Kimerling, L. C., Design guidelines for optical resonator biochemical sensors. *Journal of the Optical Society of America B-Optical Physics* **2009,** *26* (5), 1032-1041.
18. Petit, L.; Carlie, N.; Zdyrko, B.; Luzinov, I.; Richardson, K.; Hu, J. J.; Agarwal, A.; Kimerling, L.; Anderson, T.; Richardson, M., Development of novel integrated bio/chemical sensor systems using chalcogenide glass materials. *International Journal of Nanotechnology* **2009,** *6* (9), 799-815.
19. Giammarco, J.; Zdyrko, B.; Petit, L.; Musgraves, J. D.; Hu, J.; Agarwal, A.; Kimerling, L.; Richardson, K.; Luzinov, I., Towards universal enrichment nanocoating for IR-ATR waveguides. *Chemical Communications* **2011,** *47* (32), 9104-9106.

CHAPTER 6. GMA-BASED GRAFT COPOLYMERS BY "GRAFTING THROUGH" METHOD

6.1. Introduction

"Grafting through" in a form of copolymerization of macromonomers is a very promising strategy to synthesize functional GMA-based copolymers. In this chapter, I present synthesis and basic properties of such materials which builds a solid fundament for their applications discussed in the following chapters.

The modification of surfaces and colloidal structures allows for the fine tuning of their properties, which becomes crucially important for design and compatibilization of components within complex functional systems.[1-2] The natural variability of substrates and diversity of the desired properties call for methods of surface modification that could deliver required characteristics to a wide range of materials in the most straightforward and cost-effective way. To this end, grafted polymer layers have drawn considerable attention due to the ability to control surface properties of modified substrates, robustness of the layers, and diversity of chemistries suitable for the layer formation.[1-10] Despite the fact that significant advancements in synthesis of the grafted polymer layers have been made over the recent years, the developed protocols of interface modifications face challenges when being implemented in large-scale manufacturing set-up. Indeed, typical grafting procedure is a multi-step process where every stage inevitably imposes limitations on the nature of substrate, generates solvent/chemical waste and complicates the overall operation. Thus,

there is a demand on environmentally-friendly surface modification protocol with a minimum number of technological steps. To this end, we have demonstrated that using reactive copolymers functional grafted polymer layers can, in principle, be obtained in a single step from water or with minimal use of solvents and without post-processing rinsing. Specifically, the present chapter focuses on a cross-linkable amphiphilic (statistical) copolymers (**Figure 6.1**) containing oligo(ethylene glycol) methyl ether methacrylate (OEGMA), glycidyl methacrylate (GMA), and lauryl methacrylate (LMA), which can be straightforwardly covalently attached to a number of solid surfaces and colloidal objects.

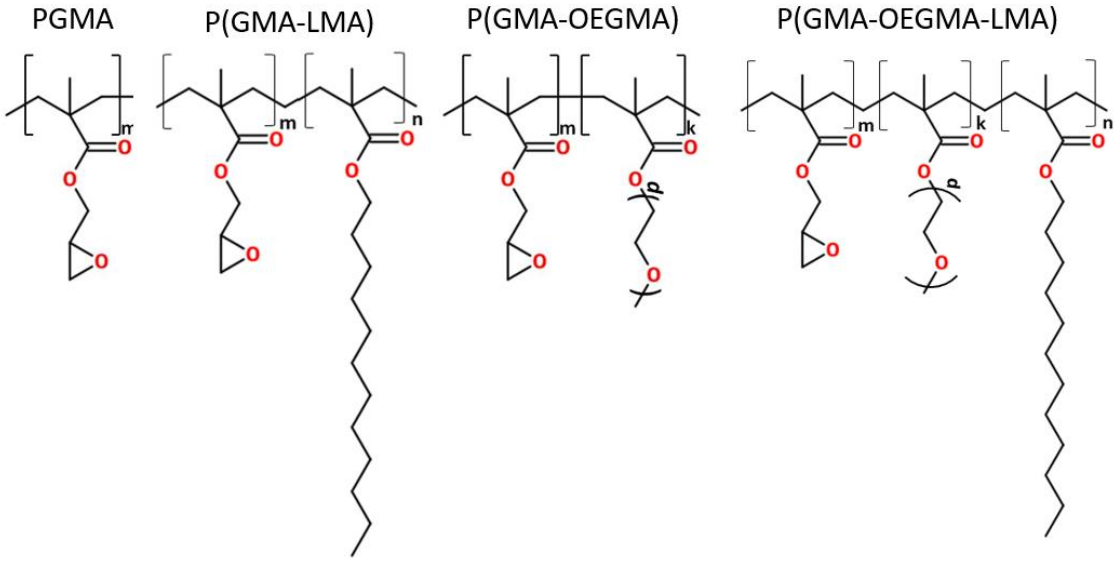

Figure 6.1. Structure of polymers synthesized in this work from the following monomers: glycidyl methacrylate (GMA), lauryl methacrylate (LMA), and oligo(ethylene glycol) methyl ether methacrylate (OEGMA).

The selection of monomers for the making copolymers with tailored affinity is based on their complementary functionality. Poly(oligo(ethylene glycol) methyl ether methacrylate) (POEGMA) has drawn significant attention over the recent years due to its

thermosensitivity, protein repellency, and ability to compatibilize materials with water.[11-17] Indeed, OEGMA monomers bear reactive methacrylate fragment that is capable of undergoing polymerization while quite long oligo(ethylene glycol) side moiety provides water compatibility to the synthesized macromolecule. Thus, POEGMA can be considered as a comb-shape graft copolymer where oligo(ethylene glycol) side chains are densely grafted to the methacrylate backbone. The balance between hydrophilic and hydrophobic parts of the molecule results in thermal switching properties that strongly depend on the side chain length.[16] It is well established that poly(ethylene glycol) demonstrates low toxicity and does not trigger immune system response, which facilitates the use of POEGMA for biological and biomedical applications.[11-17] Poly(glycidyl methacrylate) (PGMA), which is insoluble in water, found applications for the efficient "grafting to" modification of various surfaces.[18-24] GMA can be easily copolymerized with various monomers through solution free-radical copolymerization. Most importantly, epoxy groups of GMA can react with nucleophilic groups (such as hydroxyl, carboxyl and amino) which opens wide opportunities for post-synthesis modifications.[20, 25-27] As the opening of an epoxy group generates a hydroxyl group, PGMA can be thermally cross-linked forming stable permanent network layer.[18, 21, 28] Lauryl methacrylate has been employed as hydrophobic/lyophilic and low-Tg/crystallizable component in a number of studies[29-31] and selected here to tune the hydrophilic/hydrophobic balance of the resulting copolymers.

In this chapter, the copolymers have been synthesized by free-radical polymerization. To this end, I have performed a detailed investigation of the copolymerization of GMA, OEGMA and LMA. I have identified reactivity ratios in this

system, which are necessary for the control of the copolymer composition. The thermal properties, surface energy and water solubility of the series of copolymers have been characterized. It is demonstrated that these materials can be straightforwardly grafted to macroscopic surfaces or colloidal objects from melt and solution to form functional coatings.

6.2. Materials and methods

6.2.1. Materials

Glycidyl methacrylate (97%), azoisobutyronitrile (AIBN), poly(ethylene glycol) methyl ether methacrylate (average Mn 950, containing 100 ppm MEHQ and 300 ppm BHT as inhibitor), lauryl methacrylate and inhibitor removers (replacement packing for removing hydroquinone and monomethyl ether hydroquinone (MEHQ) and replacement packing for removing tert-butylcatechol (BHT)) were purchased from Sigma-Alrdich. All solvents used here were purchased from VWR International and used as received.

6.2.2. Synthesis of the binary copolymers

MEHQ inhibitor remover beads were added to GMA and LMA prior to the synthesis. MEHQ and BHT inhibitor remover beads were added to OEGMA dissolved in methyl ethyl ketone (MEK) prior to synthesis. Solutions then have been filtered through the 0.2 μm syringe filters. The resulting monomers as well as pure solvent and AIBN solution were purged under nitrogen for 45 min and then added in proper amounts to vials in the nitrogen-purged glovebox. These vials have been sealed with a septum and then immersed into a water bath preheated to 50 °C. Overall molar monomer concentration was

0.5 mol L^{-1} and the AIBN concentration was 0.01 mol L^{-1}. GMA/OEGMA synthesis was terminated after 1.5 hours, OEGMA/LMA after 2 hours and GMA/LMA after 5 hours. The resulting copolymers were precipitated by diethyl ether, centrifuged and redissolved in MEK. This procedure was repeated three times in order to remove unreacted monomers and initiator.

6.2.3. Synthesis of the terpolymers and homopolymers

Homopolymers (PGMA, POEGMA) and copolymers were synthesized by solution free-radical polymerization. Monomers were prepared using the same technique as during the study of binary systems. The charged LMA:OEGMA:GMA molar ratio was 0:0:100, 0:100:0, 0:80:20, 12.5:75:12.5 and 20:60:20 respectively. The overall monomer concentration was 0.5 mol L^{-1} and the AIBN concentration was 0.01 mol L^{-1}. The solution was kept under nitrogen purge for 45 min and then immersed into a water bath preheated to 50°C. The polymerization reaction was terminated after 1.5 h by opening flask to the ambient atmosphere and removal the reactor form the water bath. The product of the reaction was purified using the same technique as for the study of the binary systems. In order to prepare P(GMA-OEGMA) copolymer with lower molecular weight carbon tetrabromide (0.02 mol L^{-1}) was added to the reaction mixture.

6.2.4. Analysis of the copolymer composition

Nuclear magnetic resonance (^{1}H NMR) analysis was done using Bruker AVANCE-300 spectrometer and TopSpin 1.3 PL4 software and processed with Delta 5.0.4 software. The copolymer composition was also investigated by Attenuated Total Reflectance Fourier Transform Infrared Spectroscopy. Thermo Nicolet Magna 550 FTIR spectrometer with the

Thermo-Spectra Tech Endurance Foundation Series Diamond ATR accessory was used, and 16 scans were averaged. An ATR correction and baseline correction were performed using Thermo Scientific OMNIC software version 8.0. Data processing and plotting was completed using Origin MicroCal 9.

6.2.5. Analysis of the copolymer thermal properties

Differential scanning calorimetry (DSC) (Model 2920; TA Instruments) was carried out at a heating/cooling rate of 20 °C/min. The temperature range of the experiment was set from -100 °C to 100 °C. The samples were heated, cooled and the reheated again. The second heating was used to measure the glass transition temperature and meting point. The glass transition is reported as the inflection point on the heat flow graph.

6.2.6. Analysis of the copolymer molecular weight and water compatibility

The dynamic light scattering has been used to estimate the molecular weight of the synthesized polymers. Malvern Zetasizer ZS Dynamic Light Scattering and Zeta Potential (DLS-Zeta) instrument was utilized to characterize the size of polymer coil in water and methyl ethyl ketone and estimate the molecular weight. A set of monodisperse polystyrene standards with molecular weights ranging from 200 up to 3000 kDa dissolved in methyl ethyl ketone was used for calibration. The resulting data was fitted with a linear function in $MW^{0.5}$-size coordinates. It was further recalculated into the molecular weight using NMR data regarding copolymer composition. Atomic force microscopy was performed using Bruker multimode 8, tapping mode. Samples have been deposited by spin-coating on the mica surface. The AFM micrographs presented here were further processed using the grain analysis module in the Gwyddion modular program for SPM. Analysis of water and

hexadecane contact angles has been done using KRUSS DSA10 drop shape analyzer at 20 seconds after droplet deposition on the grafted copolymer surface.

6.2.7. Grafting of copolymers to silicon wafer surface

The polymer layers were deposited and grafted according to a previously published procedure.[21] In brief, highly polished, single crystal, undoped silicon wafers (University Wafer: <100>, 10000-20000 ohm·cm, 500 um) were used as a substrate. The wafers were cleaned in "piranha" solution (3:1 concentrated sulfuric acid/30% hydrogen peroxide) for 4 h, and then rinsed several times with deionized water. After rinsing, the substrates were dried under a stream of dry nitrogen. Copolymers were deposited on the surface of the clean dry wafers by dip coating (Mayer Feintechnik dip coater, model D-3400) from MEK solution. After evaporation of the MEK, the samples were placed on the temperature gradient stage[21] with the temperature varying along the stage surface for different times. After the grafting, the samples were removed from the stage and thoroughly washed to remove any ungrafted copolymer. The film thickness was investigated by home-built scanning spectroscopic reflectometer.[21] A total of 114 points on a 6×19 mm scan with 1 mm resolution were measured with 10 ms acquisition time per point. The thicknesses at the points exposed to the same temperature have been averaged for each copolymer film and then subsequently plotted in the Origin 9.0 software.

6.3. Free-radical copolymerization of GMA, LMA and OEGMA

GMA provides the copolymers with the ability to bind with the surfaces and cross-link in a one-step procedure, while OEGMA and LMA deliver compatibility of the modified object with hydrophilic and hydrophobic surfaces/media, respectively. Through composition, the properties of the copolymers can be finely tuned for a specific application. In order to obtain precise control over this process, it was necessary to identify the reactivity ratios for the monomers participating in copolymerization reaction. It is well established that the monomer composition in the feed and in the synthesized polymer are generally different because of different ability of the monomers to attach to a growing polymer chain.[32] Classical Mayo–Lewis equation considers this effect, and the process of (free-radical) copolymerization generally can be described in terms of reactivity ratios r_{12} and r_{21}.

Here, I have identified three pair of reactivity ratios for each of the GMA-OEGMA, LMA-OEGMA and OEGMA-LMA binary systems. For GMA-OEGMA and GMA-LMA systems four copolymers were prepared with 0.2, 0.4, 0.6 and 0.8 GMA molar fraction in the feed. For OEGMA-LMA system LMA molar fraction was ranged from 0.1 to 0.3. To establish the ratios the composition of the synthesized copolymers they were investigated with nuclear magnetic resonance (NMR) and further analyzed with Finemann-Ross, inverted Finemann-Ross and Kelen-Tüdos plots (see below). These methods are commonly used to extract the reactivity ratios from the experimental datasets.[33] In brief, the composition of the copolymers is plotted against the monomer ratio in the feed in a certain

system of coordinates, which is different for each method. The linearization of these data allows for the calculation of the reactivity ratios which should be reasonable close for all three methods. The composition of the copolymers synthesized in this work is listed in **Table 6.1**

Copolymer	**OEGMA fraction**		**LMA fraction**		**GMA fraction**	
P(GMA-OEGMA)	molar	weight	molar	weight	molar	weight
P(G_{85}-O_{15})	0.15	0.54	-		0.85	0.46
P(G_{73}-O_{27})	0.27	0.71	-		0.73	0.29
P(G_{61}-O_{39})	0.39	0.81	-		0.61	0.19
P(G_{34}-O_{66})	0.66	0.93	-		0.34	0.07
P(GMA-LMA)						
P(G_{83}-L_{17})	-		0.17	0.27	0.83	0.73
P(G_{65}-L_{35})	-		0.35	0.49	0.65	0.51
P(G_{46}-L_{54})	-		0.54	0.68	0.46	0.32
P(G_{26}-L_{74})	-		0.74	0.84	0.26	0.16
P(GMA-OEGMA-LMA)						
P(G_{15}-O_{66}-L_{19})	0.66	0.90	0.19	0.07	0.15	0.03
P(G_{28}-O_{56}-L_{16})	0.56	0.87	0.16	0.01	0.28	0.06

Table 6.1. The composition of the copolymers synthesized here.

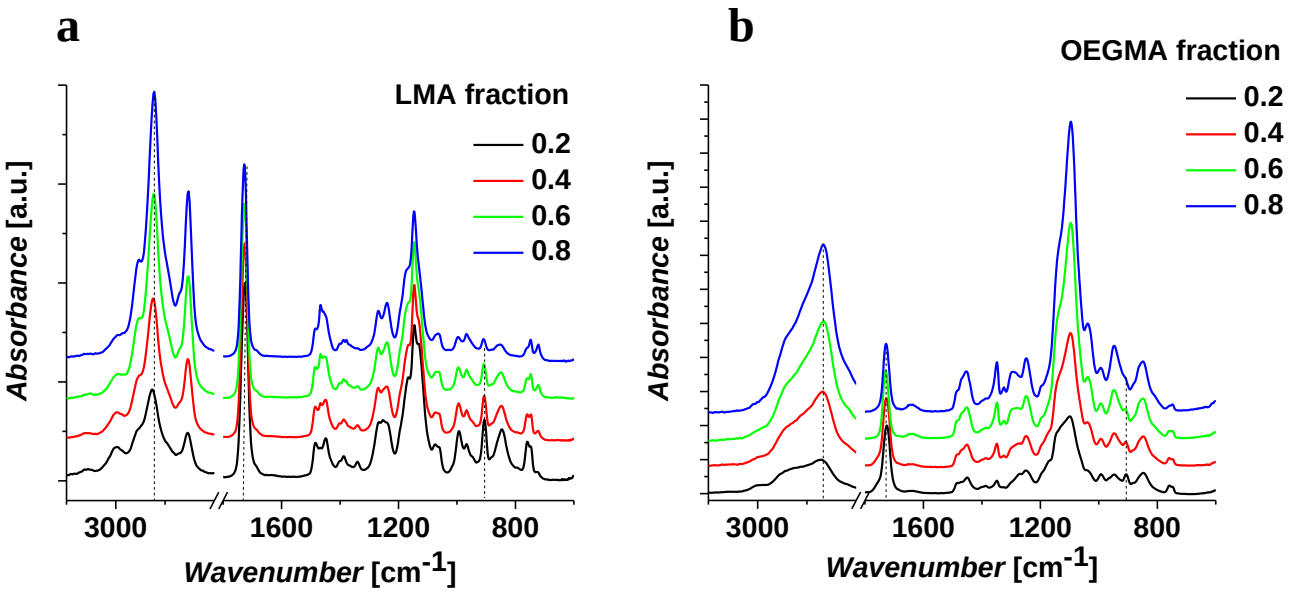

Figure 6.2. Fourier-transform infrared spectra of P(GMA-LMA) (a) and P(GMA-OEGMA) (b) copolymer systems.

Fourier-transform infrared spectroscopy is generally a powerful tool for characterization of polymer materials, so it can be compared to NMR to confirm the correctness of the composition analysis. **Figure 6.2** and **Table 6.2** displays the IR data for polymers in GMA/LMA and GMA/OEGMA series normalized by the intensity of the ester peak (1730 cm^{-1}). The ether peak at 1100 cm^{-1} is clearly pronounced in GMA/OEGMA samples which corresponds to the increase of PEG content. The epoxy peak (900 cm^{-1}) is heavily overlapping with other peaks for these samples, however, in case of GMA/LMA the peak is clearly visible and its area decreases with GMA content. While the results of FTIR and NMR analysis match quite closely, however, as NMR is more quantitative than FTIR, in this study it will be primarily relied on. In general, FTIR data coincides with the NMR results.

GMA/LMA				GMA/OEGMA			
LMA content	C-H stretch (~3000 cm^{-1})	Epoxy (900 cm^{-1})	Ester (1730 cm^{-1})	OEGMA content	C-H stretch (~3000 cm^{-1})	Ester (1730 cm^{-1})	Ether (1100 cm^{-1})
0.17	34.2	3.2	29.1	**0.15**	64.4	30.7	83.4
0.35	51.1	2.3	27.4	**0.27**	127.9	33.1	140.7
0.54	71.6	1.6	26.6	**0.39**	189.5	26.5	210.8
0.74	89.1	0.7	24.9	**0.66**	262.2	24.6	282.8

Table 6.2. The areas of the key peaks in FTIR spectra.

Once the composition of the copolymers is identified, the reactivity ratios have to be calculated. Parameters *X* and *Y* are defined as follows: [32]

$$Y = \frac{r_{12}X + 1}{1 + r_{21}X^{-1}}, \tag{2}$$

$$\text{where } Y = \frac{d[M_1]}{d[M_2]} \text{ and } X = \frac{[M_1]}{[M_2]}, \; r_{12} = \frac{k_{11}}{k_{12}}, \; r_{21} = \frac{k_{22}}{k_{21}} \tag{3}$$

Constants k_{ij} reflect the rate constant for the reaction of monomer *j* with a growing polymer chain terminated with monomer *i*, $[M_1]$ and $d[M_i]$ are molar concentrations of monomer *i* in the feed and in the polymer respectively. In the case of unknown reactivity ratios, the *X* and *Y* values have to be experimentally identified for a series of copolymerization with varying monomer feed ratios. In order to calculate r_{12} and r_{21} from this dataset the parameters *G* and *H* are defined as follows:

$$G = \frac{X(Y-1)}{Y}, \quad H = \frac{X^2}{Y} \tag{4}$$

Fineman-Ross method (**Figure 6.3a**) can then be used to find the reactivity ratios using the equation (5):

$$G = Hr_{12} - r_{21} \tag{5}$$

Alternatively, inverted Finemann-Ross method (5) (**Figure 6.3b**) can be utilized:

$$\frac{G}{H} = r_{12} - \frac{1}{H} r_{21} \tag{6}$$

Yet another method is Kelen-Tüdos method (6) (**Figure 6.3c**):

$$\eta = (r_{12} + r_{21}/\alpha)\xi - r_{21}/\alpha \text{, where} \tag{7}$$

$$\eta = \frac{G}{\alpha + H}, \quad \xi = \frac{H}{\alpha + H}, \alpha = \sqrt{H_{\min} H_{\max}} \tag{8}$$

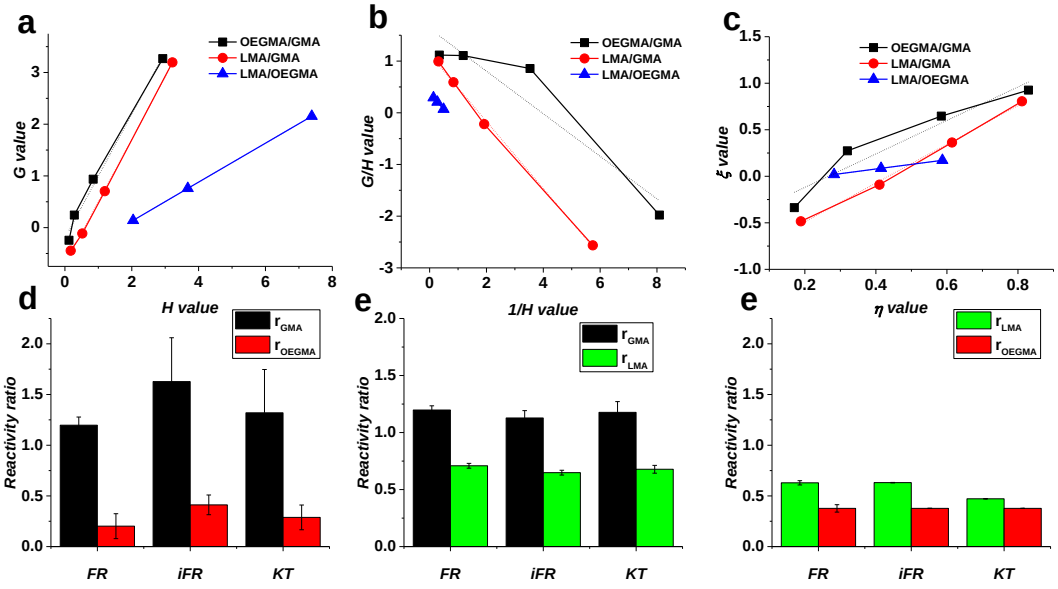

Figure 6.3. Finemann-Ross (a), inverted Finemann-Ross (b) and Kelen-Tüdos (c) plots reflecting copolymerization of binary systems. The resulting reactivity ratios are presented for OEGMA/GMA (d), LMA/GMA (e) and LMA/OEGMA (f) monomeric pairs.

Here H_{min} and H_{max} are minimum and maximum H values for a series of copolymerizations. By linear fitting of the experimental data in the corresponding coordinates (*H*-*G* for Finemann-Ross, 1/*H*-*G*/*H* for inverted Fineman-Ross, η-ξ for Kelen-Tüdos) the r_{12} and r_{21} values can be calculated.

The reactivity ratios for GMA/OEGMA system were determined to be r_{GMA}=1.4 and r_{OEGMA}=0.3, for GMA/LMA r_{GMA}=1.2 and r_{LMA}=0.7 and for LMA/OEGMA r_{LMA}=0.6 and r_{OEGMA} =0.4 (**Figure 6.3d-f**). In a general case, the reactivity ratio indicates the tendency of the growing polymer chain terminated with the certain type of monomer to interact with the same type of monomer. The r_{12} value above 1 indicates tendency of the monomer 1 to participate in homopolymerization over heteropolymerization with monomer 2, while r_{12} below 1 points out an opposite trend. All three monomers studied here belong to the methacrylate class of monomers which implies that the stabilization of the monomer radical is roughly the same, however, their diffusion properties are vastly different due to the difference in the molecular weight. This leads to GMA being the most active monomer in these systems, while LMA and especially OEGMA show suppressed reactivity during the copolymerization. This effect has been previously demonstrated for macromonomer copolymerization and specifically for OEGMA copolymerization with 2-vinyl pyridine.[33] Interestingly enough, OEGMA 300 has been shown to be more reactive than OEGMA 1100 highlighting the influence of molecular weight on the reactivity of the polymer.[33]

Composition	Feed	Calculated	Experimental (measured by NMR)
P(G_{15}-O_{66}-L_{19})			
GMA	0.10	0.20	0.15
OEGMA	0.80	0.65	0.66
LMA	0.10	0.15	0.19
P(G_{28}-O_{56}-L_{16})			
GMA	0.13	0.23	0.28
OEGMA	0.75	0.60	0.56
LMA	0.13	0.17	0.16

Table 6.3. The composition of the terpolymers prepared in this work.

Using the reactivity ratios we predicted the terpolymer compositions using copolymerization equations.[32] $d[M_i]$ and $[M_i]$ are the fractions of monomer i in the copolymer and in the feed, respectively and r_{ij} is the reactivity ratio between monomers i and j.

$$
\begin{aligned}
& d[M_1]:d[M_2]:d[M_3]= \\
& =[M_1]\left\{\frac{[M_1]}{r_{31}r_{21}}+\frac{[M_2]}{r_{21}r_{32}}+\frac{[M_3]}{r_{31}r_{23}}\right\}\left\{[M_1]+\frac{[M_2]}{r_{12}}+\frac{[M_3]}{r_{13}}\right\}: \\
& :[M_2]\left\{\frac{[M_1]}{r_{12}r_{31}}+\frac{[M_2]}{r_{12}r_{32}}+\frac{[M_3]}{r_{32}r_{13}}\right\}\left\{[M_2]+\frac{[M_1]}{r_{21}}+\frac{[M_3]}{r_{23}}\right\}: \\
& :[M_3]\left\{\frac{[M_1]}{r_{13}r_{21}}+\frac{[M_2]}{r_{23}r_{12}}+\frac{[M_3]}{r_{13}r_{23}}\right\}\left\{[M_1]+\frac{[M_2]}{r_{31}}+\frac{[M_3]}{r_{32}}\right\}
\end{aligned}
\qquad (9)
$$

The calculated compositions quite closely matched the experimentally measured ones (**Table 6.3**). The observed deviation lies within 5% and is typical for the calculations involving reactivity ratios. It is evident that the detailed analysis of the copolymerization between GMA, LMA and OEGMA monomers allows for the controlled synthesis of the copolymers with a particular composition.

Atomic force microscopy performed by Dr. Nataraja Sekhar Yadavalli working under the supervision of Dr. Minko in University of Georgia reveals (**Figure 6.4**) that copolymers [as exemplified by $P(G_{34}\text{-}O_{66})$] have linear structure, beside randomly distributed side chains no branching is observed. 75 macromolecules have been analyzed and found that the average contour length of this copolymer molecule is equal to 497±216 nm. The contour length L of the polymer molecule can be expressed mathematically as follows[34]:

$$L = 2X_n d \sin(\frac{109.5}{2}), \quad (10)$$

where X_n is the number average degree of polymerization, d – the length of carbon-carbon bond (0.154 nm) and 109.5 degrees is the angle between two bonds in the case of sp^3-hybridized carbon atom. The number average degree of polymerization and molecular weights are and M_n=1334 kg mol^{-1} respectively.

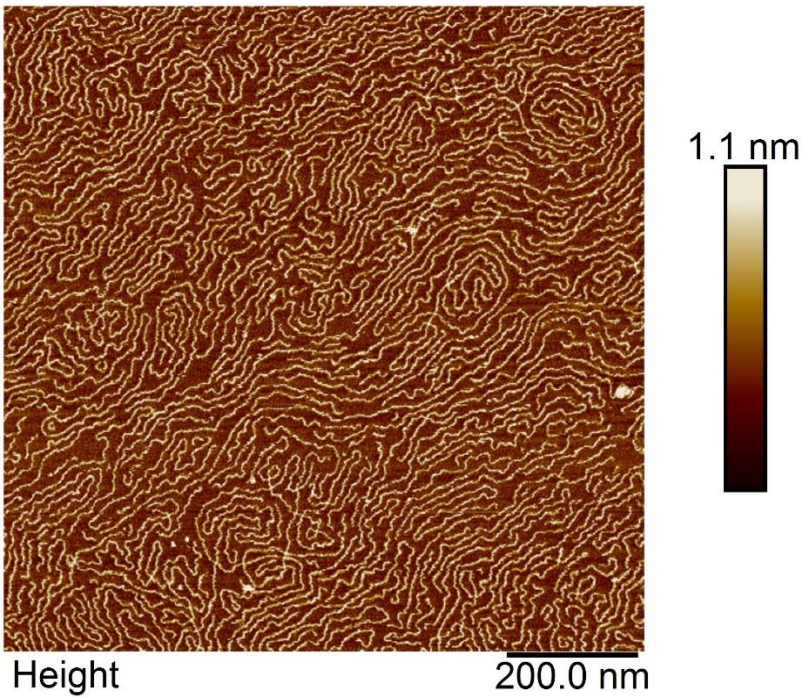

Figure 6.4. Atomic force microscopy topographical image of P(G_{66}-O_{34}) copolymer solvent casted on mica surface

The weight average degree of polymerization and molecular mass were found to be 2677 and M_w=1.807 kg mol^{-1}, respectively, which yields the polydispersity index 1.36. These values are in good agreement with the molecular weight values obtained by dynamic light scattering (DLS, see below). The difference between the data calculated using two methods is originating from a) the difference between expansion factors for poly(GMA-ran-OEGMA) and polystyrene that was used for DLS calibration and b) the small sampling size of the AFM visualized chains (75 molecules). The end-to-end size and radius of gyration of the poly(GMA-ran-OEGMA) molecules on the surface (2D-chain conformations) were found to be 225±123 nm and 88±40 nm respectively. The ratio of those values was found to be 2.56 which is very close to $\sqrt{6}$ = 2.45 which is predicted for an ideal linear chain.

6.4. Molecular weights and degrees of polymerization of GMA, LMA and OEGMA copolymers

The molecular weight of the surface coating agent play crucial role in their performance and the properties of the resulting layer. Thus, a detailed investigation of the degrees of polymerization is essential for the usage of poly(GMA-ran-OEGMA-ran-LMA) copolymers in practical application. Even though expansion factor for polystyrene and poly(GMA-ran-OEGMA) in methyl ethyl ketone may by different, the calibration curve can be used to estimate the range of poly(GMA-ran-OEGMA) molecular weight by dynamic light scattering (DLS). It yields the hydrodynamic radius R_H, which is proportional to the square root of the number of the monomeric units in the chain (X_n) (b is the carbon-carbon bound bond length, M_{PS} is the molecular weight of polystyrene monomeric unit).[35]

$$\frac{1}{R_H} = 16\left(\frac{1}{3\pi}\right)^{1/2} \frac{1}{bX_n^{1/2}} \tag{11}$$

$$2R_H = 1.152 + 0.043 \cdot (X_n \cdot M_{PS})^{1/2} \tag{12}$$

Figure 6.5a displays the degrees of polymerization of the copolymers in three binary systems calculated using this relationship. It is evident that products of LMA/GMA and OEGMA/GMA reactions have about 500-1500 units while decreasing of GMA content leads to increase of degrees of polymerization up to 2000-3000. LMA/OEGMA system is generally characterized by higher values reaching 7000 which decreases when more LMA

is presented in the copolymer. These trends are stemming from the steric hindrance of the termination step during the macromonomer radical copolymerization.[36]

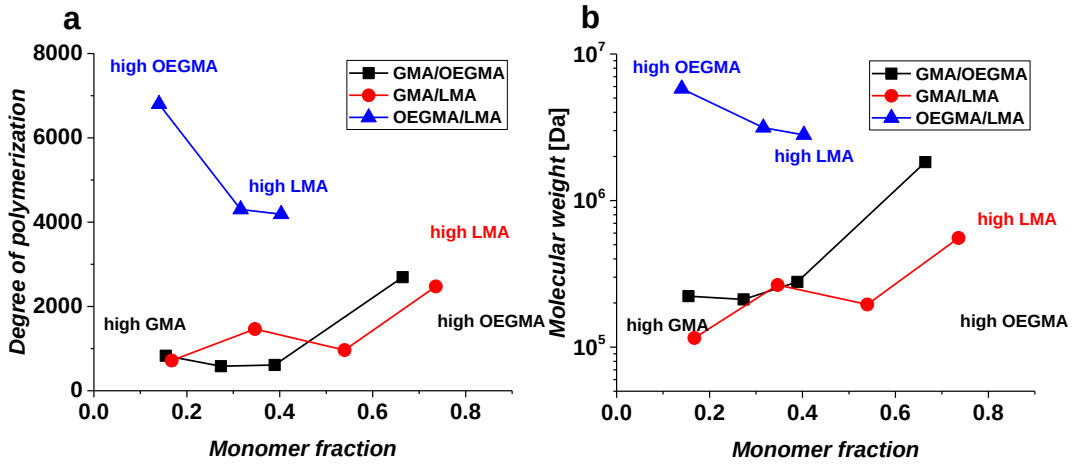

Figure 6.5. Degrees of polymerization (a) and molecular weights of GMA/OEGMA, GMA/LMA and LMA/OEGMA copolymers

Using the NMR data regarding copolymer composition, degrees of polymerization can be converted to molecular weights (**Figure 6.5b**) by multiplying the X_n by the average molecular weight of a monomeric unit ($M(i)$ is a molecular weight of a monomer i):

$$M_n = X_n \sum_i d[M_i] \cdot M(i) \qquad (13)$$

The resulting values can be finely tuned during the reaction using chain transfer agents (CTAs) that can effectively decrease the obtained degrees of polymerization of the product. Carbon tetrabromide was found to be an efficient CTA that decreased the molecular weight of poly(GMA-ran-OEGMA) with 0.66 OEGMA fraction (poly(G_{34}-O_{66})**)** copolymer) by a factor of 10 while the composition remained the same.

6.5. Thermal characteristics of the copolymers

Thermal properties of polymers such as glass transition (T_g) and meting temperature (T_m) significantly affect the parameters for the polymer grafting, since polymer solubility and diffusion are involved in the anchoring process. To this end, Deferential Scanning Calorimetry (DSC) studies for the synthesized copolymers have been performed (**Figure 6.6)**. It is well established that thermal properties of statistical copolymers are related to the thermal properties of homopolymers made of the monomers constituting the copolymers.[35]

The properties of the homopolymers are following. PGMA does not exhibit any crystallinity, while glass transition temperature is found to be ~ 75 °C. PLMA is a semicrystalline polymer[37] with T_m at ~ -26 °C and T_g at ~ -50 °C.[38] To determine the thermal characteristics for OEGMA homopolymer POEGMA was obtained using the same radical polymerization procedure as was used to synthesize the copolymers. DSC indicated that POEGMA is a semicrystalline polymer with $T_g \approx -60^oC$ and $T_m \approx 26^oC$. It is necessary to point that crystallinity for the atactic PLMA and POEGMA is originating from crystallization of the high molecular weight side-groups. Therefore, the copolymers can retain this side-group crystallization or the crystallization observed for the homopolymers can disappear as a result of the copolymerization. T_g for the statistical copolymers have to be somewhat between T_g of PLMA/POEGMA and T_g of PGMA and related to weight fractions of the monomeric units in the copolymers.[35]

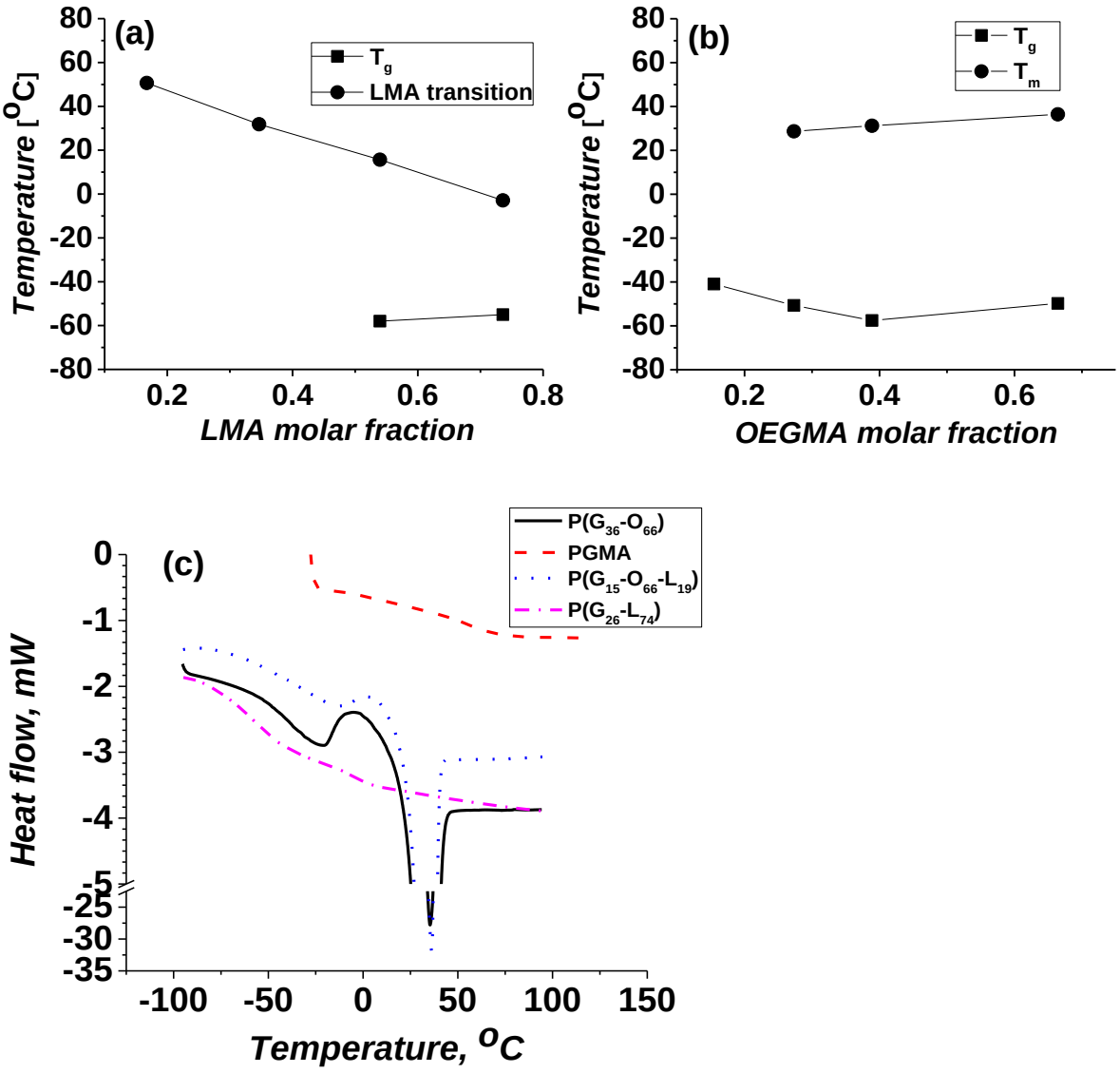

Figure 6.6. Temperature transitions observed in P(GMA-LMA) (a) and P(GMA-OEGMA) (b) copolymers. Lines are only guide for eyes, (c) exemplary DSC curves for PGMA, P(G_{34}-O_{66}), P(G_{26}-L_{74}) and P(G_{15}-O_{66}-L_{19}).

The analysis of DSC curves is shown in **Figure 6.6**. There is no crystallinity observed for P(GMA-LMA) copolymers (**Figure 6.6c**). The glass transition for the copolymers is observed to gradually decrease from 55°C to -10°C with increasing LMA

content from 0.15 to 0.74 molar fraction (from 0.27 to 0.84 weight fraction) (**Figure 6.6a**). LMA side-chain related thermal transition was also observed when LMA mole fraction equal to 0.54 and 0.74 (0.68 and 0.84 weight fraction) at about -60 ^{o}C. This transition is to a certain extent below T_g for LMA homopolymer. This transition is associated with onset of lauryl side-chains movement. On the contrary, P(GMA-OEGMA) copolymers demonstrates crystallinity originating from the side groups when OEGMA molar fraction is above 0.15 (0.54 weight fraction) (**Figure 6.6b,c**) with T_m approximately the same as the one for POEGMA. P(GMA-OEGMA) copolymers have T_g between -40^{o}C and -60. T_g is dominated by OEGMA because of the high monomer weight fraction. The transitions for terpolymer P(G_{15}-O_{66}-L_{19}) synthesized here possess thermal properties, which are close to the properties of P(GMA-OEGMA) copolymers with glass transition at ~ -31 °C and melting temperatures at ~ 32 °C (**Figure 6.6c**). The properties of the terpolymer are dominated by OEGMA because of high weight fraction (0.9) of the monomeric unit in the macromolecule. It is obvious that the surface modification by the melt "grating to" method has to be conducted above T_g for P(GMA-LMA) copolymers and above T_m for OEGMA containing copolymers.

6.6. Grafting from melt

Here, I have used "grafting to" approach for surface modification using the copolymers synthesized.[20] This method involves reaction of functionalized polymers with

complimentary functional groups located on the substrate surface. The major advantage of the "grafting to" technique over other methods is that the polymer chains can be carefully characterized prior to attachment resulting in well-defined grafted layers. Furthermore, the "grafting to" technique is often less challenging from a chemical standpoint because it does not involve elaborate synthetic protocols. In this method processes of synthesis and modification are separated in space and time thus the conditions of the synthesis are no longer restrained by substrate and chemical proficiency of the operator. Surface modification with these copolymers is a straightforward process, where the copolymer, dissolved in water or solvent can be deposited as a film on a surface by dip-coating, spin-coating, spray-coating or drop-casting. The copolymer concertation and processing parameters are dictating the film thickness. The resulting layer then is anchored to the surface and cross-linked by annealing in order to ensure the effective surface binding and stability in liquid media. The kinetics of this process is a key component enabling for the synthesis where all deposited polymer is grafted and cross-linked, and therefore, grafted film does not require post-treatment with solvents to extract unbounded polymer.

GMA contains the reactive epoxy groups that allows for surface binding through reactions with nucleophilic groups on the substrate of the modification.[20] Such chemical groups as amino, carboxyl and hydroxyl groups that are commonly found on the various surfaces can promote the opening of the GMA epoxy rings. In case when the surface lacks the required groups the plasma treatment can be conducted to initiate the binding with the polymer.[39-40] Once the GMA has reacted with the surface, it can further undergo cross-linking through the following mechanism: the opening of an oxirane ring creates newly

formed hydroxyl group that can further react with the neighboring epoxy groups. Thus, the process of GMA-based copolymer surface modification is essentially the same for a variety of the objects and can be easily transferred between different types of substrates.[20] The formation of a non-soluble covalently attached layer is proceeding from the surface and propagates into the polymer bulk. Since this process is temperature dependent (similarly to the curing of the epoxy resin), the duration of the surface modification and the temperature of this process are two primary parameters influencing the resulting thickness of the coating.

Figure 6.7 displays the kinetics of the Si wafer modification with copolymers P(G_{34}-O_{66}) and P(G_{15}-O_{66}-L_{19}) conducted at 80 °C. The thickness of the layer deposited initially on the wafer by dip-coating is ~150 nm. It is evident that upon fast reaction with the hydroxyl groups located on the surface and formation of the initial 100 nm thick layer the reaction proceeds further in a decelerating fashion. However, by selecting a proper period of annealing it is possible to fully graft and crosslink film of several hundred nm. In general, from multiple grafting experiments using combinatorial approach (employing temperature gradient stage)[20-21] an empirical conclusion has been made that there is a certain threshold grafting temperature. Below this temperature it is impossible to obtain the grafted film with non-extractable by solvent polymer, even if the grafting is conducted for several days. For PGMA homopolymer used in this work it is ~90^{o}C. There is also threshold time that is needed at threshold temperature to reach the complete grafting/cross-linking for submicron film with any thickness. For PGMA the threshold time at 90^{o}C is

about 2 hours. Addition of LMA increases this temperature by 35 degrees to about 120-125 ^{o}C (**Figure 6.8a**).

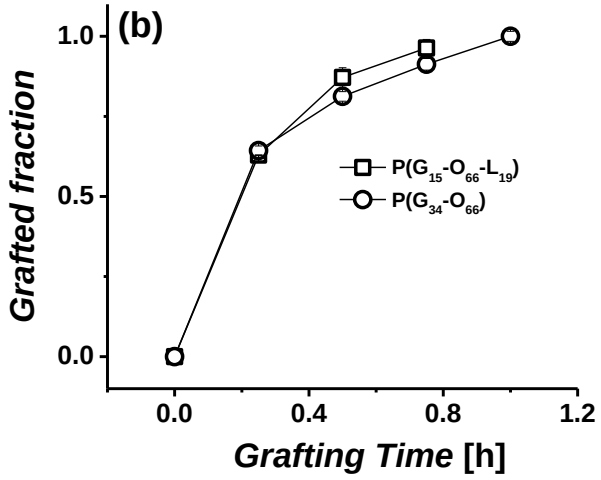

Figure 6.7. Grafted fraction (thickness of the grafted film/thickness of the deposited film) versus grafting time dependence for $P(G_{66}\text{-}O_{34})$ and $P(G_{15}\text{-}O_{66}\text{-}L_{19})$. Thickness of the initially deposited copolymer film - 150 nm. Temperature – 80^{o}C.

The threshold time is also increased to about 4 hours for the GMA-LMA copolymers. Entirely different dependence is observed for GMA-OEGMA copolymers, where with OEGMA addition the threshold time is increased to 10-16 hours. At the same time the threshold temperature is significantly (10-30 ^{o}C) decreased when OEGMA is incorporated into the copolymer chain (**Figure 6.8b**). It was found that the process of the (complete) grafting/crosslinking can be well controlled.

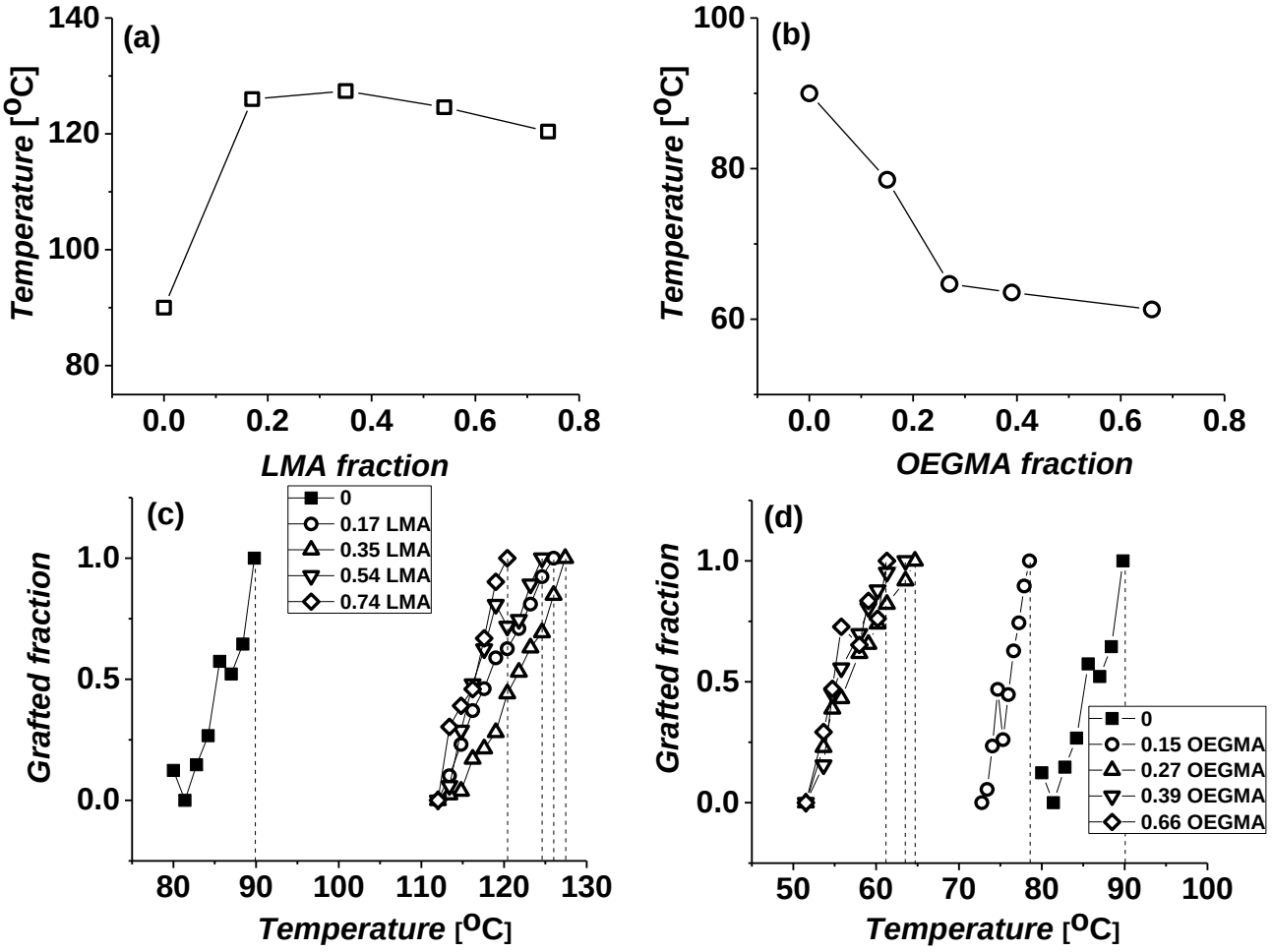

Figure 6.8. Threshold temperature required for the complete grafting of submicron layer made of (a) P(GMA-LMA) and (b) P(GMA-OEGMA) as a function of the molar copolymer composition. Grafted fraction (thickness of the grafted film/thickness of the deposited film) as a function of the grafting temperature for: (c) - P(GMA-LMA) and (d) P(GMA-OEGMA). Grafting time: (a,c) - 4 hours and (b, d) - 16 hours. In the legend for the figures (c,d) molar fractions of LMA/OEGMA are indicated. For PGMA the grafting time is 4 hours (c,d).

For instance, **Figure 6.8c,d** illustrates how the variation of the grafting temperature at constant time influence thickness of the grafted layer. Indeed, grafting of P(GMA-OEGMA) and P(GMA-LMA) binary copolymers is strongly promoted as the temperature

increases. However, since the grafting of the submicron films depends on multiple parameters (e.g. concentration and spatial distribution of GMA units in the copolymer; diffusion rate of the macromolecules, chain segments and side groups; rate and extend of the reaction between substrate surface and GMA groups) at this time comprehensive description of the observed dependencies cannot be made. However, effective combinatorial methodology to determine threshold temperature and time for the copolymers has been identified.

6.7. Surface energy and wettability

In the next step wettability and surface energy were determined for the grafted copolymer films with the submicron thickness on the level of 200 – 800 nm. The water contact angle (WCA) and hexadecane contact angle (HCA) were measured. In turns out that hexadecane virtually completely wets all the studied copolymer and PGMA films yielding extremely low contact angle. WCA for PGMA homopolymer film was found to be about 75^{o}. As it can be anticipated, WCA is systematically increasing with LMA fraction (**Figure 6.9a**) and decreasing with increasing OEGMA fraction (**Figure 6.9b**). Specifically, addition of OEGMA monomeric units decreases the contact angle to up to 30^{o}, while LMA addition increases WCA to as high as 100^{o}. It is obvious that for copolymers containing all three monomeric units the contact angle can be tuned between 30 and 100 ^{o}. For example, for the grafted film made of P(G_{15}-O_{66}-L_{19}) copolymer WCA is equal to 74°. Using WCA values derived from this experiment and assuming that HCA is effectively zero, the surface energy of the coatings can be calculated:[41]

$$\gamma_{l1}(1+cos\theta_1) = 2\sqrt{(\gamma_s^d \gamma_{l1}^d} + 2\sqrt{(\gamma_s^p \gamma_{l1}^p}$$

$$\gamma_{l2}(1+cos\theta_2) = 2\sqrt{(\gamma_s^d \gamma_{l2}^d} + 2\sqrt{(\gamma_s^p \gamma_{l2}^p}$$

$$\gamma_s = \gamma_s^d + \gamma_s^p \tag{14}$$

where γ_s and γ_l are the surface tensions of the solid and liquid, respectively. The subscripts *d* and *p* correspond to dispersion and polar components of the surface tension, respectively. Surface free energy (γ_s) and its polar (γ_s^p) and dispersion (γ_s^d) components of the surfaces were determined using two sets of contact angle measurements of water and hexadecane. The γ_l^p and γ_l^d components of liquids shown in **Table 6.4** were used in the calculations.

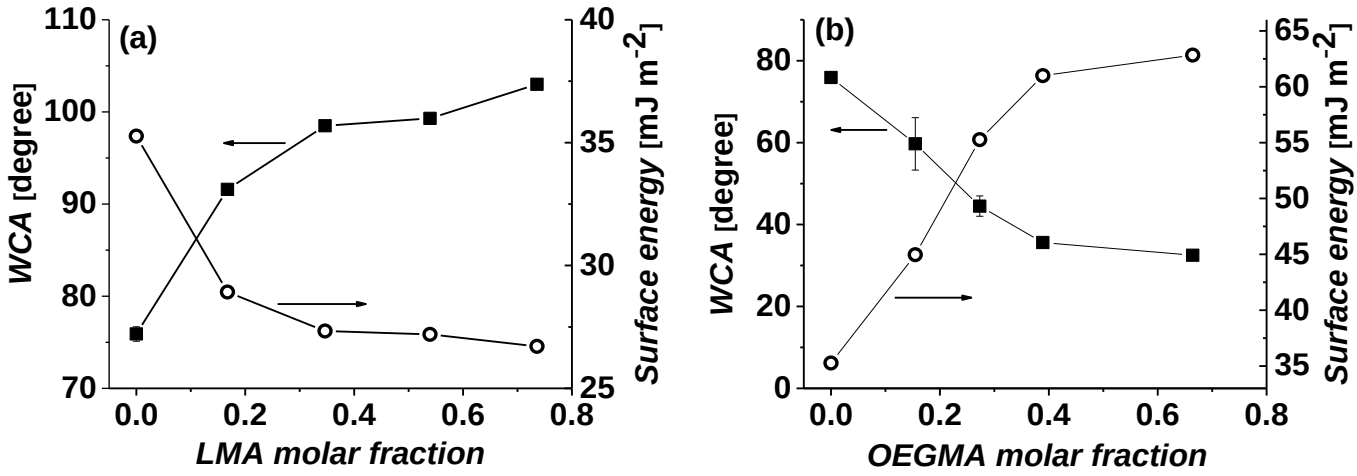

Figure 6.9. Water contact angles and surface energies of: (a) – P(GMA-LMA) and (b) - P(GMA-OEGMA) copolymer grafted from melt coatings.

	γ_l^d	γ_l^p	γ_l
hexadecane	26.35	0	26.35
water	**21.8**	**51**	**72.8**

Table 6.4. The γ_l^p and γ_l^d components of liquids.[42]

As shown in **Figure 6.9a,b** the surface energy values for the grafted films range from 27 up to 62 mJ m^{-2}. Terpolymer P(G_{15}-O_{66}-L_{19}) has the surface energy of 36.4 mJ m^{-2}. The obtained results demonstrate the tunability of the resulting properties of the copolymer coatings.

6.8. Water solubility

The copolymers reported in this work can be anchored to colloidal objects from solution as well. In this method of surface modification the copolymer solution is added to a colloidal suspension first. After the grafting, the colloidal objects are evacuated by centrifugation and redispersed in fresh solvent. Although the surface modification with the copolymers can be conducted from a number of solvents, grafting from water is practically very interesting as it is preferred solvent for biomedical applications and from ecological points of view. Therefore, water solubility of the copolymers containing OEGMA has been evaluated.

We found that the copolymers could be transferred to water from MEK solution and dissolved as individual chains and/or in micellar form. DLS studies showed that increasing OEGMA content leads to progressively better water solubility as the intensity of the DLS peaks related to single molecules rather than micelles is increasing (**Figure 6.10a)**. P(G_{85}-O_{15}) with low OEGMA fraction leaves undispersed flakes in concentrated water solutions. Moreover, as indicated by the comparison of the hydrodynamic diameters (**Figure 6.10b**), this polymer has more affinity to MEK rather than the water as the size of the coil is larger in this organic solvent.[35] The P(GMA-OEGMA) copolymers with higher OEGMA content have excellent compatibility with water as they show higher tendency to dissolve as single molecules and have high chain expansion parameter (larger size of polymer coil) in water (**Figure 6.10b**).

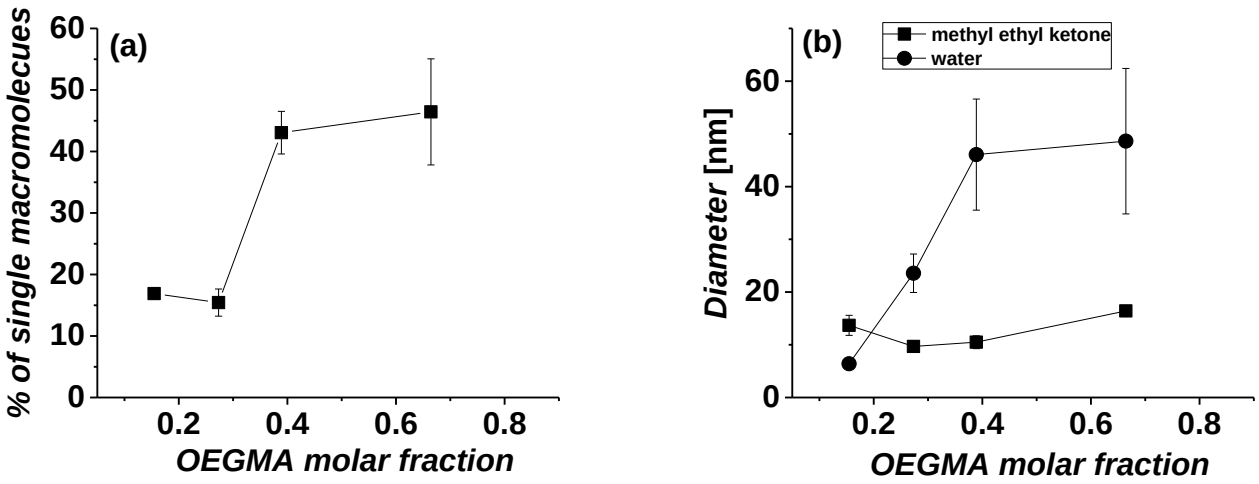

Figure 6.10. Results of DLS measurements for P(GMA-OEGMA): (a) - % of single macromolecules signal in DLS by intensity in water solution; (b) - hydrodynamic diameter of single macromolecules dissolved in water and methyl ethyl ketone.

Terpolymer P(G_{15}-O_{66}-L_{19}) containing all three monomers (GMA/OEGMA/LMA) is soluble in water as well. The increase of the hydrodynamic diameter of the terpolymer macromolecules from 73±9 nm in MEK to 167±32 nm in water clearly indicated significant affinity of the copolymer to water.[35] The ability of P(GMA-OEGMA-LMA) copolymer (containing hydrophobic LMA) to dissolve in water is essential to the process of surface modification as it opens venues to reduce the use of potentially environmentally hazardous solvents

6.9. Conclusions.

Synthesis and properties of novel amphiphilic cross-linkable poly(GMA-ran-OEGMA-ran-LMA) copolymers have been performed. Specifically, reactivity ratios in GMA/OEGMA/LMA free-radical copolymerization and trends in thermal properties, solubility and graftability of the copolymers in this system have been identified. The kinetics of the surface modification for these copolymers for melt and solution-based grafting has been characterized. These results compose a detailed guide through the synthetic procedure that is vital for preparation of a product with desired specific characteristics. These copolymers are a flexible tool for advanced surface modification that is available through simple solution free-radical copolymerization, has minimal requirements for the substrate and can be applied in a controllable fashion through the simple one step procedure delivering desired properties.

6.10. References

1. Cohen Stuart, M. A.; Huck, W. T. S.; Genzer, J.; Muller, M.; Ober, C.; Stamm, M.; Sukhorukov, G. B.; Szleifer, I.; Tsukruk, V. V.; Urban, M.; Winnik, F.; Zauscher, S.; Luzinov, I.; Minko, S., Emerging applications of stimuli-responsive polymer materials. *Nat. Mater.* **2010,** *9* (2), 101-113.
2. Luzinov, I.; Minko, S.; Tsukruk, V. V., Adaptive and responsive surfaces through controlled reorganization of interfacial polymer layers. *Prog. Polym. Sci.* **2004,** *29* (7), 635-698.
3. Liu, Y.; Klep, V.; Luzinov, I., To patterned binary polymer brushes via capillary force lithography and surface-initiated polymerization. *J. Am. Chem. Soc.* **2006,** *128* (25), 8106-8107.
4. Olivier, A.; Meyer, F.; Raquez, J.-M.; Damman, P.; Dubois, P., Surface-initiated controlled polymerization as a convenient method for designing functional polymer brushes: From self-assembled monolayers to patterned surfaces. *Prog. Polym. Sci. 37* (1), 157-181.
5. Akiyama, Y.; Kikuchi, A.; Yamato, M.; Okano, T., Ultrathin poly(N-isopropylacrylamide) grafted layer on polystyrene surfaces for cell adhesion/detachment control. *Langmuir* **2004,** *20* (13), 5506-5511.
6. Lokitz, B. S.; Messman, J. M.; Hinestrosa, J. P.; Alonzo, J.; Verduzco, R.; Brown, R. H.; Osa, M.; Ankner, J. F.; Kilbey, S. M., II, Dilute Solution Properties and Surface Attachment of RAFT Polymerized 2-Vinyl-4,4-dimethyl Azlactone (VDMA). *Macromolecules* **2009,** *42* (22), 9018-9026.
7. Zhao, B.; Brittain, W. J., Polymer brushes: surface-immobilized macromolecules. *Prog. Polym. Sci.* **2000,** *25* (5), 677-710.
8. Armini, S.; Burtovyy, R.; Moinpour, M.; Luzinov, I.; De Messemaeker, J.; Whelan, C. M.; Maex, K., Interaction forces between a glass surface and ceria-modified PMMA-Based abrasives for CMP measured by colloidal probe AFM. *J. Electrochem. Soc.* **2008,** *155* (4), H218-H223.
9. Keating, J. J.; Imbrogno, J.; Belfort, G., Polymer Brushes for Membrane Separations: A Review. *ACS Appl. Mater. Interfaces* **2016,** *8* (42), 28383-28399.
10. Zoppe, J. O.; Ataman, N. C.; Mocny, P.; Wang, J.; Moraes, J.; Klok, H.-A., Surface-Initiated Controlled Radical Polymerization: State-of-the-Art, Opportunities, and Challenges in Surface and Interface Engineering with Polymer Brushes. *Chem. Rev.* **2017,** *117* (3), 1105-1318.
11. Hu, J.; Wang, G.; Zhao, W.; Liu, X.; Zhang, L.; Gao, W., Site-specific in situ growth of an interferon-polymer conjugate that outperforms PEGASYS in cancer therapy. *Biomaterials* **2016,** *96*, 84-92.
12. Smeets, N. M. B.; Patenaude, M.; Kinio, D.; Yavitt, F. M.; Bakaic, E.; Yang, F.-C.; Rheinstädter, M.; Hoare, T., Injectable hydrogels with in situ-forming hydrophobic domains: oligo(D,L-lactide) modified poly(oligoethylene glycol methacrylate) hydrogels. *Polym. Chem.* **2014,** *5* (23), 6811-6823.

13. Shi, X.; Wang, Y.; Li, D.; Yuan, L.; Zhou, F.; Wang, Y.; Song, B.; Wu, Z.; Chen, H.; Brash, J. L., Cell Adhesion on a POEGMA-Modified Topographical Surface. *Langmuir* **2012,** *48* (49), 17011-17018.
14. Liu, M.; Leroux, J. C.; Gauthier, M. A., Conformation-function relationships for the comb-shaped polymer pOEGMA. *Progress in Polymer Science* **2014,** *48*, 111-121.
15. Skandalis, A.; Pispas, S., PLMA-b-POEGMA amphiphilic block copolymers: Synthesis and self-assembly in aqueous media. *Journal of Polymer Science Part A: Polymer Chemistry* **2017,** *55* (1), 155-163.
16. Wang, G.; Chen, M.; Guo, S.; Hu, A., Synthesis, self-assembly, and thermosensitivity of amphiphilic POEGMA-PDMS-POEGMA triblock copolymers. *J. Polym. Sci., Part A: Polym. Chem.* **2014,** *52* (18), 2684-2691.
17. Knop, K.; Pretzel, D.; Urbanek, A.; Rudolph, T.; Scharf, D. H.; Schallon, A.; Wagner, M.; Schubert, S.; Kiehntopf, M.; Brakhage, A. A.; Schacher, F. H.; Schubert, U. S., Star-shaped drug carriers for doxorubicin with POEGMA and POEtOxMA brush-like shells: A structural, physical, and biological comparison. *Biomacromolecules* **2013,** *14* (8), 2536-2548.
18. Borodinov, N.; Giammarco, J.; Patel, N.; Agarwal, A.; O'Donnell, K. R.; Kucera, C. J.; Jacobsohn, L. G.; Luzinov, I., Stability of Grafted Polymer Nanoscale Films toward Gamma Irradiation. *ACS Applied Materials & Interfaces* **2015,** *7* (34), 19455–19465.
19. Lin, P. T.; Giammarco, J.; Borodinov, N.; Savchak, M.; Singh, V.; Kimerling, L. C.; Tan, D. T. H.; Richardson, K. a.; Luzinov, I.; Agarwal, A., Label-Free Water Sensors Using Hybrid Polymer–Dielectric Mid-Infrared Optical Waveguides. *ACS Appl. Mater. Interfaces* **2015,** *7*, 11189-11194.
20. Zdyrko, B.; Luzinov, I., Polymer brushes by the "grafting to" method. *Macromolecular Rapid Communications* **2011,** *32*, 859-869.
21. Borodinov, N.; Soliani, A. P.; Galabura, Y.; Zdyrko, B.; Tysinger, C.; Novak, S.; Du, Q.; Huang, Y.; Singh, V.; Han, Z.; Hu, J.; Kimerling, L.; Agarwal, A. M.; Richardson, K.; Luzinov, I., Gradient Polymer Nanofoams for Encrypted Recording of Chemical Events. *ACS Nano* **2016,** *10* (12), 10716-10725.
22. Hoy, O.; Zdyrko, B.; Lupitskyy, R.; Sheparovych, R.; Aulich, D.; Wang, J. F.; Bittrich, E.; Eichhorn, K. J.; Uhlmann, P.; Hinrichs, K.; Muller, M.; Stamm, M.; Minko, S.; Luzinov, I., Synthetic Hydrophilic Materials with Tunable Strength and a Range of Hydrophobic Interactions. *Adv. Funct. Mater.* **2010,** *20* (14), 2240-2247.
23. Zdyrko, B.; Klep, V.; Li, X.; Kang, Q.; Minko, S.; Wen, X.; Luzinov, I., Polymer brushes as active nanolayers for tunable bacteria adhesion. *Mater. Sci. Eng. C.* **2009,** *29* (3), 680-684.
24. Zdyrko, B.; Hoy, O.; Kinnan, M. K.; Chumanov, G.; Luzinov, I., Nano-patterning with polymer brushes via solvent-assisted polymer grafting. *Soft Matter* **2008,** *4* (11), 2213-2219.
25. Soto-Cantu, E.; Lokitz, B. S.; Hinestrosa, J. P.; Deodhar, C.; Messman, J. M.; Ankner, J. F.; Kilbey, S. M., Versatility of alkyne-modified poly(glycidyl methacrylate) layers for click reactions. *Langmuir* **2011,** *27* (10), 5986-96.

26. Benaglia, M.; Alberti, A.; Giorgini, L.; Magnoni, F.; Tozzi, S., Poly(glycidyl methacrylate): a highly versatile polymeric building block for post-polymerization modifications. *Polym. Chem.* **2013,** *4* (1), 124-124.
27. Safa, K. D.; Nasirtabrizi, M. H., One-pot, novel chemical modification of glycidyl methacrylate copolymers with very bulky organosilicon side chain substituents. *European Polymer Journal* **2005,** *41* (10), 2310-2319.
28. Galabura, Y.; Soliani, A. P.; Giammarco, J.; Zdyrko, B.; Luzinov, I., Temperature controlled shape change of grafted nanofoams. *Soft Matter* **2014**, 2567-2573.
29. Scheibe, P.; Barz, M.; Hemmelmann, M.; Zentel, R., Langmuir−Blodgett Films of Biocompatible Poly(HPMA)-block-poly(lauryl methacrylate) and Poly(HPMA)-random-poly(lauryl methacrylate): Influence of Polymer Structure on Membrane Formation and Stability. *Langmuir* **2010,** *26* (8), 5661-5669.
30. Feng, Y.; Xiao, C. F., Research on butyl methacrylate–lauryl methacrylate copolymeric fibers for oil absorbency. *J. Appl. Polym. Sci.* **2006,** *101* (3), 1248-1251.
31. Chatterjee, D. P.; Mandal, B. M., Triblock Thermoplastic Elastomers with Poly(lauryl methacrylate) as the Center Block and Poly(methyl methacrylate) or Poly(tert-butyl methacrylate) as End Blocks. Morphology and Thermomechanical Properties. *Macromolecules* **2006,** *39* (26), 9192-9200.
32. Odian, G. G., *Principles of Polymerization*. Wiley-Interscience: Hoboken, N.J., 2004.
33. Driva, P.; Bexis, P.; Pitsikalis, M., Radical copolymerization of 2-vinyl pyridine and oligo(ethylene glycol) methyl ether methacrylates: Monomer reactivity ratios and thermal properties. *Eur. Polym. J.* **2011,** *47* (4), 762-771.
34. Yamamoto, T., Normal mode analysis of the conformational fluctuation of polymethylene chains in their nearly extended states. *J. Chem. Phys.* **1991,** *95* (10), 7717-7725.
35. Sperling, L. H., *Introduction to Physical Polymer Science*. Fourth ed.; Wiley-Interscience Hoboken, New Jersey, 2006; p 845.
36. Ito, K.; Tanaka, K.; Tanaka, H.; Imai, G.; Kawaguchi, S.; Itsuno, S., Poly(ethylene oxide) macromonomers. 7. Micellar polymerization in water. *Macromolecules* **1991,** *24* (9), 2348-2354.
37. Hempel, E.; Huth, H.; Beiner, M., Interrelation between side chain crystallization and dynamic glass transitions in higher poly(n-alkyl methacrylates). *Thermochimica Acta* **2003,** *403* (1), 105-114.
38. Floudas, G.; Placke, P.; Stepanek, P.; Brown, W.; Fytas, G.; Ngail, K. L., Dynamics of the "Strong" Polymer of n-Lauryl Methacrylate below and above the Glass Transition. *Macromolecular Chemistry and Physics* **1995,** *28*, 6799-6807.
39. Burtovyy, O.; Klep, V.; Turel, T.; Gowayed, Y.; Luzinov, I., Polymeric Membranes: Surface Modification by "Grafting to" Method and Fabrication of Multilayered Assemblies. In *Nanoscience and Nanotechnology for Chemical and Biological Defense*, Nagarajan, R.; Zukas, W.; Hatton, T. A.; Lee, S., Eds. Amer Chemical Soc: Washington, 2009; Vol. 1016, pp 289-305.

40. Burtovyy, O.; Klep, V.; Chen, H. C.; Hu, R. K.; Lin, C. C.; Luzinov, I., Hydrophobic modification of polymer surfaces via "grafting to" approach. *J. Polym. Sci. Part B Polym. Phys.* **2007,** *46* (1), 137-154.
41. Owens, D. K.; Wendt, R. C., Estimation of the surface free energy of polymers. *J. Appl. Polym. Sci.* **1969,** *13* (8), 1741-1747.
42. Janczuk, B.; Wojcik, W.; Zdziennicka, A.; Bruque, J. M., Components of the surface free energy of low rank coals in the presence of n-alkanes. *Powder Technol.* **1996,** *86*, 229-238.

CHAPTER 7. APPLICATION OF FUNCTIONAL PGMA-BASED GRAFT COPOLYMERS OBTAINED BY "GRAFTING THROUGH" METHOD FOR SURFACE MODIFICATIONS

7.1. Multi-frequency volatile organic compound sensing

In **Chapter 6** I have provided a detailed guide on how to synthesize PGMA-based copolymers by polymerization of GMA, OEGMA and LMA and characterized thermal properties, graftability, molecular weights, water solubility and surface energy of these materials. Such tunability of copolymer properties can be successfully used for many practical applications. Specifically, in this chapter I am going to be investigating two examples of surface modification: sensor design and regulation of cell adhesion.

In **Chapter 4** and **5** I have demonstrated principles on how PGMA-based films can be used as active enrichment layers in sensor design. In those chapters I focused on copolymers prepared by "grafting to" technique. However, P(G_{34}-O_{66}) copolymers made by "grafting through" method also can be used for detection of volatile organic compounds. In collaboration with Yongzhi Shao and Zhe Chen working under supervision of Dr. Pingshan Wang from Clemson University Department of Electrical and Computer Engineering we were able demonstrate effective detection of several volatile organic compounds (VOCs) over a broad frequency range with a simple RF (radio frequency)

interferometer, which uses polymer coated coplanar waveguides (CPW A and CPW B, **Figure 7.1**) as the detection electrodes.

We also show that different VOCs induce different frequency responses, which may be further explored to enhance selective VOC sensing. The results indicate that RF interferometer based broadband measurements are promising to provide a new approach for VOC detection and identification.

70 nm layer of P(G_{34}-O_{66}) copolymer is used as a sensing layer due to its ability of polyethylene glycol monomeric units to interact with a wide range of chemical compounds.[1-2] As it turns out the polymer coating is stable during ~ 8 months testing period, consistent with our previous results.[3] Currently, we have experimented at least hundreds of sensing cycles, the polymer is still effective.

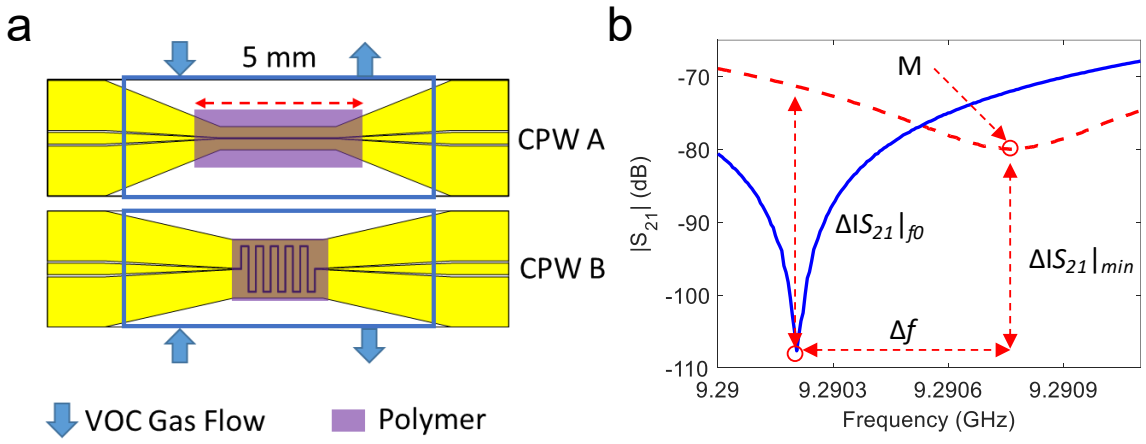

Figure 7.1. a) A layout of two coplanar waveguides used for VOC measurements, b) a typical reponse of the resonator after the exposure of the sensors to VOC vapor.

7.1.1. Materials and methods

Sensor coating

The copolymer prepared by free-radical polymerization using glycidyl methacrylate and oligoethylene glycol methacrylate (average Mn 950) monomers which was described in **Chapter 6**. Prior to the grafting, the CPWs were cleaned in air plasma with the input power of 30W for 15 minutes. The copolymer was deposited from 1.5% solution in chloroform by dip-coating at 320 mm/min and annealed for 4 hours at 120 ˚C in the oven. The ungrafted copolymer was been washed in chloroform. This procedure resultd in approximately 70 nm thick P(G_{34}-O_{66}) copolymer coating on the CPWs.

Measurement set-up

This work has been done in tight collaboration with Yongzhi Shao and Zhe Chen working under supervision of Dr. Pingshan Wang from Clemson University Department of Electrical and Computer Engineering.

VOC gases, i.e. ethanol, acetone, and isopropyl (IPA) in this work, are evaporated from VOC liquids. The liquids are stored in a bottle, which is placed in a thermal bath. Dry nitrogen (with 99.9997% N_2 and 0.41 ppm moisture) is used as the carrier gas to dilute VOC gas concentration, i.e. $C_i = F_1 \times Vp_i/(F_1+F_2)$, where C_i is the concentration of the i^{th} VOC component, F_1 and F_2 the flow rates in the two channels, and $Vp_i = v_{pi} \times x_i$ with v_{pi} the partial vapor pressure of the i^{th} VOC and x_i its molar fraction. The use of two mass flow controllers (MFCs) is to help monitor and maintain a constant flow rate, $F=F_1+F_2$, in measurements.

7.1.2. Response of the polymer coated RF sensor

To demonstrate the viability of this approach, we have studied the responses of copolymer-coated resonators to acetone, ethanol and isopropyl alcohol. The sensor in enclosed container was subjected to the VOC-enriched nitrogen with on-line recording of the sensor response. Each set of measurements takes 6-30 minutes depending on VOC gases and the targeted concentration level. Once the protocol of measurements has been established, the dependency between the concentration and the resonance shift was investigated.

Figure 7.2 summarizes acetone and IPA measurement results with CPW B, which has ~ 5 times longer sensing electrodes than CPW A. A 5-time longer sensing zone enables 5-time larger phase shifts, and 5-time larger frequency shifts. For the shorter CPW A, the achieved LOD is ~ 600 ppm for ethanol, ~ 270 ppm for acetone and ~ 330 ppm for IPA at 9.29 GHz. The 5 times longer CPW B has ~ 4 times lower LODs at ~ 11 GHz due to the use of traveling waves for sensing.

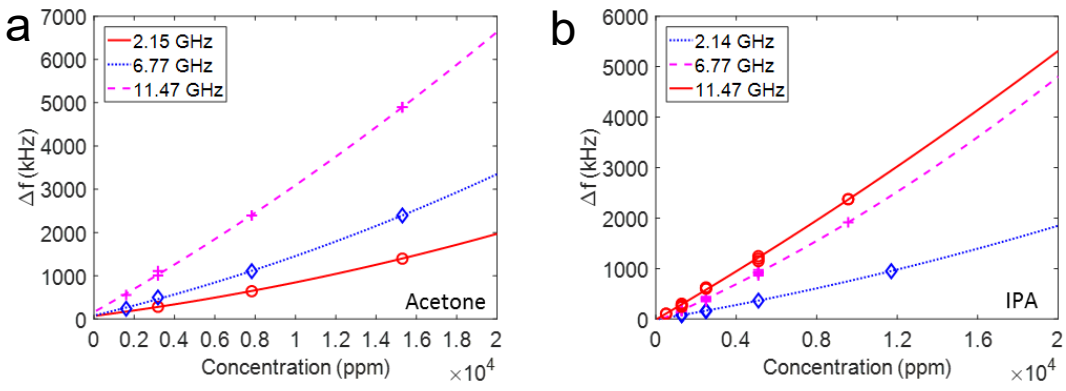

Figure 7.2. Measured CPW B responses at different frequencies and VOC concentration levels for (a) acetone, and (b) IPA. The curves are obtained from binomial data fitting.

7.1.3. The summary of radio-frequency results

A simple RF interferometer for multi-frequency VOC measurements from ~ 2 GHz and 11 GHz has been demonstrated. Two CPWs are built with conventional micromachining techniques and used as RF sensing electrodes. P(G_{34}-O_{66}) copolymer was coated on the electrodes to adsorb and concentrate VOCs for their enhanced sensing. Harmonic frequency operations were exploited to characterize ethanol, acetone and IPA vapors at concentration levels down to ~ 200 ppm. The measurement results depend on RF frequency, VOC species, concentration levels, and CPW devices, which may be exploited for better sensor selectivity operation

7.2. PGMA-based copolymer coating of surgical implants.

In order to demonstrate the applicability of copolymer coating for the control over the biological processes, we have focused our research on the osteoblast attachment. The clinical implication for controlling osteoblast adhesion and spreading is of critical importance.[4] Many orthopaedic implants are made of titanium, cobalt chromium, or stainless steel, which are relatively biologically inert materials. Some implants, especially those used in joint replacement, rely on osseous integration (bone growth directly onto or into the implant surface) to provide the proper functioning of the implant and withstand the repetitive mechanical stress, while walking.[5] Once osteoblasts adhered to the implant surface, an enhanced proliferation, production of extracellular matrix and mineralization occur. Therefore, there is a specific interest in bioactive coatings that can be deposited onto

implants in order to enhance osteoblast adhesion and at the same time decreasing bacterial adhesion.[6]

The bioactive coatings must resist sheer stress, prevent bacterial adherence, and be both osteoinductive and osteoconductive.[7] Osteoinductive materials help to recruit local stem cells and induce osteogenesis, while osteoconductive materials promote osteoblast differentiation and proliferation. In another scenario, surgeons might wish to prevent osteoblast adherence since some implants are to be taken out within a few weeks to months from the patient's body. Such examples are Kirschner wires or external fixation pins used to help with deformity correction or temporary stabilize fractures or arthrodesis.[8] Usually these implants interact with both the internal and external environment. Therefore, an implant is needed that can withstand bacterial adherence to prevent infection (since it is interacting with the environment), while preventing local on-growth of osteoblasts, so that it may be easily removed in the outpatient setting.[9] Polymer-coatings on implants provide a unique opportunity to regulate the internal and external environment of the implant to ensure surgical success.

7.2.1. Materials and methods

This work has been done in tight collaboration with Dmitry Gil working under supervision of Dr. Vertegel from Clemson University Department of Chemical and Biomolecular Engineering.

K-wire modification and results visualization

Prior to the modification, the wires were activated in air plasma with the input power of 30W for 15 minutes. For coating, 1 ml of monolaurin solution in ethanol (10

mg/ml) was transferred into a sterile centrifuge tube with a cleaned K-wire. After 10 min, the wire was removed from the solution and air-dried for 10 minutes at room temperature under sterile conditions. Uncoated control wires were prepared by incubating in pure ethanol for 10 min followed by air-drying for 10 min, similarly to the coated wires.

Polished silicon wafers prepared as specified above were coated with polymer solutions in MEK via dip-coating and annealed for 4 h at 130 °C (PGMA and P(G_{26}-L_{74})) or at 80 °C (P(G_{34}-O_{66}) and P(G_{15}-O_{66}-L_{19})). The resulting films were mashed in pure MEK in order to remove the ungrafted polymer. Same procedure was applied to the actual K-wires.

Cytotoxicity of the PGMA-based coatings

In addition, the viability of osteoblasts attached to the samples was assessed by the LIVE/DEAD® assay according to the protocol described elsewhere[29] Four replicates were performed for each of the time points.

In vitro evaluation of antibacterial activity

The antimicrobial activity of monolaurin-coated wires was evaluated against *S. aureus* (ATCC® 14775), *S. epidermidis* (ATCC® 12228) and Methicillin-resistant *Staphylococcus aureus* (MRSA, ATCC® 33591).

Studies of planktonic bacteria

Bacteria have been cultured in soy broth until reaching the stationary phase. Coated and plain wires were placed into a sterile test tube containing 1 ml of 10^6 CFU/ml bacterial

suspension. Samples under study were kept at 37 °C under mild shaking. The aliquots of bacterial suspension were analyzed by the spread-plate method according to the ISO 4833:2.

Analysis of adherent bacteria

The biofilm formation was quantified using crystal violet assay (CV assay) as described by Kobayashi et al.[10] Optical density of the resulting solution was measured at 590 nm using a microplate reader (Bio-Tek Synergy HT, Winooski, VT).

7.2.2. Regulation of cell adhesion with PGMA-based copolymers

Considering the unique properties, tunability and versatility of the copolymers studied herein, multiple applications of the material can be envisioned. For example, it can be used as a bioactive coating for medical devices. As was mentioned before, the hydrophilic and hydrophobic properties of the copolymers can be precisely controlled by changing the ratio between the monomers constituting the copolymers. Interactions of human body with an implant are largely determined by the level of hydrophobicity of its surface.[11] In particular, it was shown that numerous processes, including protein adsorption, cell adhesion and osseointegration, occur more likely on moderately hydrophobic surfaces.[12] On the other hand, a large body of evidence suggests that the use of the surfaces with pronounced hydrophilic properties completely eliminates protein adsorption and, therefore, prevents cell adhesion. With this in mind, in the present work we hypothesized that cell attachment to the polymeric coating can be controlled by tuning the ratio between the components in the copolymers.

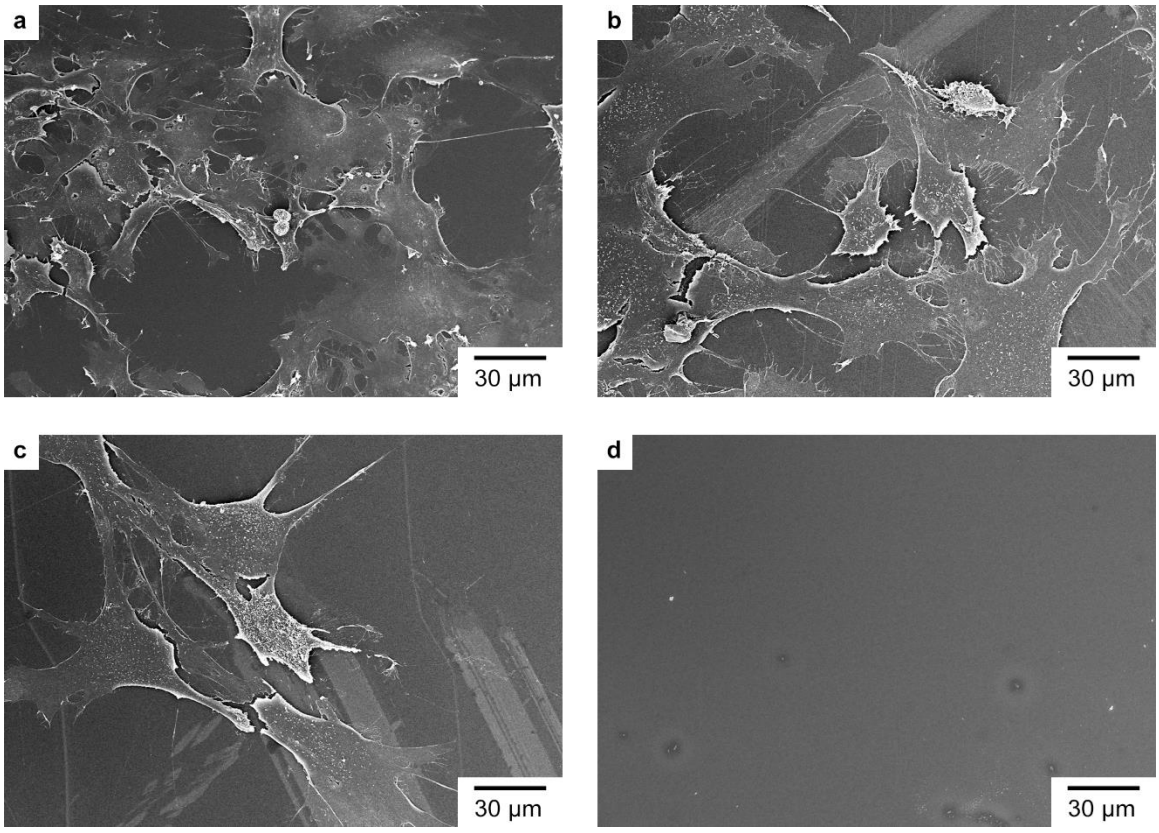

Figure 7.3. The scanning electron micrographs of the osteoblasts attached to the silicon wafers coated with PGMA (a), P(G_{26}-L_{74}) (b), P(G_{15}-O_{66}-L_{19}) (c) and P(G_{34}-O_{66}) (d).

In order to demonstrate the ability to finely tune cell adhesion, mouse osteoblasts were cultured in the presence of silicon wafers coated with PGMA homopolymer, poly(GMA-ran-LMA) with 0.74 LMA mole fraction (P(G_{26}-L_{74})), P(G_{15}-O_{66}-L_{19})and P(G_{34}-O_{66}) copolymers. Cells were allowed to adhere to the surfaces; osteoblast attachment was assessed by means of SEM (**Figure 7.3**) and the LIVE/DEAD® assay (**Figure 7.4**). SEM studies revealed different levels of cell adhesion and protein adsorption to the polymeric coatings.

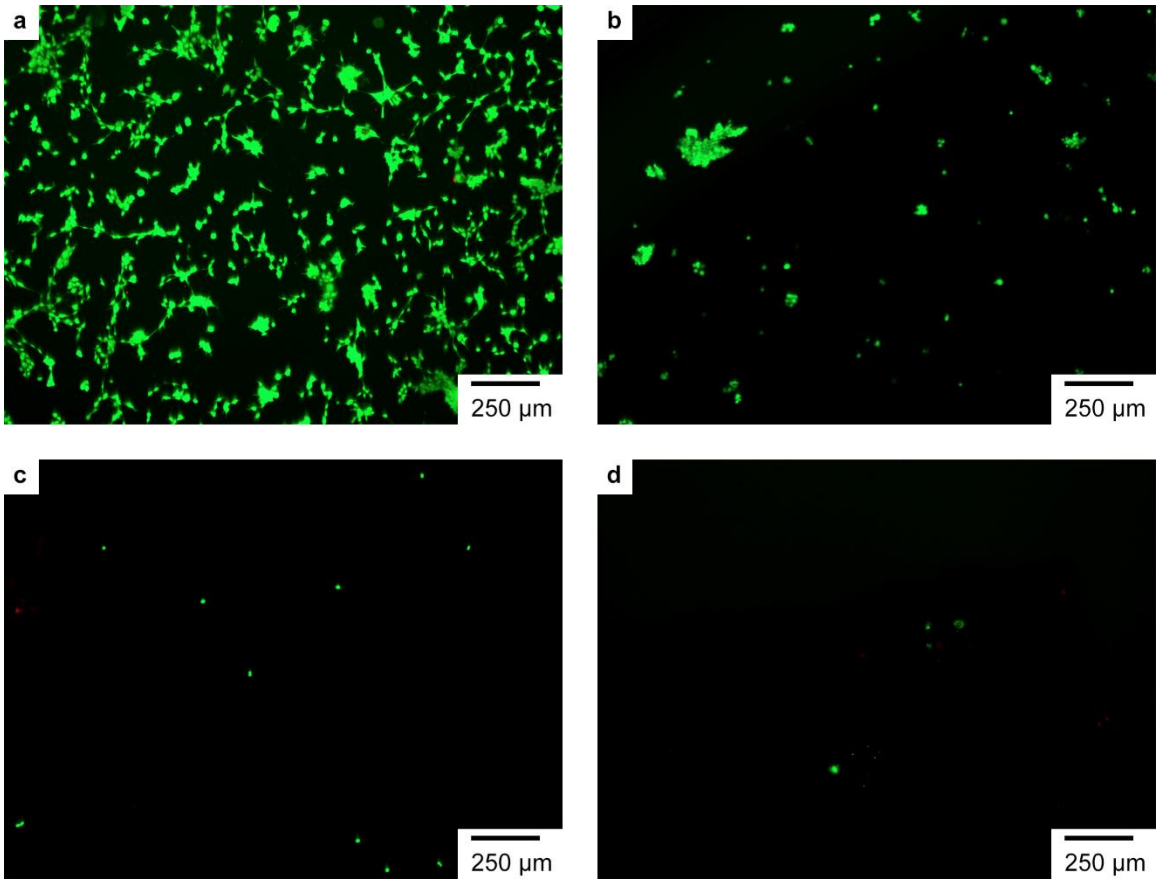

Figure 7.4. Fluorescent microscopy images of the osteoblasts attached to the silicon wafers coated with PGMA (a), P(G_{26}-L_{74}) (b), P(G_{15}-O_{66}-L_{19}) (c) and P(G_{34}-O_{66}) (d). The cells were stained with Calcein AM and Ethd-1 prior to visualization. Osteoblasts stained green are viable, while those stained red are dead.

The osteoblast attachment and spreading was shown for PGMA and P(G_{26}-L_{74}) coatings. At the same time, little to no evidence of cell adhesion was observed for the P(G_{34}-O_{66}) coating. Moreover, in the latter case the surface of the sample was found to repel proteins, in contrast to the PGMA and P(G_{26}-L_{74}) coatings. These samples appeared to be covered with thick and developed layers of proteins that are, apparently, secreted by attached osteoblasts. The P(G_{15}-O_{66}-L_{19}) coating represents an intermediate case: although,

osteoblast attachment was evident from the images and the cells exhibited conventional morphology, no proteins were adsorbed on the surface.

Proteins tend to have high affinity towards hydrophobic surfaces, facilitating cell adhesion and spreading. Considering strong hydrophobic nature of PGMA and P(G_{26}-L_{74}) coatings, the obtained results were not unexpected. At the same time, it is well-known that PEGylated surfaces possess strong protein- and, as a result, cell-repulsive properties. Therefore, no adhesion of osteoblasts on the P(G_{34}-O_{66}) coating is, apparently, due to the high percentage of PEG-containing components. Since the P(G_{15}-O_{66}-L_{19})system exhibit lower content of PEG, osteoblasts were able to adhere and spread across the surface. However, due to the low work of adhesion, this system was still demonstrating protein-repulsive properties. These findings allow for fine control over the cell adhesion that can be tuned depending on the current application.

7.2.3. Cytotoxicity of PGMA-based coatings

The LIVE/DEAD® assay was used to assess the number and viability of osteoblasts attached to the polymeric coatings. The results are presented on **Figure 7.4**. These images confirmed the results of SEM and revealed a large number of cells attached to the PGMA and P(G_{26}-L_{74}) coatings, while only a few osteoblasts adhered to the surface of the P(G_{34}-O_{66}) samples. In the case of P(G_{15}-O_{66}-L_{19}) coating, the number of cells lodging the sample was higher than for P(G_{34}-O_{66}). However, compared to PGMA and P(G_{26}-L_{74}) coatings, the P(G_{15}-O_{66}-L_{19}) polymer system exhibited significantly less adherent cells, demonstrating moderate cell-repulsive properties. It is important to emphasize that all four

polymer systems demonstrated high biocompatibility and low cytotoxicity resulting in little to no evidence of non-viable osteoblasts attached to the samples.

The MTT assay was conducted in order to monitor the effect of the PGMA/POEGMA ($P(G_{34}\text{-}O_{66})$) coatings on the osteoblast proliferation rate. The results (**Figure 7.5**) were compared with plain tissue-grade polystyrene. Absorbance at 570 nm reflects cell count and as evident from the analysis, the difference between the control and studied samples was not found to be statistically different (p-value>0.05, for n=6 samples). Hence, multiple evidences suggest that polymer coatings are non-cytotoxic which confirms the findings observed with LIVE/DEAD® assay.

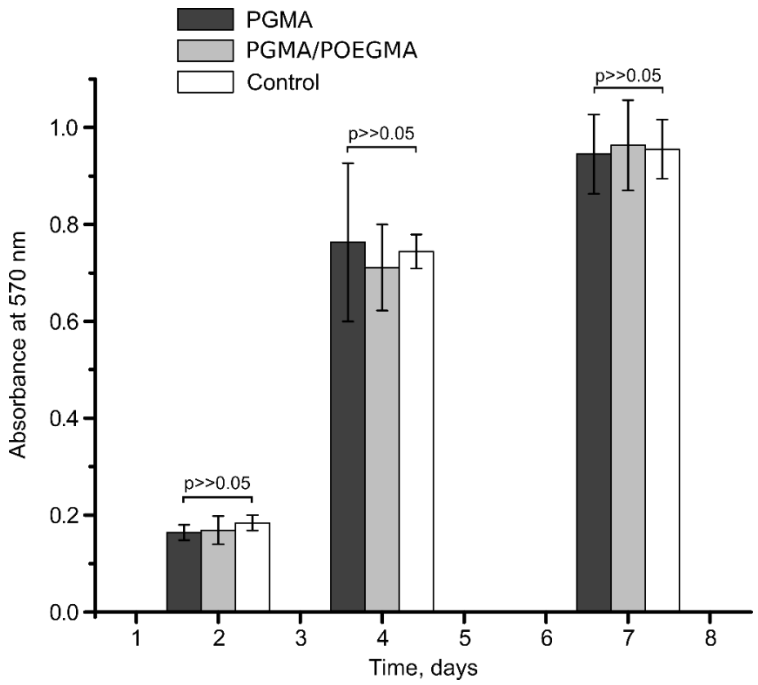

Figure 7.5. The results of MTT assay for PGMA and PGMA/POEGMA ($P(G_{34}\text{-}O_{66})$).

Overall, these results demonstrate that poly(GMA-ran-OEGMA-ran-LMA)-based coatings offer high variability of its cell adhesion properties achieved through the one-step process of deposition and annealing while showing no signs of cytotoxicity.

7.2.4. The *in-vitro* evaluation of biological activity of PGMA-based coated implants

The characterization of mechanical stress

As the K-wires are going to undergo mechanical shear stress in the body during their operation, they must preserve their antibacterial properties after being subjected to this stress. In order to investigate this effect the K-wires were dragged through the Septa and the resulting force was measured using the Instron machine. The wires were dragged with different rates (1, 5 and 8 mm/s). Average value of shear stress is essentially independent on the speed and is ca 0.5 MPa (**Figure 7.6**). Here the force measured by Instron has been divided by the inner area of the hole in the septa.

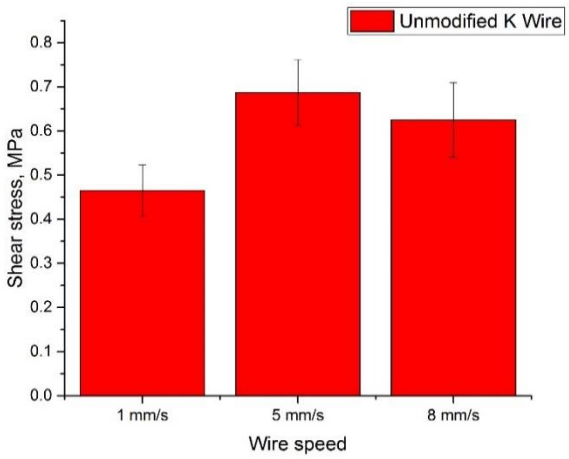

Figure 7.6. The shear mechanical stress imposed to the K-wire dragged through septum.

Analysis of planktonic bacteria

Monolaurin is a naturally occurring antibiotic that shows significant promise in the combating bacterial contamination that happens when the orthopaedic implants are inserted into the human body. The analysis of the planktonic bacteria demonstrates the ability to bacteria to grow in the regions within the vicinity of the implant. This is an important characteristic as in a body the bacterial grow must be suppressed on only directly on the surface of an implant but also in the surrounding space. The analysis of planktonic bacteria consists of determining the highest concentration of bacteria that cannot proliferate due to antibacterial activity of the coating. Once the maximum concentration is established, the kinetics of this process must be investigated with viability curves.

ML concentration	**No polymer**	**No polymer dragged through the septa**	**P(G_{15}-O_{66}-L_{19})**
1	≈$6*10^6$	0	≈$6*10^6$
3	≈$7*10^6$	0	≈$8*10^7$
5	≈$6*10^6$	0	≈$7*10^8$
10	≈$8*10^6$	0	≈$2*10^9$

Table 6.1. The analysis of the planktonic bacteria on the coated K-wires.

According to the results, K-wires coated with P(G_{15}-O_{66}-L_{19})/ML possess excellent antibacterial activity against planktonic SA. Moreover, it was shown that even after being dragged through septa P(G_{15}-O_{66}-L_{19})/ML coated samples are capable of inhibiting up to $2*10^9$ CFU of SA. At the same time, it was shown that the ML coated wires are capable of

killing "only" $8*10^6$ CFU. Furthermore, ML coating does not possess mechanical stability and can be easily peeled off when exposed to shear stress. A total number of 9 replicates were performed for each concentration. Given the results shown above, the wires were coated using 10%ML/5% P(G_{15}-O_{66}-L_{19})solutions in order to get the samples with the highest antibacterial activity.

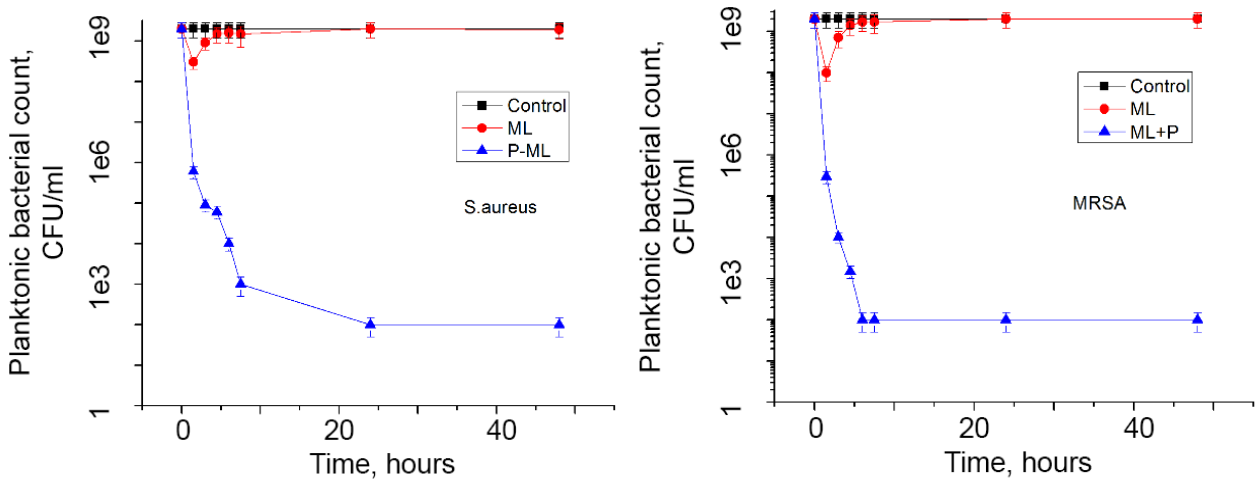

Figure 7.7. The bacterial viability curves for *S. aureus* and MRSA.

Bacterial viability curves that demonstrate the kinetics of the bacterial proliferation are presented on **Figure 7.7**. As can be seen, the P(G_{15}-O_{66}-L_{19})/ML coating is capable of inactivating more than 10^9 CFU of bacteria, in contrast to the ML coating. Moreover, it was noticed that the activity of the coating against MRSA is higher than that against SA. Another interesting finding is that the P(G_{15}-O_{66}-L_{19})/ML coating does not kill all the bacteria. There are always ~100 bacteria left in the vials and this number remains over at least 24 hours.

For the following experiments the ML sample has not been dragged through the septum. The **Figure 7.8** compares the planktonic antibacterial activity of the ML and P/ML

wires after being stored for 5 days at 50°C (which corresponds to 45 days at RT). Samples were exposed to 10^5 CFU of *S.aureus*. As can be seen, ML-coated wires loose their antibacterial activity over time, Concurrently, when polymer layer is added, the antibacterial activity retains (though a mild drop of one was noticed). The observed drop is, apparently, caused by the degradation of monolaurin.

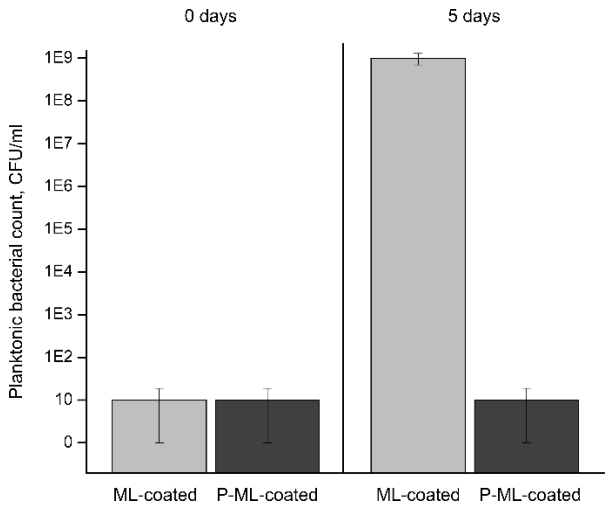

Figure 7.8. Planktonic bacterial count for coated wires before and after storage.

Analysis of adherent bacteria

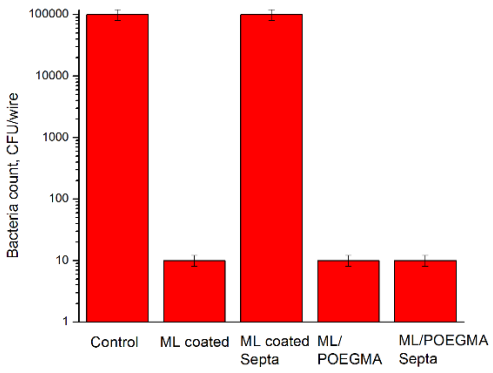

Figure 7.9. Adherent bacteria on the wires

The obtained results (**Figure 7.9**) demonstrate that although the monolaurin coating is utterly efficient against adherent *S. aureus*, it lacks the mechanical stability – after being dragged through a rubber septa, the samples lose their antibacterial activity against adherent bacteria. In contrast, the samples coated with ML/P demonstrate an excellent antibacterial activity even after being exposed to the shear stress.

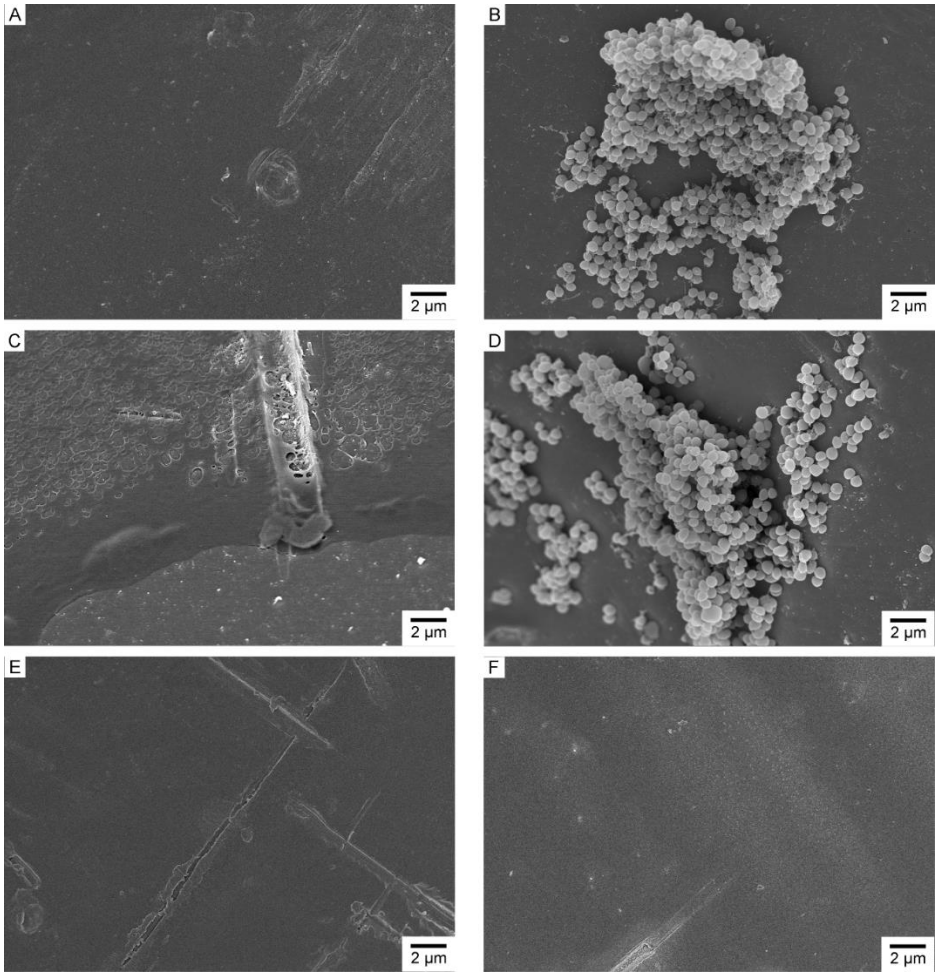

Figure 7.10. SEM of K-wire: (a) coated with ML, (b) coated with ML after being dragged through septa, (c) coated with ML+PLA, (d) coated with ML+PLA after being dragged through septa, (e) coated with ML+ P(G_{15}-O_{66}-L_{19}), (e) coated with ML+ P(G_{34}-O_{66}) after being dragged through septa

The results of the SEM imaging (**Figure 7.10**) confirmed pronounced antibacterial activity of ML/ P(G_{15}-O_{66}-L_{19})coated wires that were exposed to the shear stress. Again, ML-coated wires did not retain its antimicrobial properties. For these studies, the wires coated with PLA+ML were also tested and used as a reference. Initial experiments showed that PLA+ML coating is not mechanically stable. However, after the coating protocol was optimized, PLA+ML coating was capable of withstanding the shear stress.

7.2.5. The summary of results for PGMA-based copolymer coatings for biomedical applications.

The investigation PGMA-based copolymers usage for biomedical applications clearly demonstrated that these materials can be used to ensure the mechanical stability of antibacterial coatings while showing no signs of being cytotoxic. This is a highly promising result that opens wide opportunities for another practical applications of these materials.

7.3. Conclusions for the modification of surfaces using GMA-based copolymer obtained by “grafting through” method

It has been demonstrated that GMA-based copolymers obtained by “grafting through” method via copolymerization with macromonomers has be attached to surfaces in a similar manner as well-studied PGMA by thermal-activated grafting. Due to large variability of these copolymers, it is possible to regulate biologically-relevant properties such as cell adhesion, create drug-loaded coatings and utilize them for sensor design.

7.4. References

1. Kianpour, E.; Azizian, S., Polyethylene glycol as a green solvent for effective extractive desulfurization of liquid fuel at ambient conditions. *Fuel* **2014,** *137*, 36-40.
2. Li, Z.; Ma, R. Y.; Bai, S. S.; Wang, C.; Wang, Z., A solid phase microextraction fiber coated with graphene-poly (ethylene glycol) composite for the extraction of volatile aromatic compounds from water samples. *Talanta* **2014,** *119*, 498-504.
3. Borodinov, N.; Giammarco, J.; Patel, N.; Agarwal, A.; O'Donnell, K. R.; Kucera, C. J.; Jacobsohn, L. G.; Luzinov, I., Stability of Grafted Polymer Nanoscale Films toward Gamma Irradiation. *ACS applied materials & interfaces* **2015,** *7* (34), 19455-19465.
4. Anselme, K., Osteoblast adhesion on biomaterials. *Biomaterials* **2000,** *21* (7), 667-681.
5. Albrektsson, T.; Johansson, C., Osteoinduction, osteoconduction and osseointegration. *Eur Spine J* **2001,** *10 Suppl 2*, S96-101.
6. Lyndon, J. A.; Boyd, B. J.; Birbilis, N., Metallic implant drug/device combinations for controlled drug release in orthopaedic applications. *Journal of Controlled Release* **2014,** *179*, 63-75.
7. Beardmore, A. A.; Brooks, D. E.; Wenke, J. C.; Thomas, D. B., Effectiveness of Local Antibiotic Delivery with an Osteoinductive and Osteoconductive Bone-Graft Substitute. *JBJS* **2005,** *87* (1), 107-112.
8. Albrektsson, T.; Albrektsson, B., Osseointegration of bone implants: A review of an alternative mode of fixation. *Acta Orthopaedica Scandinavica* **1987,** *58* (5), 567-577.
9. Goodman, S. B.; Yao, Z.; Keeney, M.; Yang, F., The Future of Biologic Coatings for Orthopaedic Implants. *Biomaterials* **2013,** *34* (13), 3174-3183.
10. Guillaume, O.; Garric, X.; Lavigne, J.-P.; Van Den Berghe, H.; Coudane, J., Multilayer, degradable coating as a carrier for the sustained release of antibiotics: preparation and antimicrobial efficacy in vitro. *J Control Release* **2012,** *162* (3), 492-501.
11. Anderson, J. M.; Rodriguez, A.; Chang, D. T., Foreign body reaction to biomaterials. *Seminars in Immunology* **2008,** *20* (2), 86-100.
12. Dee, K. C.; Puleo, D. A.; Bizios, R., *An Introduction To Tissue-Biomaterial Interactions*. Wiley-Liss, Inc: 2002.

CHAPTER 8. APPLICATION OF FUNCTIONAL PGMA-BASED COPOLYMERS BY "GRAFTING THROUGH" METHOD FOR MODIFICATION OF COLLOIDAL PARTICLES

8.1. Graphene oxide functionalization, deposition and thermal reduction

The scope of the objects for the modification by PGMA-based copolymers is not limited to solid surfaces only. Colloidal particles can be modified with copolymer as well. As it was established in **Chapter 6** the surface energy of copolymers can be finely tuned within a wide range. Once the modified particles have the proper values of surface energy, they will tend to not aggregate and spread uniformly. This principle can be used for the preparation of highly conductive coatings using flakes of graphene oxide as a precursor. The interest in this material is mainly due to its physical and electrical properties: high carrier charge mobility (conductivity on the order of 10^5 S cm^{-1}), outstanding mechanical (1 TPa Young's modulus, high flexibility) and optical (90% transmittance for corresponding sheet resistance of 20 Ω sq^{-1}). To this end, reduced graphene (rGO) based films have not yet approached pristine graphene in terms of its conductive properties, although its optical properties showed a great promise.[1] Reasons for that are the quality of individual rGO sheets and properties of the entire layer. The increased electrical resistivity originates from the residual sp^3 regions, nanoscopic defects in atomic arrangements,[2-4]

irregular distribution of sheets and multiple in plane (edge-to-edge) as well as plane-to-plane (stacking) contacts.[5] Therefore, to obtain highly conductive rGO film useful for electronic application it is very crucial to achieve ordered and controlled sheet packing of graphene oxide.

8.1.1. Materials and methods

This work has been done in tight collaboration with Mykhailo Savchak working under Dr. Luzinov's supervision.

Preparation of graphene oxide sheets modified with P(G_{34}-O_{66}) and P(G_{15}-O_{66}-L_{19}) copolymers

The graphene oxide (GO) aqueous suspension was prepared by Hummers method.[6] The as-synthesized graphene oxide suspension was purified by water rinsing and ultracentrifugation (10000 rpm for 1 hour) for five times to remove the electrolytes and protons. GO water suspension (~ 3 mg ml^{-1}) was mixed with water solution of P(G_{34}-O_{66})/ P(G_{15}-O_{66}-L_{19}) (~ 5 mg ml^{-1}) in mass ratio 1:6, so to have polymer in abundance. The mixture has been rigorously shaken for 15 minutes and then it was kept at room temperature on an orbital shaker. After at least 4 hours GO sheets were evacuated from the solution by centrifugation at 10000 rpm for 5 minutes and rinsed 3-4 times with DI water to remove unattached polymer chains. Then this suspension was centrifuged at 1000 and 500 rpm for 15 min at least two times in order to get rid of all flocculated sheets. To achieve the very dense packing of graphene oxide sheets on any substrate it is necessary to let the colloidal suspension stabilize not less than one week.

Analysis of kinetics of graphene oxide modification

To reveal thermal decomposition behavior of graphene oxide before and after modification with P(G_{34}-O_{66}) and P(G_{15}-O_{66}-L_{19}) TGA was performed using a Q-5000 TA Instruments and AutoTGA 2950HR V5.4A under N_2 environment from room temperature to 600 °C using a ramp rate of 15 °C min^{-1}. To study the adsorption kinetics 3 mg ml^{-1} of concentrated water solution of adsorbent (GO) was mixed with 5 mg ml^{-1} P(G_{34}-O_{66}) or P(G_{15}-O_{66}-L_{19}) in water in ratio 1:6. Such system was held at constant room temperature. Then the suspension was gently evacuated after 20 minutes, 1, 2.5, 4.5 hours of adsorption and rinsed it well with DI water at least 3 times.

8.1.2. Modification of graphene oxide for the deposition of the uniform layers

Atomic force microscopy has been performed by Mykhailo Savchak working under Dr. Luzinov's supervision to determine the thickness of individual GO sheet modified with P(G_{34}-O_{66}), P(G_{15}-O_{66}-L_{19}). Cross-sectional analysis revealed that thickness of pristine GO sheet increased roughly by 1.5 nm for both P(G_{34}-O_{66}) and P(G_{15}-O_{66}-L_{19}). It implies polymer layer was indeed anchored to graphene oxide sheets. As it turns out, deposition of pristine GO does not result in uniform coverage on the piranha-treated hydrophilic surface (**Figure 8.1a**) and produces no coverage on the hydrophobic surface of silane-treated silicon wafer (**Figure 8.1b**). In contrast, individual GO/P(G_{34}-O_{66}) sheets were uniformly distributed on the surface of hydrophilic SiO2 (**Figure 8.1c**). However, **Figure 8.1d** reveals that GO/P(G_{34}-O_{66}) on hydrophobic surface resulted in non-uniform coverage and crumpling of GO flakes, which may be due to poor adhesion of OEGMA units to the hydrophobic surface and capillary forces from fast solvent evaporation.[7-8] By using P(G_{15}-

O_{66}-L_{19}) copolymer it was possible to achieve formation of uniform layers on both hydrophilic and hydrophobic surfaces (**Figure 8.1e** and **8.1f**, respectively). Moreover, by adjusting the GO/ P(G_{15}-O_{66}-L_{19}) concentration it is possible to deposit multilayer through the single dip-coating which has not been seen for pristine GO and GO/P(G_{34}-O_{66}). By selecting an appropriate material for the modification of graphene oxide it is possible to tune its compatibility with the surfaces of drastically different hydrophilicity.

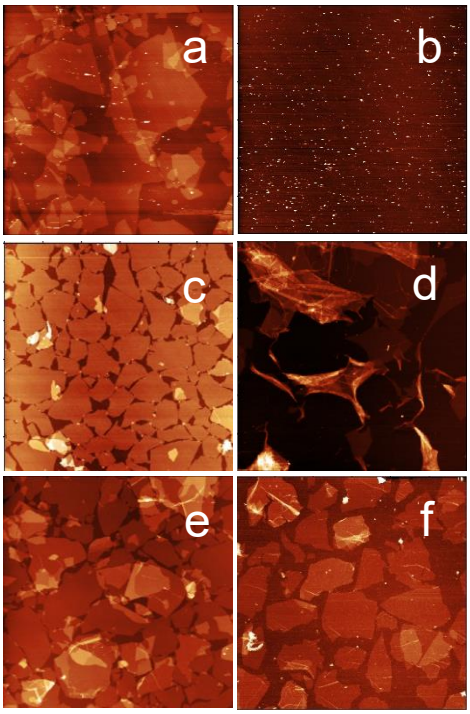

Figure 8.1. Atomic force microscopy of pristine graphene oxide deposited on hydrophilic (a) and hydrophobic (b) surface, GO/P(G_{34}-O_{66}) on hydrophilic (c) and hydrophobic (d) surface and GO/ P(G_{15}-O_{66}-L_{19}) on hydrophilic (e) and hydrophobic (f) surface. The size of the scans is 30x30 μm, height bar is 30 nm (a, c), 2 nm (b), 70 nm (d, e, f).

8.1.3. Kinetics of graphene oxide modification.

In order to confirm that P(G_{34}-O_{66}) and P(G_{15}-O_{66}-L_{19}) have been grafted on GO sheets, thermogravimetric analysis (TGA) was conducted by Mykhailo Savchak working under Dr. Luzinov's supervision to study the thermal stability and adsorption kinetics of GO/P(G_{34}-O_{66}) and GO/ P(G_{15}-O_{66}-L_{19}). The samples are heated to 600 ^{o}C at a rate of 15 ^{o}C/min in a nitrogen atmosphere. From **Figure 8.2a**, it can be observed that pristine GO is not thermostable: mass loss of GO started already below 100 ^{o}C, which is attributed to the volatilization of stored water in its π-stacked structure.[9] The main weight loss of GO around 200 ^{o}C is caused by the decomposition of labile oxygen-containing functional groups yielding CO, CO_2 and steam.[10] The overall weight loss of pristine GO at 500 ^{o}C is 40%. The curve of P(G_{34}-O_{66}) shows a fast weight reduction at about 350-400 ^{o}C, while P(G_{15}-O_{66}-L_{19}) starts to lose weight already at 150 ^{o}C (which may be attributed to the release of trapped) and decomposes entirely at 440 ^{o}C. As for GO/P(G_{34}-O_{66}) and GO/ P(G_{15}-O_{66}-L_{19}), about 70% weight fraction loss is observed from 200 to 500 ^{o}C (**Figure 8.2b,c**), which is due to the decomposition of polymer and some oxygen functional groups on GO sheets. Based on the area under the corresponding derivative curves (**Figure 8.2b,c**, insets it was found that after first 20 minutes there was adsorbed approximately 47% of P(G_{34}-O_{66}) and 53% of P(G_{15}-O_{66}-L_{19}) to the surface of GO sheets. After 4.5 hours 52% of P(G_{34}-O_{66}) and 58% of P(G_{15}-O_{66}-L_{19}) was observed. It suggests that adsorption process is very fast at initial stage. Also, P(G_{15}-O_{66}-L_{19}) unlike P(G_{34}-O_{66}) has higher affinity for adsorption to GO sheets, since its additional LMA side-chain can directly attach to the hydrophobic sites

on GO. Before TGA experiments each sample was thoroughly rinsed with DI at least three times to remove all unattached polymer.

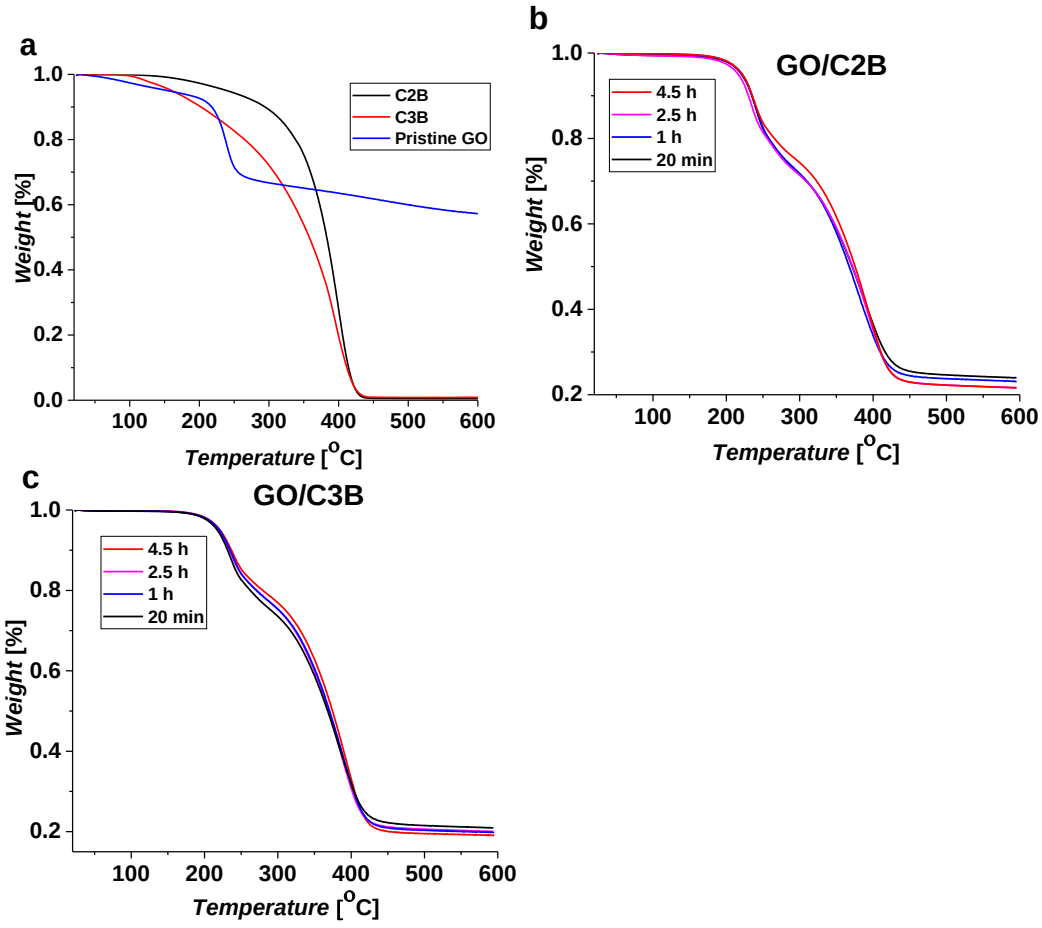

Figure 8.2 Thermogravimetric analysis of P(G_{34}-O_{66}), P(G_{15}-O_{66}-L_{19}) polymers and pristine GO (a). Kinetics of adsorption of P(G_{34}-O_{66}) (b) and P(G_{15}-O_{66}-L_{19}) (c) copolymers to GO sheets.

It suggests that adsorption process is very fast at initial stage similar to what is observed for the melt grafting. Also, P(G_{15}-O_{66}-L_{19}) unlike P(G_{34}-O_{66}) has higher affinity for adsorption to GO sheets since its additional LMA side-chain can directly attach to the hydrophobic sites on GO.

8.1.4. Electrical properties

In order to directly assess the extent to which the GO samples have been reduced and a defect repair degree[11-12] electrical conductivity measurements were performed by Mykhailo Savchak working under Dr. Luzinov's supervision. 34 measurements on about 15 different samples consisted of sequentially deposited r(GO/P(G_{34}-O_{66})) conjugate, polyacrylic acid and another layer (GO/P(G_{34}-O_{66})) that were deposited on undoped Si/SiO_2 substrates and thermally carbonized at 1000 °C in nitrogen flow. The defects in the graphene oxide double layer are getting "healing" through the formation of carbon radicals similar to what was observed for CVD of hydrocarbons.[13-14]

Two-point transport measurements indicated an average sheet resistance 1200 Ω/sq (by a multimeter) and 1508 Ω/sq (from I-V measurements) at room temperature, which resulted in an average conductivities of 2424 S/cm and 3605 S/cm respectively. Thermal reduction of GO/PAA/GO films resulted in better graphitization of graphene sheets and hence further increased conductivity values than for rGO, r(GO/P(G_{34}-O_{66})) or rGO/PAA films. Notably, electrical conductivity values for the bi-layer film is one of the highest reported results[15-26] obtained under the similar thermal treatment conditions.

By selecting the appropriate copolymer for the modification, it is possible to achieve a uniform monolayer free of crumbles, wrinkles and sheet overlapping. This allows for consequent thermal reduction that yields highly conductive films of reduced graphene oxide. The technique of colloid substrate modification with PGMA-based graft copolymers can be transferred to other layered systems to compatibilize them with the surface they are applied to.

8.2. Polymer Cocoons for Thermal Stability of Mesophilic Enzymes over 100˚C

Enzymes are poised to become major commercial catalysts for sustainable chemical technologies, in food industry, biofuel production, deactivation of toxic materials and chemical weapons, laundry, cleaning of oil spills, biosensors, medicine, and many other applications owing to their unparalleled catalytic efficiency and substrate specificity.[27-31] However, quite often the industrial adaptations of biocatalysts are hurdled by the fact that the majority of enzymes can function only at mild aqueous conditions similar to biological cell environment while many industrial processes and real life applications are known to inflict harsh processing conditions such as variations of temperature, *p*H, solvents, and the high concentration of reactants.[32-33] Enzymatic industrial processes tend to be expensive due to a short life-span, poor resiliency and low reusability of biocatalysts. Long-term enzyme thermal stability is vital to harness their catalytic performance beyond their natural environment.[34-37]

Herein, a reported original conjugation strategy has a potential to become a virtually universal thermal stabilization approach for a range of enzymes. The method is based on a spontaneous formation of a semipermeable single polymer molecule cocoon enveloping the enzyme. The cocoon is permeable for substrates and products. It was found that the enzymes stabilized by the cocoon retained their biocatalytic activity after exposure to the temperatures well above 100 ^{o}C. Indeed, the enzyme-cocoon conjugates extended the

temperature range of thermal stability up to 150 ^{o}C in the case of Hen Egg-White Lysozyme.

8.2.1. Materials and methods

This work has been done in collaboration with Dr. Nataraja Sekhar Yadavalli working under the supervision of Dr. Minko in University of Georgia.

Materials

Lysozyme is a 14.3 kDa enzyme that is found in orthologous forms in many different organisms. One of the best-studied forms is found at relatively high amounts in hen egg-white. To estimate the activity levels of lysozyme-PL conjugate at the elevated temperatures, the EnzChek® lysozyme assay kit (Catalog # E22013) purchased from the ThermoFischer Scientific was used. The assay measures lysozyme activity down to 20 U/mL on *Micrococcus lysodeikticus* (new name: *Micrococcus luteus*) cell walls, which are labelled to a high degree that the fluorescence is quenched. Active lsyozyme hydrolyzes the β-(1-4)-glucosamine linkages, relieving the quenching and yielding an increase in the fluorescence that is proportional to lysozyme activity.

8.2.2. The basic concept of the polymer cocoon

The basic architecture of the enzyme-polymer conjugate is explained on **Figure 6.6**. The enzyme is fortified by conjugation with water-soluble polymer ligand P(G_{34}-O_{66}) that has been described in details in **Chapter 6**. P(G_{34}-O_{66}) is designed to impose on the enzyme a broad range of intermolecular forces and covalent bonding in order to stabilize the favorable molecule conformation of the protein. This required a combining of reactive

epoxy functional groups and oligomeric polyethylene glycol (OEGMA) side groups in the P(G_{34}-O_{66}) structure. Epoxy functionalities react with multiple amino groups of lysine (Lys) monomeric units of the enzyme (**Figure 8.3**) creating an enzyme-polymer covalent conjugate (**EPC**) wrapping the enzyme molecule into a cocoon-like structure. OEGMA side chains rally multiple hydrogen bonding to provide the stabilizing effect of the polymeric cocoon. At the same time, OEGMA fragments secure solubility of the copolymer in aqueous solutions, steric stabilization of EPC, and favorable local EPC environment for the enzyme biocatalytic behavior as discussed below.

This design was verified for two examples of Hen-Egg White Lysozyme. The selection is based upon their three dimensional structural analysis for the availability of surface Lys functional residues, their distance from the active site, and spatial location of disulfide bridges. For both enzymes, it was found a very favorable distribution of Lys residues (**Figure 8.3**) for the formation of the targeted cocoon structure and uphold of catalytic activity of the reactive site.

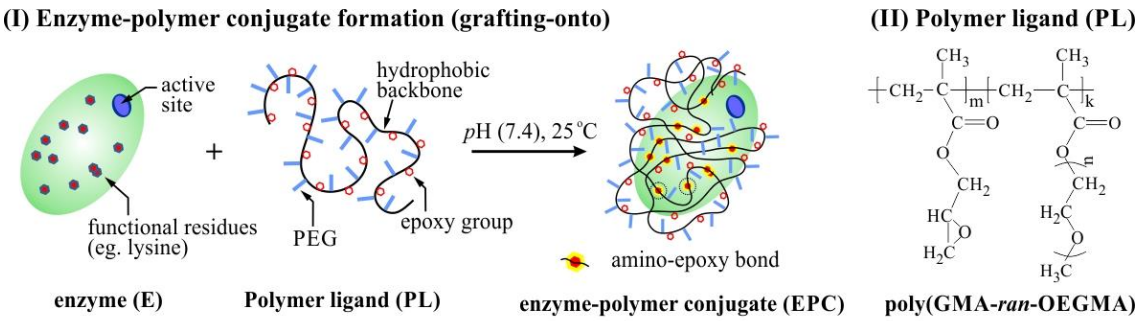

Figure 8.3. (I) Schematic representation of the enzyme (E) and polymer ligand (P(G_{34}-O_{66}), **PL**) conjugate (EPC) formation at 25 °C. **(II)** Polymer ligand (P(G_{34}-O_{66})) – a random copolymer of glycidyl methacrylate (GMA) and oligo(ethylene glycol) methacrylate (OEGMA).

8.2.3. The study of enzyme thermal stability

The LPCs were evaluated by Dr. Nataraja Sekhar Yadavalli working under the supervision of Dr. Minko in University of Georgia for their biocatalytic performance upon incubation at elevated temperatures using fluorescence based biocatalytic activity assays. A comparison of catalytic activity of native enzymes and their P(G_{34}-O_{66}) conjugates undoubtedly demonstrates that the EPCs improved the rate of enzyme activity by severalfold as shown on **Figure 8.4** in terms of relative fluorescence counts (cumulative activity). The native lysozyme completely denatured at 80 ^{o}C, while LPC outperformed and demonstrated excellent levels of activity up to 150 ^{o}C (nearly 100 % at 100 ^{o}C).

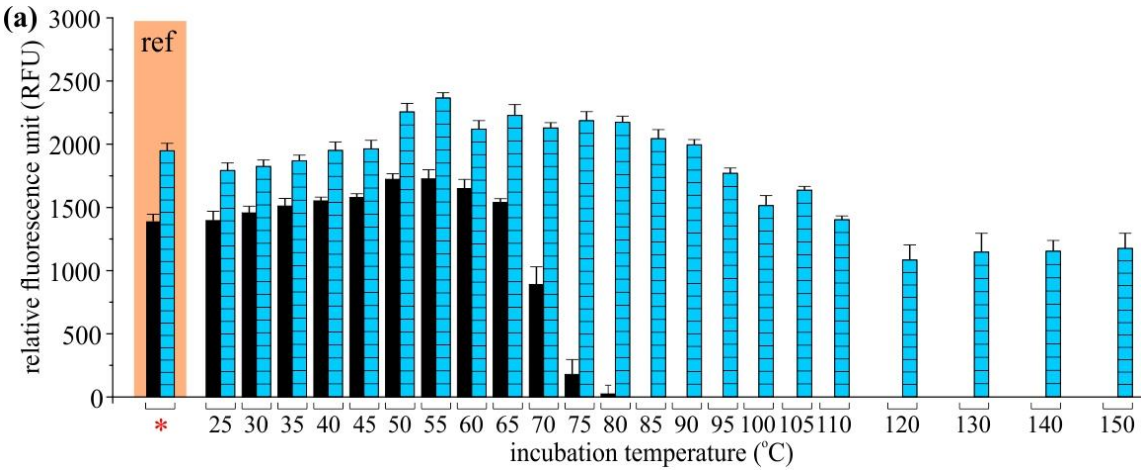

Figure 8.4. Comparison of biocatalytic activity of the native lysozyme (0.44 µM) and LPC at elevated temperature (bio-assay: 1h at 45 ^{o}C) and an incubation period of 1h is used for all samples up to 110 ^{o}C; 45 min for 120 ^{o}C; 30 min for 110 ^{o}C and 15 min for 140 ^{o}C and 150 ^{o}C. Cumulative activity: the black solid and cyan pattern bars correspond to the native lysozyme and LPC, respectively. The data sets inside orange highlighted regions (*) labelled 'ref' represent the activities of native lysozyme and the LPC at 45^{o}C without prior incubation at elevated temperature and used as a reference point to compare with the activity of samples at elevated temperatures

8.2.4. Summary of enzyme thermal stabilization

An effective conjugation approach to enzyme stabilization with a polymer ligand was demonstrated. At high temperatures, a number of hydrogen bonds remains high and conformational changes in the protein remains low, indicating a high degree of resilience of the secondary structure and thereby contributing to the high rates of relative activity. Despite challenges of vulnerable conformations of enzymes the conjugates demonstrate an unmatched ability to stabilize enzymes allowing to reach much higher temperatures than in previously proposed stabilizing methods.[38-41] The polymer ligand creates a cocoon-like structure by engulfing the enzyme into the stabilizing polymeric environment and significantly improves its efficiency and the thermal stability. The stabilization effect is originated from the deployment of a delicate synergetic combination of a strong covalent binding to the protein globule and multiple weak hydrogen bonding between the cocoon and protein. The stabilizing effect is preserved in the powdered lyophilized conjugates making the proposed method promising and virtually universal for many applications.

8.3. References

1. Eda, G.; Fanchini, G.; Chhowalla, M., Large-area ultrathin films of reduced graphene oxide as a transparent and flexible electronic material. *Nature Nanotechnology* **2008,** *3* (5), 270-274.
2. Gomez-Navarro, C.; Weitz, R. T.; Bittner, A. M.; Scolari, M.; Mews, A.; Burghard, M.; Kern, K., Electronic Transport Properties of Individual Chemically Reduced Graphene Oxide Sheets. (vol 7, pg 3499, 2007). *Nano Letters* **2009,** *9* (5).
3. Luo, Z. T.; Vora, P. M.; Mele, E. J.; Johnson, A. T. C.; Kikkawa, J. M., Photoluminescence and band gap modulation in graphene oxide. *Applied Physics Letters* **2009,** *94* (11).
4. Pacile, D.; Meyer, J. C.; Rodriguez, A. F.; Papagno, M.; Gomez-Navarro, C.; Sundaram, R. S.; Burghard, M.; Kern, K.; Carbone, C.; Kaiser, U., Electronic properties and atomic structure of graphene oxide membranes. *Carbon* **2011,** *49* (3), 966-972.
5. Mohan, V. B.; Jayaraman, K.; Stamm, M.; Bhattacharyya, D., Physical and chemical mechanisms affecting electrical conductivity in reduced graphene oxide films. *Thin Solid Films* **2016,** *616*, 172-182.
6. Hummers, W. S.; Offeman, R. E., PREPARATION OF GRAPHITIC OXIDE. *Journal of the American Chemical Society* **1958,** *80* (6), 1339-1339.
7. Wang, W. N.; Jiang, Y.; Biswas, P., Evaporation-Induced Crumpling of Graphene Oxide Nanosheets in Aerosolized Droplets: Confinement Force Relationship. *Journal of Physical Chemistry Letters* **2012,** *3* (21), 3228-3233.
8. Becton, M.; Zhang, L. Y.; Wang, X. Q., Mechanics of graphyne crumpling. *Physical Chemistry Chemical Physics* **2014,** *16* (34), 18233-18240.
9. Jung, I.; Dikin, D.; Park, S.; Cai, W.; Mielke, S. L.; Ruoff, R. S., Effect of Water Vapor on Electrical Properties of Individual Reduced Graphene Oxide Sheets. *Journal of Physical Chemistry C* **2008,** *112* (51), 20264-20268.
10. Stankovich, S.; Dikin, D. A.; Piner, R. D.; Kohlhaas, K. A.; Kleinhammes, A.; Jia, Y.; Wu, Y.; Nguyen, S. T.; Ruoff, R. S., Synthesis of graphene-based nanosheets via chemical reduction of exfoliated graphite oxide. *Carbon* **2007,** *45* (7), 1558-1565.
11. Guo, H. L.; Wang, X. F.; Qian, Q. Y.; Wang, F. B.; Xia, X. H., A Green Approach to the Synthesis of Graphene Nanosheets. *Acs Nano* **2009,** *3* (9), 2653-2659.
12. Shang, Y.; Zhang, D.; Liu, Y. Y.; Guo, C., Preliminary comparison of different reduction methods of graphene oxide. *Bull. Mat. Sci.* **2015,** *38* (1), 7-12.
13. López, V.; Sundaram, R. S.; Gómez-Navarro, C.; Olea, D.; Burghard, M.; Gómez-Herrero, J.; Zamora, F.; Kern, K., Chemical Vapor Deposition Repair of Graphene Oxide: A Route to Highly-Conductive Graphene Monolayers. *Advanced Materials* **2009,** *21* (46), 4683-4686.
14. Dai, B.; Fu, L.; Liao, L.; Liu, N.; Yan, K.; Chen, Y.; Liu, Z., High-quality single-layer graphene via reparative reduction of graphene oxide. *Nano Res.* **2011,** *4* (5), 434-439.
15. Shi, H. F.; Wang, C.; Sun, Z. P.; Zhou, Y. L.; Jin, K. J.; Yang, G. Z., Transparent conductive reduced graphene oxide thin films produced by spray coating. *Science China-Physics Mechanics & Astronomy* **2015,** *58* (1), 5.

16. Li, Z. J.; Yang, B. C.; Zhang, S. R.; Zhao, C. M., Graphene oxide with improved electrical conductivity for supercapacitor electrodes. *Applied Surface Science* **2012,** *258* (8), 3726-3731.
17. Lopez, V.; Sundaram, R. S.; Gomez-Navarro, C.; Olea, D.; Burghard, M.; Gomez-Herrero, J.; Zamora, F.; Kern, K., Chemical Vapor Deposition Repair of Graphene Oxide: A Route to Highly Conductive Graphene Monolayers. *Advanced Materials* **2009,** *21* (46), 4683-+.
18. Vlassiouk, I.; Polizos, G.; Cooper, R.; Ivanov, I.; Keum, J. K.; Paulauskas, F.; Datskos, P.; Smirnov, S., Strong and electrically conductive graphene-based composite fibers and laminates. *ACS Appl. Mater. Interfaces* **2015,** *7* (20), 10702-9.
19. Becerril, H. A.; Mao, J.; Liu, Z.; Stoltenberg, R. M.; Bao, Z.; Chen, Y., Evaluation of solution-processed reduced graphene oxide films as transparent conductors. *Acs Nano* **2008,** *2* (3), 463-470.
20. Wang, X.; Zhi, L. J.; Mullen, K., Transparent, conductive graphene electrodes for dye-sensitized solar cells. *Nano Letters* **2008,** *8* (1), 323-327.
21. Eda, G. a. C. M., Chemically derived graphene oxide: towards large-area thin-film electronics and optoelectronics. *Advanced materials (Deerfield Beach, Fla.)* **2010,** *22* (22), 2392--415.
22. Zheng, Q. B.; Ip, W. H.; Lin, X. Y.; Yousefi, N.; Yeung, K. K.; Li, Z. G.; Kim, J. K., Transparent Conductive Films Consisting of Ultra large Graphene Sheets Produced by Langmuir-Blodgett Assembly. *Acs Nano* **2011,** *5* (7), 6039-6051.
23. Fan, T.-J.; Yuan, C.-Q.; Tang, W.; Tong, S.-Z.; Liu, Y.-D.; Huang, W.; Min, Y.-G.; Epstein, A. J., A Novel Method of Fabricating Flexible Transparent Conductive Large Area Graphene Film. *Chinese Physics Letters* **2015,** *32* (7), 076802.
24. Li, L.; Sun, Q.; Bellehumeur, C.; Gu, P., Composite Modeling and Analysis for Fabrication of FDM Prototypes with Locally Controlled Properties. *Journal of Manufacturing Processes* **2002,** *4* (2), 129-141.
25. Su, Q.; Pang, S. P.; Alijani, V.; Li, C.; Feng, X. L.; Mullen, K., Composites of Graphene with Large Aromatic Molecules. *Advanced Materials* **2009,** *21* (31), 3191-+.
26. Dai, B. Y.; Fu, L.; Liao, L.; Liu, N.; Yan, K.; Chen, Y. S.; Liu, Z. F., High-Quality Single-Layer Graphene via Reparative Reduction of Graphene Oxide. *Nano Res.* **2011,** *4* (5), 434-439.
27. Ansari, S. A.; Husain, Q., Potential applications of enzymes immobilized on/in nano materials: A review. *Biotechnol Adv* **2012,** *30* (3), 512-23.
28. Ariga, K.; Ji, Q.; Mori, T.; Naito, M.; Yamauchi, Y.; Abe, H.; Hill, J. P., Enzyme nanoarchitectonics: organization and device application. *Chem Soc Rev* **2013,** *42* (15), 6322-45.
29. Min, K.; Yoo, Y. J., Recent progress in nanobiocatalysis for enzyme immobilization and its application. *Biotechnol Bioproc E* **2014,** *19* (4), 553-567.
30. Es, I.; Vieira, J. D.; Amaral, A. C., Principles, techniques, and applications of biocatalyst immobilization for industrial application. *Appl Microbiol Biotechnol* **2015,** *99* (5), 2065-82.
31. Misson, M.; Zhang, H.; Jin, B., Nanobiocatalyst advancements and bioprocessing applications. *J R Soc Interface* **2015,** *12* (102), 20140891.

32. Liese, A.; Hilterhaus, L., Evaluation of immobilized enzymes for industrial applications. *Chem Soc Rev* **2013,** *42* (15), 6236-49.
33. Stepankova, V.; Bidmanova, S.; Koudelakova, T.; Prokop, Z.; Chaloupkova, R.; Damborsky, J., Strategies for Stabilization of Enzymes in Organic Solvents. *Acs Catal* **2013,** *3* (12), 2823-2836.
34. Prakash, O.; Jaiswal, N., alpha-Amylase: an ideal representative of thermostable enzymes. *Appl Biochem Biotechnol* **2010,** *160* (8), 2401-14.
35. Zamost, B. L.; Nielsen, H. K.; Starnes, R. L., Thermostable Enzymes for Industrial Applications. *J Ind Microbiol* **1991,** *8* (2), 71-81.
36. Haki, G. D.; Rakshit, S. K., Developments in industrially important thermostable enzymes: a review. *Bioresour Technol* **2003,** *89* (1), 17-34.
37. Yeoman, C. J.; Han, Y.; Dodd, D.; Schroeder, C. M.; Mackie, R. I.; Cann, I. K. O., Thermostable Enzymes as Biocatalysts in the Biofuel Industry. *Adv Appl Microbiol* **2010,** *70*, 1-55.
38. Lucius, M.; Falatach, R.; McGlone, C.; Makaroff, K.; Danielson, A.; Williams, C.; Nix, J. C.; Konkolewicz, D.; Page, R. C.; Berberich, J. A., Investigating the Impact of Polymer Functional Groups on the Stability and Activity of Lysozyme-Polymer Conjugates. *Biomacromolecules* **2016,** *17* (3), 1123-34.
39. Buck, F. F.; Vithayathil, A. J.; Bier, M.; Nord, F. F., On the mechanism of enzyme action. LXXIII. Studies on trypsins from beef, sheep and pig pancreas. *Archives of Biochemistry and Biophysics* **1962,** *97* (2), 417-424.
40. Andrade, C. M. M. C.; Pereira Jr, N.; Antranikian, G., Extremely thermophilic microorganisms and their polymer-hidrolytic enzymes. *Revista de Microbiologia* **1999,** *30* (4), 287-298.
41. Kashefi, K.; Lovley, D. R., Extending the upper temperature limit for life. *Science* **2003,** *301* (5635), 934.

CHAPTER 9. CONCLUSIONS AND RECOMMENDATIONS FOR FUTURE STUDIES

Graft copolymers are a very promising tool for surface modification which can provide materials in a complex system with the desired properties on the interface. However, to expand the area of their practical applicability, the modification protocols have to be scalable but at the same time tunable. Within the present dissertation I have focused on the development of such approach using GMA-based graft copolymers. These materials can form surface-attached cross-linked networks capable of undergoing further chemical reactions and show great variability of properties.

In the first part of the study, **Chapters 3-5**, I have investigated GMA-based graft copolymer films synthesized by "grafting to" method. I have demonstrated the challenges that post-synthetic modification of a polymer network can face as well as designed the efficient methods to bypass these complications for grafting of polystyrene and poly(2-vinyl pyridine) into PGMA films. I have demonstrated the unexpected swelling behavior of the resulting films and provided the qualitative explanation of the observed phenomena. The gamma-radiation stability of these nanoscale layers has been identified as well as the pathways to mitigate the damage done to the ability of the films to interact with volatile organic compounds. These findings are required for advanced design of a new generation of photonic sensors that could operate in extreme environments. Finally, I have demonstrated a prototype of nanofoam-based sensor and showed a proof-of-concept for qualitative analysis of chemical vapors in post-exposure regime.

At the same time, the optimization of the response of the nanoscale sensor coating towards specific analytes (such as actual agents of chemical warfare and/or explosives) and testing the radiation stability of the operation of the sensor as a whole are necessary. From fundamental standpoint, a theoretical quantitative description of swelling of the polymer graft-copolymer nanolayers and the composition-dependent collapse of nanofoam coatings should be performed to have better general understanding of these systems and design nanolayers with customized response. Finally, a large library of both swelling and nanofoam collapse caused by different chemicals for different polymer systems needs to be created to enable the use of nanofoam-based sensors for the field operations. This dissertation paves to way for further engineering efforts to improve the performance of such systems and apply them for combating the proliferation of dangerous compounds.

The second part of the dissertation, **Chapters 6-8**, reveals the potential of "grafting through" process to prepare copolymers to control the surface properties of both solid surfaces and colloid objects. I have developed a series of water-compatible copolymers that retain the basic reactivity of PGMA but can be used in an aqueous process. I have performed a detailed study of the composition-dependent properties in this system including thermal properties, surface energy, water solubility and kinetics of melt-grafting. I have demonstrated that such systems can be used to control materials wettability using the deposition of modified graphene oxide as an example to yield transparent conductive coating. At the same time, GMA copolymers show no signs of cytotoxicity and can be used to control cell adhesion, moreover, they are a highly-promising platform for mechanically robust drug-loading. In addition, GMA-copolymer can provide enzymes with

unprecedented thermal stability through simple one-step conjugation. In a broader prospective, GMA-based copolymers can be used in a one-step process to compatibilize the interfaces and are especially interesting for biological applications.

Future studies for graft copolymers synthesized by "grafting through" procedure should be concentrated on theoretical explanation of thermal stabilization observed for polymer-enzyme conjugates and creation of the predictive models. Stability to pH and non-aqueous solvents should be investigated as well as it can significantly boost the processing windows for industrial processes involving selected enzymes. As GMA-based copolymers were showed to be extremely effective for the design of mechanically resistant drug-loaded coatings, their action needs to be verified during *in-vivo* animal studies. Also, other drugs can be investigated for the loading into copolymer layers. If the results are promising, these findings should be considered for commercialization.